SONNE-Berichte

Dynamics of sedimentation processes and their impact on biogeochemical reactions on the continental slope off Argentina and Uruguay (MARUM)

Cruise No. SO260/Leg 1 & Leg2

Leg 1: January 12 – January 30, 2018
Buenos Aires (Argentina) – Montevideo (Uruguay)

Leg 2: February 2 – February, 14, 2018
Montevideo (Uruguay) – Buenos Aires (Argentina)

DosProBio

Kasten, S., Schwenk, T., Aromokeye, D., Baques, M., Baumann, K.-H., Bergenthal, M., Bösche, J., Bozzano, G., Brune, R., Bülten, J., Chiessi, C.M., Coffinet, S., Crivellari, S., Dehning, K., Dohrmann, I., Dröllner, M., Düßmann, R., Durica, J.T., Frederichs, T., Garcia Chapori, N., Gonzalez, L., Hanebuth, T.J.J., Hilgenfeldt, C., Hüttich, D., Jones, C.K., Klann, M., Klar, S., Klein, T., Kockisch, B., Köster, M., Lantzsch, H., Linowski, E., Long, J.H., Melcher, A.-C., Ogunleye, O.J., Pereyra, N., Rehage, R., Riedinger, N., Rosiak, U., Schmidt, W., Schnakenberg, A., Spieß, V., Steinmann, L., Thieblemont, A., Volz, J., Warnke, F., Warratz, G., Wenau, S., Zonneveld, K.A.F.

Chief Scientist: Prof. Dr. Sabine Kasten

Alfred Wegener Institute Helmholtz Centre for Polar and Marine Research

2019

We dedicate this cruise report to Niels Jacobi, Uwe Rosiak and Monika Segl

Table of Contents

1 Cruise Summary

1.1 Summary in English

RV SONNE cruise SO260 "DosProBio" was carried out in two legs from January 12th until February 14th 2018. The study area was the continental margin off Argentina and Uruguay, which represents a highly dynamic depositional environment and is also a key location of the global thermohaline circulation due to the confluence of northward and southward flowing contour currents. With a multidisciplinary team consisting of geoscientists from various disciplines, biologists and oceanographers the objective of the cruise was to study the fundamental interaction between bottom currents and sediment deposition as well as how sedimentation processes control biogeochemical reactions and element cycling in the seabed. Moreover, the sediments deposited in contourites and canyons were targeted as valuable high-resolution archives to study paleo-oceanographic changes. In order to reach our scientific aims we conducted detailed sediment echosounder and seismic surveys. Based on these mappings we chose suitable sites for sediment and water column sampling. The water column was sampled using a Rosette/CTD system and *in situ* pumps. The sediment surface and the uppermost meters of the sediments were sampled by means of multiple corer, giant box corer, sediment grab, and gravity corer. In order to retrieve older/deeper sediments the MARUM MeBo70 drill rig was deployed. The expedition contributed to and was carried out in the framework of the DFG-funded Cluster of Excellence MARUM "The Ocean in the Earth System" (MARUM – Center for Marine Environmental Sciences, University of Bremen).

1.2 Zusammenfassung

Die FS SONNE Expedition SO260 "DosProBio" wurde in der Zeit vom 12. Januar bis 14. Februar 2018 in Form von zwei Fahrtabschnitten durchgeführt. Das Arbeitsgebiet umfasste den Kontinentalrand vor Argentinien und Uruguay, der ein hoch-dynamisches Ablagerungsgebiet repräsentiert und aufgrund der Konfluenz von nord-und südwärts-gerichteten Kontourströmungen eine Schlüsselregion der globalen thermohalinen Zirkulation darstellt. In einem multidisziplinären Team bestehend aus Geowissenschaftlern, Biologen und Ozeanographen war es das Ziel der Expedition die grundlegenden Wechselwirkungen zwischen Bodenströmungen und Sedimentationsregimen zu untersuchen und zu ermitteln in welcher Weise die verschiedenen Ablagerungsprozesse die biogeochemischen Prozesse und Elementflüsse im Sediment steuern. Darüber hinaus wurden Contourit- und Canyon-Ablagerungen beprobt, um diese als zeitlich hochauflösende Archive zur Rekonstruktion der Änderungen der paläozeanographischen Bedingungen zu nutzen. Um diese Ziele zu erreichen, wurden detaillierte Echolot- und seismische Vermessungen durchgeführt. Auf der Basis dieser Kartierungen erfolgte die Auswahl geeigneter Lokationen für die Beprobung der Wassersäule und des Sedimentes. Die Beprobung der Wassersäule erfolgte mittels eines Rosetten-Wasserschöpfer/CTD-Systems und *in situ* Pumpen. Die Sedimentoberfläche und die oberstern Meter des Sedimentes wurden mit Hilfe von Multicorer, Großkastengreifer, Sediment-Greifer und Schwerelot beprobt. Für die Gewinnung längerer Kerne bzw. älterer Sedimente kam das Meeresbodenbohrgerät MeBo70 des MARUM zum Einsatz. Die Expedition wurde im Rahmen des von der DFG finanzierten Exzellenzclusters MARUM "The Ocean in the Earth System" (MARUM – Zentrum für Marine Umweltwissenschaften, Universität Bremen) durchgeführt.

2 Participants

2.1 Principle Investigators

Name	Institution *
Prof. Dr. Sabine Kasten	AWI, UBremen-FB5, MARUM
Dr. Tilmann Schwenk	UBremen-FB5, MARUM
Prof. Dr. Volkhard Spieß	UBremen-FB5, MARUM
Prof. Dr. Natascha Riedinger	OSU
Prof. Dr. Till J. J. Hanebuth	CCU
Dr. Hendrik Lantzsch	UBremen-FB5
Dr. Thomas Frederichs	UBremen-FB5, MARUM
Dr. Sarah Coffinet	MARUM
Dr. David Aromokeye	UBremen-FB2, MARUM
Dr. Graziella Bozzano	SHN-CONICET
Dr. Natalia Garcia Chapori	UBA-CONICET
Prof. Dr. Cristiano M. Chiessi	USP
Prof. Dr. Karin A. F. Zonneveld	UBremen-FB5, MARUM
Dr. Karl-Heinz Baumann	UBremen-FB5
Markus Bergenthal	MARUM

* for abbreviations, please, see chapter 2.3

2.2 Scientific Party

Table 2.2.1: Scientific Party of Leg 1 of RV SONNE cruise SO260

Name	Discipline/Task	Institution*
Kasten, Sabine, Prof. Dr.	Chief scientist	AWI UBremen-FB5 MARUM
Spieß, Volkhard, Prof. Dr.	Geophysics	UBremen-FB5
Wenau, Stefan, Dr.	Geophysics	UBremen-FB5
Steinmann, Lena, Dr.	Geophysics	UBremen-FB5
Brune, Rouven	Geophysics	UBremen-FB5
Thieblemont, Antoine, Dr.	Geophysics	RHU-London
Warnke, Fynn	Geophysics	UBremen-FB5
Ogunleye, Opeyemi Jesse	Geophysics	UBremen-FB5
Riedinger, Natascha, Prof. Dr.	Geochemistry	OSU
Köster, Male	Geochemistry	AWI
Volz, Jessica, Dr.	Geochemistry	AWI
Dohrmann, Ingrid	Geochemistry	AWI
Dröllner, Maximillian	Geochemistry	AWI
Melcher, Anne-Christin	Geochemistry	AWI
Jones, Christopher K.	Geochemistry	OSU
Bösche, Janina	Sedimentology	UBremen-FB5
Warratz, Grit, Dr.	Sedimentology	UBremen-FB5
Kockisch, Brit	Sedimentology	UBremen-FB5
Hanebuth, Till J. J. Prof. Dr.	Sedimentology	CCU
Long, Joshua Handfield	Sedimentology	CCU
Durica, John Taylor	Sedimentology	CCU
Bozzano, Graziella, Dr.	Sedimentology	SHN-CONICET
Crivellari, Stefano, Dr.	Sedimentology	USP
Frederichs, Thomas, Dr.	Sediment physics, MSCL	UBremen-FB5
Hilgenfeldt, Christian	MSCL	UBremen-FB5
Coffinet, Sarah, Dr.	Organic geochemistry	MARUM
Schnakenberg, Annika	Microbiology	UBremen-FB2
Aromokeye, David, Dr.	Microbiology	UBremen-FB2
Dehning, Klaus	Core technician	MARUM
Klann, Marco	Geo Lab, sample labelling	MARUM
Zonneveld, Karin A. F., Prof. Dr.	Palynology, Water column	MARUM
Baumann, Karl-Heinz, Dr.	Sedimentology, Water column	UBremen-FB5
Baques, Michele	Observer, Argentina	DIIV-UNIDEF

* for abbreviations, please, see chapter 2.3

Table 2.2.2: Scientific Party of Leg 2 of RV SONNE cruise SO260.

Name	Discipline/Task	Institution*
Kasten, Sabine, Prof. Dr.	Chief scientist	AWI UBremen-FB5 MARUM
Schwenk, Tilmann, Dr.	Geophysics	UBremen-FB5
Spieß, Volkhard, Prof. Dr.	Geophysics	UBremen-FB5
Riedinger, Natascha, Prof. Dr.	Geochemistry	OSU
Köster, Male	Geochemistry	AWI
Volz, Jessica, Dr.	Geochemistry	AWI
Dohrmann, Ingrid	Geochemistry	AWI
Dröllner, Maximilian	Geochemistry	AWI
Melcher, Anne-Christin	Geochemistry	AWI
Jones, Christopher K.	Geochemistry	OSU
Lantzsch, Hendrik, Dr.	Sedimentology	UBremen-FB5
Kockisch, Brit	Sedimentology	UBremen-FB5
Bösche, Janina	Sedimentology	UBremen-FB5
Long, Joshua Handfield	Sedimentology	CCU
Chiessi, Christiano M., Prof. Dr.	Sedimentology	USP
Frederichs, Thomas, Dr.	Sediment physics, MSCL	UBremen-FB5
Coffinet, Sarah, Dr.	Organic geochemistry	MARUM
Schnakenberg, Annika	Microbiology	UBremen-FB2
Aromokeye, David, Dr.	Microbiology	UBremen-FB2
Hüttich, Daniel	Core technician	MARUM
Klann, Marco	Geo Lab, sample labelling	MARUM
Bergenthal, Markus	MeBo	MARUM
Klein, Thorsten	MeBo	MARUM
Düßmann, Ralf	MeBo	MARUM
Bülten, Jutta	MeBo	MARUM
Linowski, Erik	MeBo	MARUM
Schmidt, Werner	MeBo	MARUM
Klar, Steffen	MeBo	MARUM
Rosiak, Uwe	MeBo	MARUM
Rehage, Ralf	MeBo	MARUM
Garcia Chapori, Natalia, Dr.	Sedimentology	UBA-CONICET
Baques, Michele	Observer, Argentina	DIIV-UNIDEF
Gonzalez, Lorena	Observer, Uruguay	
Pereyra, Noelia	Observer, Uruguay	

* for abbreviations, please, see chapter 2.3

Fig. 2.2.1 Cruise participants of Leg 1 of RV SONNE cruise SO260.

Fig. 2.2.2 Cruise participants of Leg 2 of RV SONNE cruise SO260.

2.3 Participating Institutions

AWI	Alfred Wegener Institute Helmholtz Centre for Polar and Marine Research
CCU	Coastal Carolina University
CONICET	National Scientific and Technical Research Council of Argentina
DIIV	Argentinian Navy Research Office
MARUM	MARUM – Center for Marine Environmental Sciences, University of Bremen
OSU	Oklahoma State University
RHU-London	Royal Holloway University of London
SHN	Servicio de Hidrografía Naval
SOHMA	Servicio de Oceanografía, Hidrografía y Meteorología de la Armada
UBA	University of Buenos Aires
UBremen-FB2	University of Bremen, Faculty of Biology and Chemistry
UBremen-FB5	University of Bremen, Faculty of Geosciences
UNIDEF	CONICET – Ministry of Defense of Argentina
USP	University of São Paulo

3 Research Program

3.1 Description of the Work Area

The continental slope off Argentina and Uruguay (cf. Fig. 3.1.1) represents a highly dynamic depositional environment and is also a key location of the global thermohaline circulation due to the confluence of northward and southward flowing contour currents. Results from RV Meteor cruise M78/3 in 2009 and earlier cruises have shown that this region offers a unique depositional setting to study the fundamental interaction between bottom currents and sediment deposition as well as how sedimentation processes control biogeochemical reactions and element cycling. Moreover, the sediments deposited in contourites and canyons represent valuable high-resolution archives to study paleo-oceanographic changes.

3.2 Aims of the Cruise

The main scientific goals of the cruise were:

- Analyze the sedimentation of contourite systems in a process-oriented approach with respect to the interaction with regional and local factors as ocean currents, sediment supply and bottom topography.
- Determine the sedimentation modes in submarine canyons in relation to the regional oceanography and climatic regime.
- Utilize the deposits in contourites and canyons for paleo-oceanographic and -climatic reconstructions with special emphasis on the shifting of the BMCZ over longer and shorter time scales.
- Determine the factors other than mass transport deposits (contourites) that can induce transient pore-water profile shapes in the study area – including the role of changes in upward methane flux.
- Determine the changes in origin of the contourite material by investigating the palynomorph composition (pollen/spores, dinoflagellates) of nepheloid layers and slope sediments.
- Investigate how depositional conditions control the preservation and reduction of Fe(III) and Mn(IV)-bearing minerals in sub-seafloor sediments, in particular methanic zones.
- Elucidate the processes and microbial communities that mediate iron and manganese reduction below the sulfate-methane transition.
- Identify the carbon sources of iron and manganese reducing microbial communities below the sulfate-methane transition.
- Investigate how variations in the depositional regime and other environmental factors control the distribution, abundance and composition of benthic archaeal communities in marine sediments.

3.3 Agenda of the Cruise

In order to reach the aims outlined above we conducted detailed sediment echosounder and seismic surveys. Based on these mappings we chose suitable sites for sediment and water column sampling. The water column was sampled using a Rosette/CTD system and *in situ* pumps. The sediment surface and the uppermost meters of the sediments were sampled by means of multiple corer, giant box corer, sediment grab, and gravity corer. In order to retrieve older/deeper sediments the MARUM MeBo70 drill rig was deployed.

The expedition contributed to and was carried out in the framework of the DFG-funded Cluster of Excellence MARUM "The Ocean in the Earth System" (MARUM – Center for Marine Environmental Sciences, University of Bremen).

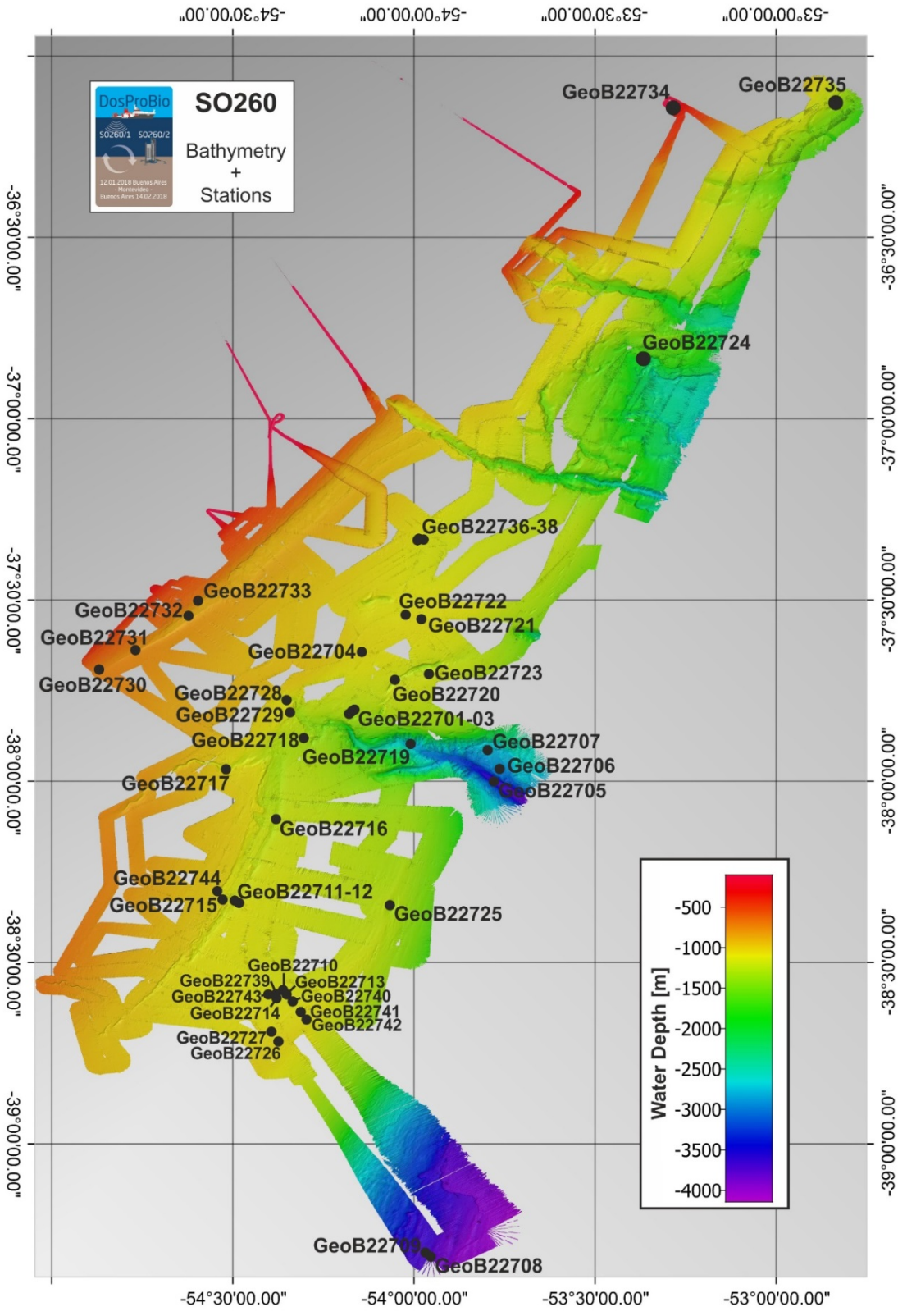

Fig. 3.1.1 Bathymetry and stations of cruise SO260.

4. Narrative of the Cruise

In the morning of Jan 9, 2018 RV SONNE entered the port of Buenos Aires, Argentina. A few members of the scientific party arrived at noon onboard the vessel to delegate laboratory space among the scientists and talk to the ship's command and ship agents. All scientists boarded the RV SONNE on Jan 10, 2018. Container and transport boxes that were loaded onto the vessel in the shipyard in Emden, Germany, were unloaded with highly appreciated help from the deck personnel. Large equipment was assembled on deck and labs and workspaces were prepared.

After an official opening ceremony on Jan 11, 2018, an Open Ship Event was carried out on board RV SONNE organized by the German Embassy in Buenos Aires and the Leitstelle Deutsche Forschungsschiffe. Representatives from the Argentine Ministry of Science (MinCyT), the German Embassy in Buenos Aires, the port authority, and numerous universities and research institutes of Argentina participated in the official opening ceremony. Between 11 am and 5 pm the RV SONNE was open to the public, and about 600 visitors toured the ship and were informed on research and life onboard the ship. The high participation was remarkable, as there were summer holidays in Argentina, and with a temperature around 38°C it was one of the warmest days of the summer. Because of the perfect organization by the ship's command, the German Embassy in Buenos Aires, the Ship agency AMI / Ultramar, as well as the wonderful help of the crew and science party, the event was a great success. We were all impressed by the great interest the visitors showed towards the ship and our research.

In the morning of Jan 12, 2018 the RV SONNE embarked from Buenos Aires on schedule beginning research expedition SO260. On board was an international team of researchers from the Alfred Wegener Institute Helmholtz Centre for Polar and Marine Research, the faculties of Geosciences and Biology/Chemistry at the University of Bremen, the MARUM – Center for Marine Environmental Sciences, the Oklahoma State University, the Coastal Carolina University, the Royal Holloway University of London, the Servicio de Hidrografia Naval in Buenos Aires as well as one observer from Argentina (Argentinian Navy Research Office and UNIDEF). After a 24-hour transit, we arrived at our first work area off Argentina. We were running a survey program with multi-channel seismics to gain information about the sediment structure on the upper continental margin off Argentina near the Mar del Plata Canyon.

After an extended seismic survey along the continental slope off Argentina during the first two days of our expedition, we started to collect water column samples and to core seabed sediments. The main geographic targets were contouritic drift bodies, and associated terraces and channels around the Mar del Plata Canyon. Our scientific aim was to understand how the interaction between water masses, bottom current regimes and seabed topography controls the sediment dynamics inside and outside this canyon system.

We focused on a major morphological terrace on Jan 16, which is located inside the canyon's lower reach. Thick packages of accumulated sediment suggested that this location would provide us with a high-resolution sediment archive. The successful sampling program resulted in two 9-m long sediment cores which seem to cover 5 to 6 meters of Holocene within the uppermost part of the core.

On Jan 17 we proceeded to our up to now deepest sampling station located at about 3.600 m water depth in the South of the Argentine working area. The objective was to recover sediment cores at sites where we had indication from previous expedition M78/3 that intense iron reduction occurs in the deeper sediments. As yet it is not known which biogeochemical process is responsible

for the observed liberation of reduced iron into the pore water of these deep subsurface sediments and how this process is controlled by the particular sedimentation conditions. There is evidence that iron oxides can be reduced by methane, which is present in these sediment layers in dissolved form. There may thus exist a strong coupling between the biogeochemical cycles of iron and methane. By means of joint sampling of the pore water and the sediments by the Inorganic and Organic Geochemistry groups as well as the Microbiologists we seek to elucidate by which biogeochemical process, based on which organic substrates and by which microbial organisms this process is mediated.

Based on PARASOUND and Airgun data, which we collected during a previous cruise in 2009, we found hints on assumedly deep water coral mounds in association with a slope-parallel contouritic channel. Our combined echosounder-seismic survey revealed that these mounds are very common in the region. Coring brought confirmation that these mounds represent an ancient deep-sea coral habitat. On Jan 21 research activity focused on the sampling of various contouritic channels with giant box corer and grab sampler. We received large amounts of gravel and rock fragments, which indicate that the channel floors are very much influenced by strong bottom currents. These currents probably transport a lot of finer material but do not allow for a permanent deposition.

On Monday Jan 22 we continued sediment and water sampling with a focus on erosion structures and canyons. Box corer, multi corer (MUC), gravity corer, and grab corer were deployed again. The recovered sediments were sampled by each scientific group, including geochemistry, microbiology, and organic geochemistry. During the night of Jan 23 to 24, CDT/Rosette and *in situ* pumps were deployed and water column samples were collected. Our colleagues from MARUM and the Faculty of Geosciences of the University of Bremen were interested in sampling nepheloid layers within the water column and near the seafloor to gain information about the origin of particles within these layers.

According to the weather forecast, on Jan 24, wind intensity increased to 5-7 with gusts reaching 9. Despite the tough weather conditions and waves of up to 4 meters high, the RV SONNE stayed steady in the waters and we were able to continue our sediment sampling program using MUC and gravity corer at a designated biogeochemistry-MeBo station. Unfortunately, during the day the weather conditions worsened, with increasing waves, and coring activity had to be stopped. We decided to move to the northernmost station of our research area for further water column sampling. This location was intended to sample the transition to the warm Brazil current from the cold Malvinas current in the uppermost water column. Preliminary shipboard results indicated that the plankton community in the warm surface water differs distinctively from the community found in the cold Malvinas current sampled in the southernmost research area, which is characterized by Antarctic species.

In the night of Thursday Jan 25 to Friday Jan 26, strong winds were chased away by sunny weather and blue sky and a calm sea. The remaining part of the week was used for seismic survey to find a suitable location for MeBo70 deployment during the second leg of SO260.

During the cruise, the richness of seismoacoustic data from multibeam, sediment echosounder and multichannel seismic has revealed a particularly detailed image of the seafloor, which is a clear step forward in understanding the seafloor processes shaping the Northern Argentine Margin. Based on the combined survey and sampling program to visit the most relevant structures as

channels, scours and canyons and associated contouritic deposits, we could develop a possible sampling strategy for the upcoming second leg of our cruise.

Most of the work had so far been concentrated on the Ewing Terrace north and south of the Mar del Plata Canyon, with the hope that sampling may allow the evaluation of the influence of the canyon on along-slope currents and deposition. Several potential areas had been picked for more detailed surveying. A particularly suitable site was found in ~1100 m water depth, representing a very fine-grained succession of drift sediments. PARASOUND at this site penetrates over 80 meters - resembling the rapid fill of a previous depression. This site was assumed to provide a good stratigraphic and contouritic record and to document biogeochemical processes and zonation in the sediments of the terrace. South of the Mar del Plata Canyon, several sites had been surveyed, including scours, the most recent drift body on the terrace and an area of mixed erosion and accumulation next to a contourite channel. Further data processing and site selection kept us busy until the following week, when the first MeBo deployment was planned.

On Monday Jan 29 we continued our surface-sediment sampling program with the grab corer and giant box corer on the upper continental margin off Argentina in water depths of 600 to 800 m. Most of the sampled sites are characterized by strong erosive conditions. Samples of rock fragments with sessile organisms, cold-water coral pieces, and other macro faunal organisms such as solitary corals, mollusca, bryozoans, and sponges were retrieved. Coring activities of RV SONNE cruise Leg SO260-1 were completed Jan 29 at noon and we left the working area towards Montevideo, Uruguay. After reaching the pilot station at 6 am, we entered port in Montevideo at 8 am on Jan 30. Briefly after arrival in Montevideo, the MARUM-MeBo Team came on board to set up the seafloor drill rig MeBo70. The work on the MeBo continued through Jan 31, and was successfully completed Febr 1 with a practice run in the harbor.

While the first leg of our research cruise was dominated by seismic surveys; the second leg focussed on the retrieval of long sediment cores using the seafloor drill rig MeBo70. We therefore had to say goodbye to 15 of our first-leg colleagues, including most of the seismic group from the Faculty of Geosciences, University of Bremen. In return, 15 new scientists came onboard the ship, including 9 members of the MeBo Team and two Uruguayan observers from the Servicio de Oceanografía, Hidrografía y Meteorología de la Armada (SOHMA).

Besides preparation and device assembly work for the second leg of RV SONNE expedition SO260, a ship tour was carried out on Febr 1, for invited guests and the press initiated by the German ambassador in Montevideo, Ingo von Voss. In the evening of Febr 1, a reception was hosted by Ambassador von Voss in a nearby Hotel for members of the RV SONNE crew and of the scientific party. It was a very nice evening with stimulating conversations with, among others, Uruguayan scientists and Naval officers, and other ambassadors in Montevideo.

In the morning of Febr 2, we disembarked for our second leg of the research expedition and arrived after a 12-hour transit at our working area on the continental margin off Uruguay. After sampling two sites with the gravity corer and multi corer, we headed towards our first MeBo station off Argentina, where we arrived Sunday, Febr 3. This first MeBo target was a deep-depression structure near the Mar del Plata Canyon filled with 80-meter thick, undisturbed sediments. The site was picked based on detailed seismic surveys taken during our first expedition leg. After the first MeBo70 deployment had to be cancelled due to technical difficulties, drilling was continued at this location on Monday Febr 5, 2018. Sediments down to 32.80 m depth were retrieved and

revealed, in contrast to the expected fine-grained material, mostly sandy deposits with some intercalated cohesive sediment intervals.

Prior to the next deployment of MeBo70, surface sediments were sampled using the grab corer in areas where, based on PARASOUND surveys, coral mounds were expected. In contrast to our expectations, the hard substance turned out to be sandstone and not a coral mound and thus no gravity cores were taken at this location.

The goal of the second MeBo70 deployment was the recovery of sediments for biogeochemical and microbial studies with a focus on the impact that depositional conditions, as well as the quality and quantity of organic material, have on biogeochemical processes and the microbial communities – especially regarding deep-subsurface iron reduction processes. The site selected for these studies was located off Uruguay, at 1400 m water depth. Pore water data of a 10-meter long gravity core retrieved during previous expedition M78/3 indicated iron reduction processes below the sulfate-methane transition as well as the occurrence of deep sub-seafloor gas hydrates at this location. The MeBo70 drilling was very successful, and after 36 hours of drilling the maximum drill depth of 70.2 meters was accomplished on Febr 8. Sediments were recovered on the morning of Febr 9, after the retrieval of MeBo70. As expected, the sediments showed gas expansion below approximately 20-meter sediment depth related to high methane concentrations. Preliminary data from samples taken for geochemistry revealed the occurrence of dissolved iron for the entire sediment column below approximately 7 m sediment depth, indicating the iron reduction process. Core recovery less gas-expansion gaps was almost 80 %.

After our way back to the Argentine work area we reached again the southern part of the Ewing Terrace and dedicated the entire weekend to the third MeBo70 drilling. Seismic surveys in this area suggested the occurrence of buried coral mound structures. On Monday Febr 12, we completed the third and last MeBo drill site in the area of the Southern Ewing Terrace at a sediment depth of 20 meters and the MeBo70 drill rig was brought back on deck of the RV SONNE around lunch time. The retrieved sediments were mostly sand with a layer of coarse sand and shell fragments at the base. The remaining station time was used to deploy the gravity corer and the giant box corer in an area where – based on PARASOUND surveys – we expected a coral mound structure. The 5 m long sediment core and the sediments retrieved by means of the box corer contained numerous fragments of cold-water corals and sessile fauna at the sediment surface and thus confirmed our assumption. Coring activities of RV SONNE cruise SO260 were completed on Febr 12 in the late afternoon and we left the working area towards Buenos Aires. After reaching the pilot station located within the inner Rio de la Plata mouth at around 10:00 pm of Febr 13 we entered port in Buenos Aires at 8 am the next day. Loading of containers took place on Febr 15.

In the evening of Febr 16, a reception took place on board of the RV SONNE on invitation of the German ambassador in Buenos Aires, Jürgen Christian Mertens. Among others the reception was joined by the Argentine parliamentarian Cornelia Schmidt-Liermann (Cambiemos), representatives of MinCyT, of the port authorities and numerous universities and research institutes, the Master of RV AUSTRAL (the former/old SONNE) and ambassadors of several G20 countries (AUS, EU, FRA, GBR, ITA, MEX). After the welcoming speeches of Master Oliver Meyer and Ambassador Mertens as well as a short scientific presentation of RV SONNE expedition SO260 by chief scientist Sabine Kasten, the guests of the reception had the opportunity to tour the ship and talk to members of the crew and the scientific party to find out about research and life onboard the RV SONNE. After the Open Ship Event in Jan 2018 also this reception was

again a great success due to the perfect organization by the ship's command, the German Embassy in Buenos Aires – in particular by Mrs Kathrin Megerle – the Ship Agency AMI / Ultramar, as well as the wonderful help of the crew and science party.

5 Preliminary Results

5.1. Hydroacoustics

(T. Schwenk, R. Brune, O. Ogunleye, V. Spiess, L. Steinmann, A. Thieblemont, F. Warnke, S. Wenau)

5.1.1. Swath Bathymetry

Technical description

During Expedition SO260, the hull-mounted Kongsberg Simrad system EM122 was used for bathymetric mapping. The shallow- and mid-water EM710 multibeam echo sounder was not used during this cruise. The EM122 system allows bathymetric mapping down to full ocean depth. It was operated continuously in a 24-hour schedule in all permitted survey areas. For calibration of the depth determination algorithms, sound velocity profiles from two XSV deployments as well as various CTD stations were used (see Chapter 5.7). The system operated reliably throughout the cruise with only very few short interruptions. Few data gaps exists which could not be tracked. The duals swath mode did not work by corrupting acquisition, swath width and water column recording. Altogether, a total of ~6800 profile-kilometers were surveyed (Fig. 5.1.1).

Basic components of the EM122 system are two linear transducer arrays in a Mills Cross configuration with separate units for transmitting and receiving. The nominal sonar frequency is 12 kHz with an angular coverage sector of up to 150° and 432 soundings per swath. The emission cone is 150° wide across track, and 0.5° in along track direction. The reception is obtained from 288 beams, with widths of 1° across track and 20° along track. Thus, the actual footprint of each beam has a dimension of 0.5° by 1°. The achievable swath width on a flat bottom will usually be up to 6 times the water depth dependent on the roughness of the seafloor. The angular coverage sector and beam pointing angles may be set to vary automatically with depth according to achievable coverage. Using the high-density mode, which creates 432 soundings out of the 288 beams, finally 432 isolated equidistant depth values are obtained perpendicular to the track for each ping. Using the detected two-way travel time and the beam angle known for each beam, and taking into account the ray bending due to refraction in the water column due to sound speed variations, depth is calculated for each beam. A combination of amplitude (central beams) and phase (slant beams) is used to provide a measurement accuracy practically independent of the beam pointing angle. Besides the depths values the EM122 provides also backscatter information and pseudo-sidescan images. For planning purposes, the data were roughly processed and gridded with the software MB-System (Leg 1) and Fledermaus Pro (Leg 2). However, for detailed analysis a time-consuming processing is necessary after the cruise.

Preliminary results

Along the northern Argentine/Uruguayan continental margin, a multibeam dataset covering an area of 25,000 km^2 (Fig. 5.1.1) was acquired from the upper slope through the middle slope to the transition between the lower slope and the continental rise. Water depths within the surveyed region range from 100 to 4,100 m. Due to similar working areas, the map is complementary to and partly overlapping with multibeam data from cruise RV Meteor M78/3 that operated in the same region.

The Mar del Plata Submarine Canyon separates the northern from the southern part in the Argentine study area. Around the Mar del Plata Canyon the 2 major terraces – the La Plata and Ewing Terraces – as well as their adjacent contouritic channel were surveyed. The deeper Necochea Terrace was covered just by two lines. With its head at ~1000 m of water depth, the Mar del Plata Canyon cuts into the Ewing Terrace and extends to the Necochea Terrace. North of the Mar del Plata Canyon, the Querandi Canyon was partly mapped as well. Further to the North, a significant portion of the southern Uruguayan margin could also be mapped by several visits during Leg 2 between the shelf edge and ~2800 m water depth, but mostly concentrating on water deeper than 1000 m (Fig. 5.1.1). Two large canyon structures, the Rio de la Plata and the Montevideo canyons, were surveyed, as well as the large depressions between them.

Beside these large structures, the multibeam data provided an image of smaller scale surface features as erosional surfaces, contouritic channels, minor and larger elongated depressions, and smaller scale as well as larger scale drift bodies. However, to image these small scale structures properly, a dedicated processing is necessary. As seismic and sampling work focused on the southern Ewing terrace, the previously known area could be significantly extended to the South, thus allowing a comparison between the northern and southern Ewing terrace and the role of the canyon in the contouritic depositional system.

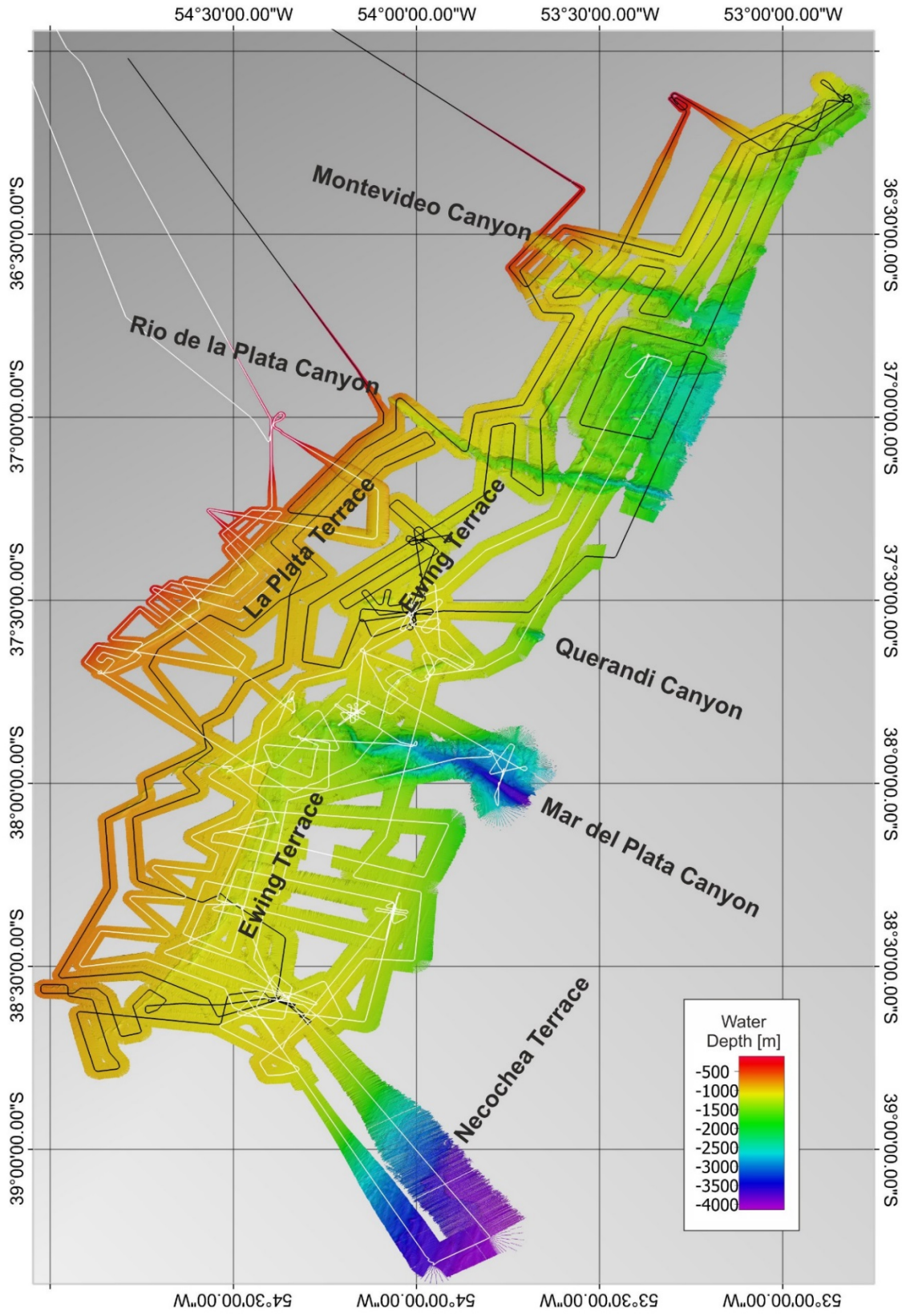

Fig. 5.1.1 Map of bathymetric data gathered during cruise SO260. White lines represent the cruise track of Leg 1, black lines show the cruise track of Leg 2.

5.1.2. PARASOUND Sediment Echosounder

Technical Description

The PARASOUND P70 is a hull-mounted narrow-beam parametric sub-bottom profiler distributed by Teledyne ATLAS HYDROGRAPHIC (Teledyne RESON GmbH). It provides very high-resolution information on the uppermost ~100 m of the subsurface sedimentary layers, thereby allowing also a precise detection of suitable coring locations. A further usage of the PARASOUND system was to image acoustic backscatter within the water column caused by e.g. organisms or suspended material. The PARASOUND was operated in 24-hour watch schedule during the cruise. During the expedition a total of ~ 6800 profile-kilometers were surveyed (Fig. 5.1.1). Small data gaps exist due to crashing of the PARASTORE software roughly once per day.

The PARASOUND system uses the parametric effect to generate a Secondary Low Frequency (SLF) in the range of 0.5 to 6 kHz and a Secondary High Frequency (SHF) in the range of 36.5 to 40 kHz by emitting two primary high frequency signals (Primary High Frequency, PHF). These PHFs are adjustable between 18.5 and 33 kHz. The secondary frequencies develop through non-linear acoustic interaction of the primary waves at high signal amplitudes (*parametric effect*). The transmission beam angle of the PARASOUND P70 is extremely narrow with only 4.5° aperture for a transducer of ~1 m² in size. Consequently, the footprint size is only 7% of the water depth and vertical and lateral resolution is significantly improved compared to conventional sediment echosounder systems. This guarantees a high lateral resolution and, thus, allows an imaging of small scale structures on the sea floor.

During the whole cruise, a SLF frequency of 4 kHz and a non-rectangular pulse shape of ~0.25 ms length were chosen as standard operation setting to provide a good relation between signal penetration and vertical resolution. On most lines during Leg 1 (i.e. all multichannel seismic surveys), the PARASOUND system was operated in quasi-equidistant mode, meaning that a signal is transmitted at equal intervals irrespective of whether the previously transmitted signal was already received back at the receiver. Hence, there can be more than one signal in the water column, which allows for an optimal lateral coverage and, thus, horizontal resolution. On selected profiles during Leg 1 and during stations, as well as during the complete Leg 2, the system was operated in single pulse mode to record the entire water column. This mode implies that there is only one pulse in the water column at every point in time. To adapt the ping rate of all modes, depth information from the EM122 was used as system depth.

The software ATLAS PARASTORE was used for displaying and storing echograms, while the program ATLAS Hydromap Control (AHC) transmits the hydroacoustic settings during acquisition and transfers data from the acquisition unit. The PHF, SLF and SHF data were acquired and stored in the PARASOUND format ASD. The PHF and SLF data were additionally converted into the more common PS3 and SGY formats. For the identification of suitable coring locations as well as for profile planning, the PS3 data were then routinely converted into SGY data with the custom-made program ps32sgy (H. Keil, University of Bremen) and loaded into the interpretation software *The Kingdom Software 2016.1*. During the conversion, outliers within the navigation data in the header were eliminated and the data were re-projected to UTM. Moreover, for further use of the data, the envelope of the seismic trace had to be calculated using The Kingdom Software, as the phase representation of the data is incorrect. In addition, heave compensation was not properly applied to converted data due to a software bug after maintenance, and heave was still present in the data, significantly degrading the use of the data.

Preliminary Results

Figure 5.1.2 shows a PARASOUND profile crossing coring stations GeoB22701, GeoB22702 and GeoB22703 located inside a local depression north of the Mar del Plata Canyon. This depression is characterized by the presence of an upper and a lower terrace. Seafloor reflectors at those terraces are showing high amplitudes and, in case of the upper terrace, several horizontally aligned, continuous reflectors of low amplitude beneath. The signal penetration into the undisturbed sediments exceeds 60 m. All of those reflectors are truncated at the slope between both terraces. Directly adjacent, a lens-shaped body of diverging reflector patterns with medium amplitudes is visible. That sedimentary structure is interpreted as a contouritic drift deposit. Furthermore, the lower drift boundary is associated with an erosional process truncating into the undisturbed sediments deposited inside the depression. The result is a terraced seafloor, which is clearly visible in the PARASOUND profile (Fig. 5.1.2). The amount of sediment accumulation adds up to 30 m in the central part of the drift deposit.

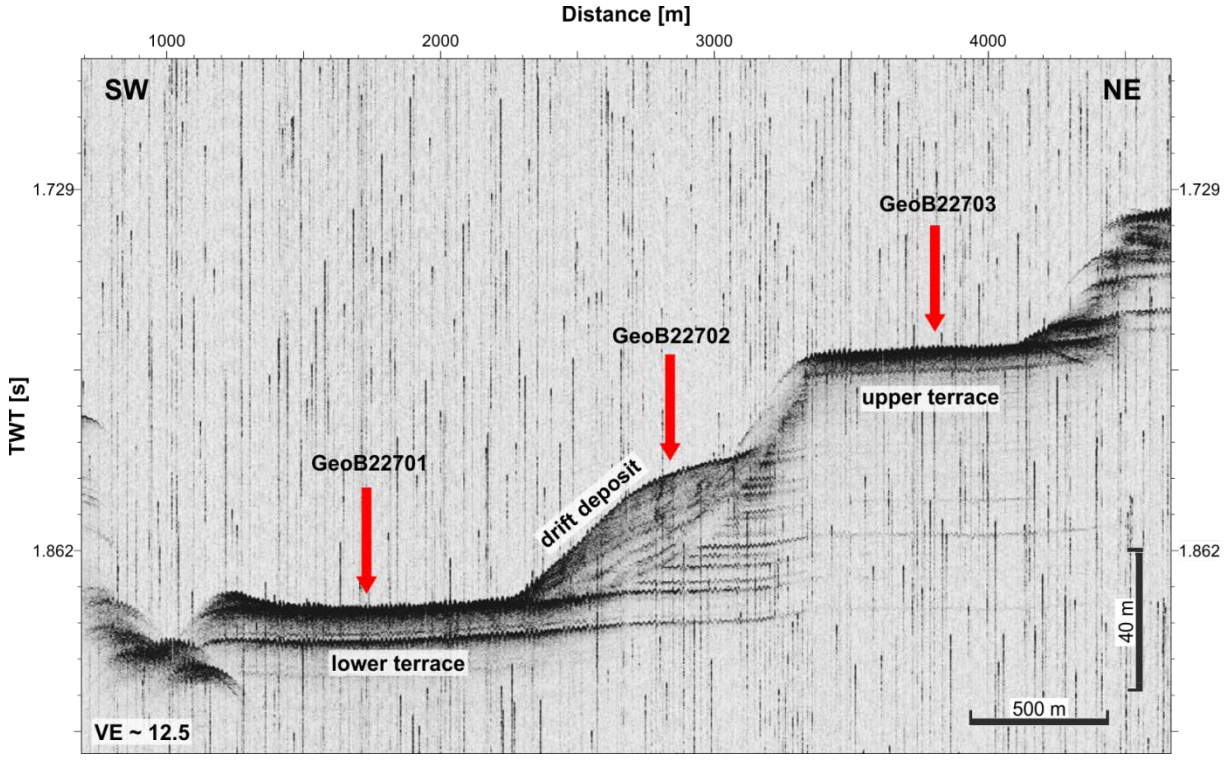

Fig. 5.1.2 PARASOUND profile (SLF, 4 kHz) crossing a local depression north of the Mar del Plata Canyon. A contouritic drift is imaged on the slope between two horizontal terraces. The positions of one CTD station (GeoB22701) and two coring sites are indicated with red arrows.

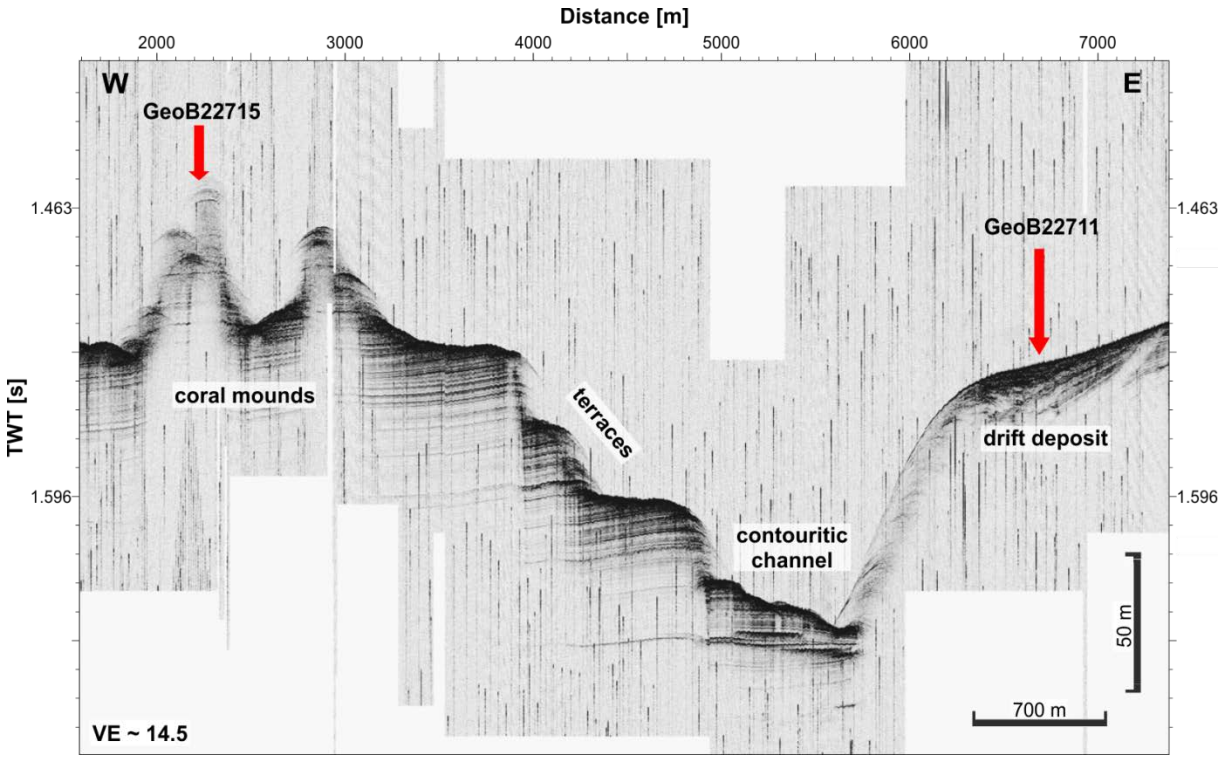

Fig. 5.1.3 PARASOUND profile (SLF, 4 kHz) crossing an N-S aligned contouritic channel associated with erosional surfaces at the western flank and drift deposits at the eastern side. The positions of two coring sites are indicated with red arrows.

The PARASOUND profile shown in Fig. 5.1.3 images an incision more than 100 m deep and approx. 2.5 km wide, which is interpreted as a contouritic channel. The profile shows at least four terraces separated by steep slopes of ~40 m height each at the western side of the channel. Further west, two prominent pinnacles of up to 30 m height are visible. Both features reveal several diffraction hyperbolae and almost no penetration of the acoustic signal. The structures are interpreted as deep water coral mounds which is consistent with findings in sedimentary samples recovered at station GeoB22715. In contrast to the coral mounds, the surrounding subseafloor shows distinct and continuous reflectors of medium to high amplitudes down to a depth of 50 mbsf. Comparable to the PARASOUND profile shown in Fig. 5.1.2, all reflectors west of the contouritic channel are truncated at the steep slopes in between the terraces. East of the channel, acoustic penetration is limited on the steep slope. The PARASOUND profile shows a lens-shaped deposit of divergent reflector patterns on top of the channel flank. This deposit is interpreted as a drift deposit related to the channel system.

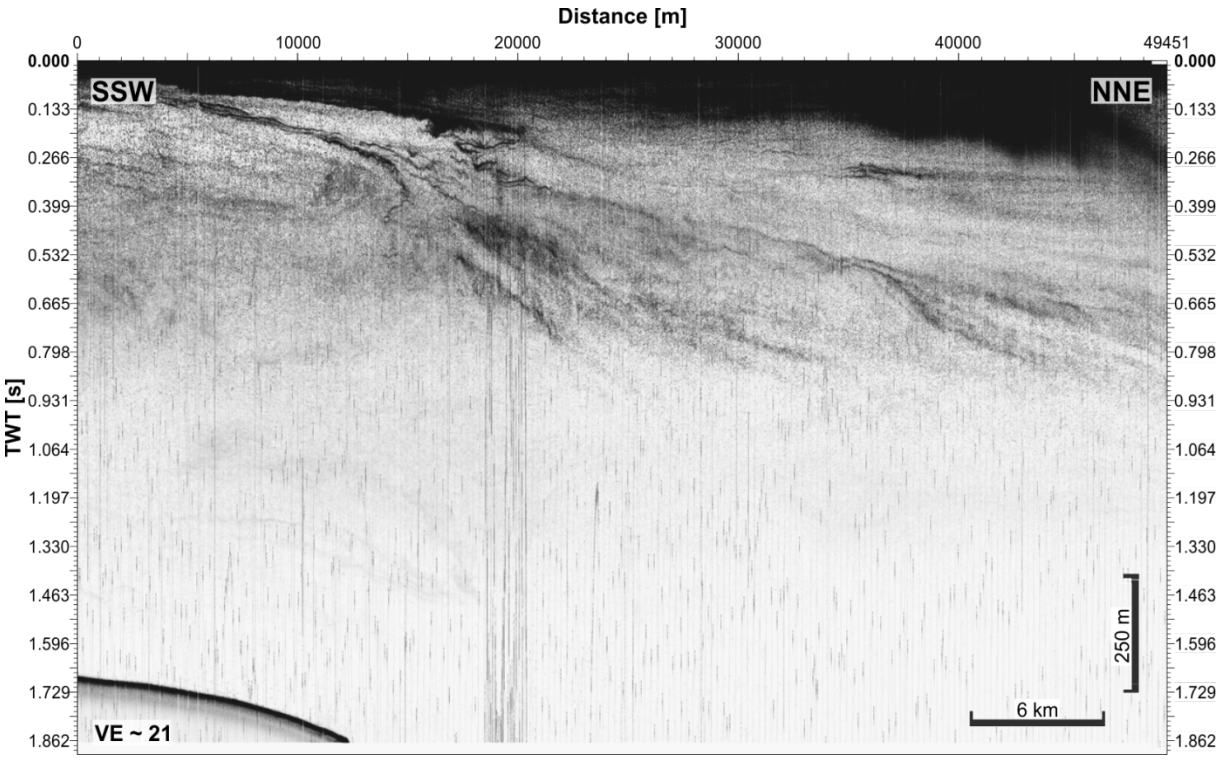

Fig. 5.1.4 PARASOUND profile (18 kHz; PHF) along a transect from Argentina to Uruguay images the water column across the Brazil-Malvinas Confluence zone.

In addition to mapping subseafloor structures, the water column was imaged using the primary high frequency (PHF, 18 kHz) signal of the PARASOUND echosounder. As example, Fig. 5.1.4 shows a 50 km long profile with two depth ranges of different backscatter intensities. Whereas the water column beneath a depth of 500 m is characterized by very low backscatter intensities, the upper water column is obviously more diverse. From SSW to NNE, the profile reveals an area of high backscatter intensity increasing in thickness from approx. 50 m up to 200 m below the sea surface. In the central part of the profile, there are elongated layers of high backscatter intensity inclined northwards. Those layers could be interpreted as the boundary of two different water masses varying both in temperature and salinity. In case of the study area, the overlaying water mass flowing southwards is designated as the Brazil Current, which converges with the northward flowing Malvinas Current in the so called Brazil-Malvinas Confluence zone.

5.2. High-Resolution Multichannel Seismics

(T. Schwenk, R. Brune, O. Ogunleye, V. Spiess, L. Steinmann, A. Thieblemont, F. Warnke, S. Wenau)

5.2.1. Introduction

During Leg 1 of cruise SO260, the multichannel seismic (MCS) equipment of the working group Marine Technology/Environmental Research from the Faculty of Geosciences, University of Bremen was utilized. In contrast to conventional seismic systems, this customized set-up allows for the acquisition of high-resolution MCS data imaging sedimentary structures on a meter scale. The main system components include a seismic source, a seismic streamer, a recording unit, a trigger unit, and the GPS/navigation system from the ship (Fig. 5.2.1).

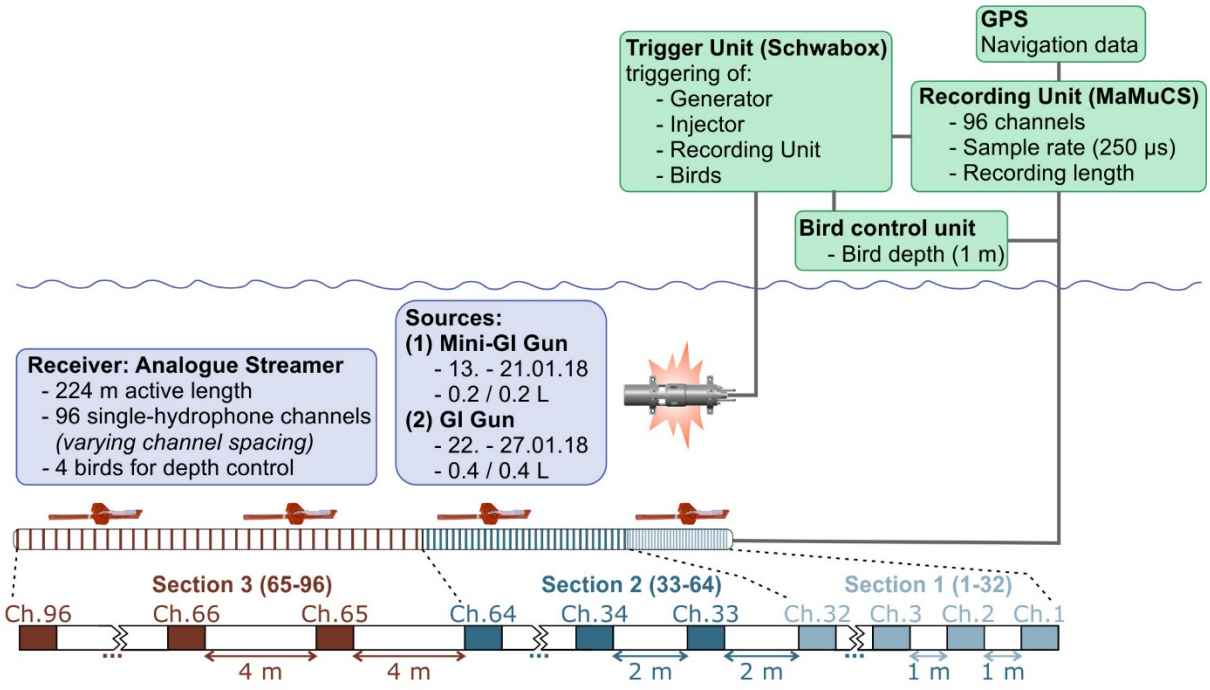

Fig. 5.2.1 Components and set-up of the MCS system during Leg SO260-1.

During the cruise, a total of 89 seismic profiles were acquired, with a total length of ~1200 km (Fig. 5.2.2). Altogether 6 deployments covered a time of 122 hours of seismic data acquisition, mixing objectives of larger scale imaging of sedimentary structures with site surveys for cores and MeBo drilling. The survey grids were designed to optimize the use of seismic, sediment echosounder and multibeam data for a better understanding of the processes acting on the northern Argentine margin within the contouritic depositional system.

5.2.2. System Components

As seismic sources, two GI Guns with different configurations were used during different surveys of the cruise. For the MCS surveys conducted between 13. and 21.01.2018 (Surveys 1-4, see Fig.

5.2.2 and profile list in attachment), a SERCEL Mini-GI Gun with 0.24 L generator and 0.24 L injector volume (frequency range of approximately 30 – 700 Hz) was operated in harmonic mode. The gun depth was controlled by a buoy above the hanger resulting in a towing depth of ~1 m. It was towed ~29 m behind the ship's stern. Its across-track position varied slightly during the different surveys as illustrated in the deckplans (Fig. 5.2.3). The gun was connected via an umbilical to the ship and shot at intervals of 4 to 6 seconds depending on the water depth, yielding shot spacing of ~10-15 m at a ship's speed of 5 to 5.5 knots. With this source, a signal penetration of ~1 s TWT was achieved. On 21.01.2018, the Mini-GI Gun was damaged beyond repair due to a lack of spare parts and, thus, was replaced by a SERCEL GI Gun for Surveys 5 and 6 with chamber volumes of 0.4 L for the generator and injector, respectively (frequency range of approximately 30 – 600 Hz). This gun was towed at a depth of 1.5 m on a steel cable, ~40 m behind the ship's stern (Fig. 5.2.3). Buoyancy was provided by a buoy attached to the steel cable and a tail of three small buoys that stabilize the gun in the water. The gun was shot at an interval of 4.5 seconds, yielding shot spacing of ~11 m at a ship's speed of 5 to 5.5 kn. With the 0.4 L GI gun, a signal penetration of more than 1 s TWT could be achieved at, however, lower resolution than with the Mini-GI.

A custom-designed analog TELEDYNE streamer characterized by a broad bandwidth of 3 – 1000 Hz was deployed at the port side behind the ship's stern (Figs. 5.2.1 and 5.2.3). The streamer comprises 96 single-hydrophone channels divided into four sections with varying channel spacing: channels 1 – 32 (section 1) have a spacing of 1 m, channels 33 – 64 (section 2) have a spacing of 2 m, and channels 65 – 96 (sections 3 and 4) have a spacing of 4 m (Fig. 5.2.1). In front of the active streamer, which has an overall length of 224 m, a 10 m stretch is attached to partially decouple the streamer from the ship's movements. The stretch is connected via the lead-in and deck's cable to the seismic lab. To stabilize the streamers position in the water column, a buoy was attached to the streamer's end with a ~20 m of rope.

For depth control of the streamer, 4 so-called birds (Digicourse Inc., Model 7010) were attached to the streamer (Fig. 5.2.1). The bird positions were as follows: at the stretch, at the end of the first active section, at the start of the third section and at the end of the streamer. During seismic acquisition using the Mini GI-Gun, the birds were set to 1 m depth in order to optimize the data acquisition for high-frequency content. The birds were controlled through the Digi-Bird Control PC where they were accessed via induction coils included in the streamer at the Bird positions. This allowed a real-time monitoring of the streamer position in the water.

Data were recorded with the custom-designed MaMuCS-System (Marine Multi Channel Seismic Acquisition System), which was developed at the University of Bremen. It consists of an Intel i7 based PC (32GB RAM, Windows 7) with three NI6052E 16bit AD-converters. Each ADC is connected to a 32-channel multiplexer (NI-SCXI1102-C) with onboard pre-amplification and anti-alias filter. The system digitizes a maximum of 96 channels at a maximum sampling rate of 10 kHz per channel. The acquisition software provides nearly continuous recording of the 96 channels with data storage in demultiplexed SEG-Y format (floating-point IEEE) to hard disk. The software allows online quality control by displaying shot gathers and an online profile plot using brute stacks of selected channels. The MaMuCS-PC is also used for logging the ship's GPS data, which is distributed via another PC in the lab over the network. Seismic data acquisition parameters generally included a sample rate of 0.25 ms and recording lengths between 3 and 6 s depending on the water depth, to cover the full water column.

A crucial part of the multichannel seismic data acquisition is the accurate triggering of seismic sources and recording instruments (Fig. 5.2.1). For this purpose a custom-built 6-channel trigger module was used (Schwabox, A. Schwab) which includes a custom software that allows the design of different trigger schemes. The GI-Guns were triggered with a delay of 30 ms between the generator and injector chambers. Two trigger amplifiers provided the necessary voltage for the solenoid valves of the gun. MaMuCS was triggered with the seismic source simultaneously. After the recording of the seismic signal with MaMuCS (max. 6 s), the birds were triggered, allowing a communication with them by the Digi-Bird PC through the streamer.

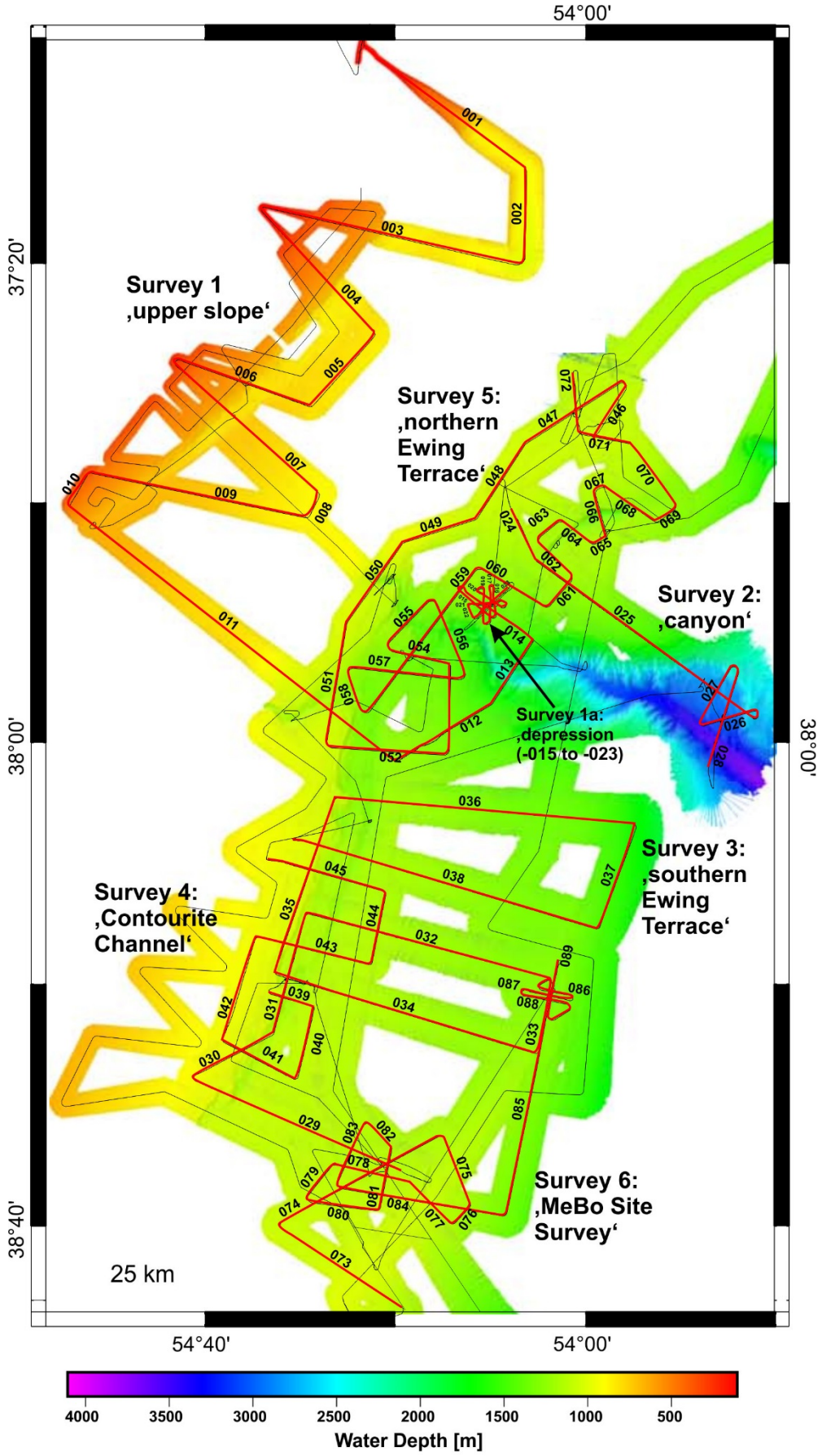

Fig. 5.2.2 Map of seismic surveys performed during Leg SO260-1.

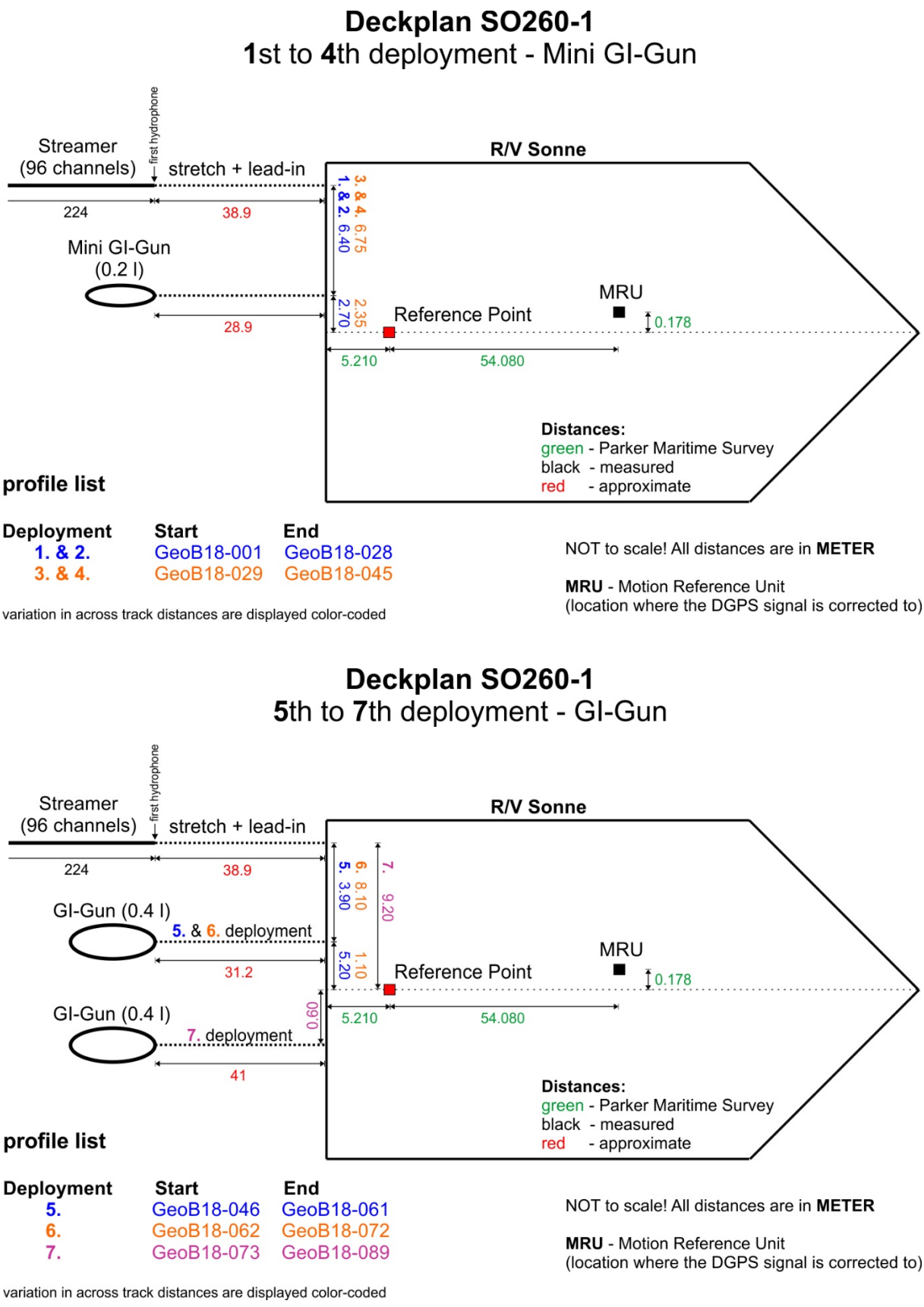

Fig. 5.2.3 Deckplans showing the different towing configurations of the seismic equipment deployed during Leg SO260-1.

5.2.3. Preliminary Shipboard Results

The seismic work is separated into five different surveys. The first seismic survey along the 'upper slope' started on January, 13th around 14:00 UTC and finished on January 15th at 06:50 UTC in the upper part of the Mar del Plata submarine canyon. Data were collected on 23 Profiles with a total length of ~388 km (GeoB18-001 through -023) (Fig. 5.2.2). The survey was shortly interrupted during Line GeoB18-012 due to a metal part of the gun was broken, because a connection between buoy and gun hanger had failed. Profile GeoB18-007 was shot during Survey 1 perpendicular to the upper slope across a contourite channel (Fig. 5.2.4), which seems to deepen northward, but is absent to the South (see also Fig. 5.1.1). It reveals the slope architecture in this area with respect to the distance of the shelf break. The profile highlights the so-called La Plata Terrace with reflectors showing toplap terminations at the seafloor on its landward position and a contouritic moat, which reaches a width of up to 1 km and depth of 0,1s TWT on its seaward position. The NNW-flank of the moat is characterized by a steep erosive slope. On its SSE flank, sediments are characterized by parallel continuous reflectors separated by erosive surfaces. Several contourite drifts were identified through the sedimentary record demonstrating the impact of bottom currents on the shape of the margin here.

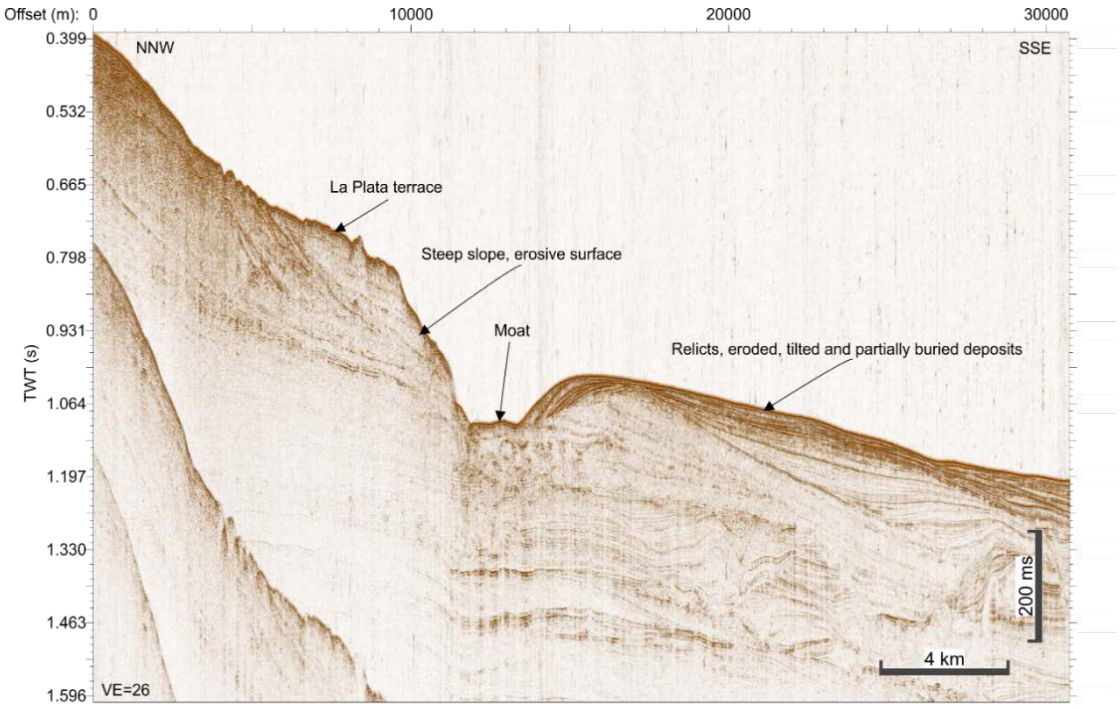

Fig. 5.2.4 Brute stack of seismic data from Profile GeoB18-007 crossing the upper slope from NNW to SSE.

The second (night) survey ("Canyon") of 5 profiles with a total length of ~90 km (GeoB18-024 to -028; Fig. 5.2.2) started on the Ewing terrace on January 15th at 22:59 UTC and finished on January 16th at 06:56 UTC on the northern flank of the Mar del Plata submarine canyon. During the third survey the "southern Ewing Terrace" was surveyed between January 18th 12:49 UTC and January 19th 16:05 UTC, targeting to gain a first overview. Data were collected on 10 Profiles with a total length of ~300 km (GeoB18-029 to -038) (Fig. 5.2.2).

The fourth survey was designed to collect more information around the location of the third survey where coral mounds had been sampled and identified in echosounder data (Fig. 5.1.3). Acquisition started at the 20.01.2018 at around 23:01 UTC to stop the 21.01.2018 at 07:03 UTC due to a shooting rate problem with the Mini GI-Gun. Data were collected on 7 Profiles with a total length of ~94 km (GeoB18-039 to -045) (Fig. 5.2.2). Profile GeoB18-041 (Fig. 5.2.5) was shot perpendicular to the slope, the seismic data show thick sediments packages separated by unconformities overlying a more chaotic and transparent package between 1.729 and 1.789 s TWT. The upper NW part of the profile above ~1,330 s TWT shows high amplitude chaotic reflections interpreted as coral mounds. As visible in the profile, these coral mounds are located along the steepest NW side of a contouritic moat, and absent on the eastern drift.

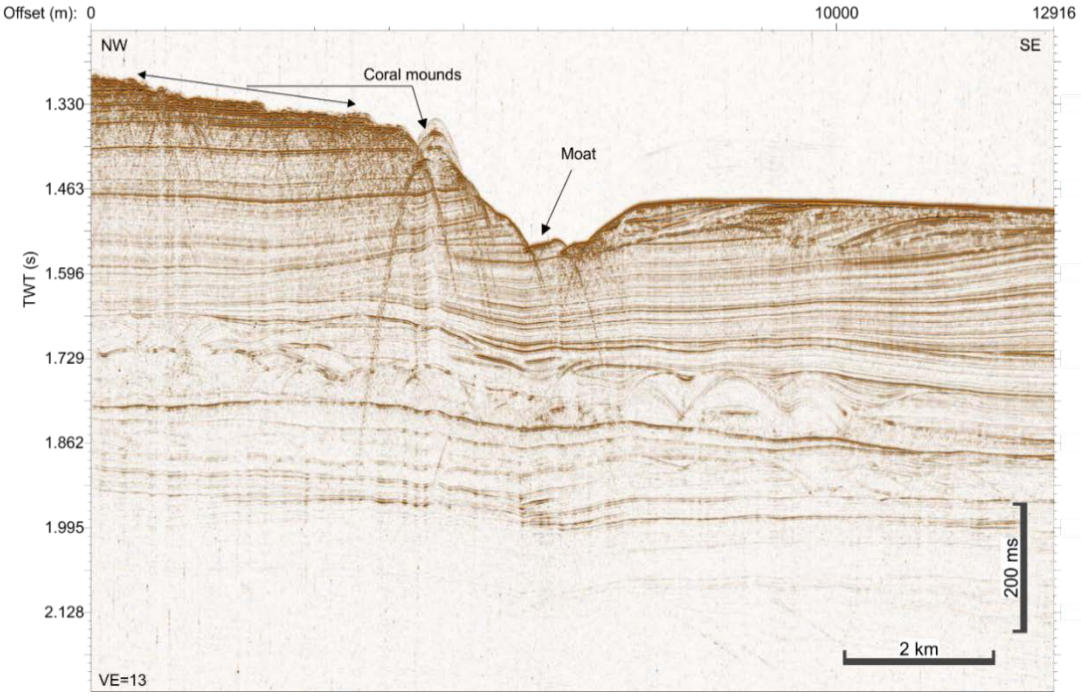

Fig. 5.2.5 Brute stack of seismic data collected on Profile GeoB18-041 crossing coral mounds.

The fifth survey started on January 22nd at 20:37 UTC, finished on January 24th at 00:49 UTC, and was dedicated to the northern Ewing Terrace. Data were collected on 27 Profiles with a total length of ~310 km (GeoB18-046 to -072) (Fig. 5.2.2). Here, a larger GI-Gun was deployed (volume of 0,4l instead of 0,2l) and bad weather conditions have led to a change of the GI-Gun position relative to the streamer cable (see Fig. 5.2.3). Seismic Profile GeoB18-047 (Fig. 5.2.6) was collected along a filled depression on the northern Ewing terrace. High amplitude reflectors (bright spots) can be recognized at depth, suggesting that the sediments may have trapped gas hydrate/free gas in this area. The profile highlights the infilling of the depression (interpreted as a contourite channel) by packages of sub-parallel medium to low amplitude reflectors which are thinning toward its edges.

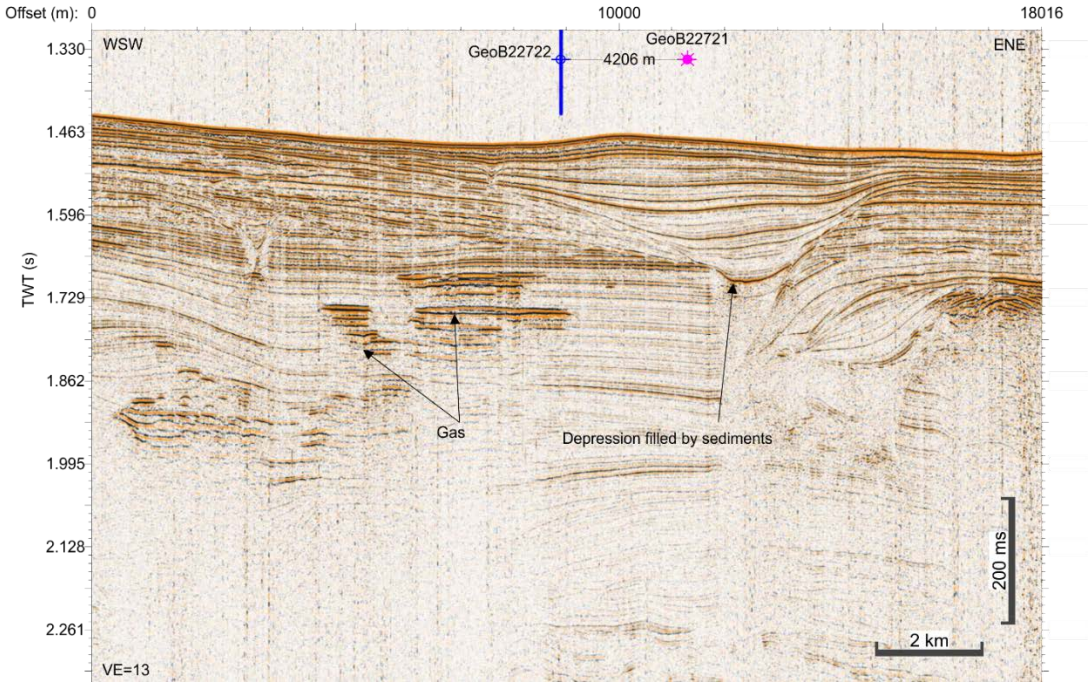

Fig. 5.2.6 Brute stack of seismic data collected on Profile GeoB18-047 along the Ewing terrace.

The last survey was a dedicated MeBo Site Survey along the southern part of the Ewing Terrace in the study area. The survey started on January 26th at 10:45 UTC and finished on January 27th at 08:46 UTC. Data were collected on 17 Profiles with a total length of ~235 km (GeoB18-073 to -089) (Fig. 5.2.2). Towing configuration for this survey was changed again (Fig. 5.2.3).

5.3. Sediment Sampling

(T.J.J. Hanebuth, H. Lantzsch, G. Bozzano, J. Bösche, J.H. Long, J.T. Durica, N. Chapori, C.M. Chiessi, S. Crivellari, K. Dehning, D. Hüttich, M. Klann, B. Kockisch, G. Warratz)

5.3.1 Introduction

We targeted various environmental settings which were often located in close proximity to each other. The current-dominated continental slope off Uruguay and northern Argentina consists of several contourite terraces, which are mainly sandy with various portions of mud, erosional features such as channels and depressions, and biogenous coral mounds. We accordingly used a variety of sediment sampling tools: Multicorer (*Multilot*), Giant Box Corer (*Großkastengreifer*), and Grab Sampler (*Backengreifer*) for sampling the uppermost seabed sediment, as well as Gravity Corer (*Schwerelot*) and the sea floor drill rig MeBo (*Meeresboden-Bohrgerät*) for deeper penetration.

In total, we cored at 19 stations during the 1st Leg and at 22 stations during the 2nd Leg. The latter included 3 MeBo sites. We recovered 151 m of sediment with gravity coring, while 81 m were drilled with MeBo. The individual systems and first shipboard results are summarized in the following.

5.3.2 Sampling Tools and Methods

Multicorer

The Multicorer (MUC) was used to retrieve undisturbed near-surface sediment, with up to 50 cm core length, the sediment-water interface, and superstitious bottom-water samples. The samples were taken in a set of twelve 60-cm long plastic tubes with a diameter of 10 cm. After retrieval, overlying water and sediment were sampled (Fig. 5.3.1). The MUC was deployed at 13 stations (Table 5.3.1).

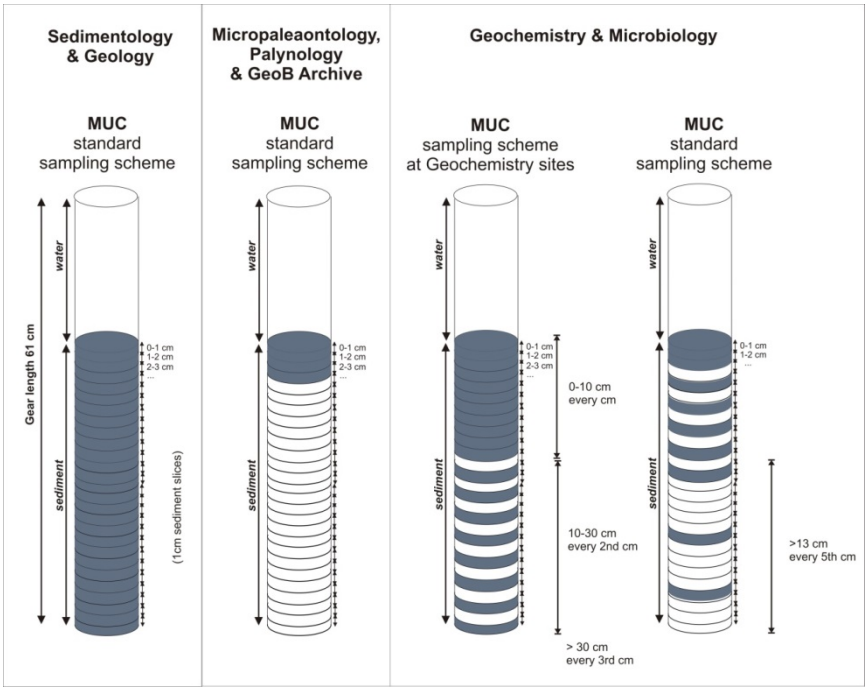

Fig. 5.3.1 Sampling schemes of MUC cores.

Table 5.3.1 List of Multicorer stations.

GeoB #	Ship #	Gear	Date	Time (UTC)	Latitude	Longitude	Water depth (m)	Recovery (cm)	REMARKS
GeoB22739-2	SO260/2-47-1 MeBo	MeBo	11.02.18	20:00:00	38°35.559´S	54°22.796´W	1112	536,5	
GeoB22702-2	SO260/1 3-2 MUC	MUC	15.01.18	15:09:00	37°48.563´S	54°10.214´W	1355	26	
GeoB22706-1	SO260/1_8-2	MUC	16.01.18	14:24:00	37°57.028´S	53°45.807´W	3006	357	
GeoB22707-2	SO260/1_9-2 MUC	MUC	16.01.18	21:50:00	37°54.829´S	53°47.716´W	2761	240	
GeoB22708-3	SO260/1-10-3 MUC	MUC	17.01.18	16:20:00	39°18.700´S	53°57.167´W	3677	296	
GeoB22711-1	SO260/1_14-1 MUC	MUC	20.01.18	00:17:00	38°20.037´S	54°28.950´W	1127	308	
GeoB22713-1	SO260/1-16-1	MUC	20.01.18	10:39:00	38°35.328´S	54°21.079´W	1115	228,5	
GeoB22721-1	SO260/1_25-1 MUC	MUC	22.01.18	16:46:00	37°33.318´S	53°58.710´W	1060	324	
GeoB22722-3	SO260/1_27-3	MUC	21.01.18	09:50:00	37°32.392´S	54° 1.342´W	1076	333	
GeoB22723-2	SO260/1_28-2 MUC	MUC	25.01.18	23:30:00	37°42.230´S	53°57.505´W	1168	316,5	
GeoB22725-1	SO260/1_31-1 MUC	MUC	27.01.18	10:56:00	38°20.536´S	54° 3.862´W	1343	289	
GeoB22734-1	SO260/2-40-1 MUC	MUC	03.02.18	09:07:00	36° 8.488´S	53°17.163´W	242	352	
GeoB22735-2	SO260/2-41-2-MUC	MUC	03.02.18	16:46:00	36° 7.668´S	52°49.898´W	1381	432	

Giant Box Corer

In areas where a coarse-grained sediment surface was expected, the Giant Box Corer (GBC) was used. The Giant Box Corer was deployed at 10 stations (Table 5.3.2). The superstitious water was carefully removed with a hose, and the sediment surface was photographically documented, visually described and sampled for various purposes (Fig. 5.3.2). One 12-cm diameter core tube for sedimentology and one 10-cm diameter core tube for geochemistry (only on stations without MUC deployment) were vertically pushed into the sediment. Afterwards, the GBC front side was opened and the downward profile was documented through photography and description.

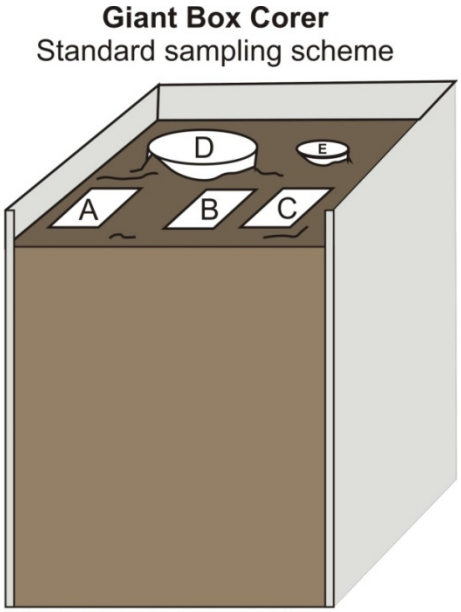

Fig. 5.3.2 Standard sampling scheme of GBC sampling including 3 surface samples and 1-2 core tubes.

Table 5.3.2 List of Giant Box Corer stations.

GeoB #	Ship #	Gear	Date	Time (UTC)	Latitude	Longitude	Water depth (m)	Recovery (cm)	REMARKS
GeoB22701-2	SO260/1_2-2 GKG	GBC	15.01.18	11:52:00	37°48.902´S	54°10.691´W	1400	1	nearly empty
GeoB22702-1	SO260/1_3-1 GKG	GBC	15.01.18	13:47:00	37°48.560´S	54°10.215´W	1349	221	
GeoB22703-1	SO260/1_4-1GKG	GBC	15.01.18	18:16:00	37°48.252´S	54° 9.805´W	1320	25	
GeoB22704-1	SO260/1_5_1 GKG	GBC	15.01.18	21:30:00	37°38.630´S	54° 8.492´W	1041	154	
GeoB22712-3	SO260/1_15-3 GKG	GBC	21.01.18	17:55:00	38°19.953´S	54°29.665´W	1214	5	GBC 200 m behind the vessel due to currents. Sample site 25 m NW of coordinates. Recovery 3kg
GeoB22715-1	SO260/1-18-1 GKG	GBC	20.01.18	19:50:00	38°19.499´S	54°31.696´W	1101	80	strong bottom currents, sample location 20 m north of the coordinates (Posidonia)
GeoB22716-1	SO260/1-20-1	GBC	21.01.18	12:46:00	38° 6.412´S	54°22.882´W	1287	1	Posidonia 38° 6.329 S / 54° 22.803 W
GeoB22726-1	SO260/1_32-1	GBC	27.01.18	16:42:00	38°43.139´S	54°22.337´W	1019	10	no recovery, box deformed
GeoB22735-4	SO260/2-41-4	GBC	07.02.18	16:29:00	36° 7.630´S	52°49.892´W	1392	0	no bottom contact: stopped due to strong drift of GBC (currents)
GeoB22744-2	SO260/2-52-1 GKG	GBC	12.02.18	20:31:00	38°18.253´S	54°32.374´W	992	33	

Grab Sampler

The Grab Sampler (GS) is a robust and simple sampling device for coarse-grained or stone-rich sediment surfaces. The GS was applied at 13 stations (Table 5.3.3). The recovered sediment was photographed and described. Up to 3 bulk samples were taken.

Table 5.3.3 List of Grab Sampler Stations

GeoB #	Ship #	Gear	Date	Time (UTC)	Latitude	Longitude	Water depth (m)	Recovery (cm)	REMARKS
GeoB22717-1	SO260/1_21-1	GS	21.01.18	16:16:00	37°58.047´S	54°31.007´W	1165	9	Posidonia location: 38°6.329S and 54°22.803W; stones
GeoB22718-1	So260/1-22-1 Grab	GS	21.01.18	20:53:00	37°52.846´S	54°18.263´W	1411	9	Posidonia
GeoB22720-1	So260/1-24-1 Grab	GS	22.01.18	10:26:00	37°43.309´S	54° 3.063´W	1273	9	Posidonia
GeoB22726-2	So260/1_32-2 Grab	GS	27.01.18	18:11:00	38°43.121´S	54°22.326´W	1019	10	
GeoB22727-1	SO260/1_33-1 Grab	GS	27.01.18	21:25:00	38°41.440´S	54°23.485´W	1044	10	
GeoB22728-3	SO260/1_34-3 Grab	GS	28.01.18	16:48:00	37°46.603´S	54°21.047´W	1255	5	
GeoB22730-1	SO260/1-36 Grab	GS	29.01.18		37°41.686´S	54°51.961´W	647	10	
GeoB22731-1	SO260/1-37-1 Grab	GS	29.01.18	08:41:00	37°38.437´S	54°45.998´W	706	10	
GeoB22732-1	SO260/1-38-1 Grab	GS	29.01.18	10:48:00	37°32.578´S	54°37.244´W	799	10	
GeoB22733-1	SO260/1-39-1 Grab	GS	29.01.18	12:39:00	37°30.113´S	54°35.788´W	636	10	
GeoB22736-1	SO260/2-44-1 Grab	GS	06.02.18	19:24:00	37°20.007´S	53°59.336´W	1110	15	Sandstone fragment with sessile fauna
GeoB22737-1	SO260/2-45-1 Grab	GS	06.02.18	20:57:00	37°20.162´S	53°59.444´W	1118	0	no bottom contact
GeoB22738-1	So260/2-46-1 Grab	GS	06.02.18	22:47:00	37°19.942´S	53°58.390´W	1117	30	1 bulk sample

Gravity Corer

Sediment gravity cores were recovered at 33 stations using a Gravity Corer (GC) with site-specific corer lengths of 3, 6, 12, and 15 m (Table 5.3.4). The top weight of the corer was 1.5 tons. After retrieval, the core liners were cut into 1-m long sections, closed with caps and labeled according to the general GeoB labeling scheme. Afterwards the cores were split into two halves: a *Work* and an *Archive* half. Most of the cores were opened onboard except for cores taken at coral mounds and cores reserved for incubation experiments.

Table 5.3.4 List of Gravity Corer stations.

GeoB #	Ship #	Gear	Date	Time (UTC)	Latitude	Longitude	Water depth (m)	Recovery (cm)	REMARKS
GeoB22702-3	SO260/1_3-3 GC	GC	15.01.18	16:30:00	37°48.567´S	54°10.211´W	1355	902	
GeoB22704-2	So260/1-5-2GC	GC	22.01.18	13:21:00	37°38.631´S	54° 8.493´W	1040	59	
GeoB22704-3	So260/1-5-3GC	GC	22.01.18	14:39:00	37°38.635´S	54° 8.484´W	1038	105	bent core barrel
GeoB22706-2	SO260/1_8-3 GC	GC	16.01.18	16:49:00	37°58.035´S	53°45.789´W	3011	935	
GeoB22707-1	SO260/1_9-1 GC	GC	16.01.18	20:00:00	37°54.829´S	53°47.722´W	2762	840	
GeoB22708-1	SO260/1_10-1 GC	GC	17.01.18	10:25:00	39°18.701´S	53°57.153´W	3690	976	
GeoB22708-2	SO260/1-10-2 GC	GC	17.01.18	13:31:00	39°18.702´S	53°57.165´W	3679	960	
GeoB22709-1	SO260/1-11-1 GC	GC	17.01.18	19:24:00	39°18.064´S	53°58.030´W	3611	932	
GeoB22709-2	SO260/1-11-2 GC	GC	17.01.18	22:12:00	39°18.060´S	53°58.023´W	3615	964	
GeoB22711-2	SO260/1_14_2 GC	GC	20.01.18	00:55:00	38°20.030´S	54°28.969´W	1130	0	
GeoB22711-3	SO260/1_14-3 GC	GC	20.01.18	16:12:00	38°20.032´S	54°28.956´W	1129	0	no recovery
GeoB22713-2	SO260/1-17-1 GC	GC	20.01.18	11:45:00	38°35.320´S	54°21.081´W	1115	561	
GeoB22714-1	SO260/1_18-1 GC	GC	20.01.18	13:24:00	38°37.775´S	54°22.717´W	1111	357	
GeoB22715-2	SO260/1_18-2 GC	GC	20.01.18	21:31:00	38°19.477´S	54°31.645´W	1105	554	strong bottom currents (Posidonia); not opened on board; contains coral fragments
GeoB22721-2	So260/1-25-2 GC	GC	22.01.18	18:16:00	37°33.313´S	53°58.723´W	1060	777	
GeoB22722-4	So260/1-27-4 GC	GC	24.01.18	11:48:00	37°32.400´S	54° 1.332´W	1077	571	overpenetrated; not opened on board; no coral fragments
GeoB22722-5	So260/1-27-5 GC	GC	24.01.18	13:25:00	37°32.399´S	54° 1.377´W	1073	901	
GeoB22723-1	SO260/1_28-1GC	GC	24.01.18	17:15:00	37°42.224´S	53°57.508´W	1167	490	bent core barrel
GeoB22723-3	SO260/1_28-3 GC	GC	26.01.18	00:28:00	37°42.221´S	53°57.497´W	1168	431	
GeoB22725-2	SO260/1-31-1 GC	GC	27.01.18	12:38:00	38°20.541´S	54° 3.864´W	1345	160	
GeoB22726-3	SO260/1_32-3 GC	GC	27.01.18	19:26:00	38°43.123´S	54°22.333´W	1021	1	bent core barrel - small bag sample
GeoB22729-1	So260/1_35-1 GC	GC	28.01.18	18:43:00	37°48.445´S	54°20.113´W	1202	183	not opened on board; contains coral fragments
GeoB22733-2	SO260/1-39-2 GC	GC	29.01.18	13:42:00	37°30.120´S	54°35.793´W	635	47	not opened on board; contains coral fragments
GeoB22733-3	SO260/1-39-3 GC	GC	29.01.18	14:33:00	37°30.119´S	54°35.793´W	635	18	not opened on board; contains coral fragments
GeoB22734-2	SO260/2-40-2 GC	GC	03.02.18	09:38:00	36° 8.483´S	53°17.160´W	240	854	
GeoB22734-3	SO260/2-40-3 GC	GC	03.02.18	10:50:00	36° 8.489´S	53°17.149´W	240	718	
GeoB22735-1	SO260/2-41-1 GC	GC	03.02.18	15:23:00	36° 7.662´S	52°49.899´W	1384	899	
GeoB22740-1	SO260/2-48-1 GC	GC	10.02.18	15:11:00	38°36.577´S	54°20.105´W	1102	162	Posidonia; bent core
GeoB22740-2	SO260/2-48-2 GC	GC	10.02.18	21:45:00	38°36.573´S	54°20.086´W	1102	0	no recovery
GeoB22741-1	SO260/2-49-1 GC	GC	10.02.18	17:06:00	38°38.216´S	54°18.674´W	1072	241	Posidonia
GeoB22742-1	So260/2-50-1 GC	GC	10.02.18	18:57:00	38°39.368´S	54°17.692´W	1054	0	Posidonia; no recovery
GeoB22743-1	So260/2-51-1 GC	GC	10.02.18	23:25:00	38°35.302´S	54°23.995´W	1108	0	no recovery
GeoB22744-1	SO260/2-52-1 GC	GC	12.02.18	19:03:00	38°18.254´S	54°32.363´W	992	507	Posidonia; not opened on board; contains coral fragments

The *Archive* halves of gravity cores were described on standard description sheets. Visual core description focused on color, grain size, lithology, composition, physical, biogenic, and diagenetic structures. Afterwards, the descriptions were drafted into condensed graphic core logs (see Fig. 5.3.3 for an example). These logs are presented in Appendix 2. The core logs are simplified from the original description and are presented on a uniform scale with one core per page.

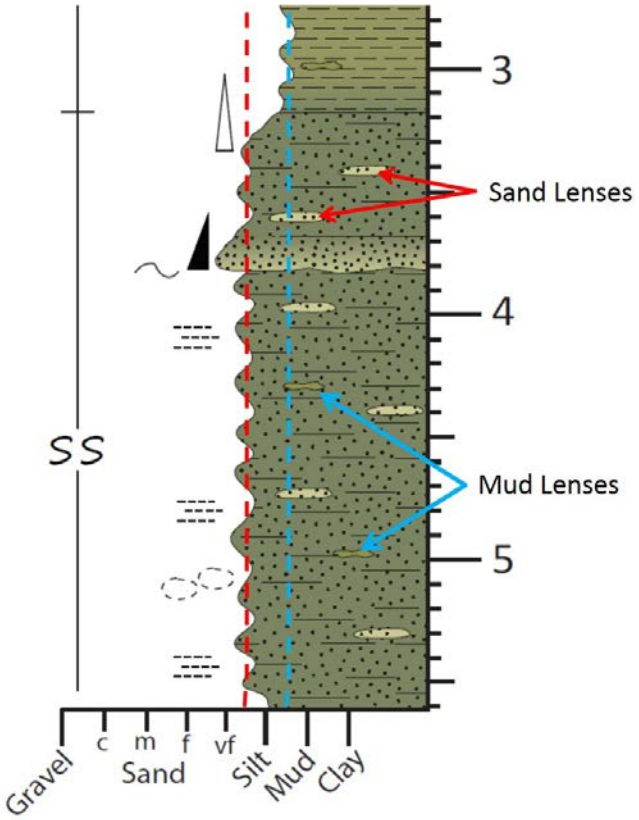

Fig. 5.3.3 Example of a core log taken from the base of core GeoB22713-02. This section of core contains two primary units; a muddy silt unit overlies a silty sand unit with a gradational contact (indicated by the white triangle) between the two at 320 cm. The silty sand unit contains a lower section that is generally a homogeneous mixture of very fine-grained sand, silt, and mud but also contains a very fine-grained, sharp-based sand that begins at 380 cm which fines upwards (as indicated by the black triangle). The estimated mean grain sizes of the mud-rich unit (muddy silt) and the sand-rich unit (silty sand) are indicated by the blue and red dashed vertical lines respectively. The irregular left edges of the column are used to show that there is variability in grain size throughout. The regularly spaced inclusions of both mud and sand lenses are used to indicate that these features occur throughout but are not intended to show the specific locations of these small-scale features. However, within many of these cores there are either muddier or sandier zones that have no discernible contacts. For these zones these lenses are used to indicate concentrations of these lithologies. Core GeoB22702-03, for example, has sandier zones at 200 and 270 cm. On the core log, numerous sand lenses aligned at these depths indicate the increase in sand content.

In order to gain a better understanding of the mechanism of sedimentation processes, radiograph slabs of 25 cm length were taken from selected *Archive halves* (Fig. 5.3.4, GeoB22706-2). Other samples were always taken from the *Work halves*. For geochemical, microbiological and geophysical (magnetic) purposes, selected cores were sampled every 40 cm and at biogeochemistry sites in 20 cm intervals (Fig. 5.3.4). Further organic geochemistry samples were taken target-specific according to facies changes based on the core description (Fig. 5.3.4). Samples for dating purposes were taken at the top, the middle and the base of most gravity cores (Fig. 5.3.4).

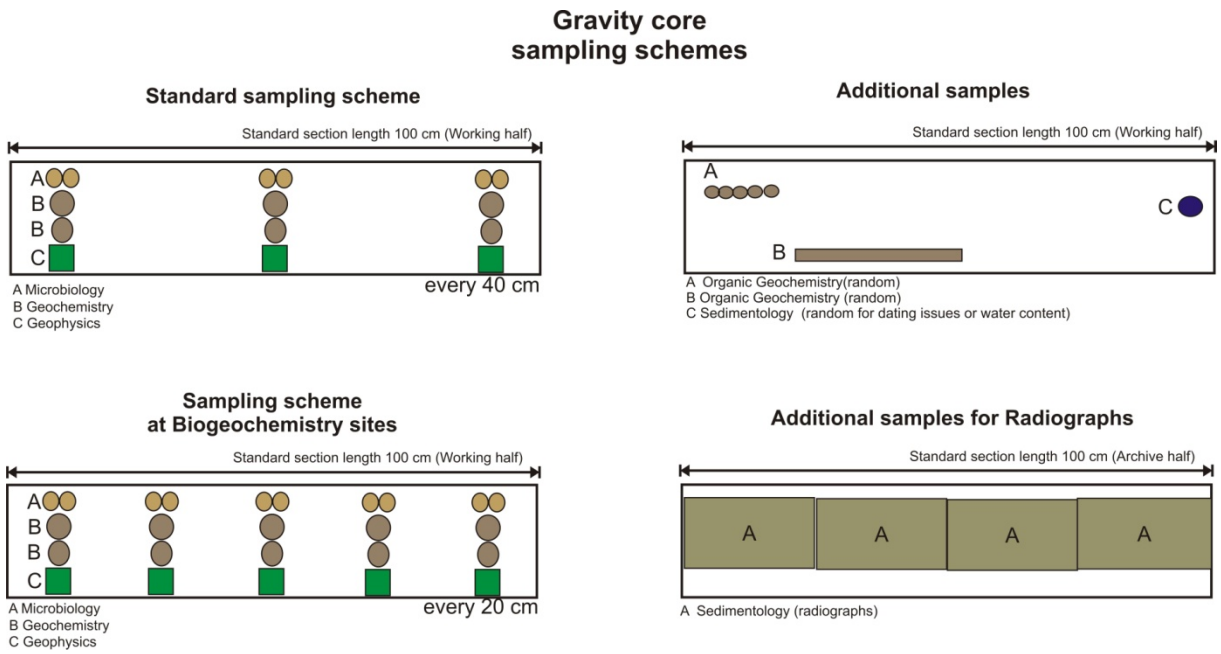

Fig. 5.3.4 Gravity core sampling schemes of the participating research groups.

Sea floor drill rig MeBo70

(M. Bergenthal, J. Bülten, R. Düßmann, S. Klar, T. Klein, E. Linowski, R. Rehage, U. Rosiak, W. Schmidt)

The sea floor drill rig MARUM-MeBo70 (Fig. 5.3.5) was used for retrieving long sediment cores. This device is a robotic drill that is deployed on the seabed and remotely controlled from the vessel (Fig. 5.3.6). The complete MeBo system, including drill, winch, launch and recovery systems, control unit, workshop, and spare drill tools is shipped in six 20' containers. A steel armored umbilical with a diameter of 32 mm is used to lower the 10-ton device to the seabed where four legs are being armed out in order to increase the stability of the rig. Copper wires and fiber optic cables inside the umbilical supply energy from the vessel and allow for the communication between MeBo and the control unit on deck. The maximum deployment water depth was 2000 m.

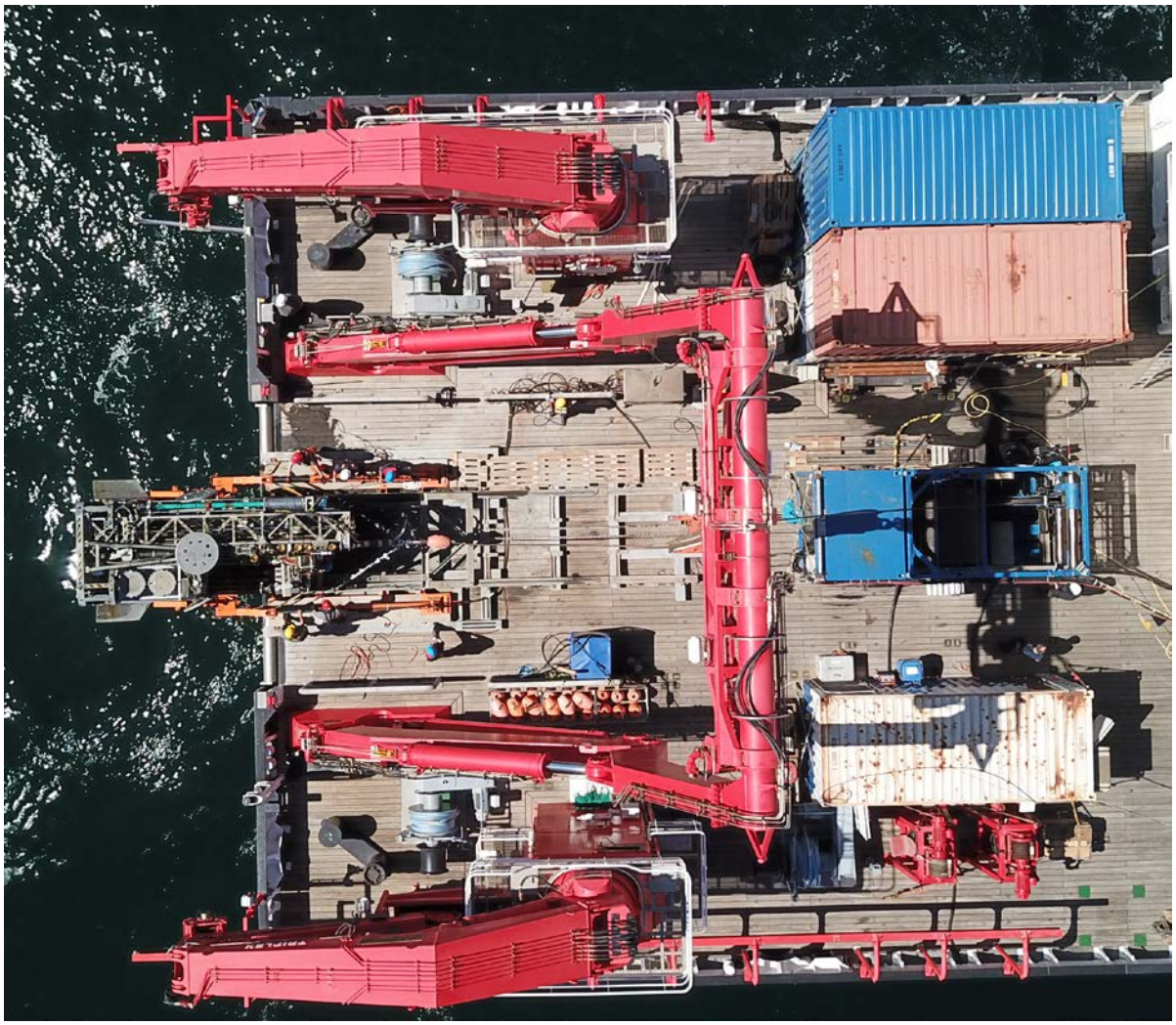

Fig. 5.3.5 Sea floor drill rig MARUM-MeBo70 on board RV SONNE during expedition SO260-2.

The mast with the feeding system forms the central part of the drill rig (Fig. 5.3.6). The drill head provides the required torque and rotary speed for rock drilling and is mounted on a guiding carriage that moves up and down the mast with a maximum push force of 4 tons. A water pump flushes the

drill string with seawater for cooling the drill bit and removing the drill cuttings. Core barrels and rods are stored in two magazines on the drill rig. We used wire-line core barrels (HQ) and hard metal drill bits with 55 mm (push coring) and 63 mm (rotary drilling) core diameters. The stroke length was 2.5 m (steel rods). With complete loading of the magazines a maximum coring depth of 70 m can be achieved. Station time may last longer than 24 hours per deployment.

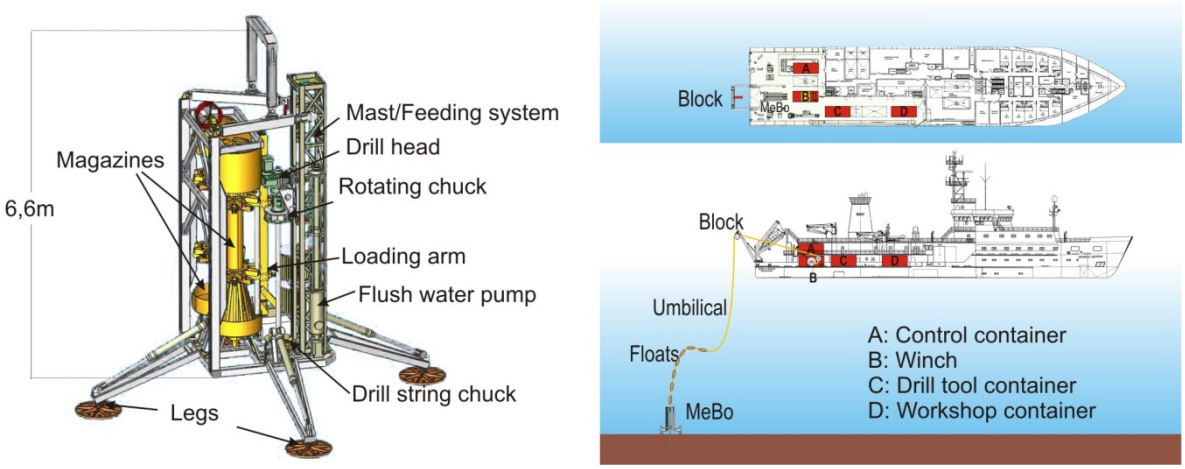

Fig. 5.3.6 Schematic overview on the MeBo drill rig (left) and its deployment from a research vessel (right).

During the cruise the MeBo was deployed five times at three sites to retrieve long cores. In total, MeBo drilled for 80 hrs and 131 m of sediment were drilled. During the first two deployments the drill string was flushed through the upper meters since interest was only in sediments below the penetration depth of the gravity corer at these sites. 125 m were cored in total with 81 m recovery and an average recovery rate of 65 %. Detailed information on deployment of MeBo and recovery of sediments is summarized in the station list (Table 5.3.5).

Table 5.3.5 Station list for MeBo deployments.

Station GeoB No. Drill #	Drilling duration [hrs:min]	Latitude [S]	Longitude [W]	Water depth (m)	Drill depth (cm)	Cored length (cm)	Recovery (cm)	Remarks
22722-6 152	3:10	37°32.407’	54°01.339'	1076	540	260	80 31 %	Rotating Chuck failure
22722-7 153	17:02	37°32,398'	54°01,336'	1076	3280	3010	1527 50 %	Wireline failure
22735-5 154	35:49	36°07,665‘	52°49.898'	1388	7020	7020	5979 85 %	Target depth reached
22739-1 155	0:37	38°'35.511’	54°22.776’	1114	220	220	0 0 %	Core was washed out during recovery
22739-2 156	22:55	38°35.506’	54°22.778’	1112	2040	2010	536,5 27 %	
Total	79:33				13100	12520	8122,5 65 %	

Core Line Scanner Imaging

(J. Bösche, B. Kockisch, G. Warratz)

A smartcube Camera Image Scanner smart CIS was used to scan the slabbed cores with the aim to archive digital copies of the fresh core surfaces. In conjunction with smartDIS the device can be used to build up virtual core archives. The smartSCAN software contains a special interface to communicate with the smartDIS-database. In advance of measurements the scanner was calibrated at a predefined position to produce a white balance calibration and to check gain and offset settings of the connected camera.

The scans were operated with a 50-mm lens. Core pictures were archived using a resolution of 500 dpi, a core diameter of 117 mm and section-specific core scan lengths and offsets. Section images were merged using the IGOR software by applying a 0.66 average of the core image to display RGB and lightness data.

Shear strength and penetrometer measurements

(J. Bösche, T.J.J. Hanebuth)

Shear strength was measured with a Humboldt H-4212MH Pocket Shear Vane Tester (Fig. 5.3.7). The Pocket Shear Vane Tester was pushed into the sediment until the fins of the probe were fully covered by sediment, with the flat-footed part of the probe just in touch with sediment surface. The analogue display shows the corresponding shear value which can be transferred into kilograms per square meter. As a complementary device, the Geotester Pocket Penetrometer is a flat-footed, cylindrical probe that was pushed slowly 6.35 mm into the split-core surface (Fig. 5.3.7). The analogue display shows the corresponding values in kilograms and kilograms per square meter. Both types of measurements were performed on the *Work* half of split gravity cores (Fig. 5.3.8). The measurements were performed in fifty centimeter increments on the sediment surface with the rotation axis of the Shear Vane Tester and the applying pressure of the Penetrometer vertical to the bedding surface (Fig. 5.3.7); a depth interval of five centimeters was defined in which both measurements, vane shear strength and shear penetration were performed each twice, starting with the shear strength measurement, which was followed by the penetration measurement. The average of each of the two value pairs was calculated for a better precision.

To determine water content and dry bulk density onshore, a sediment sample was taken with a 10-cc syringe every 100 cm to gather a defined sediment volume. The syringe was closed with a cap, carefully sealed with tape and stored at 4°C.

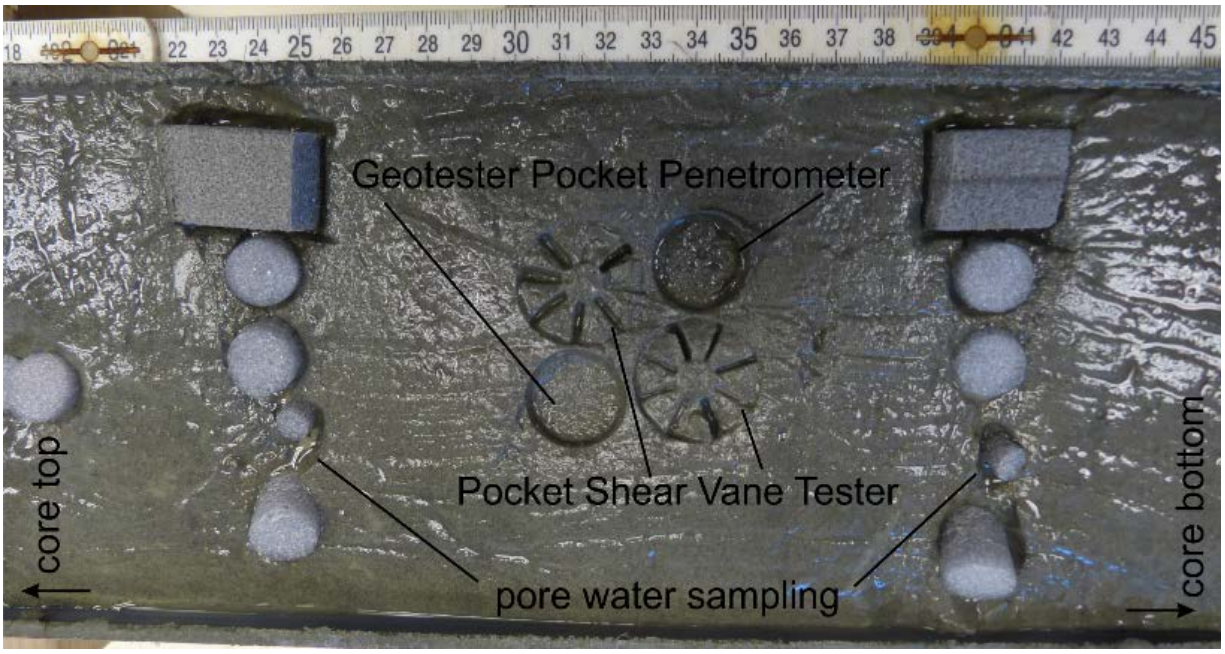

Fig. 5.3.7 Measurements with the Pocket Shear Vane Tester and the Geotester Pocket Penetrometer on the surface of the split core. Measurements were carried out between depths sampled for pore water. Each measurement was performed twice within a five-centimeter interval in the middle of the core, every fifty centimeters of core depth.

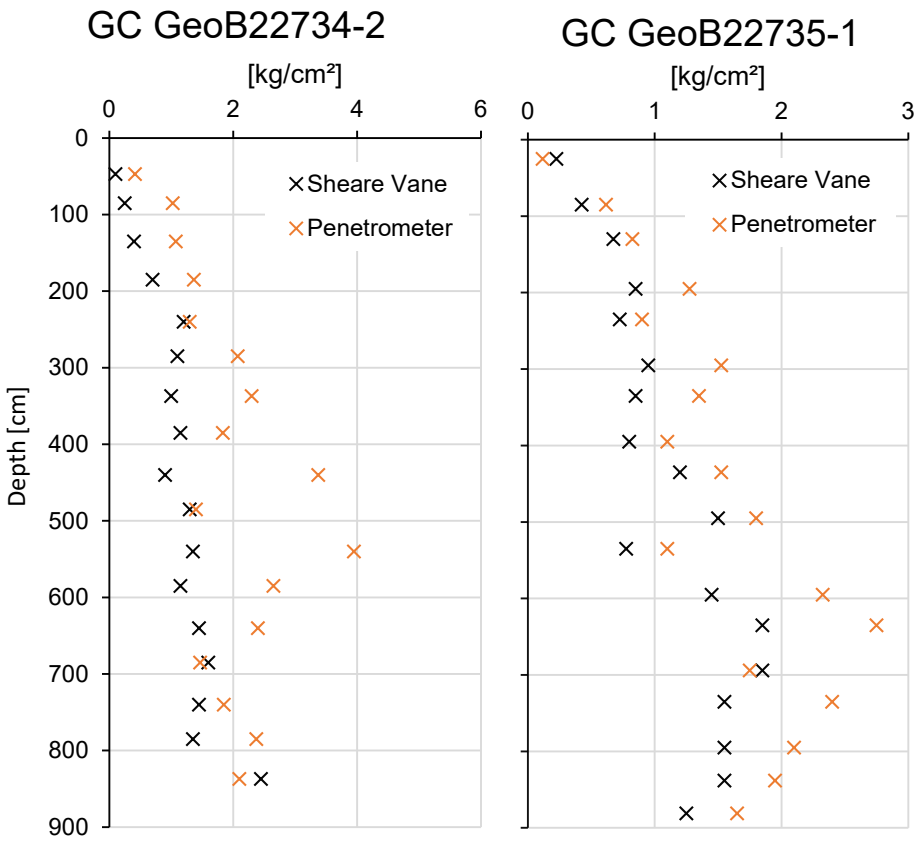

Fig. 5.3.8 Preliminary comparison of raw Vane and Penetrometer measurements suggesting stepwise changes in consolidation in the two gravity cores GeoB22734-2 and GeoB22735-1.

5.3.3 Preliminary Shipboard Results

Most of the cores are composed of mud, silt, and very fine sand with minor amounts of fine sand. The sediment color can be described as dark gray, olive, or sometimes black with the darkest colors corresponding to both sand-rich intervals and monosulfidic mineralization. Sorting is typically poor and lithologies can be divided into two primary categories: sand-rich (> 50 % sand) and mud-rich.

The coarse-grained fraction is predominantly within the coarse silt (31–63 µm) to very fine sand (62–125 µm) range except for a unit that occurs at the top of some cores (e.g., GeoB22702-3, GeoB22713-2, and GeoB22722-5). This uppermost unit contains fine sand (125–250 µm) with abundant benthic foraminifers (up to 10 %) as well as very fine sand and mud (e.g., Fig. 5.3.9). These uppermost sand layers appear to be similar to those sampled by the box corer which contained a diverse assemblage of epifaunal and infaunal organisms (worms, small arthropods, gastropods, etc.). The layer might represent a modern and still mobile sand sheet. All cores featuring this coarser-grained top unit were taken from water depths of less than 2,000 meters while cores recovered from greater depths lack this sand cover. In terms of composition, all sands observed within the gravity cores and box cores are made up of about 70 % Quartz; 20 % lithic fragments (metamorphic and igneous); and 20 % black, opaque minerals of not further determined composition.

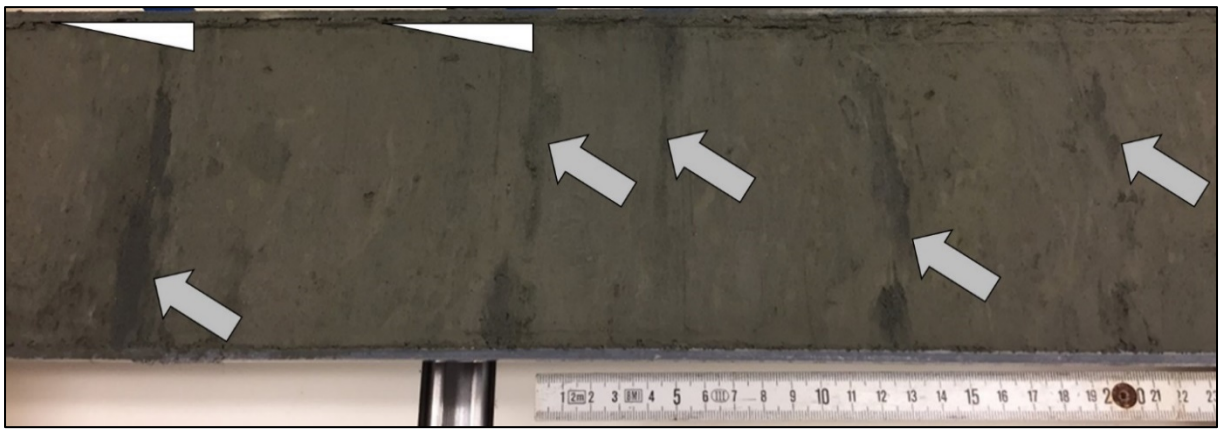

Fig. 5.3.9 Thin, sharp-based, very dark gray sands (gray arrows) in core GeoB22706-02 (~700 cm depth). These sands define the bases of thin, fining-upwards units (white triangles).

The deepest MeBo core taken at station GeoB22739-2 (core 8P-1A) recovered a succession of medium to coarse, shelly sand interbedded with fine, faintly laminated sand containing small mud clasts, which represents the coarsest sediment recovered during cruise SO260 (Fig. 5.3.10). These shell-rich, coarse-grained sands and laminated sands are intercalating over a depth interval of 1 meter, above which the succession is defined by massive, fine-grained sand.

Mud-rich lithologies are defined mostly as silty mud with sand or as mud that occurs as isolated lenses. Just as with the sand-rich lithologies, sorting is almost always poor. Cores GeoB22709-1 and GeoB22708-1, two of the longest gravity cores recovered, are predominately mud-rich throughout.

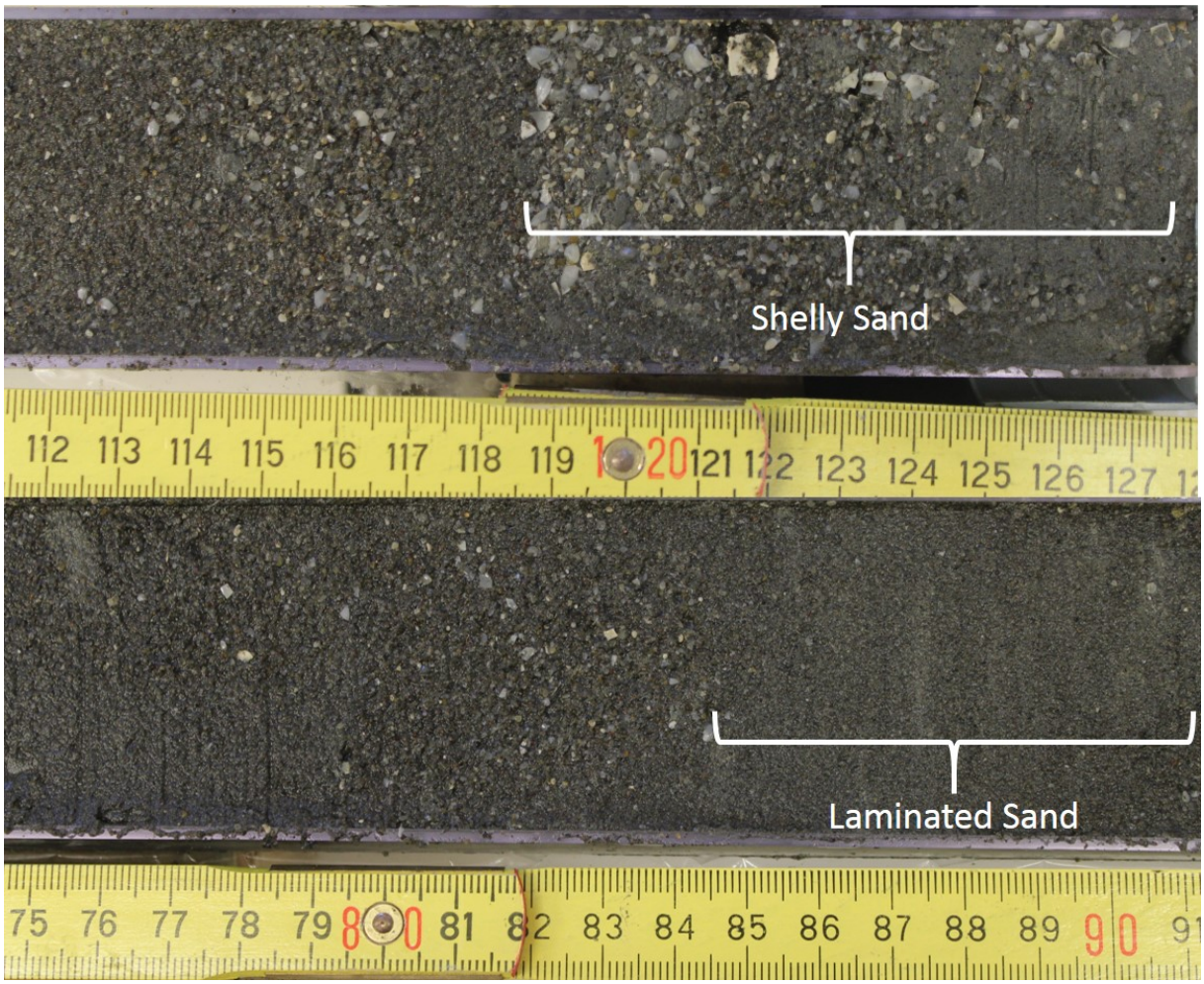

Fig. 5.3.10 Shelly, coarse-grained sand and laminated fine-grained sand from core GeoB22739-02.

One of the most striking aspects of the retrieved sediment cores is the pervasive bioturbation. This bioturbation is manifested in three ways. Firstly, as a non-distinct, chaotic to massive fabric that disrupts most primary bedding. Within this type, individual burrows are not discernible rather varying intensities of bioturbation overprints primary physical structures including bed contacts. Secondly, as large (~1 cm in diameter) irregular or elongated oval-shaped burrows with fill material that differs slightly from the host sediment (Fig. 5.3.11). These occur mostly in sand-rich lithologies. Thirdly, as small, sharp-walled, circular to cylindrical burrows that are most common within mud-rich lithologies. Finally, the least common type of burrow observed are small, mud/fecal-lined, circular burrows (Fig. 5.3.11).

The pervasive and intense bioturbation present within most of the cores limits the identification of primary sedimentary structures. However, the gravity core GeoB22734-2 contains a relatively thick succession of well-preserved beds within the lower 4 meters of the core indicating a lower degree of bioturbation relative to other cores. These beds define 20–40 cm thick fining-upwards successions which contain basal, massive, fine sands and shell fragments overlain by laminated silty sands and capped by muds. These units may be turbidites possibly triggered by storm events that remobilized large volumes of shelf sands.

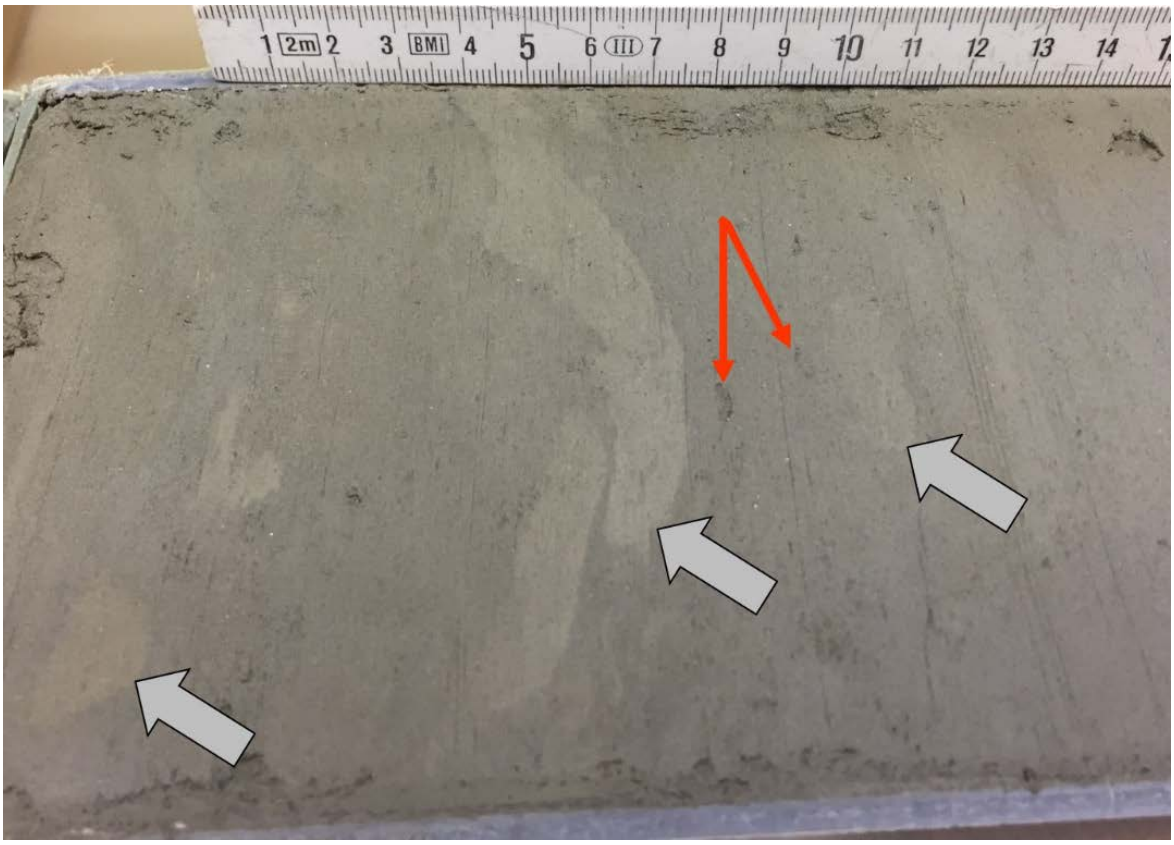

Fig. 5.3.11 Large, unlined, irregular shaped burrows with lighter colored fill (gray arrows). May be classified as *Planolites* and reflect shallow dwelling or grazing structure. The red arrows indicate smaller, lined, circular burrows which may be *Paleophycus*.

The most prominent diagenetic feature observed within the cores is the occurance of black or very dark gray patches – most likely representing iron monosulfides. These occurs as both small (1–3 m) black grains within thick, mud-rich zones (Fig. 5.3.12B) and larger black/dark gray, irregular oval-shaped features within sand-rich zones (Fig. 5.3.12A). Both features occur in discrete zones (Fig. 5.3.13) within several of the cores (see sharp contacts at 310, 430, and 590 cm in core GeoB22709-1). It should be noted that the cores with the highest abundances of these black grains are the two deepest cores recovered during this cruise at ~3,600 meters water depth.

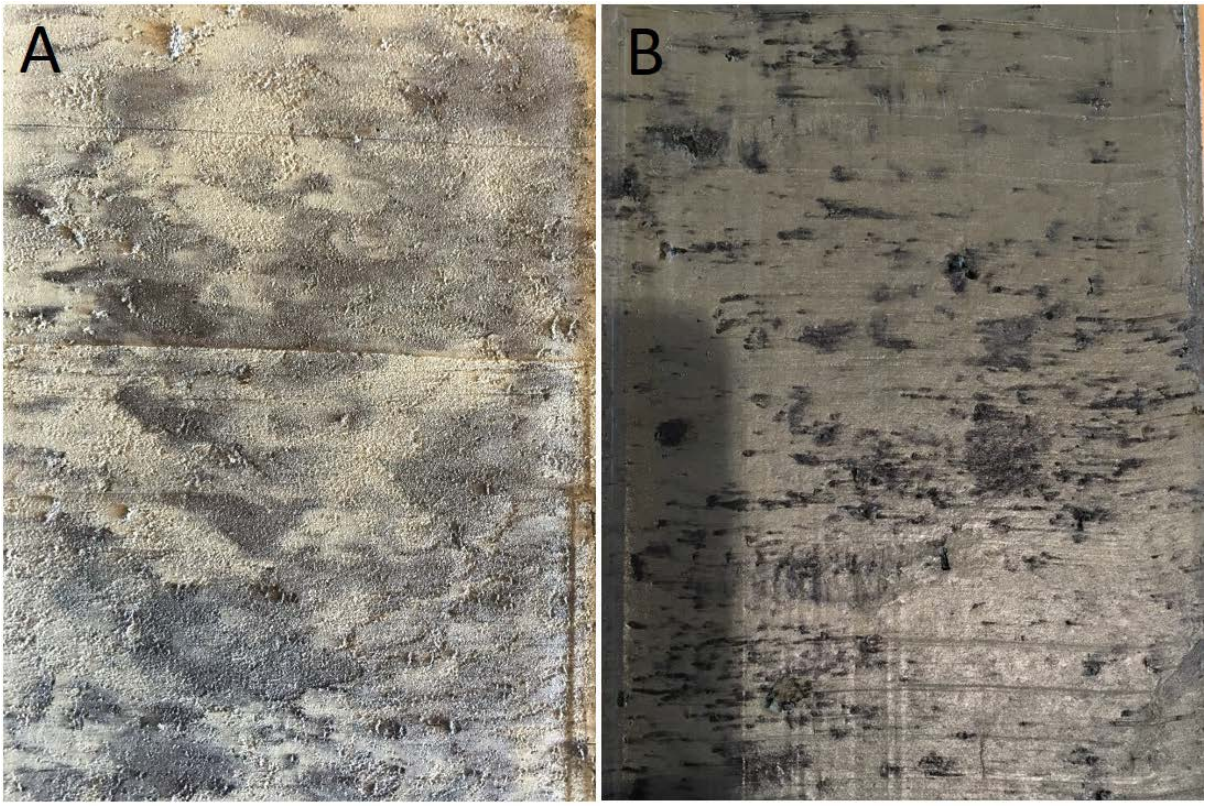

Fig. 5.3.12 Different forms and appearances of tentative iron monosulfide precipitates. A) diffuse black/very dark gray patches associated with large indistinct burrows within a sand-rich matrix. B) small, black grains within a mud-rich matrix.

Fig. 5.3.13 Contact between tentative iron monosulfide grain-bearing zone (below 101 cm) and an overlying zone, which is apparently free of iron monosulfides.

5.4 Physical Properties Studies

(T. Frederichs, C. Hilgenfeldt)

5.4.1 Introduction

The sediment series recovered during RV SONNE cruise SO260 by gravity corer and the Meeresbodenbohrgerät (MeBo70) drill rig were subjected to routine laboratory geophysical studies: shipboard measurements on the segmented cores were made using a *Multi-Sensor Core Logging System* (MSCLS) that was newly developed at MARUM (Center for Marine Environmental Sciences, University of Bremen) (Fig. 5.4.1). On research cruise SO260 the system was used for the first time.

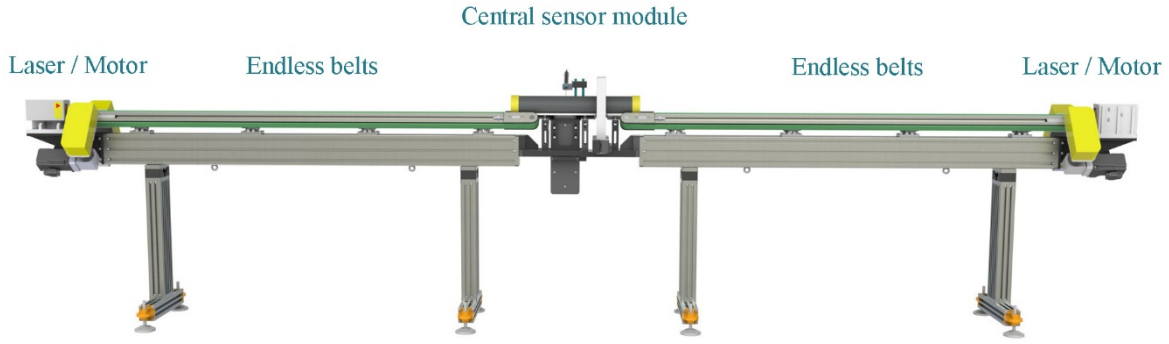

Fig. 5.4.1 CAD drawing of the Multi-Sensor Core Logging System (MSCLS) consisting of two-sided (endless) conveyor belts, the central sensor module, the drive motors and the laser distance sensors.

The MSCLS measurements routinely comprise two basic physical parameters:

- electrical resistivity R_s (as a measure of porosity and density),
- magnetic volume susceptibility κ

These properties are closely related to the lithology and grain size of the sediments. Electrical resistivity and magnetic volume susceptibility yield medium-resolution core logs available prior to most other detailed investigations. The characteristic sensor response width for these parameters is approximately 5-8 cm and all the cores were measured at 1 cm resolution.

Magnetic Volume Susceptibility

Magnetic volume susceptibility κ is defined by the equations

$$B = \mu_0 \cdot \mu_r \cdot H = \mu_0 \cdot (1 + \kappa) \cdot H = \mu_0 \cdot H + \mu_0 \cdot \kappa \cdot H = B_0 + M$$

with magnetic induction B, absolute and relative permeabilities μ_0 and μ_r, magnetizing field H, magnetic volume susceptibility κ and volume magnetization M. As can be inferred from the third term, κ is a dimensionless physical quantity. It represents the amount to which a material is magnetized by an external magnetic field.

For marine sediments, magnetic susceptibility may vary between an absolute minimum value of around -15·10-6 SI units (diamagnetic value of pure carbonate or silicate) to a maximum of some 10.000·10-6 SI for basaltic debris rich in (titano-) magnetite. In most cases κ is primarily determined by the ferrimagnetic mineral content, while paramagnetic matrix components such as

clays are of minor importance. High magnetic susceptibilities indicate high terrigenous or low carbonate deposition. Low values of magnetic susceptibility can also result from post-depositional reduction of oxic iron minerals. In absence of pervasive diagenesis, magnetic susceptibility can serve for a correlation of sedimentary sequences deposited under similar conditions.

Due its size, the sensor integrates the response signal over a core interval of about 5-8 cm. Consequently, sharp susceptibility changes in the sediment column appear smoothed in the κ log.

Electrical Resistivity, Porosity, and Density

The electrical sediment resistivity R_s is determined using an external inductive sensor. A non-contact infrared thermometer is used to measure the temperature at exactly the spot where contemporaneously electrical resistivity is determined. For sensor calibration, a series of saline solutions is measured daily.

The porosity ϕ is calculated according to the empirical Archie's equation,

$$R_s/R_w = k \cdot \phi^{-m}$$

which approximates the ratio of sediment resistivity R_s to pore water resistivity R_w by a power function of porosity ϕ. Following a recommendation by Boyce (1968) for sea water saturated clay-rich sediments, values of k=1.30 and m=1.45 are used. Density estimates are calculated assuming a mean bulk density of 2670 kg/m^3. For inductive porosity and susceptibility proxies, we join the core section data to an entire core log due to a method-immanent non-linear signal decay toward the section caps. Corrections using an adapted section end correction curve were applied, but some conspicuous peaks and discordances persist at some section boundaries and should not be over-interpreted.

Sampling for sediment magnetic investigations

Additional to the shipboard long-core measurements, selected gravity cores were sampled for onshore sediment magnetic investigations. These samples were taken with variable increments parallel to those for geochemical studies (see Appendix 4).

5.4.2 Methods

General setup of MSCLS

The MSCLS is used to measure physical parameters of sediments. Magnetic susceptibility, electrical conductivity and temperature at the time of measurement of whole-round or split cores are recorded. Individual core sections are moved along the static sensors on a horizontal conveyor belt.

The latter consists of an endless tooth belt system which is able to transport the core sections with almost no slippage, thus ensuring an accurate horizontal positioning of the objects to be measured.

Two laser distance meter (WELOTEC, Germany, type OWTB V2) measure in real time the distance to the respective edges of the core section and guarantee for a positioning accuracy and determination of section length of better than 0.1 mm.

The V-shaped layout of the four endless conveyor belts ensures an exact axial alignment. It accurately holds the core section on its position on the belt without being accidently moved (Fig. 5.4.2), even during severe ship movements. The setup consists of four AM8131 three-phase permanent magnet synchronous motors (Beckhoff, Germany) which are electrically connected to form a cluster of two pairs. Thus, it is possible to position even heavy sediment cores with a practical repeatability of better than 0.2 mm.

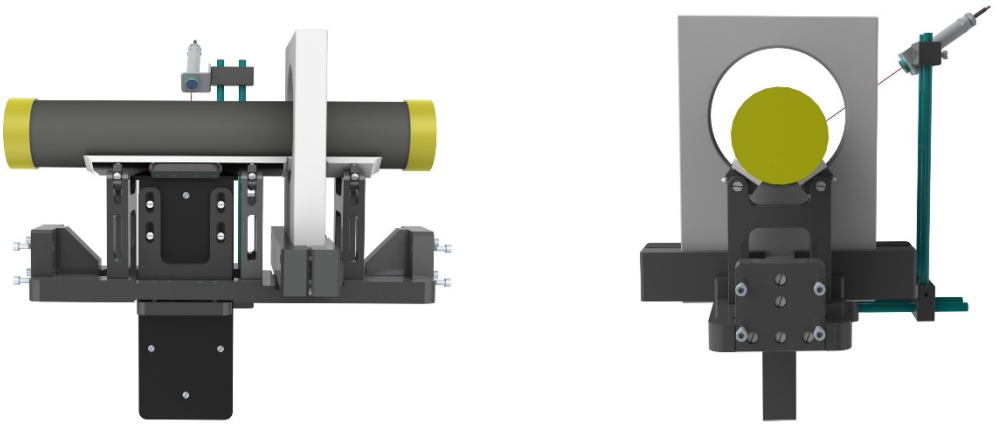

Fig. 5.4.2 CAD drawing of the central sensor module in side and front view showing the V-shaped stabilization of the section.

The sensor module is currently carrying two probes (Fig. 5.4.3) and is located in the center of the MSCLS. It is made of polyacetal (POM), which not only ensures high stability but also very small influence on the measurements of the respective probes. Two fully assembled modules are available, each with a Bartington MS2C susceptibility loop sensor with different coil diameters of 85 and 140 mm, respectively. To change between the modules only takes a few minutes and requires no readjustment of the system to adapt to different core diameters. Only the sensors for electrical conductivity and for temperature have to be exchanged between the modules due to availability.

The actual temperature of the core section to be measured is determined by means of a non-contact infrared thermometer focusing on the location of the recent electrical conductivity measurement.

Since only a single core section is measured at a time, it is possible to horizontally traverse the section forward and backward along the conveyor belt. Any number of background measurements (without a core section within the sensitive volumes of the sensors) during a measuring cycle can be conducted in order to determine any eventual sensor drift. Therefore, sediment cores were usually measured shortly after their recovery. Warming of the sections to room temperature, as on previous cruises, is no longer necessary.

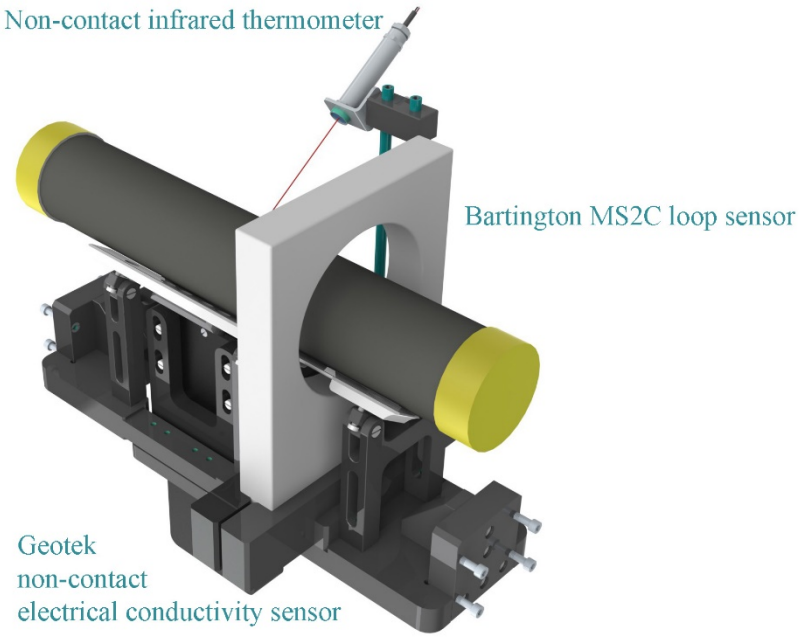

Fig. 5.4.3 CAD drawing of the central sensor module with core section, MS2C loop sensor, NCR sensor and infrared thermometer.

Magnetic volume susceptibility

Measurements on gravity cores were made on both whole-round and split core sections using a MS2C loop sensor (Bartington Instruments Ltd., UK) with a diameter of 140 mm (S/N 827), MeBo core sections were measured with a MS2C loop sensor with a diameter of 85 mm (S/N 832). The control unit was a Bartington MS3 (S/N 456), which allows an almost freely programmable time integration of the measurement signal. The functional principle of the susceptibility meter is an oscillator circuit that produces a weak (approx. 80 A/m RMS) non-saturating alternating magnetic field with a frequency of 565 Hz. A PC communicates with the MS3 via an in-house developed serial protocol (RS232) providing permanent checksum proofing of the data transfer.

At the beginning of the measurement of each core section, the MS3 unit is reset and zeroed. The zero measurement provides the reference values E0, I0, F1,0 and F2,0 while the respective parameters E, I, F1, F2 from each sample measurement are used to obtain the uncalibrated magnetic susceptibility:

$$V = (I \times 10^{E+1} - I_0 \times 10^{E0+1}) + (F_1 \times 10^{E-5} - F_{1,0} \times 10^{E0-5}) + (F_2 \times 10^{E-12} - F_{2,0} \times 10^{E0-12})$$

This value is transformed into the calibrated susceptibility κ' [SI] by applying the MS3 calibration constant k = 1.5121357037 × 10^{-3} and the value Vair which is determined after the MS3 was initially zeroed and without sediment within the sensitive volume. Vair takes into account the ambient environmental conditions.

$$\kappa' = \frac{V - Vair}{k}$$

Vair:	Measurement ‘in Air’
V:	Uncalibrated magnetic susceptibility
κ‘:	Calibrated magnetic susceptibility [SI]

Finally k’ is normalized to volume by correcting for the ratio between MS2C loop sensor diameter and the core diameter:

$$\kappa = \frac{1}{3{,}45 * (\frac{d}{D+8\,mm})3} * \kappa‘$$

d:	Core diameter
D:	Sensor diameter

Electrical resistivity, porosity and density

Electrical resistivity is a measure of how strongly a material opposes the flow of electric current and is the reciprocal of electrical conductivity. A low resistivity indicates a material that readily allows the movement of electrical charge. The SI unit of electrical resistivity is the ohm-meter and the SI unit of electrical conductivity is Siemens per meter.

Electrical resistivity was measured by means of a non-contact resistivity (NCR) sensor (Version 02.2016) by Geotek Ltd. (UK). The NCR sensor uses a transmitter coil to induce a high-frequent magnetic field in the sediment which in turn generates an electrical current in the sediment that is inversely proportional to the resistivity. A receiver coil measures the very small magnetic field regenerated by the electrical current in the sediment. These readings are compared with those from a second identical coil operating in air. This difference technique provides the required accuracy and stability. Electrical resistivities between 0.21 and 15.48 Ohm-m (at 20ºC) can be measured with a spatial resolution along the core of approximately 2 cm.

The analog output Q-signal (± 2,500 mV) of the NCR sensor was digitized using a 16-bit, 250 kS/s National Instruments PCIe-6320 analog-to-digital (AD) converter.

The temperature of the object to be measured, which was used to calculate the specific resistance, was recorded using a non-contact Omega OS151 infrared thermometer. In its simplest construction, an infrared thermometer consists of a lens that focuses the infrared energy on a detector. This energy is then converted into an electrical signal (4 - 20 mA) which has also been digitized with 16 bits. This ensures an accuracy of ± 1% of the measured value, or a repeatability of 0.5% of the measured value.

For the necessary NCR calibration we daily measured a set of saline solutions at concentrations of 0.35 - 1.75 - 3.5 - 8.75 - 17.5 - 35 g/l. The respective voltage readings minus the zero level of the sensor are automatically saved to the control software and applied to the voltage data from the core section.

Parameter-Setup

The following parameters were usually applied for physical properties measurements during cruise SO 260:

General settings	
Distance between core section and sensors for sensor initialization	40 (50) cm
Number of drift measurements	3 (5)
Sampling interval for all sensors	1 cm
Motor velocity	150 mm/s
Motor acceleration / deceleration	100 mm/s²
Thickness of end caps	2 mm
Magnetic susceptibility	
Integration time	3500 ms
Leader distance	14 cm
Electrical conductivity	
Integration time	3.500 ms (16-Bit, 100 S/s)
Leader distance	14 cm
Temperature	
Integration time	3.500 ms (16-Bit, 100 S/s)

5.4.3 Preliminary Shipboard Results

Gravity coring

The means and trends of the porosity and susceptibility measurements, as well as core lengths and water depths, are compiled in figure 5.4.4. Physical property data of a total of 27 gravity cores (total length about 151 m) demonstrating core lengths between 0.18 and 9.76 m were collected onboard. Dots indicate the mean values of magnetic susceptibility and derived porosity and density. Vertical error bars denote the standard deviations. Each diagram is divided into groups of spatially adjacent cores. Color statistics are not included as absolute reflectance numbers are controlled by multiple factors and therefore not easy to compare.

Average porosities calculated for gravity cores ranged from about ca. 40 % to 75 %. Porosity values in their lower range appear relatively dense for unconsolidated marine sediments. Most porosity values range from 50 to 60 %. The lowest value (about 40 %) associated with a relatively large variability, expressed as standard deviation, was determined for core GeoB22740-1 which recovered material from a dark unit of a drift wave (water depth 1102 m). This is in clear contrast to the porosity of about 75 % measured for the deep-water core GeoB22708-2 from 3679 m water depth which represents the highest mean porosity of all the cores. In summary, porosity of cores from larger water depths, deeper than 1500 m, show a tendency to higher porosities compared to porosities from cores from shallower water depth as long as they are not affected by carbonates. Corresponding to these mean porosities, densities ranging from 1438 kg/m³ (GeoB22708-2, water depth 3679 m) to 2016 kg/m³ (GeoB22740-1, water depth 1102 m).

The volume magnetic susceptibility means for all gravity cores are in the ca. 147 to $3256 \cdot 10^{-6}$ SI range. Core GeoB22741-1 recovered from a hydro-acoustically light unit of a drift wave at 1072

m water depth and consisting of mainly fine to very fine-grained sand shows the highest mean susceptibility ($3256 \cdot 10^{-6}$ SI) and also the highest absolute value of magnetic susceptibility ($9045 \cdot 10^{-6}$ SI). The by far lowest absolute values were determined for cores GeoB22706-2 ($165 \cdot 10^{-6}$ SI) and GeoB22707-1 ($146 \cdot 10^{-6}$ SI) recovered from the lower and upper terraces of the Mar del Plata Canyon consisting of more muddy, silty very fined-grained sand. Even core GeoB22733-2 recovered from coral mounds exhibits a higher average magnetic susceptibility ($199 \cdot 10^{-6}$ SI) than these. The significant differences in average magnetic susceptibility (varying by an order of magnitude) demonstrate the heterogeneity of the working area where local environmental conditions dominate the physical properties signals. The highest (relative) variability with 129 % demonstrates core GeoB22735-1 (water depth 1384 m) from the former M78 station GeoB13809 where also MeBo drill site GeoB22735-5 is located. Also both cores from biogeochemistry site 1 (GeoB22708-1/2) show high relative variabilities larger than 80 % of their respective means due to wide dissolution of magnetic minerals. Furthermore, cores from carbonate/coral mounds exhibit also high relative variability of magnetic susceptibility (64 to 88 %) (GeoB22715-2, 22729-1, 22733-2, 22744-1), which is due to their variable composition. The lowest variabilities (mainly < 25 %) are shown again by cores GeoB22702-3, 22713-2, 22714-1 and 22725-2 from drifts or terraces.

As examples, physical properties data in combination with results from digital line scanning are shown in figures 5.4.5 through 5.4.8.

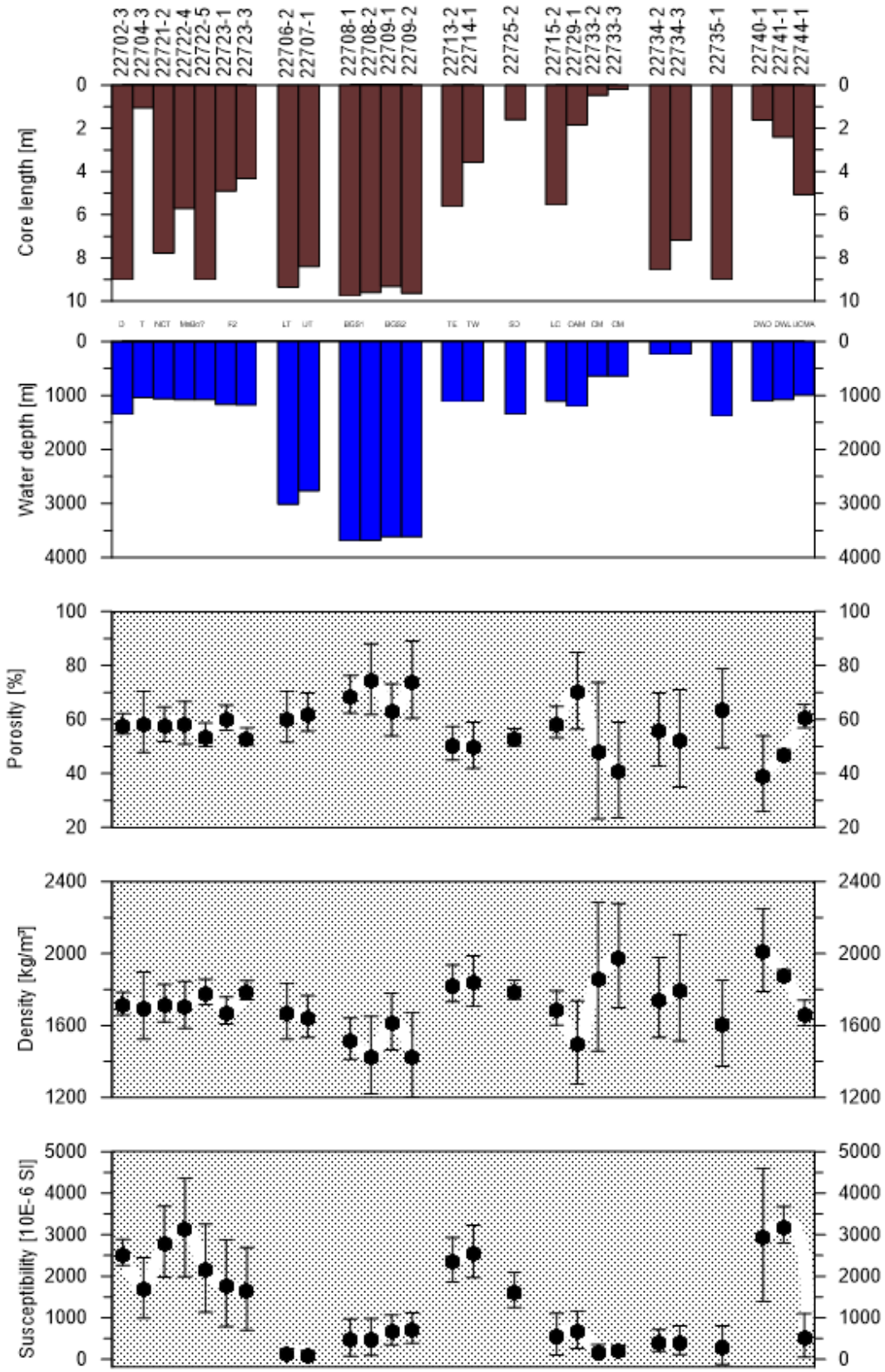

Fig. 5.4.4 Mean porosities, densities and magnetic susceptibilities of gravity cores GeoB22702-3 through GeoB22744-1 as compared to variations in water depth at the sampling sites and core recovery. Data of core GeoB22733-3 are not shown here. Vertical bars denote standard deviations. Data sets are summarized according to working areas: D – Drift, T – Terrace, NCT – Northern contourite terrace, MeBo - Potential BioGeo MeBo Site, F2 – Furrow 2, LT/UT – Lower/upper terrace of Mar del Plata canyon, BGS 1/2 - Biogeochemistry Site1/2, TE/TW – Terrace East/West, SD – Scour drift, LC - Lower carbonate mound area, CAM - Corals and mud above stones, CM – Carbonate mound, DWD – Drift wave dark unit, DWL – Drift wave light unit, UCMA – Upper carbonate mound area.

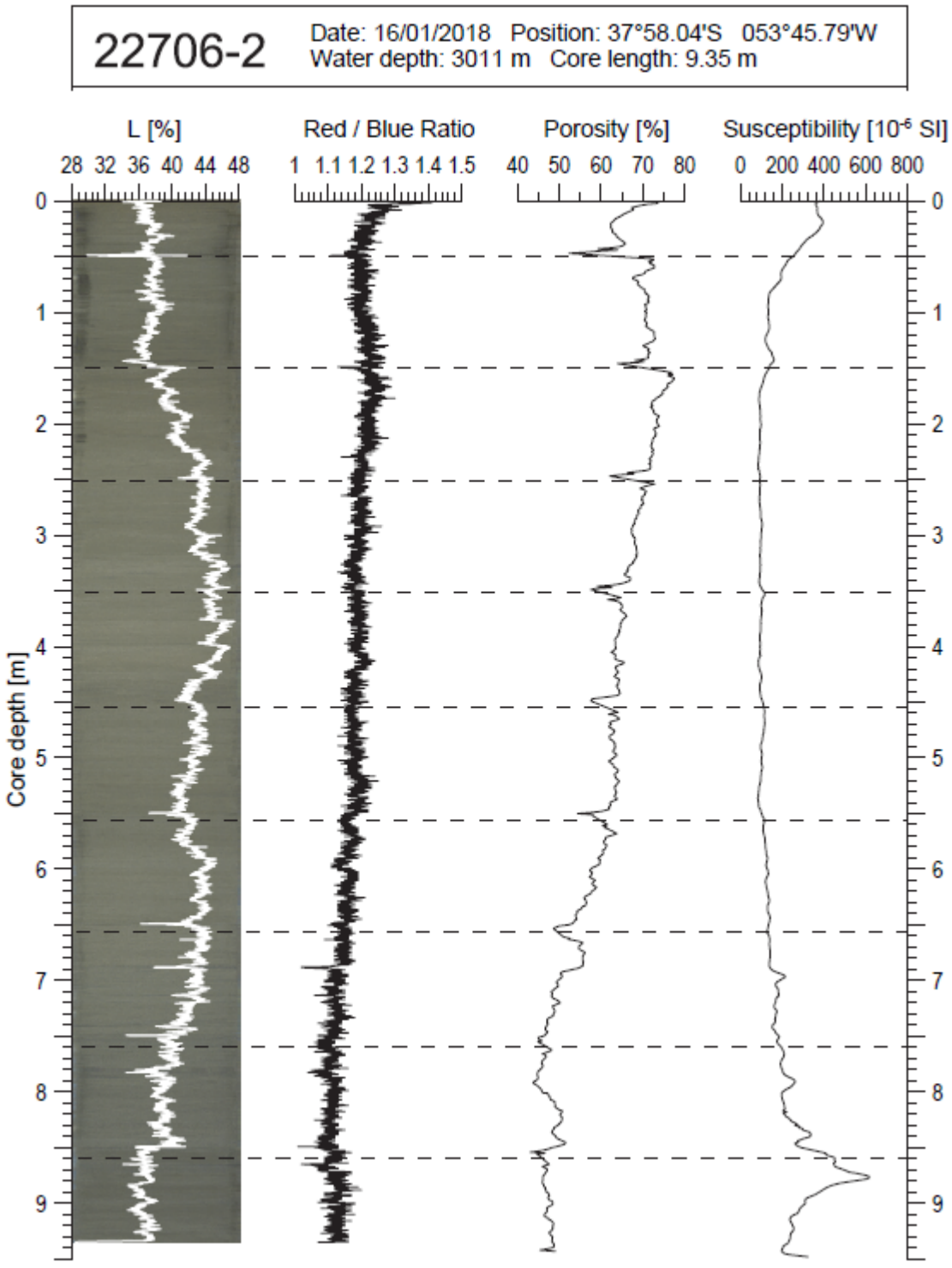

Fig. 5.4.5 Reflectance L, red/blue ratio from digital line scanning, porosity as calculated from electrical resistivity data and magnetic susceptibility for gravity core GeoB22706-2 from the lower terrace of the Mar del Plata Canyon.

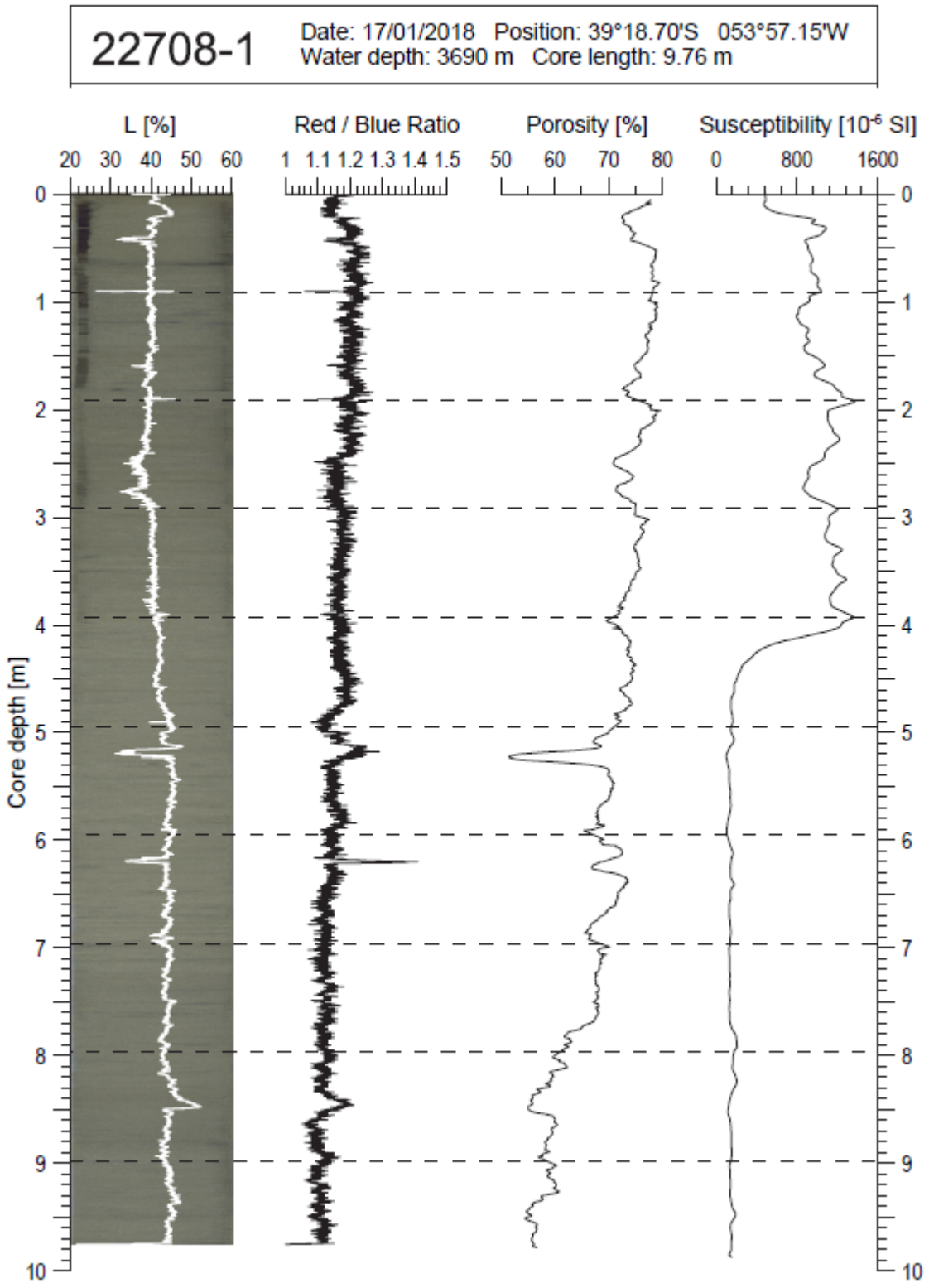

Fig. 5.4.6 Reflectance L, red/blue ratio from digital line scanning, porosity as calculated from electrical resistivity data and magnetic susceptibility for gravity core GeoB22708-1 from Biogeochemistry site 1.

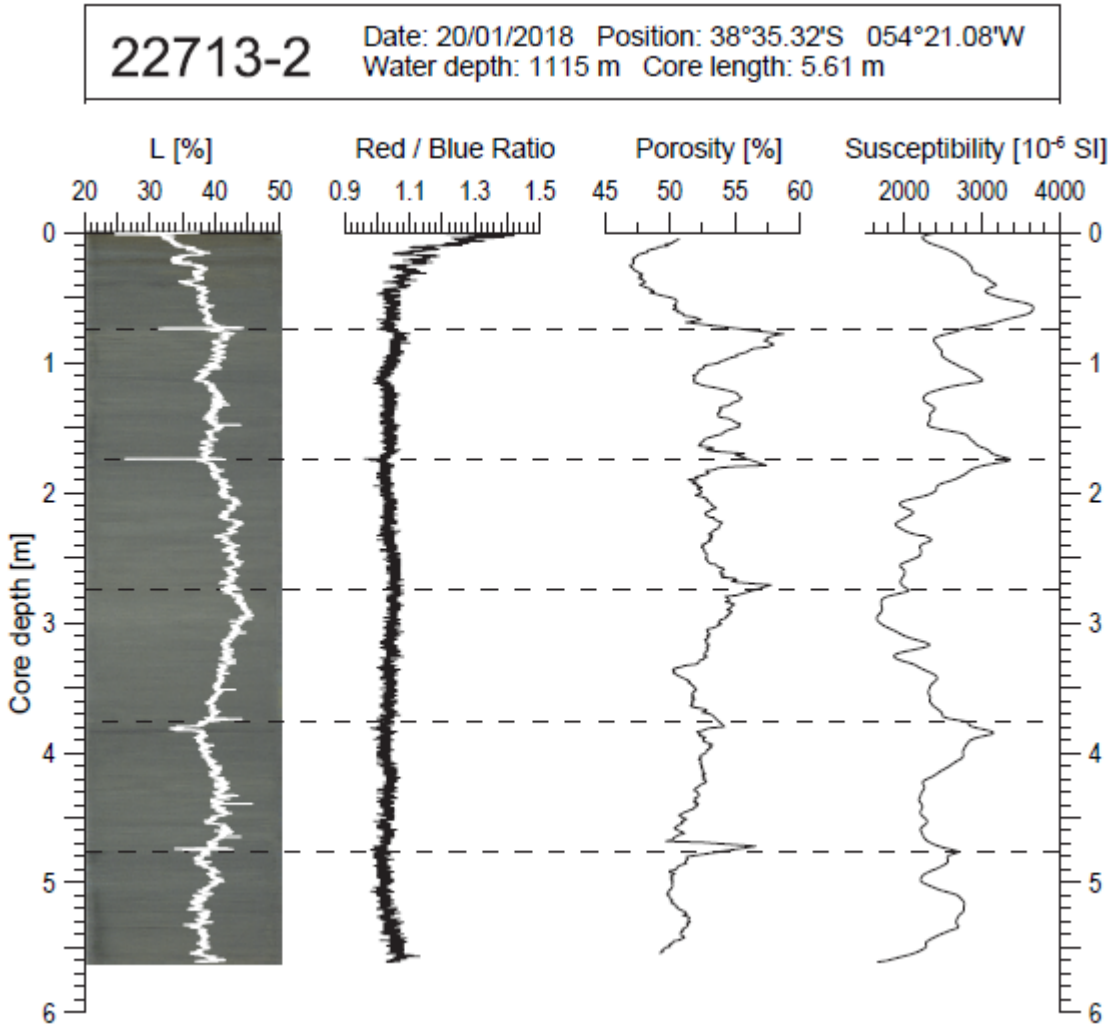

Fig. 5.4.7 Reflectance L, red/blue ratio from digital line scanning, porosity as calculated from electrical resistivity data and magnetic susceptibility for gravity core GeoB22713-2 from Terrace East.

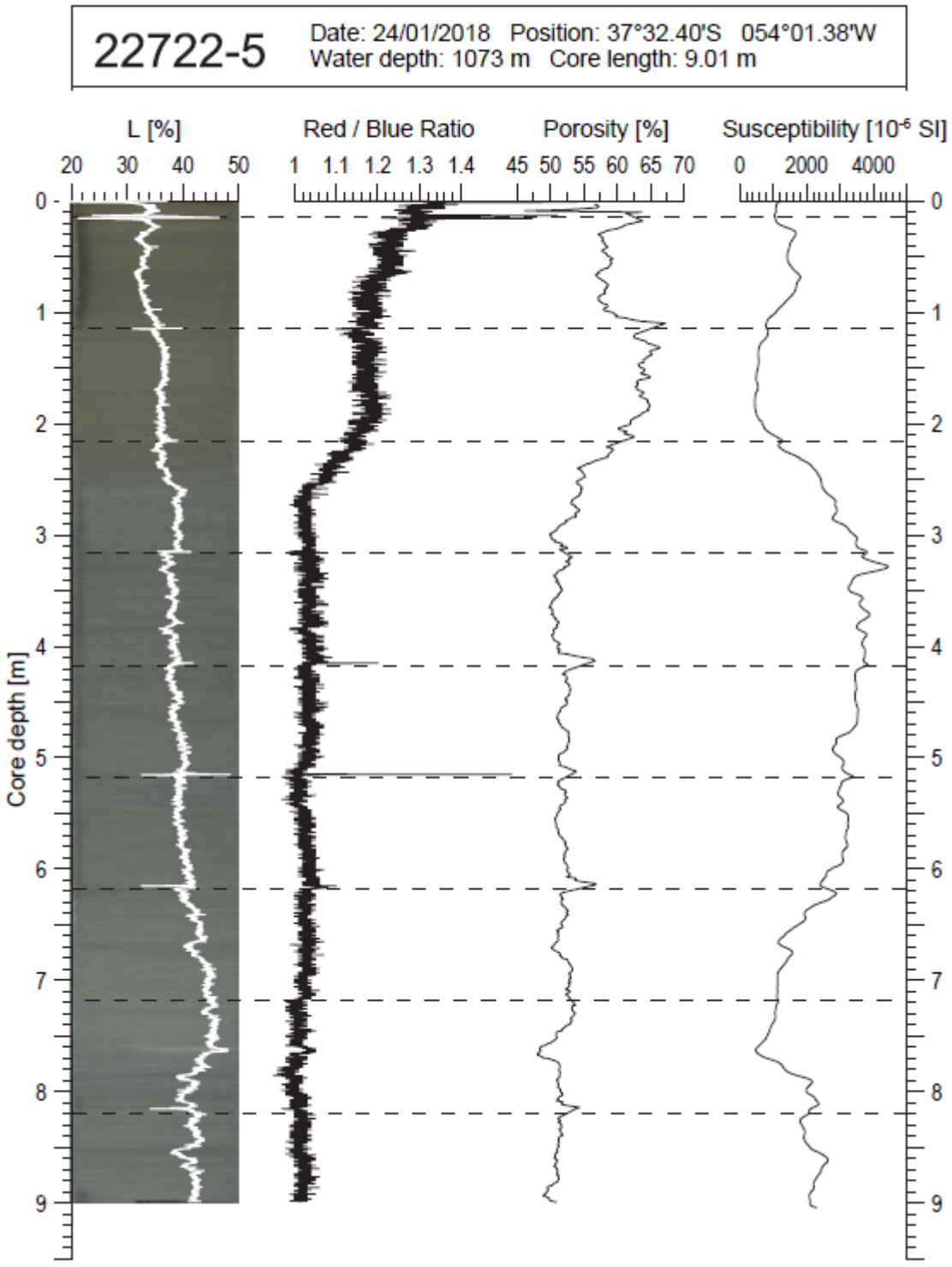

Fig. 5.4.8 Reflectance L, red/blue ratio from digital line scanning, porosity as calculated from electrical resistivity data and magnetic susceptibility for gravity core GeoB22722-5 (compare corresponding MeBo drill core).

MeBo drilling

Four MeBo drill cores (total recovery 81.225 m) were subject to physical properties measurements. Although on identical coring sites and MeBo data mirroring well the physical properties data of gravity cores, e.g., GeoB22735, GeoB22722, their absolute numbers has to be considered with caution. Incomplete filling of some liners resulted in artificially reduced (increased) values for porosity (density) if the voids were empty or vice versa if the voids were filled with water. In either case the values for magnetic susceptibility were reduced.

Down-hole core depths were assigned to the data to our best knowledge leading to numerous gaps in the records due to core recoveries of less than 100 per cent. Figure 5.4.9 shows exemplarily the data from MeBo core GeoB22735-5.

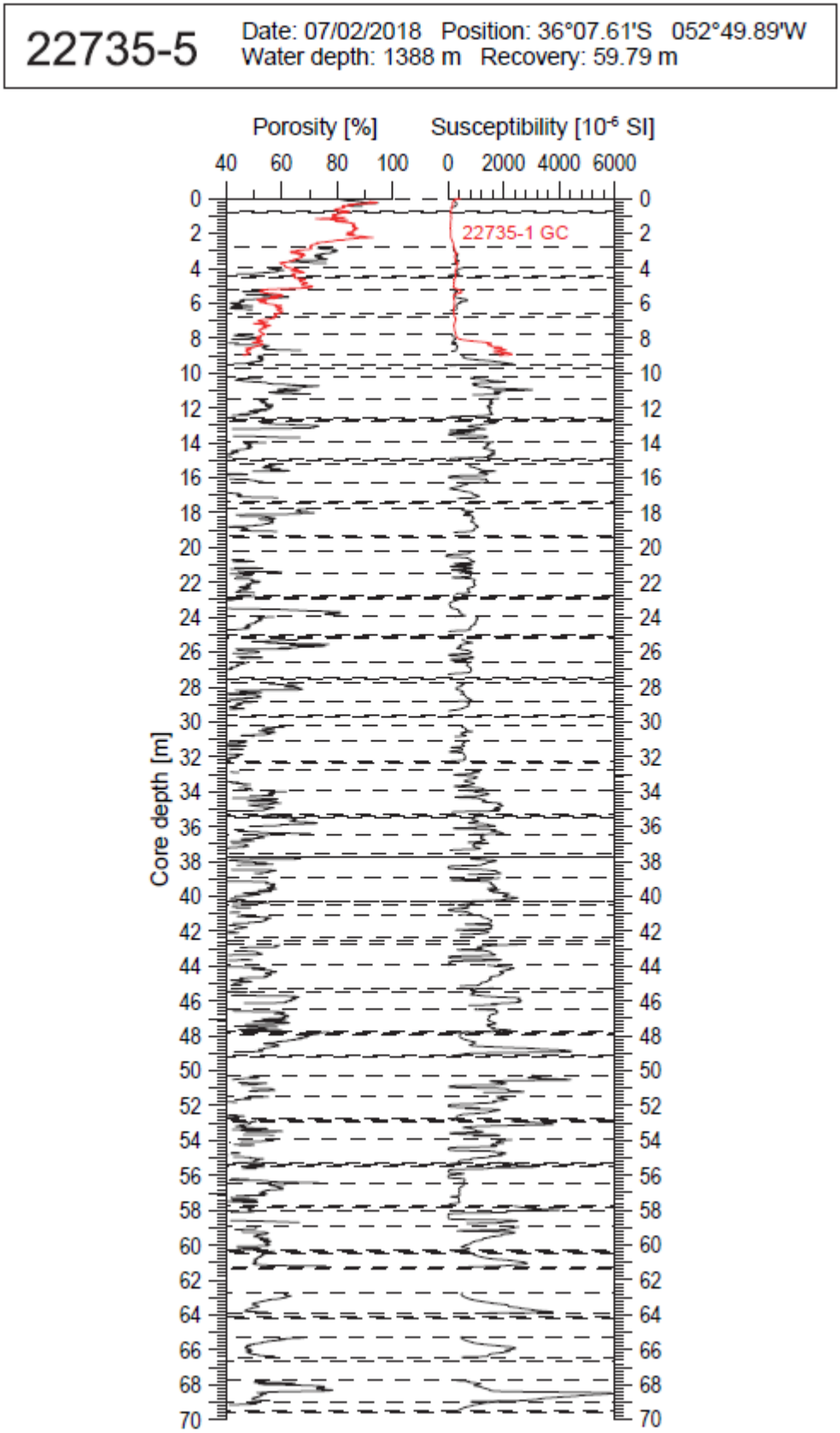

Fig. 5.4.9 Porosity as calculated from electrical resistivity data and magnetic susceptibility for MeBo core GeoB22735-5. Red lines indicate the respective data from gravity core GeoB22735-1.

5.5 Sediment and Pore-Water Geochemistry and Biogeochemistry

(I. Dohrmann, M. Dröllner, C.K. Jones, S. Kasten, M. Köster, A.-C. Melcher, N. Riedinger, J. Volz)

5.5.1 Introduction and Objectives

Previous work on sediments of the continental slope off Argentina and Uruguay has demonstrated that the different sedimentary regimes and sedimentation/accumulations rates exert a strong control on the rates and pathways of geochemical and biogeochemical processes as well as fluxes of elements (Hensen et al., 2003; Riedinger et al., 2005, 2014, 2017) – not only in surface sediments but also in more deeply buried deposits. The dynamic sedimentation conditions that are widely observed in the study area have also been demonstrated to induce transient pore-water profiles (Henkel et al., 2012). These nonsteady-state pore-water profile shapes have been successfully used to identify and date recent mass transport deposits for which traditional dating approaches usually fail (Henkel et al., 2011).

Hensen et al. (2003) and Riedinger et al. (2005) presented first indication for deep iron and manganese reduction to occur below the so-called sulfate-methane transition. A follow-up study by Riedinger et al. (2014) performed on sediment material collected during RV METEOR cruise M78/3 provided the first comprehensive inorganic dataset pointing towards Fe- and Mn-mediated anaerobic oxidation of methane to occur in natural marine sediments. This novel biogeochemical pathway had been previously proposed by Beal et al. (2009) and Segarra et al. (2013) based on laboratory experiments.

The reduction of reactive ferric iron phases in marine sediments also releases adsorbed trace metals and nutrients into the pore water of the surrounding sediments (e.g., Riedinger et al., 2014; März et al., 2018). This process can have strong implications for the application of trace metals as paleoproxies. Additionally, the release of bioavailable trace metals in deeper sub-surface sediments can stimulate microbial processes in these layers.

The main objective of the Geochemistry Group during RV SONNE cruise SO260 was to acquire high-resolution profiles of pore-water and sediment geochemistry to investigate the impact of lithology, mode of sedimentation and accumulation rate on the composition and activity of the deep sub-seafloor biosphere and biogeochemical processes, and to provide a sampling roadmap for microbiology and organic geochemistry. The main scientific goals were 1) to determine the depositional and (bio)geochemical factors that can induce transient pore-water profile shapes – including the role of upward methane flux, 2) to investigate how depositional conditions control the preservation and reduction of Fe(III) and Mn(IV)-bearing mineral phases, 3) to elucidate iron- and manganese-reducing processes in the methanic zone by the application of inorganic techniques, 4) to determine the spatial variability of trace metal cycling and how it is controlled by regional and local sedimentary and oceanographic processes, and 5) to generate high-resolution profiles of trace metal concentrations in non-sulfidic sediments and at the sediment-water transition. Specifically, canyon structures were sampled to get insights into trace metal distribution on small spatial scales and their significance for paleoceanographic reconstruction.

5.5.2 Methods

Immediately after core recovery, the multi-corer (MUC) sediment cores were transferred into the cold room at a temperature of approximately 4°C. One MUC core was used for the retrieval of the

supernatant bottom water as well as the pore water. Three parallel MUC cores were separately used for (1) oxygen measurements, (2) sediment sampling for the later determination of porosity and the performance of total acid digestions and (3) sediment sampling for the later measurement of ^{210}Pb activities.

The gravity cores (GC) were cut into 1-m segments on deck and syringe samples were taken from every freshly cut segment surface for the analysis of methane (CH_4). After the GC were cut open, the working half was transferred into the cold room at a temperature of approximately 4°C for the pore-water and solid-phase sediment sampling.

After the sediment cores from the MeBo70 were sectioned off, 20 cm whole-round sediment cores were retrieved from approximately the middle of each filled core section and immediately transferred into the cold room at about 4°C. In the refrigerated room, the 20 cm whole-round sections were cut into two pieces from which one half was processed for microbiology/organic geochemistry while the other half as well as every core catcher were used for the extraction of pore water and sediment for the later determination of inorganic geochemical parameters.

The pore water of both MUC and GC cores was extracted by means of rhizons with an average pore size of 0.1 µM according to the procedure presented by Seeberg-Elverfeldt et al. (2005). In order to allow for high resolution sampling of the MUC cores without mixing of the pore water of different depths, all MUC cores were sliced, transferred into a 50 mL Falcon tube, flushed with Argon and then sampled by means of rhizons. Sampling intervals of both pore water and sediment for the MUC cores are presented in chapter 5.3. Pore-water and sediment sampling for the GC cores was performed every 20 to 30 cm. In order to avoid any dilution or oxidation during the pore-water sampling by rhizons, the first mL of the freshly extracted pore water was discarded.

The pore water from the MeBo70 sediment cores was extracted with (1) rhizons and (2) a titanium squeezer, modified after the stainless-steel squeezer of Manheim and Sayles (1974). Gauge pressures of up to $15*10^4$N were applied using a Breitländer laboratory hydraulic press to extract the pore water. Interstitial water was passed through two Whatman No. 1 filters, fitted above and below a titanium screen, and subsequently extruded into a 24 mL plastic syringe attached to the bottom of the squeezer assembly. Collected fluids were then filtered through a 0.2 µm Sartorius (Minisart NML) cellulose acetate disposable filter. In most cases, 5-8 mL of pore water was collected from each sample after~20 min of squeezing.

Shipboard analyses include the determination of dissolved iron, total sulfide, oxygen, alkalinity, dissolved inorganic carbon and nutrients such as ammonium, phosphate and silica. Pore-water samples were stored for the later determination of the concentrations of sulfate, chloride, cations and trace metals as well as the stable iron isotopic composition. Sediment samples were stored for the later determination of the concentration and stable carbon isotopic composition of methane, total organic/inorganic carbon and total organic sulfur contents, porosity, ^{210}Pb activity, speciation and stable isotopic composition of iron as well as trace metal contents.

Table 5.5.1 Sites of geochemically investigated samples during this cruise showing parameters analyzed on board and aliquots of samples stored and conserved.

Station (GeoB)	Device	CH_4	Eh pH	Fe^{2+}	HS^- SO_4^{2-}	Alk.	O_2	PO_4^{3-}, Si, NH_4^+, DIC	OES	Fe isot.	Trace metal	Sedi-ment	^{210}Pb
22702-1	GBC			X						X	X	X	
22702-2	MUC		X	X		X		X	X			X	X
22702-3	GC	X		X	X	X		X	X		X	X	
22706-1	MUC			X		X		X	X		X	X	
22706-2	GC	X		X	X	X		X	X		X	X	
22707-2	MUC			X				X	X		X	X	
22708-1	GC	X		X	X	X		X	X	X	X	X	
22708-3	MUC			X		X	X	X	X	X	X	X	X
22709-1	GC	X	X	X	X	X		X	X	X	X	X	
22711-1	MUC			X		X		X	X		X	X	X
22713-1	MUC			X		X	X	X	X	X	X	X	X
22713-2	GC	X		X		X		X	X	X	X	X	
22715-2	GC	X		X	X	X		X	X		X	X	
22721-1	MUC			X		X	X	X	X	X	X	X	X
22721-2	GC	X		X		X		X	X	X	X	X	
22722-3	MUC			X		X		X	X	X	X	X	X
22722-5	GC	X		X	X	X		X	X	X	X	X	
22723-1	GC	X		X		X		X	X		X	X	
22723-2	MUC			X		X	X	X	X	X	X	X	X
22723-3	GC	X	X	X		X		X	X	X	X	X	
22725-1	MUC			X		X	X	X	X		X	X	X
22725-2	GC	X		X		X		X	X		X	X	
22729-1	GC	X		X		X		X	X		X		
22734-1	MUC			X	X	X	X	X	X		X	X	X
22734-2	GC	X	X	X	X	X		X	X		X	X	
22735-1	GC	X	X	X	X	X		X	X		X	X	
22735-2	MUC			X		X	X	X	X			X	X
22722-7	MeBo	X		X		X		X	X		X	X	
22735-5	MeBo	X		X	X	X		X	X	X	X	X	
22739-2	MeBo	X		X		X		X	X		X	X	
22744-1	GC	X		X	X	X		X	X		X		

Methane (CH_4) samples were taken as 3 cm^3 sediment plugs and injected into 20 mL headspace crimp vials containing 5 mL of 1M NaOH solution which were stored at 4°C. After closing and subsequent shaking, methane becomes enriched in the headspace of the vial. The concentrations and stable carbon isotopic composition ($\delta^{13}C$) of methane will be measured onshore by Dr. Thomas Pape at the University of Bremen.

Dissolved iron (Fe^{2+}) was detected photometrically (DR Lange HACH 2800 photometer) at a wavelength of 565 nm. 1.5 mL of the extracted pore water was pre-treated with 50 µL of ascorbic acid and then added to 50 µL Ferrospectral solution to complex dissolved Fe for colorimetric measurement. In the case of high concentrations of Fe^{2+} (>1 mg L^{-1}) the samples were diluted with oxygen-free artificial seawater.

Dissolved pore-water hydrogen sulfide samples were immediately fixed using a 5 % zinc-acetate solution to preserve sulfide from oxidation. Sulfide concentrations ($\Sigma H_2S = H_2S + HS^- + S^{=}$) were measured directly onboard using the methylene blue method of Cline (1969).

Ex-situ oxygen measurements (O_2) were only performed with MUC cores using amperometric Clark-type oxygen sensors with an internal reference and equipped with a guard cathode (Revsbech, 1989) according to the procedure described by Ziebis et al. (2012) and Mewes et al. (2014). The electrodes (Unisense, Denmark) are made of glass with a 6 cm long tip that was inserted into a hyperdermic needle (diameter 1.1 mm, length 50 mm) and had a response time shorter than 10 s. Signals were amplified and transformed to mV by a picoamperemeter, digitalized by an analogue/digital converter (ADC 216, Unisense, Denmark) and recorded using the software PROFIX (Unisense, Denmark). High-resolution (1 mm) vertical profiles of oxygen concentrations across the sediment/water interface were accomplished for MUC cores by use of a micromanipulator down to a maximum sediment depth of 5-6 cm.

Alkalinity was determined on a 1 mL aliquot of sample by titration with 10 or 50 mM HCl. The pH measurements were performed using a Mettler Toledo micro-electrode. The samples were titrated with a digital burette to a pH of approximately 3.8 and both titration volume and final pH were recorded. The alkalinity was calculated using a modified equation from Grasshoff et al. (1999).

A QuAAtro continuous segmented flow analyzer (Seal Analytical) was used for the (1) determination of the dissolved inorganic carbon concentrations and (2) simultaneous determination of the pore-water concentrations of ammonium, phosphate and silica. Subsamples for the determination of *dissolved inorganic carbon (DIC)* concentrations were spiked with 30 % hydrogen peroxide and then acidified with 1.5 N sulfuric acid to pH <1 to force all carbonate components into the CO_2 gas phase. DIC concentrations were determined photometrically by inverse extinction at 520-550 nm.

For the determination of *ammonium, phosphate and silica*, ideally 2 mL of the pore water were acidified with 30 µL double sub-boiling distilled HCl and rested overnight. *Ammonium (NH_4^+)* was analyzed fluorimetrically using the ortho-phtalaldehyde (OPA) method. *Phosphate (PO_4^{3-})* was determined using the molybdenum blue method (Grasshoff et al., 1999). Ammonium molybdate solution was added to the pore water aliquot and spiked with ascorbic acid solution. The phosphomolybdate complex was reduced to molybdenum blue and measured photometrically. *Silica (Si)* was also measured photometrically as a silica molybdate complex.
E_H and pH were determined by Hamilton punch-in electrodes in parallel intervals to the pore-water and sediment sampling.

Pore-water aliquots for the determination of *sulfate (SO_4^{2-}) and chloride (Cl^-)* concentrations were collected for shore based analyses and stored at 4°C. Samples containing hydrogen sulfide were fixed with 5 % ZnAc.

Pore-water cations (Al, Ba, Ca, Mg, Mn, Fe, Si, P, and S) will be analyzed in our home-laboratory at the AWI using ICP-OES. Subsamples of approximately 1 mL of pore water were acidified with double sub-boiling distilled hydrochloric acid (HCl).

For *pore-water trace metal* analyses 1 mL subsamples were acidified with sub-boiling distilled HNO_3 and will be analyzed in the home laboratory at Oklahoma State University using an ICP-MS.

Samples for ^{210}Pb analysis were collected from MUC cores at 1 cm intervals throughout the top 25 cm and stored at 4°C for the determination of sedimentation rates at the AWI.

Sediment samples for *total organic/inorganic carbon, solid-phase sulfur, trace metal, and iron species* samples were collected from GC and MUC cores for shore-based analysis, including

concentrations and stable isotope composition of total organic, inorganic carbon and solid-phase sulfur and iron species. Samples were collected with cut-off 3 or 10 mL syringes or 50 mL centrifuge tubes, respectively. Sediment samples were stored frozen at -20°C. Trace metals will be determined using a multi-acid digestion and measured on an ICP-MS. Stable iron isotopes will be extracted via a multi-leaching procedure and resin and quantified using a high mass resolution multiple collector (MC)-ICP-MS (Arnold et al., 2004; Henkel et al., 2016, 2018).

5.4.3 Preliminary Shipboard Results

Results of geochemical pore-water analyses are described below for sediments from five selected cores; two sampled using a multi-corer (MUC) and three gravity cores (GC). The results at the selected sites highlight the variable pore-water geochemistry throughout the working area of expedition SO260.

At site GeoB22706, the pore-water profile of dissolved iron (Fe^{2+}) shows a maximum at approximately 8 cm suggesting microbially mediated iron reduction in this zone (Fig. 5.5.1). Alkalinity and dissolved inorganic carbon (DIC) profiles are almost identical and show increasing concentration with sediment depth. Phosphate (PO_4^{3-}) increases with depth in the uppermost approximately 8 cm with a maximum in the zone of iron reduction indicating the release of phosphate into the pore water during iron reduction.

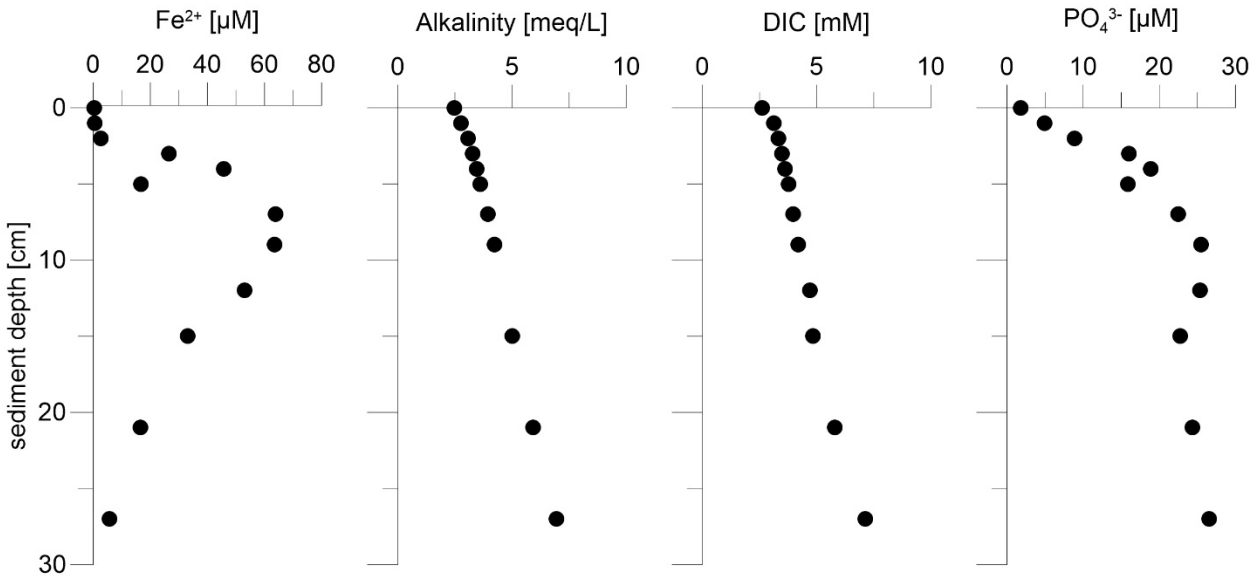

Fig. 5.5.1 Pore-water geochemistry from site GeoB22706-1. The core is located on the lower terrace in the Mar del Plata canyon off Argentina (see Fig. 3.1.1 for location).

Oxygen is depleted within the uppermost approximately 1.5 cm sediment depth at site GeoB22708 (Fig. 5.5.2). The pore-water dissolved iron profiles (measured in pore water from two adjacent MUCs) show an increase in iron with depth up to approximately 70 µM starting at 3.5-4 cm down to 20 cm below the seafloor. Alkalinity and DIC profiles display similar trends, except for one DIC outlier at the surface, with only minimal concentration increase with depth. Phosphate increases slightly with depth with maximum concentration of 10 µM at 12.5 cm.

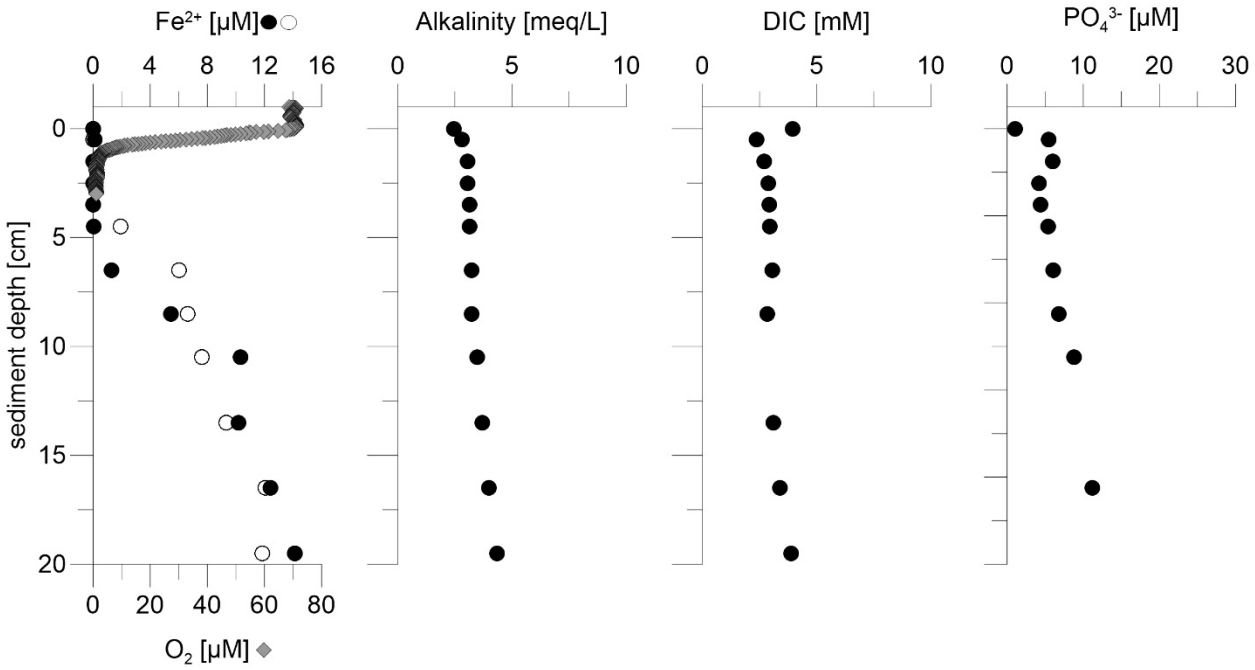

Fig. 5.5.2 Pore-water geochemistry from site GeoB22708-3. The core was taken at the Biogeochemistry Site I off Argentina (see Fig. 3.1.1 for location). Dissolved iron was measured in pore-water samples from two MUC cores adjacent to each other.

At site GeoB22702-3, dissolved iron occurs throughout the cored sediments with a minimum of 2 µM at 180 cm sediment depth; below this depth Fe^{2+} increases with depth (Fig. 5.5.3). Alkalinity and DIC show very similar pore water profiles with slight increase in concentration with sediment depth reaching concentration of 20 meq/L and 20 mM, respectively. The low alkalinity and DIC concentrations throughout the analyzed sediment column are indicative of the continual remineralization of buried organic matter through microbial processes at low rates – likely due to the low amounts organic matter or its recalcitrant nature (Riedinger et al., 2014). The phosphate profile shows an increase in concentration with sediment depth (Fig. 5.5.3). These concentrations are indicative of reducing conditions in the sediments where buried iron minerals get diagenetically altered in the anoxic zone and phosphate is liberated into the surrounding pore water (Delaney, 1998).

In contrast to sediments recovered from a drift body at site GeoB22702-3, the sediments located at the lower terrace of the Mar del Plata canyon off Argentina, site GeoB22706-2, contain high amounts of hydrogen sulfide (HS^-) with the maximum located at approximately 270 cm depth (Fig. 5.5.4).

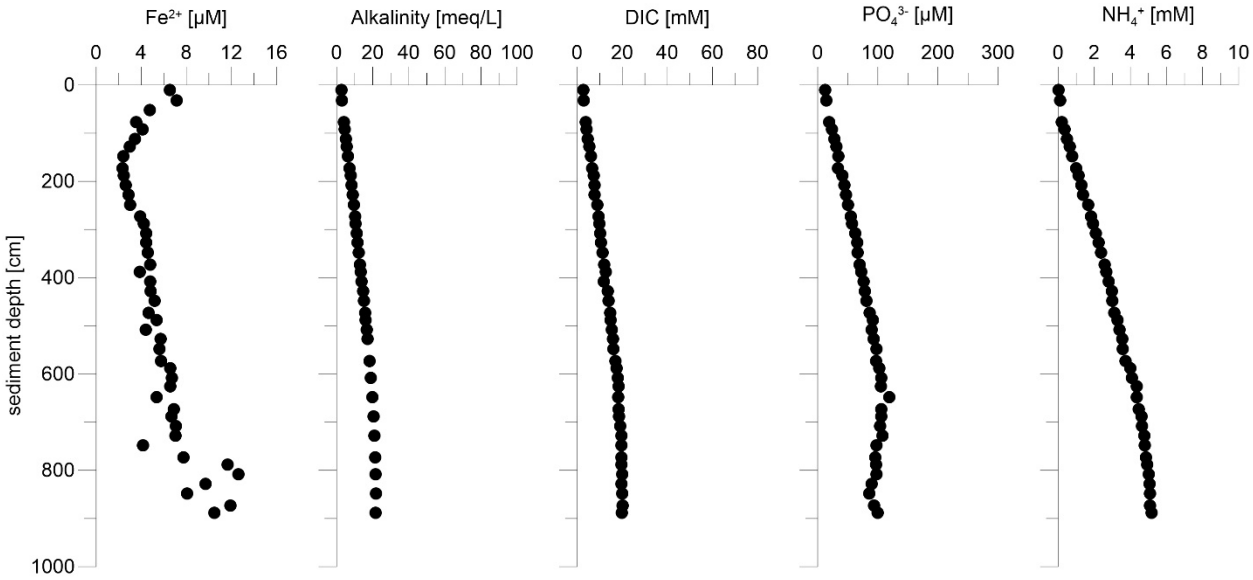

Fig. 5.5.3 Pore-water geochemistry from site GeoB22702-3. The core was taken in a drift body off Argentina (see Fig. 3.1.1 for location).

The iron pore-water concentrations indicate the occurrence of dissolved iron in the uppermost sediment layers, which is in good agreement with the surface sediment profile of Fe^{2+} at this site (Fig. 5.5.1). Below the sulfidic zone Fe^{2+} increases again. The iron concentrations only show elevated values in the shallowest and deepest samples indicative of a narrow zone of microbial iron-reduction above and below the sulfidic zone (Riedinger et al., 2014). Alkalinity concentrations increases with depth and the profile gradient becomes more linear at approximately 270 cm depth. This alkalinity kink, concurrent with the maximum of hydrogen sulfide suggest the location of the sulfate-methane transition at approximately 260-280 cm sediment depth.

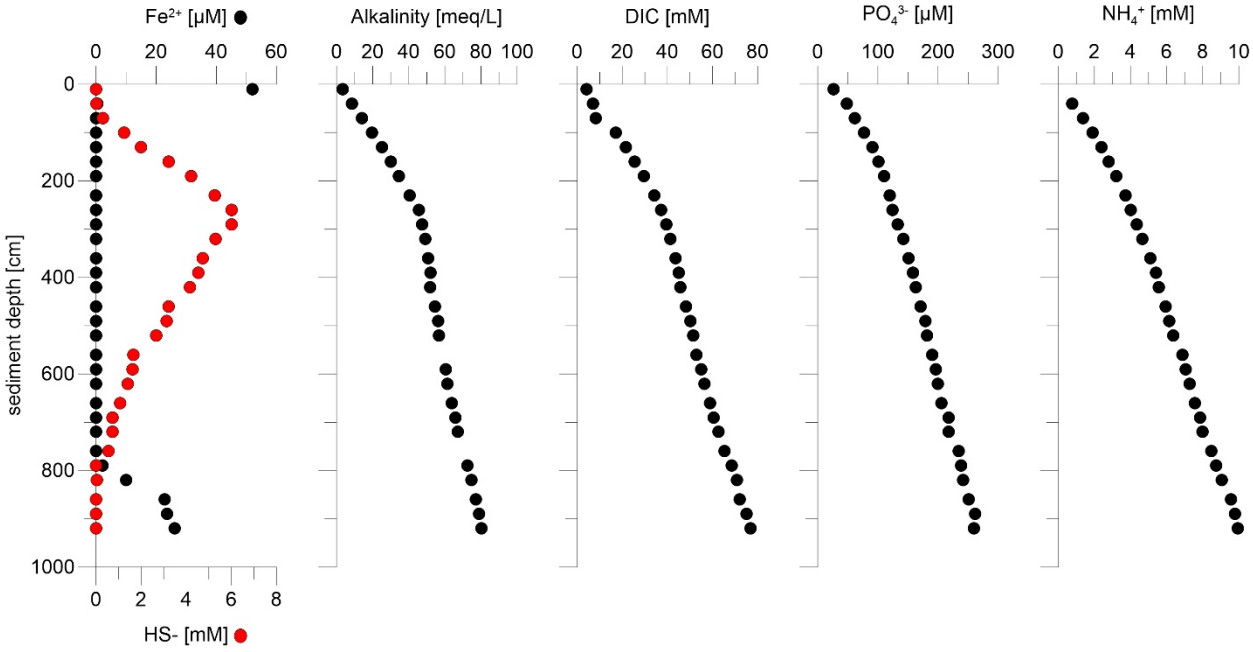

Fig. 5.5.4 Pore-water geochemistry from site GeoB22706-2. The site is located at the lower terrace of the Mar del Plata canyon off Argentina (see Fig. 3.1.1 for location).

With the exception of one data point at approximately 60 cm, the DIC pore water profile shows the same trend as the alkalinity profile. The corresponding depths of sulfide, alkalinity, and DIC profiles suggest a depth for the sulfate-methane transition at approximately 270-290 cm sediment depth. The phosphate and ammonium pore water profiles show a similar trend to alkalinity and DIC with increasing concentrations with depth.

At site GeoB22708-1, below approximately 400 cm hydrogen sulfide concentrations (HS^-) increase with depth with a maximum at approximately 750 cm (Fig. 5.5.5). Dissolved iron occurs above the sulfidic zone with a maximum at 100 cm and is depleted within the sulfidic zone. Alkalinity concentrations increase with depth down to about 750 cm depth, staying almost linear below this depth. The DIC profile shows a very similar profile compared to alkalinity. The described pore-water profiles indicate a sulfate-methane transition zone at about 750 cm depth. The phosphate and ammonium concentrations increase with depth, which suggests a release of phosphate to the pore water in the deeper sediments as a result of ongoing diagenetic alteration processes in the deeper buried sediments.

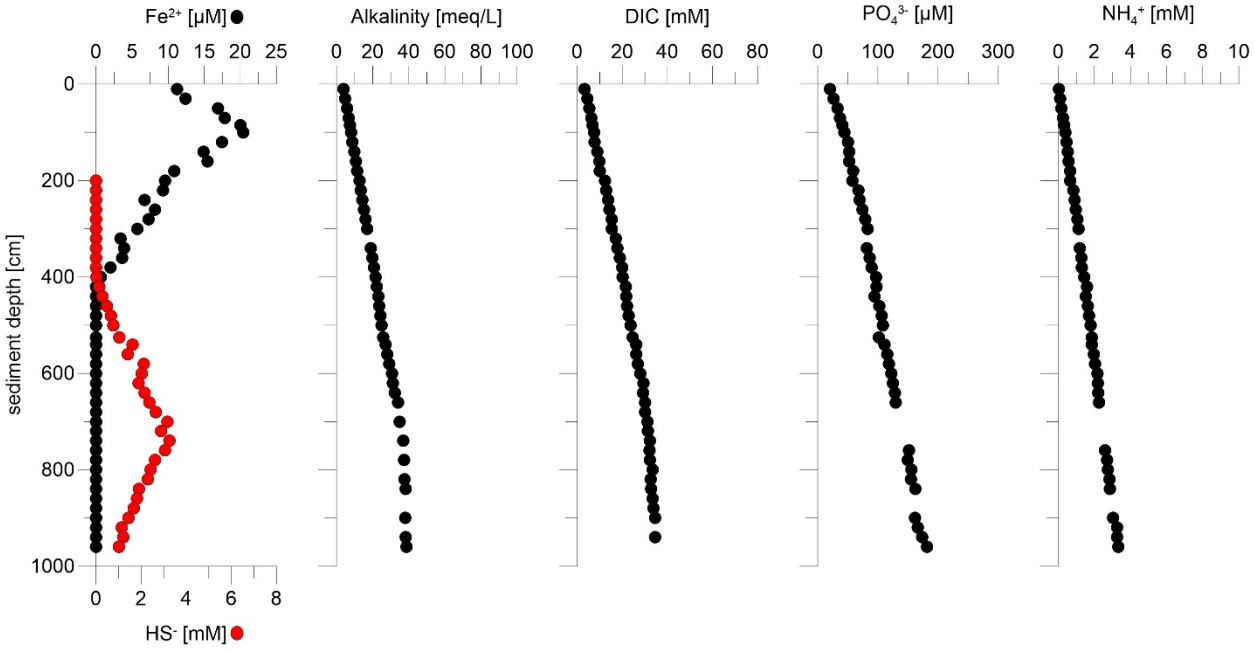

Fig. 5.5.5 Pore-water geochemistry from site GeoB22708-1. The core was taken at the Biogeochemistry site I off Argentina (see Fig. 3.1.1 for location).

5.6 Microbiology and Organic Geochemistry

(D. Aromokeye, A. Schnakenberg, S. Coffinet)

5.6.1 Introduction

The aim of the microbiology and organic geochemistry team during expedition SO260 involved (I) elucidating the various metabolic pathways and microbial communities that mediate iron and manganese reduction below the sulphate-methane transition (SMT), (II) identifying the carbon sources of iron and manganese reducing microbial communities below the SMT and (III) investigating how variations in the depositional regime and other environmental factors control the distribution, abundance and composition of benthic archaeal communities in marine sediments.

Biogeochemical cycling of iron and manganese in deep sea sediments

Microbial degradation of organic matter in sediments occurs along a cascade of electron accepting processes thereby often separating processes in marine sediments into distinct geochemical zones (Froelich et al., 1979). For example, metal oxide reduction (iron and manganese) typically occurs in the surface sediments, which transitions into a zone of sulphate reduction. Directly below the sulphate reduction zone is the methanic zone, where biological methane formation – mainly from CO_2 reduction (Whiticar et al., 1986) – predominates due to the depletion of other electron acceptors for organic matter degradation. Methane, however, diffuses upward in the sediment, such that about 90 % of methane produced in the methanic zone is oxidized with sulphate in the SMT via anaerobic oxidation of methane (AOM) by a consortium of anaerobic methanotrophs and sulphate reducing bacteria (e.g., Boetius et al., 2000). In contrast to this well-established sedimentary geochemical zonation model, elevated concentrations of dissolved iron and manganese in the methanic zone have been observed in a number of highly accumulating sediments (e.g., März et al., 2008; Oni et al., 2015) – including some of the stations of interest within the Argentine Basin (Hensen et al., 2003; Riedinger et al., 2014, 2017) and have been linked to microbial activity.

Currently, the pathways and mechanisms that drive the microbial reduction of metal oxides in methanic sediments are a subject of debate in deep sea biogeochemistry research. Riedinger et al. (2014) provided first inorganic geochemical evidence that this deep metal oxide reduction is likely linked to AOM in the Argentine Basin and this has been further supported by studies from other high accumulation marine environments (Egger et al., 2015, 2017) and from laboratory incubation experiments (Ettwig et al., 2016; Bar-Or et al., 2017). However, other potential pathways such as reduction during fermentation, respiration of fermentation intermediates and chemolithotrophic reduction during oxidation of sulphur compounds could also lead to microbial iron reduction and will also be investigated in the framework of our research.

Impact of organic matter quality and availability on biogeochemical zonation and microbial communities in marine sediments

Continental margins constitute a major sink of organic matter (OM), mainly coming from riverine transport of terrestrial OM and high primary production in the coastal surface waters. Once deposited, the OM serves as the main carbon and energy provider for the sedimentary microbial communities. The type and bioavailability of the OM will thus have a large impact on the structuring of the microbial communities within the sediment as well as on the biogeochemical zonation. Previous studies in the Argentine Margin showed that OM content was mainly

originating from reworked material brought by lateral transport downslope and deep bottom currents (Hensen et al., 2000). Riedinger et al. (2014) postulated that the mainly refractory character of the OM in this setting was one of the key factors for iron reduction to occur in the deeper parts of the sediment. During this cruise, samples for comprehensive characterization of the OM in the interstitial water and particulate phases of the sediment will be taken to test this hypothesis further.

5.6.2 Objectives

Our work on this cruise is mainly directed towards exploring the various mechanisms that could drive the biological reduction of metal oxides in the 'deep' methanic zone. We are particularly interested in understanding how microbial community composition drives the various geochemical processes in these methanic sediments, especially from the previous biogeochemistry sites from the M78 cruise where dissolved iron and manganese were detected in the methanic zone. Our approach will involve (I) sampling sediment cores for microbial community composition, microbial lipid and organic matter profiling and (II) carrying out preliminary shipboard incubation experiments with methanic sediments from previous GeoB13820 site (Riedinger et al., 2014; core GeoB22709 from SO260-1) to have a first understanding into the pathways of microbial iron and manganese reduction. In addition, specific samples will be taken in the framework of the ERC grant *ZOOMecular* (ERC Advanced Grant AdG 670115 to Prof. Dr. Kai-Uwe Hinrichs) with the aim to shed light on the spatial distribution of the microbial communities in the SMT and methanic zone and their potential association with minerals.

Specific research questions for the microbiology and organic geochemistry working group during the SO260 cruise include the following:

1. Which microbial communities drive the biogeochemical processes – in particular metal reduction – in the shallow and deeper sedimentary subsurface?
2. What is the potential importance of electron acceptors other than sulphate (i.e. Fe and Mn oxides) for anaerobic oxidation of methane below the SMT, as previously suggested in these sediments by geochemical studies?
3. How does the OM availability impact the biogeochemical processes and the microbial community activity?
4. What is the carbon metabolism of the different microbial communities related to metal reduction? How does this process affect the carbon cycle, notably methane cycling, in the subsurface?

5.6.3 Methods

During this cruise, water column, pore-water and solid-phase samples were collected from 6 CTD deployments, 10 multicore deployments (MUC), 18 gravity cores (GC), 2 grab and 2 MeBo deployments. Details and information on intended purpose of collected samples are detailed in Appendices 5 and 6.

In addition, incubation experiments were carried out to preliminarily explore the potential pathways for manganese and iron reduction below the SMT in one of the biogeochemical sites from the previous cruise M78 where Fe-AOM was suggested (Riedinger et al., 2014). Specific microbiology cores were collected from three sites (GeoB22708, GeoB22709 and GeoB22734). The first microbiology specific GC was taken from the previous GeoB13863 site (GeoB22708 from SO260-1) where Fe-AOM was suggested. However, the retrieved core did not show similar dissolved iron and manganese profiles as the core from cruise M78 from the same coordinates (see Figure 5.6.1). Therefore, we retrieved another core from the nearby site GeoB13820 (GeoB220709 from SO260-1), from which concentrations of dissolved iron and manganese were detected in the pore water (Figure 5.6.1).

Pore-water and solid-phase sampling from sediments

MUC sampling: ca. 6 ml of pore water were taken for dissolved organic matter (DOM) characterisation (complex organic matter, volatile fatty acids) and isotopic composition (δ^{13}C-DOC and δ^{13}C-DIC). Samples were transferred in 2 ml combusted vials capped with a Teflon lid and stored at -20 °C in N_2 flushed Schott bottles sealed with thick butyl stoppers. About 50 ml of sediment were taken for OM and archaeal lipid analysis. 10 ml of sediment were collected for DNA extraction and subsequent Next Generation Sequencing analysis (NGS). All samples were taken in a temperature controlled laboratory (4°C) and stored in cryo-stable Falcon tubes at -20 °C immediately after recovery in order to preserve the *in situ* microbial community distribution.

Gravity core sampling: Samples of about 50 ml of sediment were taken for OM and archaeal lipid analysis in every working half. Sampling depths were determined based on the lithology and the geochemical profiles, when available. On average, one sample for OM analysis was taken every meter. 10 ml of sediment were collected for DNA extraction and subsequent NGS analysis with an average resolution of 30 cm. When available, ca. 6 ml of pore water were taken for OM analysis every 1.5 to 2 meters. Samples were transferred in 2 ml combusted vials capped with a Teflon lid and stored at -20°C in N_2 flushed Schott bottles sealed with thick butyl stoppers. On selected cores (GeoB22734-3 and GeoB22735-1), 3 ml of sediment was sampled at ca. 50 cm resolution with autoclaved cut syringes, transferred into Falcon tube filled with 8 ml of 2,5 % NaCl, 2 % formaldehyde solution and stored at 4°C for on shore cell counts. In the framework of the *ZOOMecular* project (ERC Advanced Grant AdG 670115 to Prof. Dr. Kai-Uwe Hinrichs), 30 cm long and 1 cm large double-L channels were sampled in limited and targeted sections on cores GeoB22708-1, GeoB22709-2 and GeoB22734-2. All samples were taken in a climatized laboratory (4°C) and stored in cryo-stable Falcon tubes at -20°C immediately after recovery in order to maintain the *in situ* microbial community distribution.

Microbiology-specific gravity core sampling: three cores (GeoB22708-2, GeoB22709-2 and GeoB22734-3) were retrieved, cut in 1 m sections and kept at 4 °C as whole round cores for microbiology purposes. Sequentially, to limit the exposure time of the core to room temperature, the 1 m sections of each GC were brought to the geophysical lab for magnetic property measurements. Pore water was then extracted by inserting rhizon samplers in drilled holes in the whole round cores every 50 cm. 3 ml of pore water were sampled for iron and manganese analysis on board. Ca. 2 ml of pore water were transferred in 2 ml combusted vials with a Teflon lid for

onshore δ^{13}C-DIC analysis. Approximately 10 ml of pore water were transferred in 10 ml combusted serum vials sealed with thick butyl stoppers. All samples for DOM analysis were stored at -20°C in N_2 flushed Schott bottles sealed with thick butyl stoppers. Rhizon sampler holes were closed with thick rubber tape. Cores GeoB22708-2 and GeoB22734-3 were then stored as 1 m sections in the 4°C container for further onshore processing and analysis. GeoB22709-2 was directly sectioned at 4°C into 25 cm sections, stored away in anoxic 2.6 liter sterile glass jars under N_2 (99.999% purity, Linde, Germany) headspace at same temperature and transported back to Bremen for laboratory based incubation experiments. During the process, 50 ml of sediment was taken every 25 cm and stored at -20°C for future analysis of microbial community analysis. In addition, 50 ml of sediment was sampled every 50 cm and stored at -20°C for OM and archaeal lipid analysis and 3 ml of sediment were sampled with autoclaved cut syringes and transferred into falcon tubes filled with 8 ml of 2.5 % NaCl, 2 % formaldehyde solution and stored at 4°C for onshore cell counts.

MeBo core sampling: Whole round core sections of ca. 10 cm were cut every 2.5 m (when core recovery was sufficient). The outer part (at least 1 cm) was discarded to avoid contamination related to the drilling procedure and the inner part of the core was sampled with 10 ml cut syringes. Samples were then frozen at -20°C and shipped back for microbiology and organic geochemistry investigations.

Water column sampling

Water from different depths within the water column was sampled with the CTD/Rosette system. For each depth, approximately 400–500 ml water was filtered in duplicates using a Nucleopore polycarbonate membrane filter (Whatman) after sterilizing the filter device with 70% ethanol (see Table 5.6.1 for exact depth sampled at each CTD station). Each filter was stored in 2 ml tubes at -80°C and will be transported back to the home laboratory, where DNA will be extracted and subsequent molecular studies will be performed.

Table 5.6.1 Actual depths from which 1 L of sea water was sampled from every CTD/Rosette event and filtered using a Nucleopore polycarbonate membrane filter for future microbial community profiling.

GeoB22701-1 (depth in metres)	GeoB22710-1 (depth in metres)	GeoB22718-2 (depth in metres)	GeoB22719-1 (depth in metres)	GeoB22722-1 (depth in metres)	GeoB22722-2 (depth in metres)
10	10	20	10	20	10
40	40	40	20	40	20
60	60	60	40	60	40
80	80	80	60	80	60
100	100	100	80	100	80
125	150	150	100	150	100
150	200	200	150	200	150
200	1082	1352	200	1039	200

Dissolved manganese measurement

Concentrations of dissolved Mn^{2+} were measured via a photometric assay based on the complexation of the ions by formaldoxime, which subsequently changes its colour from colourless to pink and can be quantified at a wavelength of 450 nm. 1 ml of an original sample or diluted (with MilliQ water) sample was immediately mixed with 50 µl formaldoxime reagent (1 g formaldoxime and 0.5 ml 37% (w/v) formaldehyde in 25 ml MilliQ water) and 90 µl 30 %

ammonia. The solution was then mixed thoroughly and let to react at room temperature for 2 min. Subsequently, 50 µl 0.1 M EDTA (pH 8) and 100 µl hydroylamine hydrochloride were added, mixed thoroughly and followed by a 10-min centrifugation step at 14000 rpm and 4 °C. This allows the EDTA to destabilize complexes formed of formaldoxime with Fe^{2+}. Then, the extinction of the samples was measured with a biochrom Libra S12 spectrophotometer at 450 nm wavelength. A standard was prepared with 179.9 mg/l $MnCl_2$ and 5 ml concentrated sulfuric acid in MilliQ water with a final concentration of 50 mg/l Mn^{2+} and measured at the beginning and at the end of the cruise.

Iron reduction incubation experiments

Incubation experimental set-up: These experiments specifically aimed at testing the potential for microbial iron reduction linked to heterotrophic carbon substrates such as glucose which can be fermented; and acetate, which is hardly fermentable but can be metabolised via a respiratory mechanism. Sediments used for these experiments were taken from the depth where the highest concentration of dissolved iron was measured in core GeoB22709-2 (714-739 cm; Figure 5.6.1). Anoxic slurries were prepared using 1 volume sediment and 3 volumes of artificial sea water (ASW; composition [L^{-1}]: 26.4 g NaCl, 11.2 g $MgCl_2$, 1.5 g $CaCl_2.2H_2O$ and 0.7 g KCl). Several bottles were prepared with a final volume of 50 ml and made completely anaerobic by flushing each bottle with N_2 for 15 minutes (99.999%, Linde, Germany). In order to be able to follow substrate turnover to CO_2 and/or CH_4, together with being able to track incorporation of carbon from substrate into the biomass of active microorganisms involved in substrate turnover, stable isotope labeled glucose and acetate were used for these experiments. ^{13}C-glucose and ^{13}C-acetate were added to selected bottles to a concentration of 1 and 5 mM, respectively. The effect of exogenous iron oxides on microbial iron reduction was studied by adding poorly crystalline lepidocrocite (LanXess, Germany) or crystalline magnetite (LanXess, Germany) (30 mM each) to incubations. Finally, the bottles were incubated in the dark at 4°C, 10°C, 20°C and 30°C to study the influence of temperature on microbial iron reduction as well. Detailed information of the various treatments is given in Table 5.6.2. Microbial iron reduction was monitored for 24 days during the duration of cruise SO260 by measuring Fe(II) produced in the slurries over time.

Table 5.6.2 Summary of iron reduction incubation experiments. Treatments were made in triplicates and in 4 batches such that each set was incubated at 4°C, 10°C, 20°C and 30°C using sediments from the depth interval 714-739 cm of GC GeoB22709-2.

Treatment	^{13}C-Glucose (1mM)	^{13}C-Acetate (5 mM)	Lepidocrocite (30 mM)	Magnetite (30 mM)
I	+	-	+	-
II	+	-	-	+
III	+	-	-	-
IV	-	-	-	-
V	-	+	+	-
VI	-	+	-	+
VII	-	+	-	-

Analytical measurements: During the course of the shipboard iron reduction experiment, samples were collected every 5 days during 24 days for various measurements. As a proxy for active microbial iron reduction, measurement of Fe(II) was done at each time point. This was done by

measuring HCl extractible Fe(II) from the slurries. Therefore, collected samples (200 µL) were mixed with 0.5 M HCl (800 µL) and stored in the fume hood at room temperature for 24 hours before measurement of Fe(II). While the method has been shown to be incapable of giving an accurate determination of total Fe(II) concentrations in the sediment, it is reliable to have a conservative estimate on the amounts of Fe(II) formed in the slurries (Jensen et al., 2003). After 24 hours of HCl extraction, samples were centrifuged (15300 g, 10 mins). Fe(II) concentrations were subsequently determined spectrophotometrically at 562 nm wavelength following Viollier et al (2000). This was done by adding 100 µl of supernatant from each sample to the ferrozine reagent. Samples were diluted into concentrations that fit the standard curve absorbance spectrum with 0.5 M HCl prior to measurement. In addition to Fe (II) measurements, samples were collected for gas measurement at day 5, day 10 and day 20 by taking 1 ml of headspace gas which was directly stored in gas tight and N_2 filled 15 ml glass vials. These samples will be measured on a gas chromatography-isotope ratio mass spectrometry back at the home laboratory to track the conversion of added substrates (^{13}C-glucose or ^{13}C-acetate) into $^{13}CO_2$ and/or $^{13}CH_4$. 2 ml of slurry from day 15 and day 24 were collected and frozen at -20°C, back at home, these samples will be centrifuged to retrieve pore water to measure concentrations and isotopic composition of dissolved organic matter in the slurries. After collecting samples for analytical measurements at day 24, the incubation experiment was stopped and the rest of the slurry volume was immediately frozen at -80 °C. Back onshore, molecular stable isotope probing of RNA and lipids will be done to examine the flow of carbon from glucose and acetate during microbial iron reduction, giving the possibility to identify active members of the microbial communities participating in these processes.

Manganese reduction incubation experiments

For the purpose of studying the deep manganese oxide reduction in the sediment, a sediment slurry incubation experiment amended with MnO_2 and different reduced sulfur compounds was carried out (Table 5.6.3).

Table 5.6.3 Incubation set-up for reduced sulphur compound-dependent MnO_2 reduction.

Condition	NaN_3 (20 mM)	MnO_2 (30 mM)	S_8 (30 mM)	FeS_2 (30 mM)	$Na_2S_2O_3$ (30 mM)
1					
2	+	+	+		
3	+	+		+	
4	+	+			+
5		+	+		
6		+		+	
7		+			+
8		+			
9			+		
10				+	
11					+

For each single incubation, 10 ml of sediment from GeoB22709-2 in the depth of 914-939 cm were mixed with 30 ml artificial seawater (ASW; 20 g/l NaCl, 3 g/l $MgCl_2 \cdot 6\ H_2O$, 0.2 g/l KH_2PO_4, 0.25 g/l NH_4Cl, 0.5 g/l KCl 0.15 g/l $CaCl_2 \cdot 2\ H_2O$) and incubated in a 60 ml serum bottle under a

N_2/CO_2 (80:20, Linde, Germany) headspace at 10 °C. The amendments were made according to Table 5.6.3. Every condition was prepared in triplicates. Samples for direct photometric determination of dissolved manganese, inductively coupled plasma-optical emission spectrometry (ICP-OES of Mn, Fe, S in the liquid phase) and ion chromatography (SO_4^{2-} concentration in the liquid phase) as well as sediment for DNA extraction were collected on Day 0, 1, 2, 3, 4, 5, 7, 10, 15, 20 and 24 of incubation. Therefore, 1.8 ml of slurry was taken with an anoxic syringe and centrifuged for 20 min at 4 °C and 14000 rpm. For ICP-OES analysis, 500 µl of supernatant were stored in 4.5 ml of 0.18 M nitric acid at 4°C. For ion chromatography, 200 µl of supernatant were stored in 200 µl 5 % zinc acetate at 4°C. These measurements will be done onshore. The remaining sediment was stored at -20°C for subsequent DNA extraction.

5.6.3 Preliminary Shipboard Results and Discussion

Fe^{2+} and Mn^{2+} concentrations in microbiology cores GeoB22708-2, GeoB22709-2 and GeoB22734-3

The concentration of dissolved iron and manganese was measured over depth in all GCs taken for microbiology specific purposes (Figure 5.6.1). The Mn^{2+} profile of core GeoB22709-2 is similar to the profile of site GeoB13820 sampled at the same location during cruise M78 in 2009 (Riedinger et al., 2014). It revealed a peak in Mn^{2+} concentration in the suboxic zone above the SMT at around 225 cm bsf (16 µM; Figure 5.6.1). At the SMT, the concentration decreased with a minimum of 4.33 µM at 425 cm bsf and increased again in the methanic zone. The concentration peaked at 725 cm bsf (45 µM) and at 925 cm bsf (49 µM). The latter was the highest concentration found in the three cores. Interestingly, the Mn^{2+} profile of core GeoB22708-2, was significantly different from the corresponding core GeoB13863 profile taken during cruise M78 (Riedinger et al., 2014). Core GeoB13863 showed a maximum in concentration at 800 cm bsf (8 µM) in the methanic zone whereas dissolved Mn was not detectable in the SMT (400-550 cm bsf). Core GeoB22708-2, on the other hand, differed in the profile with only one maximum in the suboxic zone above the SMT at 185 cm bsf (10.33 µM) and low concentrations in the range of 2.2 µM – 4.2 µM between 435 and 885 cm bsf. The dissolved Mn^{2+} profile of core GeoB22734-3 (Figure 5.6.1) did not show the typical maximum in the suboxic zone above the SMT and instead only revealed one maximum at 643 cm bsf with a significantly lower concentration (12.2 µM) than measured at the similar depth of core GeoB22709-2 (625 cm bsf, 39.33 µM). At each site, the Fe^{2+} profile closely follows the Mn^{2+} one.

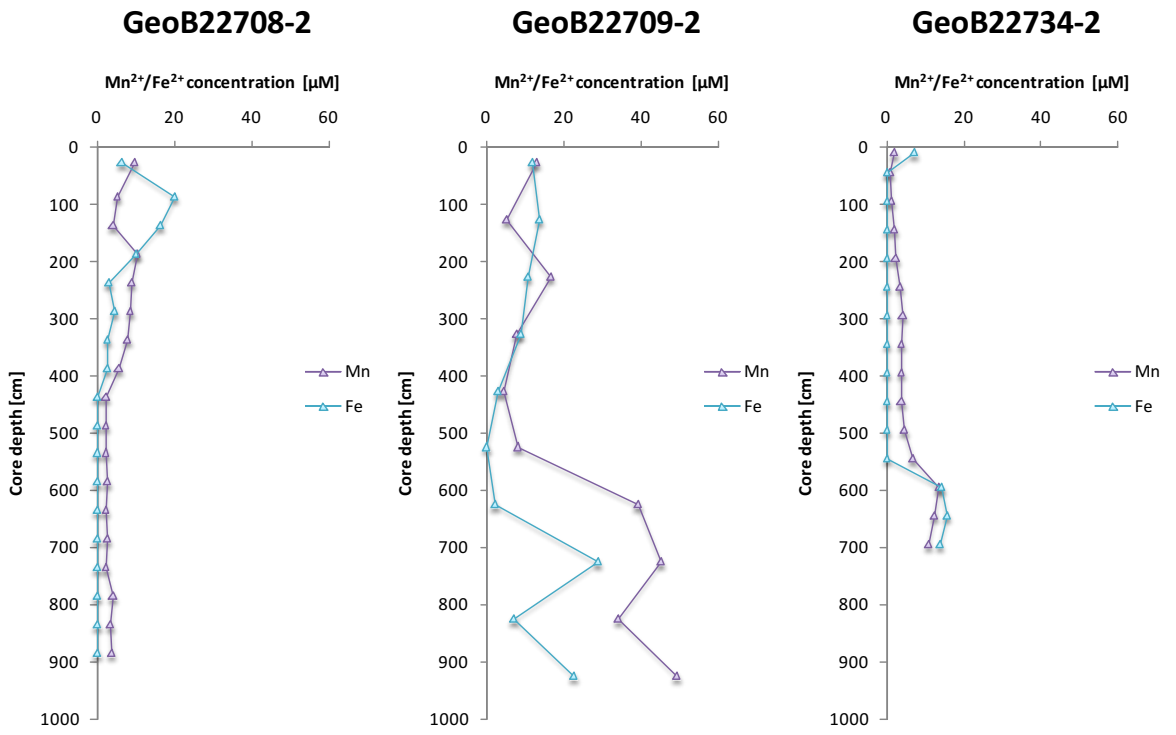

Fig. 5.6.1 Mn^{2+} and Fe^{2+} concentrations in the pore water of microbiology-specific gravity cores GeoB22708-2, GeoB22709-2 and GeoB22734-3. Cores GeoB22709-2 and GeoB22734-3 are particularly interesting due to the detection of elevated dissolved iron and manganese concentrations in the deep sediments. Dissolved iron concentrations in the cores were obtained and shown by courtesy of the geochemistry team.

Microbial iron reduction as an active process in the deep sediments of site GeoB22709-2

Microbial iron reduction, observed by increasing concentrations of HCl extractible Fe(II) in the slurries was evident in the incubation experiments across all temperatures (4, 10, 20 and 30°C; Figures 5.6.2 and 5.6.3). Therefore, our shipboard experiments support the geochemical findings that show imprints of Fe^{2+} in the pore water within the deep methanic zone linked to a microbial reduction of Fe(III) (Riedinger et al., 2014; Figure 5.6.1).

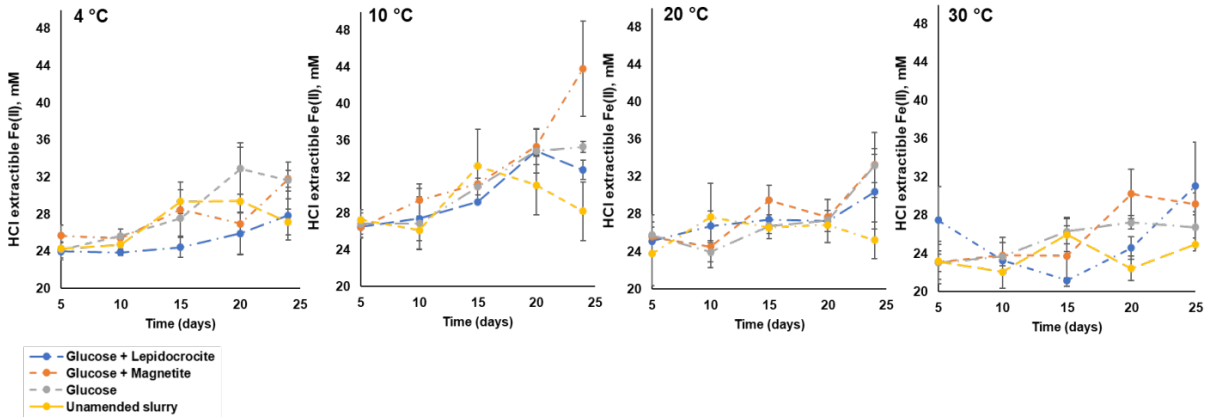

Fig. 5.6.2 Time course of microbial iron reduction with glucose as carbon substrate at varying temperatures. Microbial iron reduction was more favourable at 10°C than at other temperatures.

In general, more Fe(II) was measured in treatments amended with acetate compared to glucose across all temperatures (Figures 5.6.2 and 5.6.3), suggesting that acetate might be a more suitable substrate for microbial iron reduction in these sediments. The implication is that a microbial respiration of acetate is one potential mechanism that possibly mediates the production of dissolved Fe detected in the pore water *in situ*. However, the possibility of this mechanism needs to be further tested by onshore measurements of acetate concentrations.

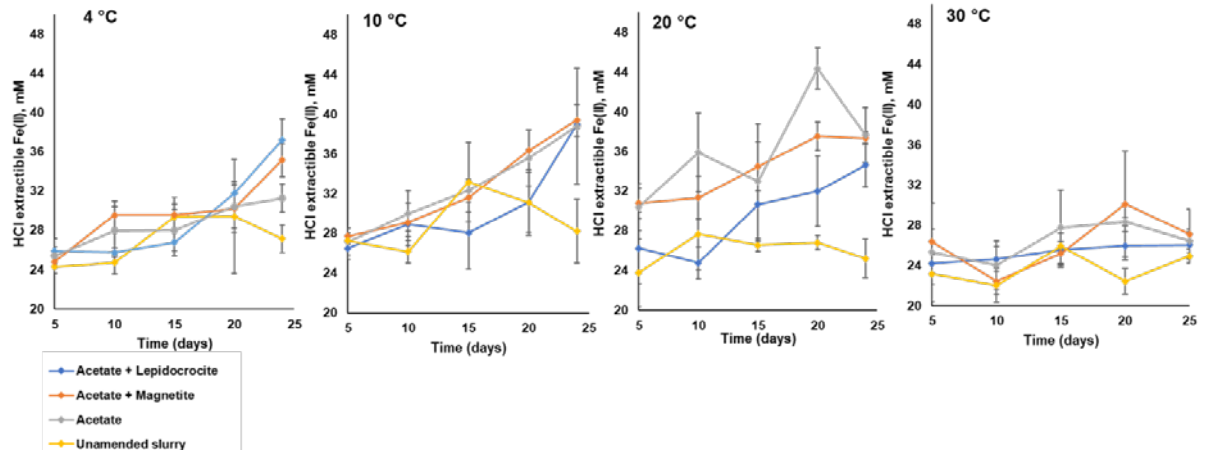

Fig. 5.6.3 Time course of microbial iron reduction with acetate as a carbon substrate at varying temperatures. Microbial iron reduction with aceate was more favourable at 20 ºC than at other temperatures.

Microorganisms prefer poorly crystalline iron oxides to crystalline forms due to easier accessibility and thermodynamic favourability (Weber et al., 2006), therefore poorly crystalline iron oxides have been widely used to test the potential for microbial iron reduction in incubations from sedimentary settings (Roden and Lovley, 1993; Zhang et al., 1999; Vandieken et al., 2006; Hori et al., 2015). Within the time-frame of these experiments, we did not observe a significant boost in produced Fe(II) when poorly crystalline lepidocrocite was added in comparison to other

amended treatments. In contrast, incubations amended with crystalline magnetite or amended with only glucose or acetate produced more Fe(II) (Figures 5.6.2 and 5.6.3). Nevertheless, addition of the iron oxides and carbon substrates stimulated microbial iron reduction above the levels observed in the unamended sediment slurry, but only after 15 days indicating that the sediment is rich in inherent iron(III) oxides that are apparently being actively reduced via a microbial process, leaving imprints in the pore water (Figure 5.6.1).

As indicated by Fe(II) concentrations after 24 days, temperature seemed to play a role in the rate of microbial iron reduction (Figures 5.6.2 and 5.6.3). More Fe(II) was measured at 10°C and 20°C in comparison to 4 °C and 30°C. This temperature effect on the rate of iron reduction is however likely governed by underlying changes in the microbial community composition and consequently community adaptation to temperature. *Geobacter spp* and *Desulfuromonas spp* are well known as respiratory iron reducers in terrestrial environments and surface marine sediments respectively (Vandieken et al., 2006; Hori et al., 2010, 2015). However, little is known about microbes mediating iron reduction in deep methanic sediments. Stable isotope probing experiments of RNA and lipids back at home will enable us to identify the active iron reducers during the 24 day incubation period and may shed more light on the mechanisms of carbon turnover into biomass in these experiments.

Manganese reduction incubation experiment

In order to investigate the origin of dissolved Mn^{2+} in the pore water in the deeper sediments of the Argentine margin, an incubation experiment was performed aboard using sediment with the highest Mn^{2+} concentration detected. Therefore, sediment slurries were prepared and incubated under a N_2/CO_2 atmosphere in serum bottles at 10°C. The incubation was set up according to Table 5.6.3 using sediment from core GeoB22709-2 (914-939 cm bsf) and incubated over 24 days on board in order to test MnO_2 reduction with three different sulphur compounds as electron acceptor (S_8, FeS_2 and $Na_2S_2O_3$). The Mn^{2+} concentration in the slurry was monitored directly aboard using formaldoxime as a chelating agent (Figure 5.6.4). Formaldoxime forms pink complexes with Mn^{2+} ions that can be detected photometrically at a wavelength of 450 nm. The unamended control showed relatively low Mn^{2+} concentration increase after 5 days and reached a maximum concentration after 20 days of incubation (275 µM). Similarly, the incubations amended with only MnO_2 (1.6 mM), MnO_2 and FeS_2 (2.1 mM) as well as MnO_2 and $Na_2S_2O_3$ (1.9 mM) revealed maximum Mn^{2+} concentrations on day 20 and slightly decreased concentrations on day 24 indicating an equilibrium in MnO_2 turnover and Mn^{2+} re-oxidation. In contrast, the incubation amended with MnO_2 and S_8 showed a maximum at day 24 without reaching the equilibrium state (1.8 mM). The incubations amended with only S_8, FeS_2 or $Na_2S_2O_3$ showed no significant MnO_2 reduction and maintained a Mn^{2+} concentration under 20 µM until the end of the incubation (Figure 5.6.4). Moreover, the incubations amended with sodium azide also revealed a significant increase in Mn^{2+} concentration after 5 days, but only reached a maximum Mn^{2+} concentration of 1 mM on day 20. The sodium azide acts as a biocide and was therefore added to remove microbiological activity and to test for geochemical reduction of MnO_2. However, in the present incubation set the sodium azide likely partially failed to eliminate microbes given the significant increase in Mn^{2+} concentration (Figure 5.6.4). Nonetheless, the incubations do not indicate a geochemical MnO_2 reduction which would have been visible promptly after the start of the incubations. The presented

incubation experiment therefore strongly indicates a microbiologically mediated manganese oxide reduction.

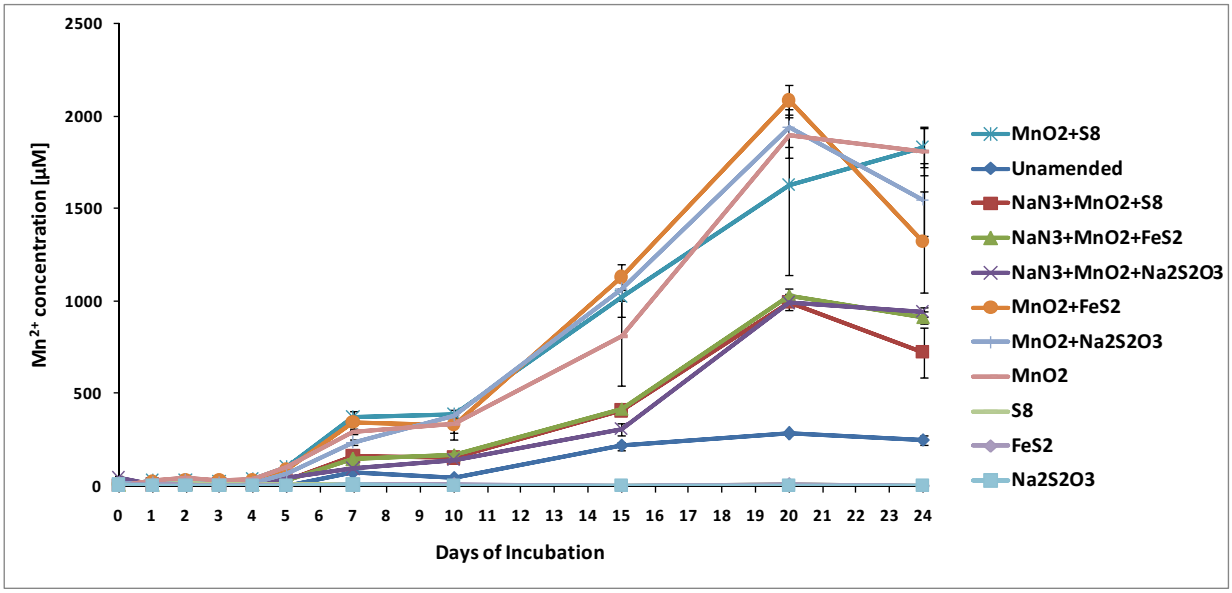

Fig. 5.6.4 Monitoring of Mn^{2+} concentrations in manganese reduction incubation experiments over time.

5.7 Water Column Characteristics, Dinoflagellate, Pollen/Spores and Coccolithophore Studies

(K.-H. Baumann, K.A.F. Zonneveld, M. Baques)

5.7.1 Introduction

The surface current circulation in the research area is characterised by the contact of two major water masses; the southward flowing Brazil Current (BC) and the northward flowing Malvinas Current (MC; Fig. 5.7.1). The MC transports cold (about 15°C in the research area) and low salinity waters (< 34.2) northwards along the continental shelf; whereas the BC is characterised by relatively high temperature and salinity values of about 22°C and 36, respectively, in the research area. At the contact zone, the so-called Brazil-Malvinas Confluence (BMC), MC waters dive under the BC waters. The mixing water masses are transported successively eastward as part of the South Atlantic current.

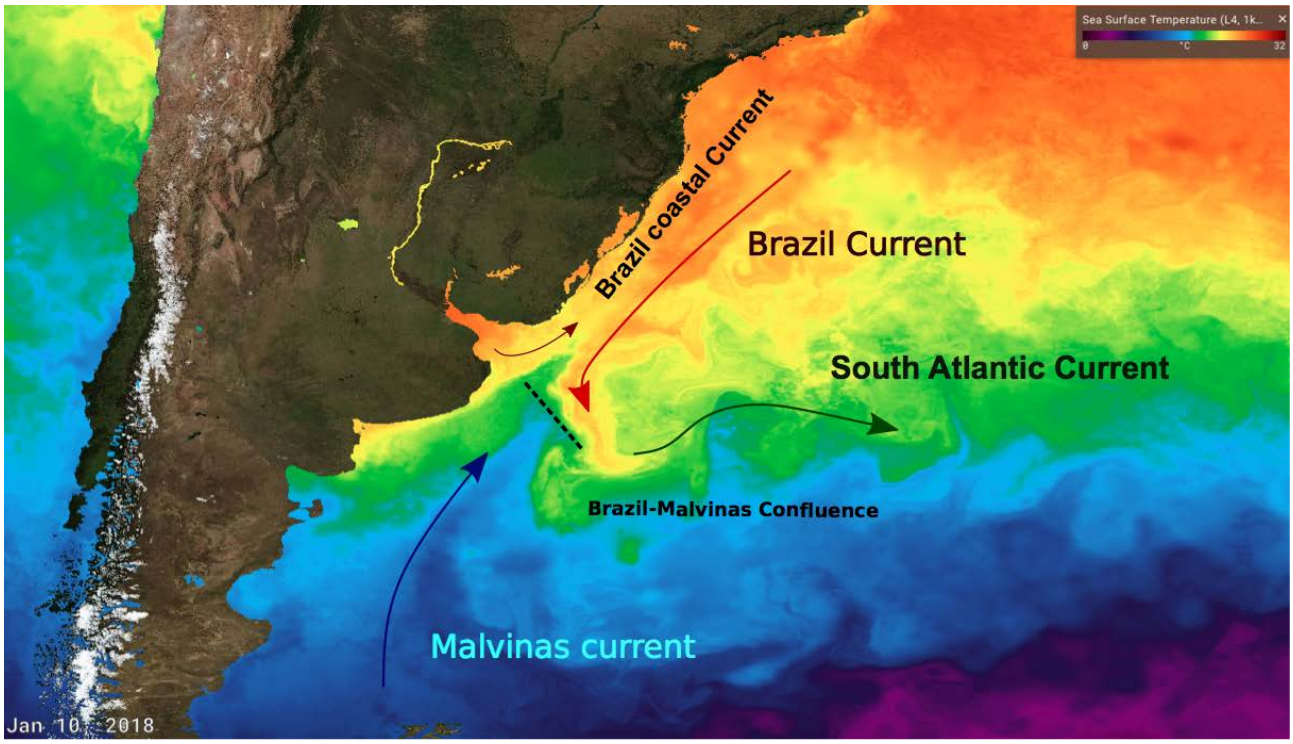

Fig. 5.7.1 Satellite image showing the upper water temperature on January 10th, 2018 of the research area as well as the major surface water currents (source satellite image: https://podaac-tools.jpl.nasa.gov/soto/, "state of the ocean, temperature").

During the last decades, major progress has been made in understanding the marine biological carbon pump; the process by which CO_2 is converted into organic matter via phytoplankton growth in sunlit surface waters, exported through sinking particles and finally sequestered in the deep ocean (e.g., Guidi et al., 2016, and references therein). Despite these large achievements, many aspects are still unknown or only partly understood. Especially the vertical and lateral displacement of particles in the water column is far from clear. The export of particulate organic matter (POM) from the upper water column typically occurs via the settling of large marine particles like marine snow (aggregates) or faecal pellets. However, apart from vertical transport,

particles can also be laterally displaced, for instance within nepheloid layers. Nepheloid layers are water layers where particle densities are higher than the surrounding waters (Inthorn et al., 2006 and references therein). They might be responsible for a major part of long distance lateral POM transport in the water column from the shelf into the open ocean (e.g., Inthorn et al., 2006; Ohde et al., 2015). It has been suggested that a major part of the particles within nepheloid layers might be resuspended especially those from layers along continental shelves. However, many aspects are still unknown, notably with respect to the degree to which nepheloid layers contain particles that have been sinking vertically through the water column or particles that have been resuspended.

Here we contribute to this discussion by studying the production, vertical and lateral transport of three POM groups of known origin, namely dinoflagellate cysts, pollen/spores and coccolithophores. In contrast to most POMs, these groups are well identifiable on species level and can be studied from their production or entrance in the upper waters, during sinking and towards their settling on the ocean floor. Moreover, by distinguishing living cysts and pollen (cyst/pollen with cell contents) from dead cysts/pollen (empty) they can provide insight into the freshness of the POM.

Dinoflagellate cysts are formed by dinoflagellates as a part of their vegetative or sexual life cycles (e.g., Bravo and Figueroa, 2014). As one of the major groups of phytoplankton, dinoflagellates are important contributors to the marine primary production and OM export production. Apart from a phototrophic life strategy, numerous species are heterotrophic. They are ecologically very diverse and association composition is dependent on many environmental factors such as differences in light availability, upper water turbulence and nutrient/trace element availability (e.g., Smayda and Trainer, 2010). Dinoflagellates can swim with help of two flagella and, as a consequence, can actively influence their position in the water column. Their cysts (size range about 10 – 100 µm) are immobile and sink passively through the water column most probably as part of larger particle clusters such as aggregates and faecal pellets (e.g., Zonneveld et al., 2010). Cysts have a species-specific morphology and can relatively easily be identified on species level by light microscopy.

Pollen and spores are produced by land plants. They are transported into the marine realm either by wind or river transport. Their morphology is species-specific and their occurrence in marine sedimentary archives can be used to reconstruct past vegetation composition and based on that past changes in climate in their source areas.

Coccolithophores are autotrophic, marine algae (Prymnesiophyceae) forming a major component of the calcareous microplankton and are one of the main open ocean primary producers. Their cell surface is covered by minute external calcite scales, which have a complex ornamentation. These so-called coccoliths constitute the single most important component of deep-sea sediments and provide floral and biomarker signals for the interpretation of environmental changes in the geological record. Therefore, they are extensively used in paleoecological and paleoceanographical studies (e.g., Winter and Siesser, 1994; Thierstein and Young, 2004). Knowledge of their distribution in surface waters as well as in surface sediments is thus a prerequisite for studies using coccoliths as proxies in Quaternary sediments. However, the environmental parameters that control the production and distribution of many coccolithophorid species are still poorly known, in particular in the study area of cruise SO260. Blooms of the species *Emiliania huxleyi* were described from the BMC (Gayoso, 1995), but there are no regular studies of this group from this area. Generally, relatively little is also known about the

transformation of living communities in the surface water into coccolith assemblages of the underlying sediment. It is obvious that assemblages in sediments are reduced by selective destruction and/or dissolution (e.g., Baumann et al., 2000; Saavedra-Pellitero and Baumann, 2016), but the influence of lateral transport on the coccolith assemblages has not been studied yet.

These aspects can be used to obtain information to what extent dinoflagellate cyst, pollen spores and coccoliths are transported vertically through the water column or laterally by nepheloid layers. In case of mainly vertical transport, cyst/pollen/coccolith associations at different water depths and in the surface sediments at the individual stations can be expected to be very similar. They will differ from associations at other locations along the Brazil-Malvinas Confluence gradient. In contrast, in case of mainly lateral transport within the bottom nepheloid layer, associations of cyst/pollen/coccoliths within this nepheloid layer can be expected to be very similar independent from their position along the surface ocean gradient.

5.7.2 Methods

Water column profiling has been performed with a seabird CTD 9.11+ equipped with additional turbidity, chlorophyll-a and oxygen sensors. In addition, the position of the BMC, which remained more or less at the same position (Fig. 5.7.2) during the cruise, was checked by satellite data.

To obtain information about the sea-surface export production, upper water column has been sampled with the ship's membrane pump (about 3m water depth; Table 5.7.2), Hydrobios and Seabird Rosettes (see Table 5.7.1) and McLane *In-situ* pumps (Table 5.7.3). In addition, sediment particles from the bottom nepheloid layer have been collected using the Rosette and *In-situ* pump systems equipped with two polycarbonate filters filters on top of each other with mesh sizes of 10 µm and 0.8 µm, respectively.

For pollen and dinoflagellate cyst analyses, filters were washed in destilled water immediately after deployment. Successively the material was treated ultrasonically and sieved over a 20 µm stainless steel high precision sieve (Storck-Veco). A known aliquot was transferred to an object glass where it was embedded in glycerin-gelatine, covered with a cover slip and sealed with wax to prevent oxidation of the organic material. The aliquots will be counted for dinoflagellate cysts using a light microscope with 400x and 1000x magnification. No chemicals were used to remove carbonate or silicate during preparation of any of the samples.

For coccolithophore sampling generally up to 5 l of water were filtered through cellulose nitrate filters (50 mm diameter, 0.45 µm pore size) by means of a vacuum pump immediately onboard. Without washing, rinsing or chemical conservation the filters were air dried for at least 24 h and then kept permanently dry with silica gel in transparent film to protect them from humidity. The filtered material will be studied by means of a Scanning Electron Microscope (SEM). Species composition and abundance will be determined by identification and counting on measured filter transects.

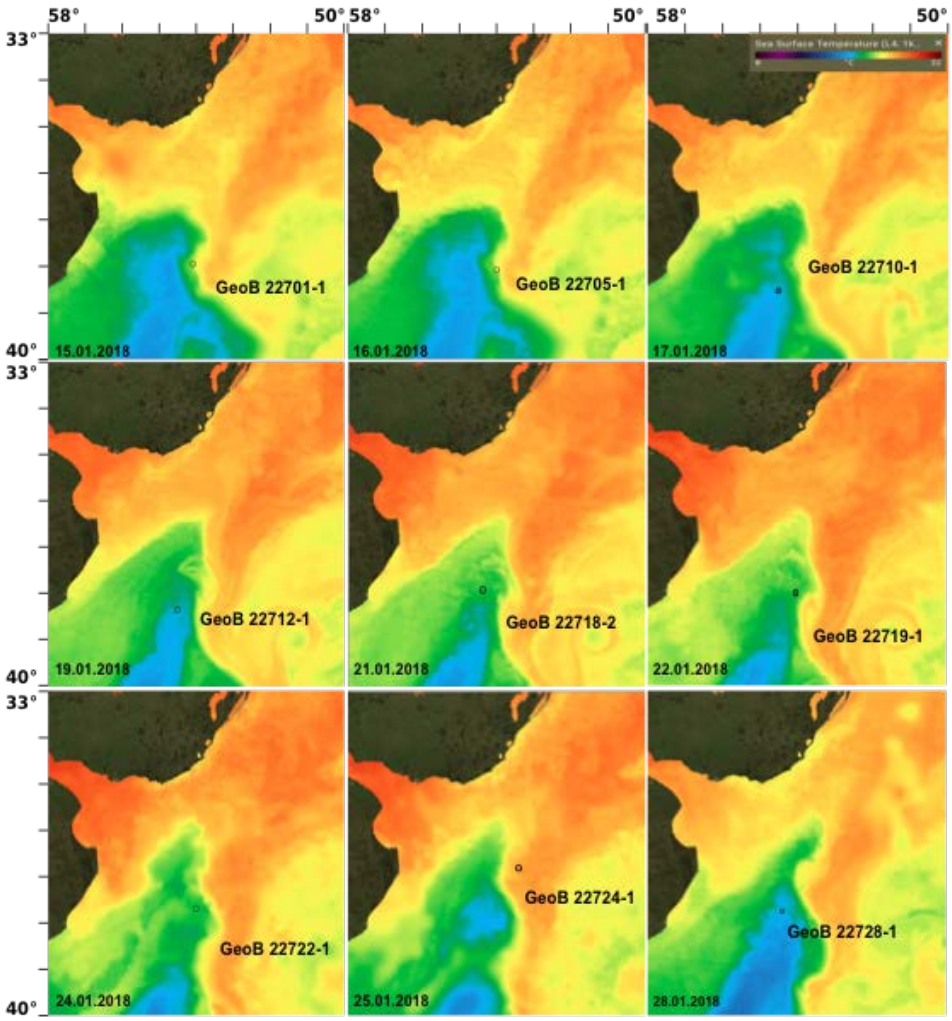

Fig. 5.7.2 Satellite image showing the surface water temperature at days of the CTD sampling and CTD-profiling positions (source satellite image: https://podaac-tools.jpl.nasa.gov/soto/, "state of the ocean, temperature")

5.7.3 CTD Profiling

CTD Profiling revealed that the MC subducts beneath the BC towards the north. The surface water layer that is characterized by relatively warm waters ranging from about 15°C in the south to about 23°C in the north. This upper layer is only a few meters thick at the southernmost positions to about 150 m at the northernmost location (Figs. 5.7.2 and 5.7.3). Below the surface currents the northward flowing Antarctic Intermediate Water (AAIW) that is characterised by relatively low salinity and high oxygen concentrations can be identified. The AAIW water is underlain by the northward flowing Circum Polar Deep Water (CDW) as well as the southward flowing well oxygenated North Atlantic Deep Water (NADW) (Figs. 5.7.3 to 5.7.6). Enhanced turbidity reflects the position of the bottom nepheloid layer that could be observed at all station located within and at the flanks of the canyons.

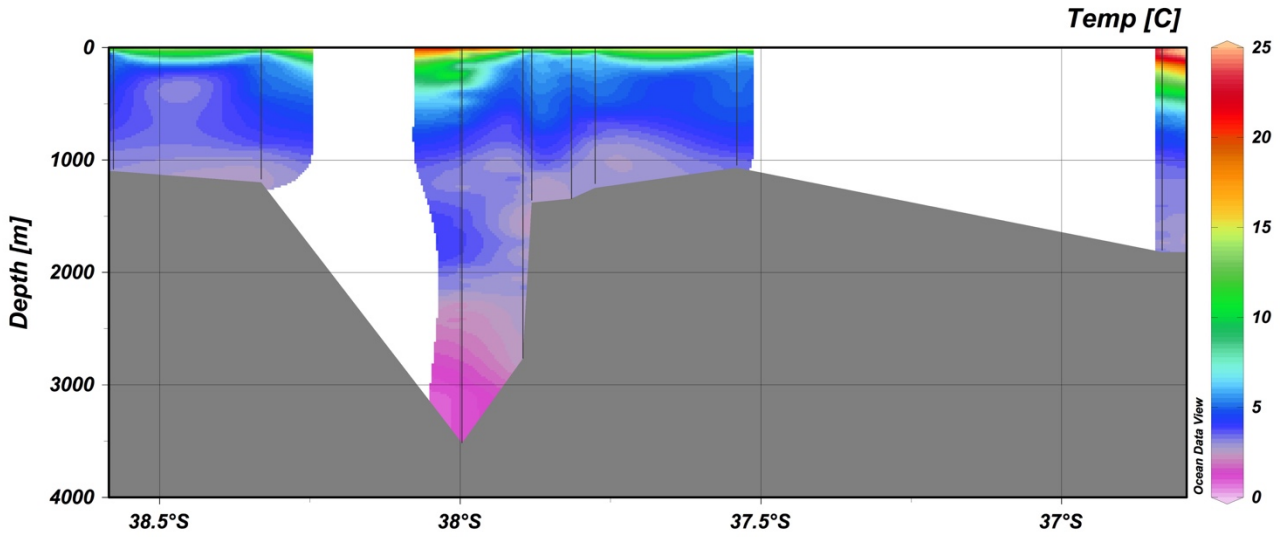

Fig. 5.7.3 Water column temperature (°C) of all CTD stations along a south-north transect.

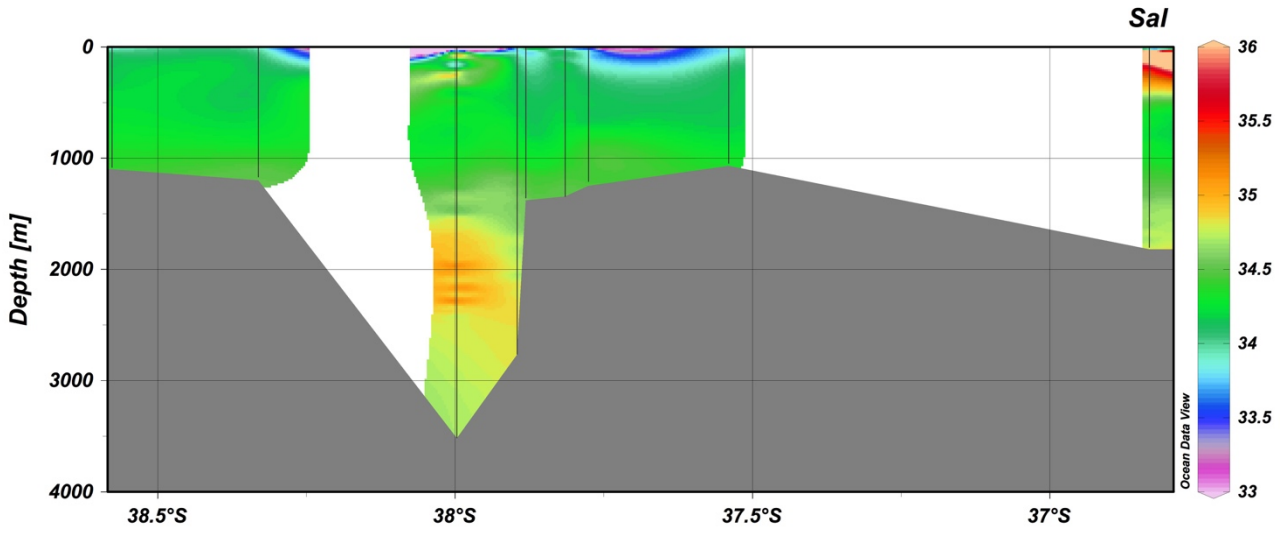

Fig. 5.7.4 Water column salinity (psu) of all CTD stations along a south-north transect.

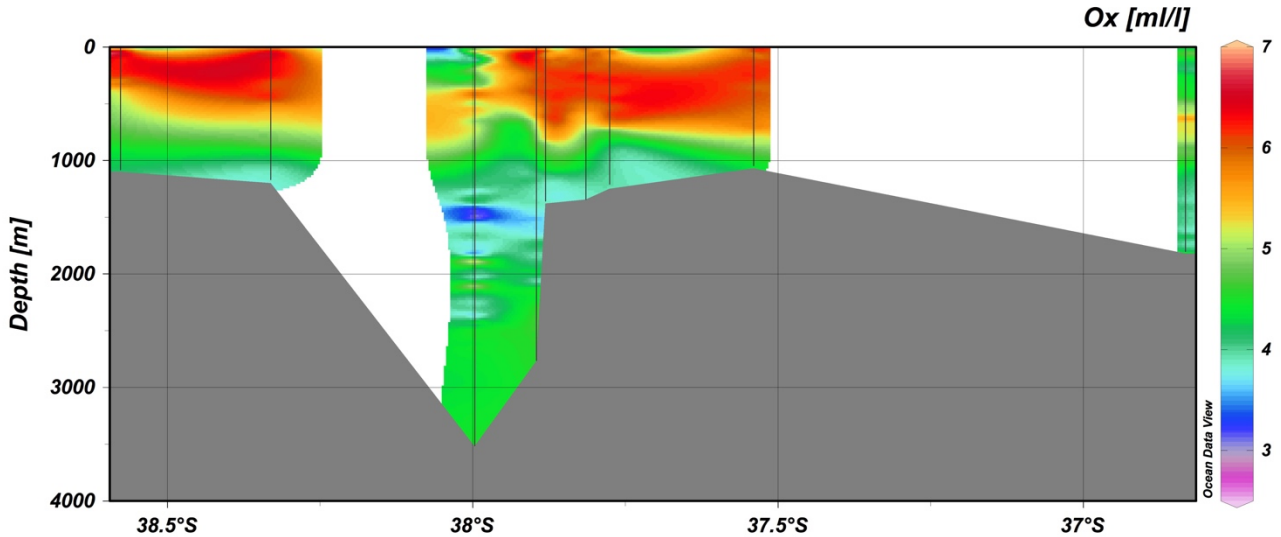

Fig. 5.7.5 Water column oxygen concentrations (ml/l) of all CTD stations along a south-north transect.

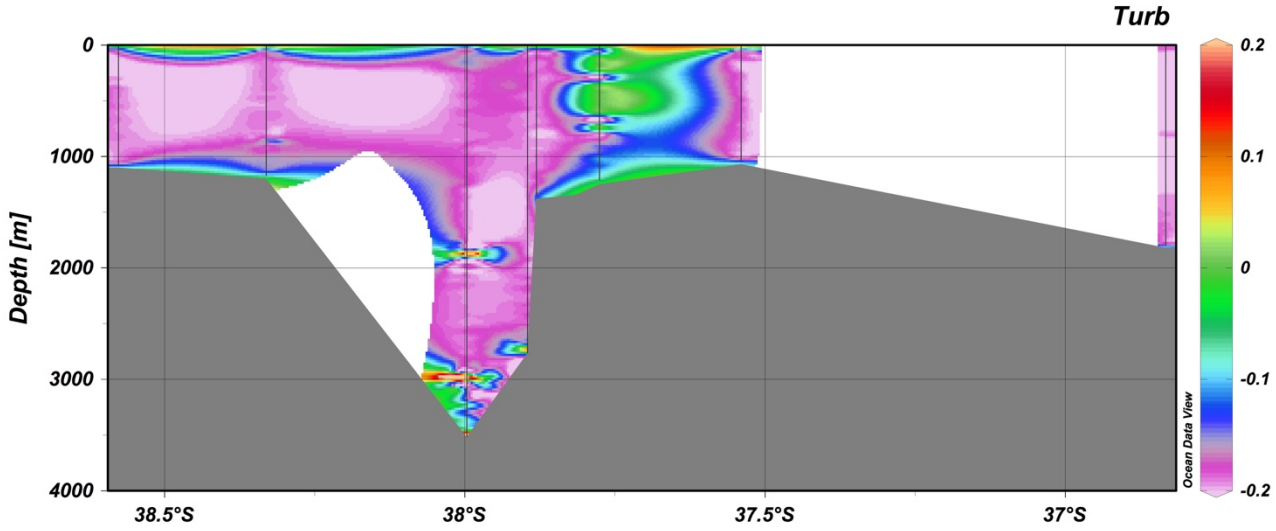

Fig. 5.7.6 Water column turbidity (standardized particle counts) of all CTD stations along a south-north transect.

5.7.4 Water Column Sampling with Membrane Pumps, Rosette and in situ Pumps

For pollen and dinoflagellate cyst analyses, 50 l of seawater collected from the ship's Membrane Pump and up to 140 l of water collected with the Rosette just above the sea floor at most stations (see Table 5.7.1), were sieved over a 20 µm stainless steel high precision sieve (Storck-Veco).

Table 5.7.1 List of CTD/Rosette deployments and depths of bottle closure.

Station	Latitude	Longitude	Bottom depth (m)	Depth Bottle closure (m)
GeoB22701-1	37°48'924"	54°10'703"	1363	1340 (1-6), 200, 150, 125, 100, 80, 60, 40, 20, 10
GeoB22705-1	37°59'997"	53°46'771"	3523	3500 (1-3), others not known, 16-18 not closed
GeoB22710-1	38°34'602"	54°21'616"	1105	1082 (1-14), 200, 150, 125, 100, 80, 60, 40, 20, 10
GeoB22712-1	38°19'887"	54°29'577"	1193	1167 (1-15), 200, 150, 125, 100, 80, 60, 40, 20, 10
GeoB22718-2	38°52'880"	54°18'267"	1352	1352 (1-15), 200, 150, 125, 100, 80, 60, 40, 20, 10
GeoB22719-1	37°53'781"	54°00'483"	2758	2758 (1-7), 2730 (8-15), 200, 150, 125, 100, 80, 60, 40, 20, 10
GeoB22722-1	37°32'404"	54°01'349"	1039	1039 (1-15), 200, 150, 125, 100, 80, 60, 40, 20, 10
GeoB22724-1	36°49'998"	53°22'001"	1798	1798 (1-9), 655 (10-15), 200, 150, 125, 100, 80, 60, 40, 20, 10
GeoB22728-1	37°46'581"	54°21'025"	1252	1238 (1-7), 2730 (8-15), 200, 150, 125, 100, 80, 60, 40, 20, 10

To retrieve additional plankton samples, 2-3 *in situ* pumps were deployed for 2.5 hours at 6 stations (Table 5.7.2). Up to 300 l of seawater were pumped through 10 µm and 0.8 µm cellulose nitrate filters at different depths. One of the *in situ* pumps was mostly situated just below the DCM, whereas with the other two the bottom nepheloid layer was sampled. Due to technical problems only two *in situ* pumps were used at the two latter stations.

Table 5.7.2 List of *in situ* pump deployments, used pumps, pumped volume and time.

Station	Pump	Pumping Depth (m)	Pumped Volume (l)	Pumped time (s)
GeoB22710-2	Jochen	20	72,11	535
	Fred	100	300	6867
	Norbert	1090	300	2624
GeoB22712-2	Jochen	40	196,99	2266
	Fred	1113	300	4963
	Norbert	1200	300	3166
GeoB22718-3	Jochen	40	49	688
	Fred	1187	300	4907
	Norbert	1400	300	3187
GeoB22722-2	Jochen	30	20,6	262
	Fred	1046	300	5185
GeoB22724-2	Fred	1805	300	4888
GeoB22728-2	Norbert	11077	282	3497
	Fred	1240	300	6212

For investigation of living coccolithophore communities of the uppermost water column water samples were taken from NISKIN-bottles of the rosette generally from 9-10 water depths between 5 and 200m (see Appendix 7). In addition, 29 surface water samples were taken from the vessel's membrane pump system at about 5 m water depth along the ships transect (Table 5.7.3). Furthermore, samples from the bottom nepheloid layer have been collected using the Rosette and *in situ* pump systems at all CTD/Rosette-stations.

5.7.5 Preliminary Shipboard Results

To obtain the species diversity within the pollen and dinoflagellate cyst samples, pilot counts were deployed in which the number of species was plotted against the number of specimens. These pilot studies showed that the maximum number of species was recovered when about 70 specimens were counted. Based on this empirical estimation and the counting error we estimated that an aliquot containing 100 specimens could be considered representative for the sample (van der Plas and Tobi, 1965). If an aliquot contained less than 100 organic-walled dinoflagellate cysts an additional aliquot was counted provided more material was still available. We distinguished between cysts and pollen/spores with cell contents and those that were empty. Cysts/pollen/spores with cell contents represented the living population whereas empty palynomorphs were either hatched or represented cysts/pollen/spores that died and had the cell contents degraded microbiologically (Bravo and Figueroa, 2014).

Detailed analyses of the coccolithophorid and dinoflagellate cyst assemblages will generally be performed by light and electron microscopy in the home laboratory at the University of Bremen.

Table 5.7.3 List of samples taken with the ship's membrane pump system.

GeoB No.	Sample No.	Date	Location Latitude (S)	Location Longitude (W")	Water Depth [m]	Sampling Depths [m]	Filtered Volume [l]
Coccolithophores							
	MP#1	14.1.18	37° 01,1'	54° 23,5'	125	3	4,0
	MP#2		37° 17,5'	54° 21,1'	788	3	1,5
	MP#3		37° 40,3'	54° 34,4'	807	3	2,0
	MP#4		37° 42,5'	54° 50,6'	647	3	1,0
	MP#5		38° 00,1'	54° 16,8'	1266	3	1,5
22701	MP#6	15.1.18	37° 58,2'	53° 49,3'	1391	3	2,5
	MP#7	16.1.18	37° 58,2'	53° 49,3'	2676	3	2,5
22705	MP#8		37° 59,8'	53° 46,3'	3562	3	2,5
	MP#9	17.1.18	38° 25,4'	54° 25,9'	1118	3	1,5
22708	MP#10		39° 18,7'	53° 57,2'	3689	3	2,0
22710	MP#11	18.1.18	38° 34,5'	54° 22,7'	1122	3	3,0
	MP#12		38° 26,6'	54° 39,0'	939	3	2,0
	MP#13		38° 13,5'	54° 29,9'	1103	3	1,5
	MP#14		38° 18,4'	54° 08,8'	1267	3	1,5
	MP#15	19.1.18	38° 05,9'	54° 05,9'	1340	3	1,5
	MP#16		38° 07,0'	53° 54,8'	1654	3	4,0
	MP#17		38° 14,8'	53° 58,4'	1446	3	3,5
	MP#18		38° 11,8'	54° 13,9'	1210	3	2,5
	MP#19		38° 09,5'	54° 25,3'	1168	3	2,0
22712	MP#20	20.1.18	38° 19,9'	54° 29,6'	1220	3	2,0
	MP#21	21.1.18	37° 58,1'	54° 31,0'	1165	3	1,5
22718	MP#22		37° 52,8'	54° 18,3'	1411	3	1,5
22719	MP#23	22.1.18	37° 53,8'	54°00,5'	2785	3	2,5
22721	MP#24		37° 33,3'	53° 58,7'	1116	3	3,0
	MP#25	23.1.18	37° 43,0'	54° 18,5'	967	3	1,7
	MP#26		37° 59,6'	53° 50,9'	1239	3	2,5
22722	MP#27	24.1.18	37° 32,6'	54° 01,3'	1074	3	1,5
22724	MP#28	25.1.18	36° 50,8'	53° 22,4'	1924	3	4,0
	MP#29	26.1.18	37° 24,5'	53° 36,6'	1268	3	4,5
Dinoflagellate Cysts							
	MP1	14.1.22	37°01'15"	54°23'5"	125	3	25
	MP2	15.1.22	37°39'93"	54°36'82"	775	3	40
	MP3	15.1.22	37°58'19"	54°25'38"	800	3	50
	MP4	15.1.22	38°00'15"	54°16'8"	1266	3	50
	MP5	17.1.22	38°02'194"	54°18'837"	1227	3	50
	MP6	18.1.22	39°18'694	53°57'165"	3682	3	50
	MP7	19.1.22	38°19'089	54°05'475"		3	51
	MP8	20.1.22	38°05'028"	54°18'243"	1209	3	50
	MP9	20.1.22	38°06'563"	53°55'910"	1565	3	50
	MP10	22.1.22	38°06'547	54°22'818"	1288	3	50
	MP11	23.1.22	38°33'313	54°58'720"	1058	3	50
	MP12	25.1.22	37°32'404"	54°01'347"	1076	3	50
	MP13	26.1.22	36°50'833"	53°22'114"	1925	3	50
	MP14	26.1.22	37°25'020"	53°36'600"	1290	3	50

5.7.6 ADCP

(M. Baqués, L. Steinmann, G. Bozzano)

Technical description

Doppler shift measurements were carried out with two hull-mounted Ocean Surveyor Teledyne RD Instruments Acoustic Doppler Current Profilers (ADCP) during both SO260 legs, providing real-time current velocity profiles in the water column. They operated continuously, during stations and also on transit routes, at two operation frequencies, 38 and 75 kHz. In addition, the ADCP also records the echo intensity, which is a measure of the signal strength of the echo returning from the transmit pulse.

The 38 kHz ADCP was configured to profile the water column at low resolution (long range) in a narrowband mode. The data were split in 120 bins of 16 m depth each, the bottom track was set on, the water temperature was measured with the ADCP sensor located at 6.4 m depth, and the salinity was set to a fixed value of 35. The instrument used the heading and tilt sensors from the Seapath 320, a positioning, attitude and heading sensor which combines inertial technology together with GPS (Global Positioning System) and GLONASS (Global Navigation Satellite System) satellite signals. The maximum range with this configuration was around 1000 m, while the depth of the first bin was 38.3 m.

The 75 kHz ADCP was configured to profile the water column at high-resolution (short range) in a broadband mode. The data were collected in 120 bins of 8 m depth each, the bottom track was set on, the water temperature was measured with the ADCP sensor located at 6.4 m depth, and the salinity was set to a fixed value of 35. The instrument used the heading and tilt sensors from the Seapath 320. The maximum range with this configuration was around 700 m, while the depth of the first bin was 22.9 m.

Two different averaged data sets were recorded in addition to the raw data. The “Short Time Average” (STA) dataset consists of a temporal averaging of the velocity record using a time window of 300 seconds, while the “Long Term Average” (LTA) dataset was produced using a time window of 600 seconds. These data sets include corrections for ships movement using the ship’s GPS navigation and gyre system and provide current velocity data in earth coordinates. The binary data were exported in Matlab format with the Teledyne RD Instruments software WinADCP. Computer programs written ad-hoc in Matlab were used to manipulate data on board, filter low quality data, average data during station, filter contributions from the reflections in the sea bottom and visualize preliminary results.

Since the transducer beam angle of the ADCP is oriented 30º from the vertical, the echo through the side lobe faces the bottom at the same time as the echo through the main lobe faces the water. This occurs at a distance of close to 85 % of the range from the ADCP to the bottom. As the echo from a hard surface - such as the sea floor - is much stronger than the echo from scatterers in the water, the velocity data from the last 15 % of the range to the bottom may be contaminated. For this reason a Lowered Acoustic Doppler Current Profiler (LADCP) attached to the CTD is recommended for future deep velocity profiling measurements.

Preliminary results

Relative Volume Backscattering Strength (dB) estimations were done from the echo intensity data following Gostiaux and van Haren (2010). This acoustic parameter is proportional to the

concentration of volume scatterers, such as zooplankton and suspended sediments that might be present in the water column and produce the echoes. Only relative backscatter measurements were done since no ADCP calibration parameters were available. These data could provide valuable information when studying biological-physical interactions in the sea.

The preliminary CTD and ADCP results from two geological stations (GeoB22712 and GeoB22716), where pebbles of different size and lithology were found, are here presented. Water masses identification in these locations, with their relative displacement velocity and direction, could be useful to correlate the presence of coarse-sized sediments with the action of strong bottom currents. Thus, the ADCP profiles collected during these stations using the 38 kHz frequency (LTA files) were averaged and the different water masses within the water column were identified from the CTD data.

At station GeoB22712, the water masses identified are the following: Subantarctic Water (SW; $5 \leq \theta$ (ºC) and $33.9 < S \leq 34.2$, where θ stands for potential temperature and S for salinity), Antarctic Intermediate Water (AAIW; $2.9 < \theta(ºC) < 5$ and $33.9 < S < 34.3$) and Upper Circumpolar Deep Water (UCDW; $2.5 < \theta < 3.5$°C, $34.3 \leq S < 34.6$ and dissolved oxygen<4.5 ml/l) (Fig. 5.7.7 (a)). In the figure, the depth boundaries between water masses are indicated with arrows. No CTD measurements were done at station GeoB22716.

The average current velocity profiles computed for stations GeoB22712 and GeoB22716 show comparable moderate to high velocities for the two stations, with values ranging from 34 cm/s (28 cm/s) at the bottom, up to 59 cm/s (48 cm/s) at the surface at station GeoB22712 (GeoB22716) (Fig. 5.7.7 (b)). As for the current direction, in the upper part of the water column (38 to 269 m), dominated by the SW, the flow points to the NE; in the intermediate layer (269 to 896 m), dominated by the AAIW, the direction also is to the NE. Finally, in the lowest portion of the water column, dominated by the UCDW, the flows points to the E.

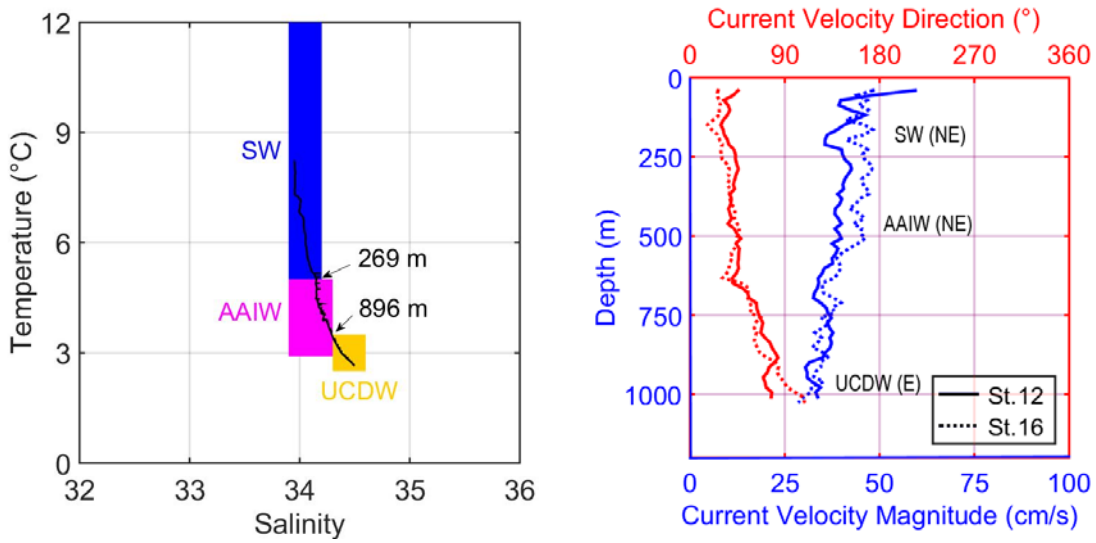

Fig. 5.7.7 (a) Water masses identified at CTD station GeoB22712. (b) Average current velocity profiles (magnitude and direction) computed for stations GeoB22712 (solid line) and GeoB22716 (dotted line).

Orthogonal components of the current velocity, cross shelf (u) and along shelf (v), were analyzed in order to study the possible link between these magnitudes and the location where coral

mounds were found. In addition, u and v distributions will provide valuable information for understanding erosion/deposition processes. The reference axes were rotated 30° from the true North due to the orientation of the continental slope. An E-W transect was chosen in the southern part of the Mar del Plata Canyon study area, crossing the location of station GeoB22715 where coral mounds were found. The ADCP data were collected on 19/01/2018, between 01:37 and 06:05 (UTC time) and on 28/01/2018, between 03:38 and 04:16 (UTC time), as shown with dots in blue and red, respectively in figure 5.7.8. The yellow dot shows the location of station GeoB22715.

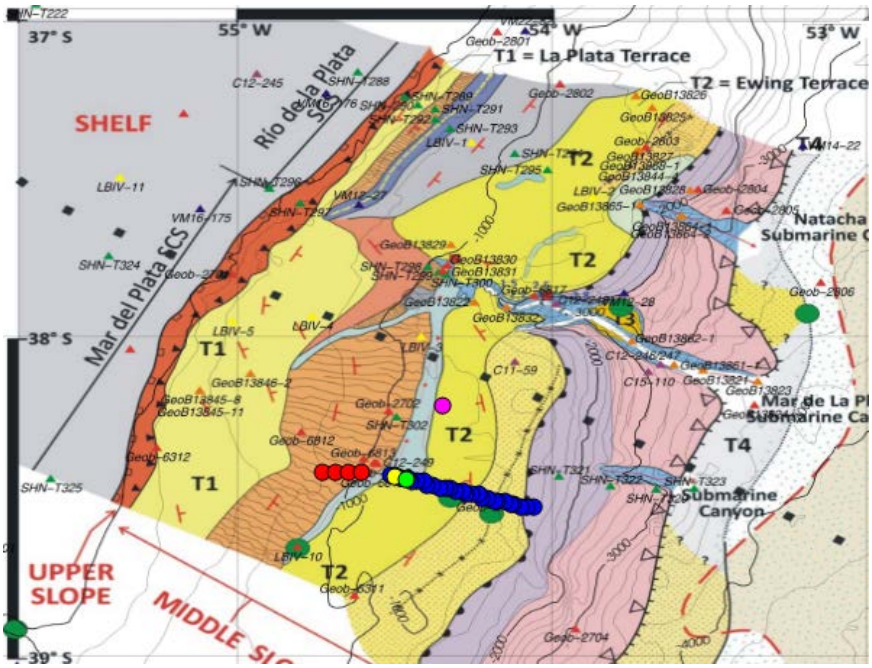

Fig. 5.7.8 Study area showing the location of ADCP measurements collected on the 19/01/2018 between 01:37 and 06:05 (UTC time) (blue dots) and on the 28/01/2018 between 03:38 and 04:16 (UTC time) (red dots). The yellow dot shows the location of station GeoB22715 where coral mounds were found, while the green and magenta dots show the locations of stations GeoB22712 and GeoB22716, respectively.

The along-shelf velocity distribution obtained for the E-W transect is shown in figure 5.7.9. In the western part of the section, the along shelf velocity decreases with increasing depth; high intensities (60-80 cm/s) are observed in the upper layers (Z<250 m) where SW was identified. In the canyon (54.5 °W), the velocity is uniform (20-40 cm/s) throughout the water column, showing higher values (40-50 cm/s) only below 800 m where the AAIW-UCDW interface was identified. East of the canyon, the current velocity is higher (30-40 cm/s) in the upper layers (Z<250 m), and displays decreasing intensity with increasing depth. An inversion of the along shelf velocity is observed below 600 m. In the Eastern part of the section, the velocity intensity is uniform (20-30 cm/s) above 800 m, with higher values (30-40 cm/s) only between 500 and 800 m. Below 800 m the velocity intensity is low (<20 cm/).

The cross shelf velocity distribution obtained for the E-W section is shown in figure 5.7.10. Intensities are generally low (<±10 cm/s), with positive values mainly in the central portion of the section and negative values towards the East. East of the canyon the cross shelf intensities are higher at Z<250 m, reaching values of 50 cm/s at 80-100 m. Below 600 m, in the area where an

inversion of the along shelf velocity was observed, the intensities are low (<14 cm/s) but still positive indicating an offshore flow (SE direction) near the bottom.

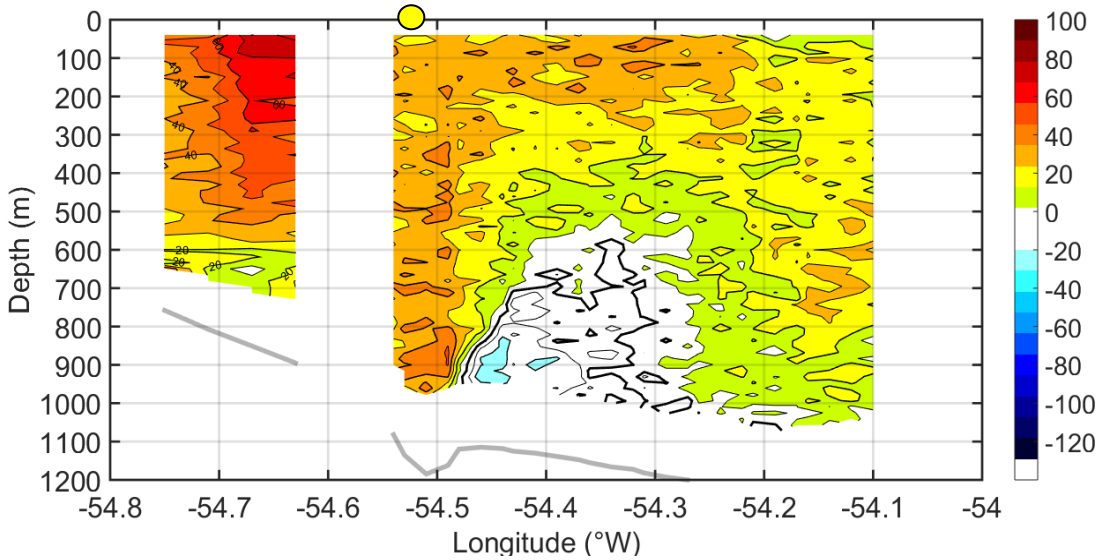

Fig. 5.7.9 Along shelf current velocity (cm/s) computed for the section shown in Fig. 5.7.8. Positive (negative) values indicate north-east (south-west) flow. The gray line indicates the water depth. The yellow dot shows the location of station GeoB22715, where coral mounds were found.

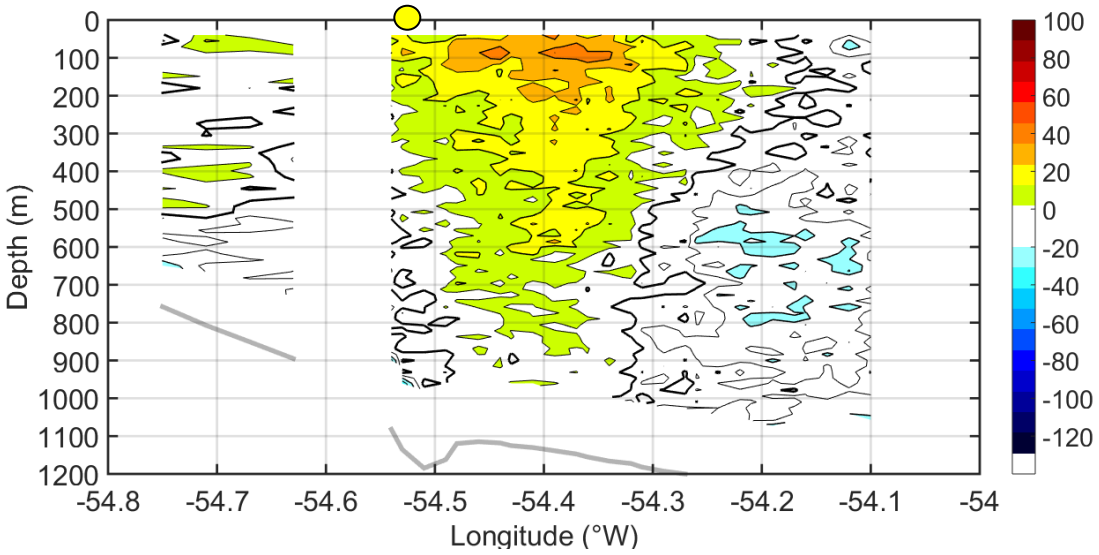

Fig. 5.7.10 Cross-shelf current velocity (cm/s) computed for the section shown in Fig. 5.7.8. Positive (negative) values indicate offshore (inshore) flow. The gray line indicates the water depth. The yellow dot shows the location of station GeoB22715, where coral mounds were found.

Future analysis should establish a possible link between the relative strong along shelf current velocity found near the bottom in the canyon and the erosional features observed in the corresponding seismoacoustic data. Moreover, a possible relationship between the SE flow found East of the canyon near the bottom and the depositional features observed in the corresponding seismic data has to be analysed.

6 Station List SO260

6.1 Overall Station List

RV SONNE station number	GeoB station number	Date	Gear	Time (UTC) (station start)	Latitude (station start)	Longitude (station start)	Water depth (m) (station start)	Remarks
SO260/1_2-1	GeoB22701-1	15.01.18	CTD+RO	09:54:00	37°48.924´S	54°10.703´W	1391,0	
SO260/1_2-2	GeoB22701-2	15.01.18	GBC	11:13:00	37°48.900´S	54°10.700´W	1389,5	nearly empty box, 10cc samples (Sedimentology and Palynology)
SO260/1_3-1	GeoB22702-1	15.01.18	GBC	13:11:00	37°48.557´S	54°10.218´W	1779,9	
SO260/1 3-2	GeoB22702-2	15.01.18	MUC	14:33:00	37°48.558´S	54°10.217´W	1354,0	
SO260/1_3-3	GeoB22702-3	15.01.18	GC	16:02:00	37°48.567´S	54°10.220´W	1355,0	
SO260/1_4-1	GeoB22703-1	15.01.18	GBC	18:07:00	37°48.251´S	54° 9.806´W	1317,0	
SO260/1_5_1	GeoB22704-1	15.01.18	GBC	21:04:00	37°38.637´S	54° 8.525´W	1041,0	
SO260/1-5-2	GeoB22704-2	22.01.18	GC	12:56:00	37°38.639´S	54° 8.495´W	1038,0	
SO260/1-5-3	GeoB22704-3	22.01.18	GC	14:09:00	37°38.633´S	54° 8.479´W	1038,0	banana
SO260/1_7-1	GeoB22705-1	16.01.18	CTD+RO	09:39:00	37°59.997´S	53°46.771´W	3565,0	problem with the system, some bottles opened
SO260/1_8-2	GeoB22706-1	16.01.18	MUC	13:16:00	37°57.966´S	53°45.780´W	2997,0	
SO260/1_8-3	GeoB22706-2	16.01.18	GC	16:00:00	37°57.608´S	53°45.691´W	2967,0	
SO260/1_9-1	GeoB22707-1	16.01.18	GC	19:34:00	37°54.829´S	53°47.722´W	2762,0	
SO260/1_9-2	GeoB22707-2	16.01.18	MUC	20:40:00	37°54.638´S	53°47.613´W	2778,0	
SO260/1_10-1	GeoB22708-1	17.01.18	GC	09:18:00	39°18.699´S	53°57.186´W	3686,0	
SO260/1-10-2	GeoB22708-2	17.01.18	GC	12:36:00	39°18.704´S	53°57.162´W	3681,0	
SO260/1-10-3	GeoB22708-3	17.01.18	MUC	15:01:00	39°18.698´S	53°57.160´W	3675,0	
SO260/1-11-1	GeoB22709-1	17.01.18	GC	18:22:00	39°18.060´S	53°58.026´W	3608,0	
SO260/1-11-2	GeoB22709-2	17.01.18	GC	21:18:00	39°18.056´S	53°58.039´W	3609,0	
	GeoB22710-1	18.01.18	CTD+RO	05:06:00	38°34.602´S	54°21.616´W	1128,0	
	GeoB22710-2	18.01.18	ISP	09:45:00	38°34.563´S	54°21.711´W	1128,0	
SO260/1_14-1	GeoB22711-1	19.01.18	MUC	23:49:00	38°20.034´S	54°28.961´W	1130,0	
SO260/1_14_2	GeoB22711-2	20.01.18	GC	00:55:00	38°20.030´S	54°28.969´W	1130,0	
SO260/1_14-3	GeoB22711-3	20.01.18	GC	15:45:00	38°20.032´S	54°28.956´W	1129,0	EMPTY, no core
SO260/1_15_1	GeoB22712-1	20.01.18	CTD+RO	02:09:00	38°19.887´S	54°29.577´W	1217,0	
SO260/1_15_2	GeoB22712-2	20.01.18	ISP	03:31:00	38°19.884´S	54°29.581´W	1217,0	
SO260/1_15-3	GeoB22712-3	20.01.18	GBC	17:11:00	38°19.917´S	54°29.544´W	1218,0	GBC 200 m behind vessel due to current, sample site 25 m NW of coordinates, recovery of 3 kg
SO260/1-16-1	GeoB22713-1	20.01.18	MUC	10:07:00	38°35.301´S	54°21.083´W	1115,0	

SO260/1-17-1	GeoB22713-2	20.01.18	GC	11:14:00	38°35.326´S	54°21.076´W	1115,0	
SO260/1_18-1	GeoB22714-1	20.01.18	GC	13:04:00	38°37.775´S	54°22.717´W	1111,0	
SO260/1-18-1	GeoB22715-1	20.01.18	GBC	19:12:00	38°19.615´S	54°31.647´W	1121,0	strong bottom currents, sample location 20 m north of the coordinates (Posidonia)
SO260/1_18-2	GeoB22715-2	20.01.18	GC	21:00:00	38°19.477´S	54°31.645´W	1105,0	strong bottom currents (Posidonia)
SO260/1-20-1	GeoB22716-1	21.01.18	GBC	11:46:00	38° 6.332´S	54°22.782´W	1292,0	Posidonia 38° 6.329 S / 54° 22.803 W
SO260/1_21-1	GeoB22717-1	21.01.18	GS	15:23:00	37°58.059´S	54°30.996´W	1167,0	Posidonia location: 38°6.329S, 54°22.803W , Recovery of stones
So260/1-22-1	GeoB22718-1	21.01.18	GS	19:46:00	37°52.850´S	54°18.213´W	1412,0	Posidonia
So260/1-22-1	GeoB22718-2	21.01.18	CTD+RO	22:10:00	37°52.880´S	54°18.267´W	1415,0	
So260/1/22/3	GeoB22718-3	21.01.18	ISP	23:25:00	37°52.885´S	54°18.250´W	1415,0	
So260/1-23-1	GeoB22719-1	22.01.18	CTD+RO	05:33:00	37°53.781´S	54° 0.483´W	2785,0	
So260/1-24-1	GeoB22720-1	22.01.18	GS	09:34:00	37°43.259´S	54° 3.111´W	1282,0	Posidonia, bulk sediment sample (G. Bozzano, GeoB Archive)
SO260/1_25-1	GeoB22721-1	22.01.18	MUC	16:19:00	37°33.287´S	53°58.746´W	1060,0	
So260/1-25-2	GeoB22721-2	22.01.18	GC	17:54:00	37°33.315´S	53°58.714´W	1060,0	
SO260/1_27-1	GeoB22722-1	24.01.18	CTD+RO	02:40:00	37°32.404´S	54° 1.349´W	1076,0	
So260/1_27-2	GeoB22722-2	24.01.18	ISP	03:41:00	37°32.391´S	54° 1.329´W	1075,0	
SO260/1_27-3	GeoB22722-3	24.01.18	MUC	09:21:00	37°32.395´S	54° 1.338´W	1077,0	
So260/1-27-4	GeoB22722-4	24.01.18	GC	11:28:00	37°32.358´S	54° 1.390´W	1077,0	overpenetrated
So260/1-27-5	GeoB22722-5	24.01.18	GC	13:05:00	37°32.362´S	54° 1.371´W	1078,0	
SO260/2-42-1	GeoB22722-6	04.02.18	MeBo	17:20:00	37°32.375´S	54° 1.342´W	1077,0	operation cancelled due to technical difficulties
SO260/2-42-1	GeoB22722-7	05.02.18	MeBo	18:00:00	37°32.373´S	54° 1.308´W	1076,0	
SO260/1_28-1	GeoB22723-1	24.01.18	GC	16:43:00	37°42.225´S	53°57.508´W	1167,0	destroyed gear
SO260/1_28-2	GeoB22723-2	25.01.18	MUC	23:01:00	37°42.218´S	53°57.547´W	1170,0	
SO260/1_28-3	GeoB22723-3	26.01.18	GC	00:08:00	37°42.231´S	53°57.503´W	1167,0	
SO260/1_29_1	GeoB22724-1	25.01.18	CTD+RO	09:00:00	36°49.998´S	53°22.001´W	1820,0	
SO260/1_29-2	GeoB22724-2	25.01.18	ISP	10:45:00	36°49.889´S	53°21.936´W	1822,0	
SO260/1_31-1	GeoB22725-1	27.01.18	MUC	10:24:00	38°20.534´S	54° 3.871´W	1347,0	
SO260/1-31-1	GeoB22725-2	27.01.18	GC	12:10:00	38°20.539´S	54° 3.859´W	1344,0	
SO260/1_32-1	GeoB22726-1	27.01.18	GBC	16:18:00	38°43.139´S	54°22.313´W	1019,0	destroyed gear => Empty box
So260/1_32-2	GeoB22726-2	27.01.18	GS	17:21:00	38°43.131´S	54°22.318´W	1019,0	
SO260/1_32-3	GeoB22726-3	27.01.18	GC	19:01:00	38°43.128´S	54°22.332´W	1019,0	banana - small bag sample
SO260/1_33-1	GeoB22727-1	27.01.18	GS	20:41:00	38°41.447´S	54°23.477´W	1044,0	

So260/1_34-1	GeoB22728-1	28.01.18	CTD+RO	09:30:00	37°46.581´S	54°21.025´W	1253,0	
So260/1_34-2	GeoB22728-2	28.01.18	ISP	10:59:00	37°46.589´S	54°21.024´W	1255,0	
SO260/1_34-3	GeoB22728-3	28.01.18	GS	15:35:00	37°47.589´S	54°22.307´W	1055,0	
So260/1_35-1	GeoB22729-1	28.01.18	GC	18:05:00	37°48.572´S	54°20.440´W	1113,0	
SO260/1-36	GeoB22730-1	29.01.18	GS	06:15:00	37°41.676´S	54°51.953´W	647,0	
SO260/1-37-1	GeoB22731-1	29.01.18	GS	08:20:00	37°38.394´S	54°45.995´W	706,0	
SO260/1-38-1	GeoB22732-1	29.01.18	GS	10:15:00	37°32.567´S	54°37.236´W	798,0	
SO260/1-39-1	GeoB22733-1	29.01.18	GS	12:08:00	37°30.071´S	54°35.786´W	638,0	
SO260/1-39-2	GeoB22733-2	29.01.18	GC	13:26:00	37°30.122´S	54°35.792´W	634,0	
SO260/1-39-3	GeoB22733-3	29.01.18	GC	14:21:00	37°30.119´S	54°35.800´W	636,0	
SO260/2-40-1	GeoB22734-1	03.02.18	MUC	09:00:00	36° 8.489´S	53°17.159´W	242,0	
SO260/2-40-2	GeoB22734-2	03.02.18	GC	09:28:00	36° 8.486´S	53°17.159´W	240,0	
SO260/2-40-3	GeoB22734-3	03.02.18	GC	10:43:00	36° 8.485´S	53°17.155´W	241,0	
SO260/2-41-1	GeoB22735-1	03.02.18	GC	14:48:00	36° 7.685´S	52°49.960´W	1381,0	
SO260/2-41-2	GeoB22735-2	03.02.18	MUC	16:10:00	36° 7.671´S	52°49.898´W	1382,0	
SO260/2-41-3	GeoB22735-3	07.02.18	MeBo	14:32:00	36° 7.369´S	52°49.670´W	1392,0	technical problems, no bottom contact
SO260/2-41-4	GeoB22735-4	07.02.18	GBC	16:09:00	36° 7.633´S	52°49.882´W	1391,0	no bottom contact, stopped due to strong drift of GBC (currents)
SO260/2-41-5	GeoB22735-5	07.02.18	MeBo	17:01:00	36° 7.630´S	52°49.892´W	1392,0	former GeoB13809
SO260/2-44-1	GeoB22736-1	06.02.18	GS	18:28:00	37°19.928´S	53°59.319´W	1112,0	
SO260/2-45-1	GeoB22737-1	06.02.18	GS	20:12:00	37°20.049´S	53°59.393´W	1114,0	
So260/2-46-1	GeoB22738-1	06.02.18	GS	21:48:00	37°19.973´S	53°58.394´W	1117,0	1 bulk sample
SO260/2-47-1	GeoB22739-1	11.02.18	MeBo	10:25:00	38°35.507´S	54°22.777´W	1113,0	first try failed
SO260/2-47-1	GeoB22739-2	11.02.18	MeBo	10:36:00	38°35.530´S	54°22.806´W	1112,0	
SO260/2-48-1	GeoB22740-1	10.02.18	GC	14:41:00	38°36.518´S	54°20.051´W	1103,0	Posidonia; Banana
SO260/2-48-2	GeoB22740-2	10.02.18	GC	21:12:00	38°36.506´S	54°20.075´W	1104,0	Empty
SO260/2-49-1	GeoB22741-1	10.02.18	GC	16:41:00	38°38.202´S	54°18.649´W	1072,0	Posidonia
So260/2-50-1	GeoB22742-1	10.02.18	GC	18:23:00	38°39.357´S	54°17.678´W	1056,0	Posidonia; empty
So260/2-51-1	GeoB22743-1	10.02.18	GC	23:02:00	38°35.277´S	54°24.014´W	1108,0	Empty
SO260/2-52-1	GeoB22744-1	12.02.18	GC	18:32:00	38°18.223´S	54°32.348´W	975,0	
SO260/2-52-1	GeoB22744-2	12.02.18	GBC	20:03:00	38°18.248´S	54°32.371´W	992,0	

6.2 Seismic Profile List

	Start					End				
Number of profile GeoB18-	Date	Time UTC	Latitude SOUTH	Longitude WEST	FFN	Date	Time UTC	Latitude SOUTH	Longitude WEST	FFN
Survey 1										
001	13/1/18	14:00	37°02,13'	54°22.39'	300	13/1/18	17:16	37°11.953	54°06.322	3698
002	13/1/18	17:28	37°12,958	54°06,270	3885	13/1/18	18:44	37°19,286	54°06,440	5024
003	13/1/18	18:53	37°19,865	54°06,897	5156	13/1/18	23:22	37°15,250	54°34,122	9170
004	13/1/18	23:28	37°15,656	54°33,836	9262	14/1/18	2:15	37°26,007	54°22,357	11777
005	14/1/18	2:15	37°26,007	54°22,357	11777	14/1/18	3:50	37°31,77	54°28,77	13207
006	14/1/18	3:54	37°31,798	54°29,299	13262	14/1/18	6:13	37°27,950	54°43,018	15338
007	14/1/18	6:20	37°28,448	54°43,066	15493	14/1/18	9:33	37°39,135	54°28,066	18345
008	14/1/18	9:38	37°39,502	54°28,143	18406	14/1/18	9:58	37°41,025	54°29,126	18719
009	14/1/18	10:02	37°41,115	54°29,591	18775	14/1/18	13:42	37°37,400	54°52,104	22070
010	14/1/18	13:46	37°37,529	54°52,400	22130	14/1/18	14:21	37°40,073	54°54,254	22671
011	14/1/18	14:25	37°40,346	54°54,087	22711	14/1/18	21:15	38°01,479	54°19,947	28877
012	14/1/18	21:18	38°01,339	54°19,635	28928	14/1/18	23:34	37°56,690	54°09,898	30155
013	14/1/18	23:37	37°56,564	54°09,780	30179	15/1/18	0:52	37°51,366	54°05,555	31117
014	15/1/18	0:57	37°51,084	54°05,916	31157	15/1/18	2:15	37°47,363	54°12,685	32325
015	15/1/18	2:33	37°47,595	54°12,779	32603	15/1/18	3:09	37°49,523	54°09,853	33159
016	15/1/18	3:16	37°49,167	59°09,438	33242	15/1/18	3:36	37°47,450	54°09,683	33560
017	15/1/18	3:55	37°47,477	54°09,993	33830	15/1/18	4:24	37°49,864	54°10,082	34271
018	15/1/18	4:26	37°50,018	54°10,720	34307	15/1/18	4:31	37°49,525	54°10,803	343463
019	15/1/18	4:35	37°49,526	54°10,804	34483	15/1/18	5:00	37°47,495	54°10,662	34823
020	15/1/18	5:16	37°47,490	54°11,094	35054	15/1/18	5:41	37°48,587	54°08,993	35403
021	15/1/18	6:03	37°48,548	54°09,521	35760	15/1/18	6:28	37°48,424	54°12,259	36139
022	15/1/18	6:32	37°48,683	54°12,378	36197	15/1/18	6:45	37°49,587	54°11,606	36409
023	15/1/18	6:50	37°49,386	54°11,307	36475	15/1/18	7:36	37°47,294	54°08,495	37900
Survey 2										
024	15/1/18	22:59	37°40,215	54°07,985	37950	16/1/18	0:03	37°44,750	54°05,214	635
025	16/1/18	0:09	37°45,032	54°04,762	723	16/1/18	4:33	37°57,895	53°42,153	4017
026	15/1/18	4:47	37°57,287	53°42,536	4113	16/1/18	5:35	37°58,47	53°47,59	4566
027	16/1/18	5:38	37°58,128	53°47.971	4627	16/1/18	6:46	37°53,570	53°44,586	5222
028	16/1/18	6:56	37°54,120	53°44,007	5311	16/1/18	8:28	38°01,667	53°47,055	6150
Survey 3										
029	18/1/18	12:49	38°35,346	54°19,506	6463	18/1/18	16:31	38°27,738	54°41,251	9833
030	18/1/18	16:36	38°27,514	54°41,187	9872	18/1/18	18:02	38°24,135	54°32,950	11158
031	18/1/18	18:03	38°24,060	54°32,858	11191	18/1/18	20:07	38°14,166	54°29,402	13038
032	18/1/18	20:09	38°14,102	54°29,188	13074	19/1/18	0:19	38°19,552	54°03,718	16825
033	19/1/18	0:24	38°19,873	54°03,722	16889	19/1/18	1:36	38°25,647	54°04,281	17964
034	19/1/18	1:39	38°25,602	54°05,625	18017	19/1/18	6:05	38°19,136	54°32,568	22008
035	19/1/18	6:09	38°18,843	54°32,692	22060	19/1/18	9:08	38°04,589	54°26,405	24757
036	19/1/18	9:13	38°04,469	54°26,113	24820	19/1/18	14:09	38°06,633	53°54,981	29269
037	19/1/18	14:16	38°07,068	53°54,806	29351	19/1/18	16:02	38°15,336	53°58,810	30770
038	19/1/18	16:05	38°15,339	53°59,074	30810	19/1/18	21:06	38°08,093	54°29,590	1701
Survey 4										
039	20/1/18	23:01	38°20,767	54°33,139	1970	20/1/18	23:39	38°21,805	54°28,625	2476
040	20/1/18	23:44	38°22,117	54°28,657	2537	21/1/18	0:53	38°27,712	54°30,392	3461
041	21/1/18	0:58	38°27,724	54°30,882	3528	21/1/18	2:16	38°24,663	54°38,161	4566

042	21/1/18	2:21	38°24,266	54°38,097	4633	21/1/18	4:04	38°16,114	54°34,705	6006
043	21/1/18	4:14	38°16,171	54°33,721	6144	21/1/18	5:52	38°18,293	54°22,703	7445
044	21/1/18	5:54	38°18,174	54°22,517	7480	21/1/18	7:00	38°12,429	54°21,07	8355
045	21/1/18	7:03	38°12,244	54°21,247	8394	21/1/18	8:35	38°10,048	54°30,917	9405
Survey 5										
046	22/1/18	20:37	37°33,019	53°57,184	10224	22/1/18	21:21	37°30,342	53°55,792	10816
047	22/1/18	21:29	37°29,912	53°56,504	10933	22/1/18	23:07	37°34,930	54°06,310	12236
048	22/1/18	23:10	37°35,060	54°06,474	12265	23/1/18	0:31	37°41,276	54°11,583	13344
049	23/1/18	0:33	37°41,352	54°11,823	13376	23/1/18	1:41	37°43,283	54°19,291	14286
050	23/1/18	1:43	37°43,366	54°19,376	14303	23/1/18	3:10	37°49,949	54°25,154	15472
051	23/1/18	3:11	37°50,068	54°25,190	15485	23/1/18	5:01	37°59,954	54°27,243	16949
052	23/1/18	5:05	38°00,244	54°26,970	17013	23/1/18	6:51	38°00,902	54°14,758	18411
053	23/1/18	6:55	38°00,628	54°14,421	18469	23/1/18	8:12	37°53,620	54°14,248	19497
054	23/1/18	8:16	37°53,335	54°14,501	19556	23/1/18	9:10	37°52,218	54° 20,577	20271
055	23/1/18	9:18	37°51,540	54°20,680	20375	23/1/18	10:08	37°48,140	54°16,494	21063
056	23/1/18	10:17	37°48,313	54°15,664	21166	23/1/18	11:27	37°54,303	54°12,746	22086
057	23/1/18	11:34	37°54,637	54°13,383	22186	23/1/18	13:13	37°53,748	54°24,781	23501
058	23/1/18	13:19	37°54,266	54°24,961	23591	23/1/18	13:55	37°57,296	54°23,505	24061
059	23/1/18	14:03	37°57,234	54°22,690	24168	23/1/18	16:42	37°45,570	54°11,624	26300
060	23/1/18	16:48	37°45,443	54°11,046	26384	23/1/18	17:53	37°48,530	54°04,500	27242
061	23/1/18	17:55	37°48,572	54°04,019	27322	23/1/18	18:28	37°46,497	54°01,626	27717
062	23/1/18	18:34	37°45,950	54°01,537	27793	23/1/18	19:17	37°43,427	54°04,808	28221
063	23/1/18	19:22	37°42,818	54°04,905	28302	23/1/18	19:45	37°41,492	54°02,829	28622
064	23/1/18	19:49	37°41,517	54°02,407	28676	23/1/18	20:20	37°43.277	53°59.515	29074
065	23/1/18	20:24	37°43,314	53°59,056	29130	23/1/18	20:34	37°42,909	53°58,040	29267
066	23/1/18	20:39	37°42,493	53°57,878	29331	23/1/18	21:16	37°39,095	53°59,019	29825
067	23/1/18	21:19	37°38,884	53°58,929	29862	23/1/18	21:25	37°38,585	53°58,336	29944
068	23/1/18	21:28	37°38,604	53°57,997	29984	23/1/18	22:21	37°41,459	53°52,757	30692
069	23/1/18	22:25	37°41,433	53°52,355	30742	23/1/18	22:43	37°40,416	53°50,666	30989
070	23/1/18	22:48	37°39,973	53°50,611	31056	23/1/18	23:54	37°35,066	53°55,186	31932
071	23/1/18	23:57	37°34,936	53°55,519	31975	24/1/18	0:42	37°34,141	54°00,571	32572
072	24/1/18	0:49	37°33,702	54°00,917	32660	24/1/18	1:27	37°30,145	54°01,163	33186
Survey 6										
073	26/1/18	10:45	38°46,492	54°19,489	33780	26/1/18	12:57	38°40,014	54°32,110	35545
074	26/1/18	13:04	38°39,505	54°31,868	35637	26/1/18	15:44	38°32,508	54°15,453	37783
075	26/1/18	15:50	38°32,633	54°14,9	37858	26/1/18	16:55	38°38,159	54°12,177	38717
076	26/1/18	16:57	38°38,360	54°12,250	38751	26/1/18	17:18	38°39,712	54°13,939	39028
077	26/1/18	17:22	38°39,671	54°14,329	39076	26/1/18	18:13	38°36,307	54°18,541	39671
078	26/1/18	18:14	38°36,259	54°18,678	39778	26/1/18	19:24	38°34,897	54°26,369	40714
079	26/1/18	19:25	38°34,968	54°26,760	40733	26/1/18	20:02	38°37,622	54°29,285	41224
080	26/1/18	20:08	38°37,965	54°28,903	41297	26/1/18	21:09	38°38,588	54°21,818	42097
081	26/1/18	21:12	38°38,319	54°21,606	42147	26/1/18	22:06	38°33,446	54°20,427	42868
082	26/1/18	22:08	38°33,317	54°20,492	42897	26/1/18	22:38	38°31,451	54°23,080	43291
083	26/1/18	22:43	38°31,667	54°23,465	43363	26/1/18	23:40	38°36,441	54°26,135	44110
084	26/1/18	23:46	38°36,838	54°25,601	44200	27/1/18	2:13	38°39,068	54°08,699	46156
085	27/1/18	2:21	38°38,507	54°08,246	46254	27/1/18	5:49	38°19,812	54°03,582	49042
086	27/1/18	6:08	38°20,438	54°04,677	49288	27/1/18	6:32	38°20,809	54°01,826	49620
087	27/1/18	6:43	38°21,283	54°01,805	49762	27/1/18	7:19	38°20,569	54°05,846	50236
088	27/1/18	7:38	38°20,940	54°06,306	50446	27/1/18	8:12	38°21,578	54°02,030	50936
089	27/1/18	8:46	38°22,447	54°03,934	51391	27/1/18	9:20	38°19,357	54°03,222	51847

7 Data and Sample Storage and Availability

Immediately after the cruise, metadata, the cruise summary report (CSR) and hydoacoustic data have been submitted to BSH/DOD. Raw seismic data are stored in the data base system of the research group "Marine Technology – Environmental Research" (Prof. Dr. Spieß) at the University of Bremen, Faculty of Geosciences on a mirrored RAID System. Data are available on request after a moratorium of three years after the cruise. Cores retrieved during this cruise are stored in the MARUM core repository and are available to other colleagues using official requests. All other samples collected during the cruise are stored in the labs of the respective principle investigators/institutions and will be processes by the groups that participated in cruise SO260. All data will be made available on request after a moratorium of 3 years.

8 Acknowledgements

We thank Master Oliver Meyer and the crew of the RV SONNE for their excellent support and helpfulness during cruise SO260. Only with their great help we were able to carry out our research and sampling activities as planned and to collect data and samples of great scientific value. All cruise participants have enjoyed the friendly and supportive atmosphere on board of the ship and for some of them – in particular some of the younger colleagues of whom some were on board of a ship for the very first time – the cruise will be a memorable, lifetime experience.

We gratefully acknowledge the German Research Foundation (DFG) for funding this expedition in the framework of the Excellence Cluster „The Ocean in the Earth System" MARUM (MARUM - Center for Marine Environmental Sciences at the University of Bremen) and the Helmholtz Association (Alfred Wegener Institute Helmholtz Centre for Polar and Marine Research, Bremerhaven) for additional financial support. We also thank Master Niels Jacobi and the Leitstelle Deutsche Forschungsschiffe, Institute of Geology, University of Hamburg and BRIESE Research for their comprehensive support in logistic preparation of the cruise.

9. References

Arnold, G.L., Weyer, S., Anbar, A.D., 2004. Fe isotope variations in natural materials measured using high mass resolution multiple collector ICPMS. Analytical Chemistry 76(2), 322-327.

Bar-Or, I., Elvert, M., Eckert, W., Kushmaro, A., Vigderovich, H., Zhu, Q., Ben-Dov, E., Sivan. O., 2017. Iron-coupled anaerobic oxidation of methane performed by a mixed bacterial-archaeal community based on poorly reactive minerals. Environmental Science & Technology 51, 12293-12301.

Baumann K.-H., Andruleit, H., Samtleben, C., 2000. Coccolithophores in the Nordic Seas: Comparison of living communities with surface sediment assemblages. Deep-Sea Research II 47 (9-11), 1743-1772.

Beal, E.J., House, C.H., Orphan, V.J., 2009. Manganese- and iron-dependent marine methane oxidation. Science 325**,** 184-187. doi: 10.1126/science.1169984

Boetius, A., Ravenschlag, K., Schubert, C. J., Rickert, D., Widdel, F., Gieseke, A., Amann, R., Jørgensen, B. B., Witte, U., Pfannkuche, O., 2000. A marine microbial consortium apparently mediating anaerobic oxidation of methane. Nature 407, 623-626.

Bravo, I., Figueroa, R.I., 2014. Towards the understanding of dinoflagellate cyst functions. Microorganisms 2, 11-32.

Cline, J.D., 1969. Spectrophotometric determination of hydrogen sulfide in natural waters. Limnology and Oceanography 14, 454-458.

Delaney, M.L., 1998. Phosphorus accumulation in marine sediments and the oceanic phosphorus cycle. Global Biogeochemical Cycles 12(4), 563-572. doi:10.1029/98GB02263

Egger, M., Rasigraf, O., Sapart, C.L.J., Jilbert, T., Jetten, M.S., Röckmann, T., Van Der Veen, C., BâNdă, N., Kartal, B., Ettwig, K.F., 2015. Iron-mediated anaerobic oxidation of methane in brackish coastal sediments. Environmental Science & Technology 49, 277-283.

Egger, M., Hagens, M., Sapart, C.J., Dijkstra, N., van Helmond, N.A., Mogollón, J.M.,Risgaard-Petersen, N., van der Veen, C., Kasten, S., Riedinger, N., Böttcher, M.E., Röckmann, T., Jørgensen, B.B., Slomp, C.P., 2017. Iron oxide reduction in methane-rich deep Baltic Sea sediments. Geochimica et Cosmochimica Acta 207, 256-276

Ettwig, K.F., Zhu, B., Speth, D., Keltjens, J.T., Jetten, M.S.M., Katal, B., 2016. Archaea catalyse iron-dependent anaerobic oxidation of methane. Proceedings of the National Academy of Sciences 113, 12792-12796.

Froelich, P.N., Klinkhammer, G.P., Bender, M.L., Luedtke, N.A., Heath, G.R., Cullen, D.,Dauphin, P., Hammond, D., Hartman, B., Maynard, V., 1979. Early oxidation of organic matter in pelagic sediments of the eastern equatorial Atlantic: suboxic diagenesis. Geochimica et Cosmochimica Acta 43, 1075-1090.

Gayoso, A.M., 1995. Bloom of *Emiliania huxleyi* (Prymnesiophyceae) in the western South Atlantic. Journal of Plankton Reseach 17 (8), 1717-1722.

Gostiaux, L., van Haren, H., 2010. Extracting meaningful information from uncalibrated backscattered echo intensity data. Journal of Atmospheric and Oceanic Technology 27, 943-949. doi: 10.1175/2009JTECHO704.1

Grasshoff, K., Kremling, K., Ehrhardt, M. (eds), 1999. Methods of seawater analysis, 3rd edition. Wiley-VCH, Weinheim, New York.

Guidi, L., Chaffron, S., Bittner, L., Eveillard, D., Larhlimi, A., Roux, S., Darzi, Y., Audic, S., Berline, L., Brum, J. R., Coelho, L. P., Espinoza, J. C. I., Malviya, S., Sunagawa, S., Dimier, C., Kandels-Lewis, S., Picheral, M., Poulain, J., Searson, S., Stemmann, L., Not, F., Hingamp, P., Speich, S., Follows, M., Karp-Boss, L., Boss, E., Ogata, H., Pesant, S., Weissenbach, J., Wincker, P., Acinas, S. G., Bork, P., de Vargas, C., Iudicone, D., Sullivan, M. B., Raes, J., Karsenti, E., Bowler, C., Gorsky, G., 2016. Plankton networks driving carbon export in the oligotrophic ocean. Nature 532, 465-470.

Henkel, S., Strasser, M., Schwenk, T., Hanebuth, T.J.J., Hüsener, J., Arnold, G.L., Winkelmann, D., Formolo, M., Tomasini, J., Krastel, S., Kasten, S., 2011. An interdisciplinary investigation of a recent submarine mass transport deposit at the continental margin off Uruguay. Geochemistry, Geophysics, Geosystems 12, Q08009, doi:10.1029/2011GC003669.

Henkel, S., Schwenk, T., Hanebuth, T. J. J., Strasser, M., Riedinger, N., Formolo, M., Tomasini, J., Krastel, S., Kasten, S., 2012. Pore water geochemistry as a tool for identifying and dating recent mass-transport deposits, Submarine Mass Movements and Their Consequences: 5th International Symposium (Advances in Natural and Technological Hazards Research, 31), Y. Yamada, K. Kawamura, K. Ikehara, Y. Ogawa, R. Urgeles, D. Mosher, J. Chaytor, M. Strasser (eds.), Springer, 87-97.

Henkel, S., Kasten, S., Poulton, S.W., Staubwasser, M., 2016. Determination of the stable iron isotopic composition of sequentially leached iron phases in marine sediments. Chemical Geology 421, 17-32.

Henkel, S., Kasten, S. , Hartmann, J. , Busso, A.S., Staubwasser, M., 2018. Iron cycling and stable Fe isotope fractionation in Antarctic shelf sediments, King George Island. Geochimica et Cosmochimica Acta 237, 320-338, doi: 10.1016/j.gca.2018.06.042.

Hensen, C., Zabel, M., Pfeifer, K., Schwenk, T., Kasten, S., Riedinger, N., Schulz, H.D., Boetius, A., 2003. Control of sulfate pore-water profiles by sedimentary events and the significance of anaerobic oxidation of methane for the burial of sulfur in marine sediments. Geochimica et Cosmochimica Acta 67, 2631-2647.

Hensen, C., Zabel, M., Schulz, H.D., 2000. A comparison of benthic nutrient fluxes from deep-sea sediments off Namibia and Argentina. Deep-Sea Research II 47, 2029-2050.

Hori, T., Müller, A., Igarashi, Y., Conrad, R., Friedrich, M.W., 2010. Identification of iron-reducing microorganisms in anoxic rice paddy soil by 13C-acetate probing. ISME Journal 4, 267-278.

Hori, T., Aoyagi, T., Itoh, H., Narihiro, T., Oikawa, A., Suzuki, K., Ogata, A., Friedrich, M.W., Conrad, R., Kamagata, Y., 2015. Isolation of microorganisms involved in reduction of crystalline iron (III) oxides in natural environments. Frontiers in Microbiology 6, 386.

Inthorn, M., Mohrholz, V., Zabel, M., 2006. Nepheloid layer distribution in the Benguela upwelling area offshore Namibia. Deep Sea Research Part I 53, 1423-1438.

Jensen, M.M., Thamdrup, B., Rysgaard, S., Holmer, M., Fossing H., 2003. Rates and regulation of microbial iron reduction in sediments of the Baltic-North Sea transition. Biogeochemistry 65, 295-317.

März, C., Hoffmann, J., Bleil, U., de Lange, G. J., Kasten, S., 2008. Diagenetic changes of magnetic and geochemical signals by anaerobic methane oxidation in sediments of the Zambezi deep-sea fan (SW Indian Ocean). Marine Geology 255, 118-130.

März, C., Riedinger, N., Sena, C., Kasten, S., 2018. Phosphorus dynamics around the sulphate-methane transition in continental margin sedimnts: Authigenic apatite and Fe(II) phosphates. Marine Geology 404, 84-96.

Manheim, F.T., Sayles, F.L., 1974. Composition and origin of interstitial waters of marine sediments, based on deep sea drill cores. In Goldberg, E.D. (Ed.), The Sea (Vol. 5): Marine Chemistry, New York (Wiley), 527-568.

Mewes, K., Mogollón, J.M., Picard, A., Rühlemann, C., Kuhn, T., Nöthen, K., Kasten, S., 2014. Impact of depositional and biogeochemical processes on small scale variations in nodule abundance in the Clarion-Clipperton Fracture Zone. Deep-Sea Reseach, Part I: Oceanogr. Res. Pap. 91, 125–141. doi:10.1016/j.dsr.2014.06.001

Ohde, T., Fiedler, B., Körtzinger, A., 2015. Spatio-temporal distribution and transport of particulate matter in the eastern tropical North Atlantic observed by Argo floats. Deep Sea Research Part I 102, 26-42.

Oni, O., Miyatake, T., Kasten, S., Richter-Heitmann, T., Fischer, D., Wagenknecht, L., Kulkarni, A., Blumers, M., Shylin, S.I., Ksenofontov, V., Costa, B.F.O., Klingelhöfer, G. Friedrich, M.W., 2015. Distinct microbial populations are tightly linked to the profile of dissolved iron in the methanic sediments of the Helgoland mud area, North Sea. Frontiers in Microbiology 6, doi:10.3389/fmicb.2015.0036.

Revsbech, N.P., 1989. An oxygen microsensor with a guard cathode. Limnology and Oceanography 34, 474–478. doi:10.4319/lo.1989.34.2.0474

Riedinger, N., Pfeifer, K., Kasten, S., Garming, J.F.L., Vogt, C., Hensen, C., 2005. Diagenetic alteration of magnetic signals by anaerobic oxidation of methane related to a change in sedimentation rate. Geochimica et Cosmochimica Acta 69, 4117-4126.

Riedinger, N., Formolo, M.J., Lyons, T.W., Henkel, S., Beck, A., Kasten, S., 2014. An inorganic geochemical argument for coupled anaerobic oxidation of methane and iron reduction in marine sediments. Geobiology. doi:10.1111/gbi.12077

Riedinger, N., Brunner, B., Krastel, S., Arnold, G.L., Wehrmann, L.M., Formolo, M.J., Beck, A., Bates, S.M., Henkel, S., Kasten, S., Lyons, T.W., 2017. Sulfur cycling in an iron oxide-dominated, dynamic marine depositional system (Argentine Basin). Frontiers in Earth Sciences 5, 33.

Roden, E.E., Lovley, D.R., 1993. Dissimilatory Fe (III) reduction by the marine microorganism *Desulfuromonas acetoxidans*. Applied & Environmental Microbiology 59, 734-742.

Saavedra-Pellitero, M., Baumann, K.-H., 2015. Comparison of living and surface sediment coccolithophore assemblages in the Pacific sector of the Southern Ocean. Micropaleontology 61 (6), 507-520.

Seeberg-Elverfeldt, J., Schlüter, M., Feseker, T., Kölling, M. 2005. Rhizon sampling of porewaters near the sediment-water interface of aquatic systems. Limnology and Oceanography: Methods 3, 361-371.

Segarra, K.E.A., Comerford, C., Slaughter, J., Joye, S.B., 2013. Impact of electron acceptor availability on the anaerobic oxidation of methane in coastal freshwater and brackish wetland sediments. Geochimica Cosmochimica Acta 115, 15-30. doi: 10.1016/j.gca.2013.03.029

Smayda, T.J., Trainer, V.L., 2010. Dinoflagellate blooms in upwelling systems: Seeding, variability, and contrasts with diatom bloom behaviour. Progress in Oceanography 85, 92-107.

Thierstein, H.R., Young, J.R., 2004. Coccolithophores – from molecular processes to global impact. Springer-Verlag Berlin, Heidelberg, 565 pp.

Vandieken, V., Mußmann, M., Niemann, H., Jørgensen, B.B., 2006. *Desulfuromonas svalbardensis* sp. nov. and *Desulfuromusa ferrireducens* sp. nov., psychrophilic, Fe (III)-reducing bacteria isolated from Arctic sediments, Svalbard. International Journal of Systematic and Evolutionary Microbiology 56, 1133-1139.

Van der Plas, L., Tobi, A.C., 1965. A chart for judging the reliability of point counting results. American Journal of Science 236, 87-90.

Viollier, E., Inglett, P., Hunter, K., Roychoudhury, A., Van Cappellen, P., 2000. The ferrozine method revisited: Fe (II)/Fe (III) determination in natural waters. Applied Geochemistry 15, 785-790.

Weber, K.A., Achenbach, L.A., Coates, J.D., 2006. Microorganisms pumping iron: anaerobic microbial iron oxidation and reduction. Nature Review Microbiology 4, 752-764.

Whiticar, M.J., Faber, E., Schoell, M., 1986. Biogenic methane formation in marine and freshwater environments: CO_2 reduction vs. acetate fermentation - isotope evidence. Geochimica et Cosmochimica Acta 50, 693-709.

Winter, A., Siesser, W.G., 1994. Coccolithophores, Cambridge Univ. Press, 242 pp.

Zhang, C., Stapleton, R.D., Zhou, J., Palumbo, A.V., Phelps, T.J., 1999. Iron reduction by psychrotrophic enrichment cultures. FEMS Microbiology Ecology 30, 367-371.

Ziebis, W., McManus, J., Ferdelman, T., Schmidt-Schierhorn, F., Bach, W., Muratli, J., Edwards, K.J., Villinger, H., 2012. Interstitial fluid chemistry of sediments underlying the North Atlantic gyre and the influence of subsurface fluid flow. Earth and Planetary Science Letters 323, 79–91. doi:10.1016/j.epsl.2012.01.018

Zonneveld, K.A.F., Susek, E., Fischer, G., 2010. Seasonal variability of the organic-walled dinoflagellate cyst production in the coastal upwelling region off Cape Blanc (Mauritania): a five-year survey. Journal of Phycology 46, 202-215.

Appendices

Appendix 1: Parasound images of core locations

Appendix 2: Core descriptions and photos

a) Giant Box Corer
b) Gravity Corer
c) MeBo
d) Grab

Appendix 3: Physical properties

Appendix 4: Core labels and depths of samples taken for rock magnetic studies

Appendix 5: List of samples collected for microbiological analyses

Appendix 6: List of samples collected for organic geochemical analysis

Appendix 7: List of samples from Rosette-casts for investigation of coccolithophore assemblages

Appendix 1: Parasound images of core locations

Appendix 1: PARASOUND figures of core locations

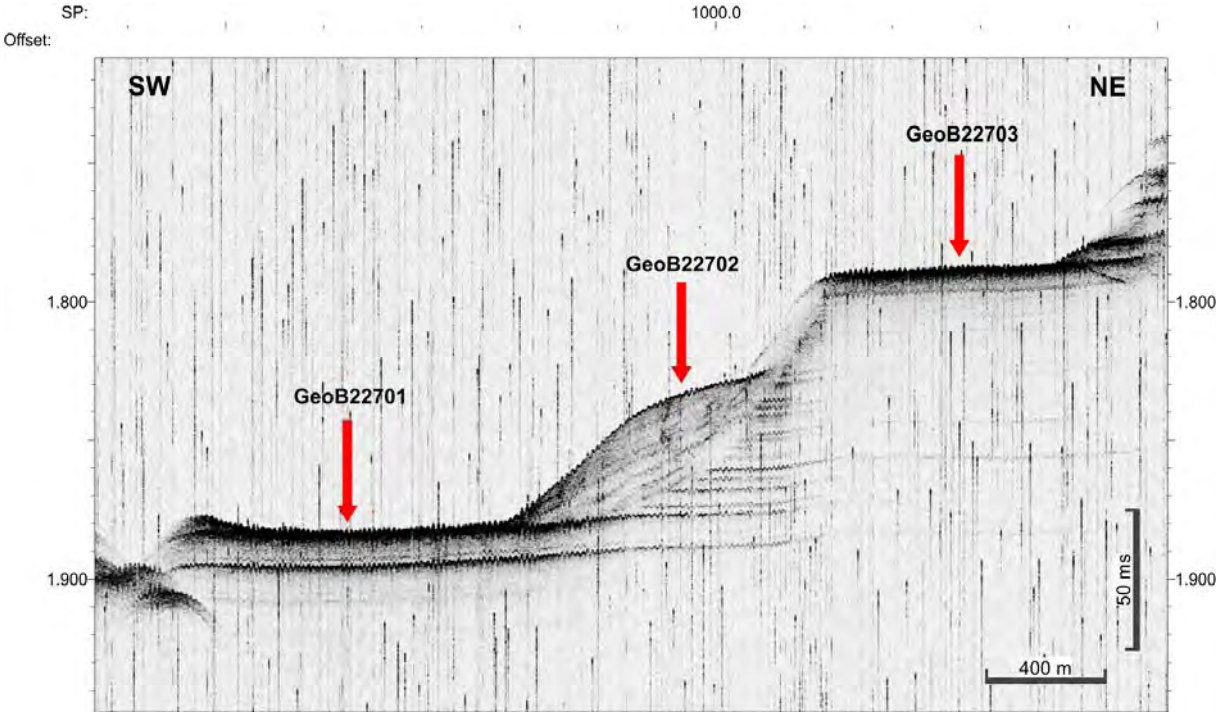

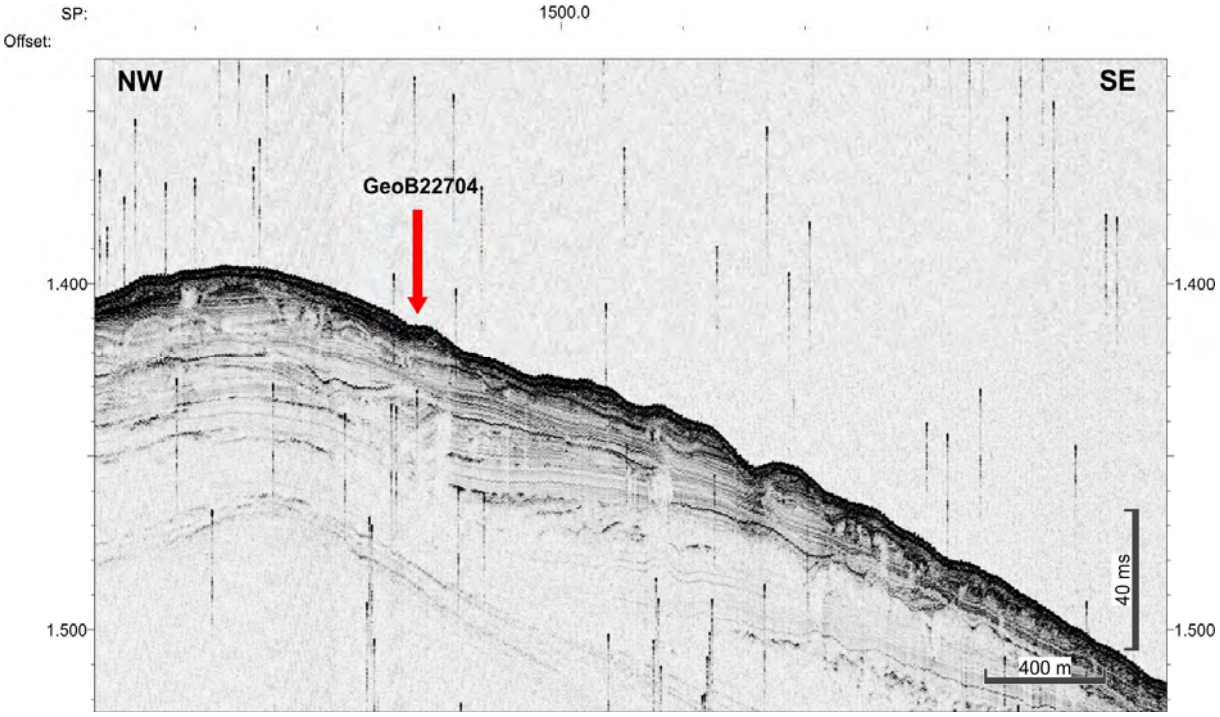

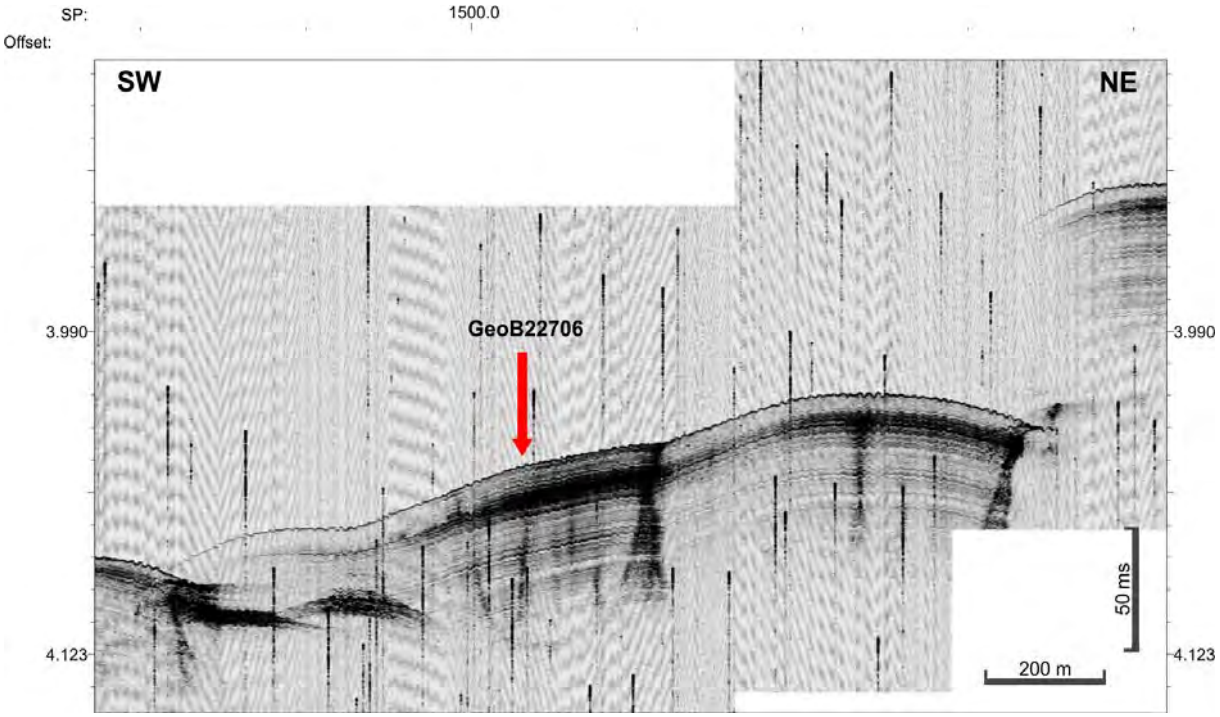
SP:
1500.0
Offset:
SW
NE
3.990
GeoB22706
3.990
50 ms
4.123
200 m
4.123

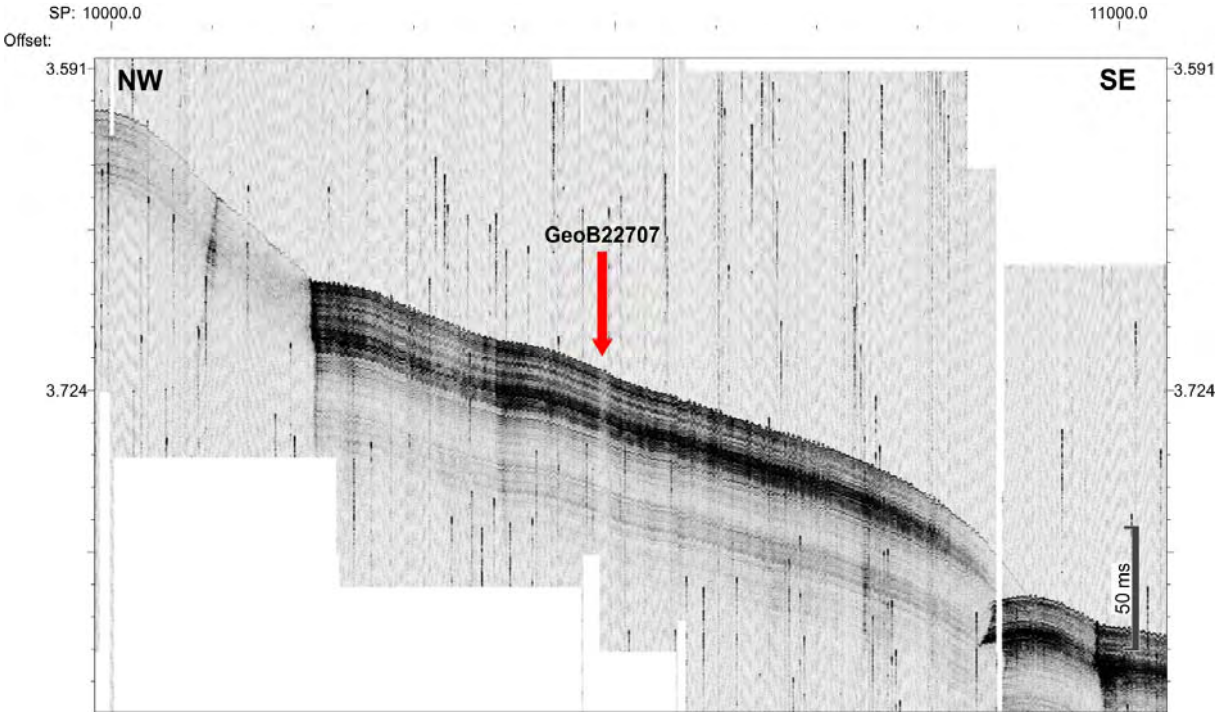
SP: 10000.0
11000.0
Offset:
3.591
NW
SE
3.591
GeoB22707
3.724
3.724
50 ms

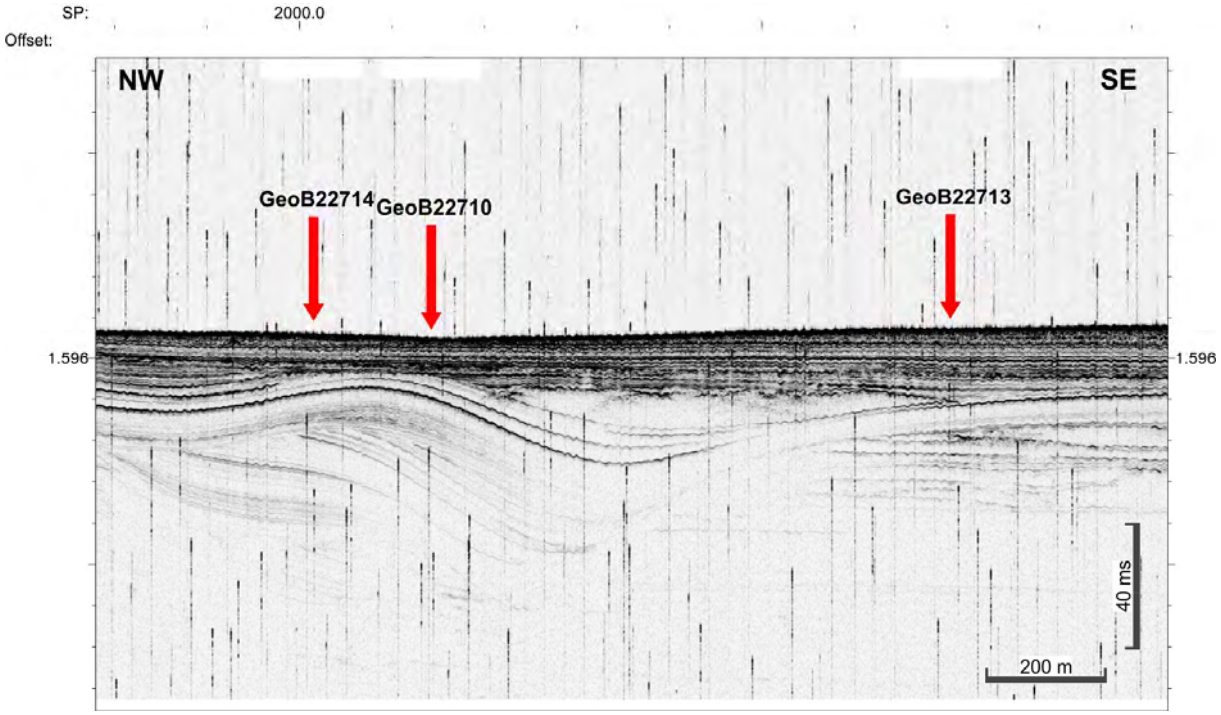
SP:
2000.0
Offset:
NW
SE
GeoB22714
GeoB22710
GeoB22713
1.596
1.596
40 ms
200 m

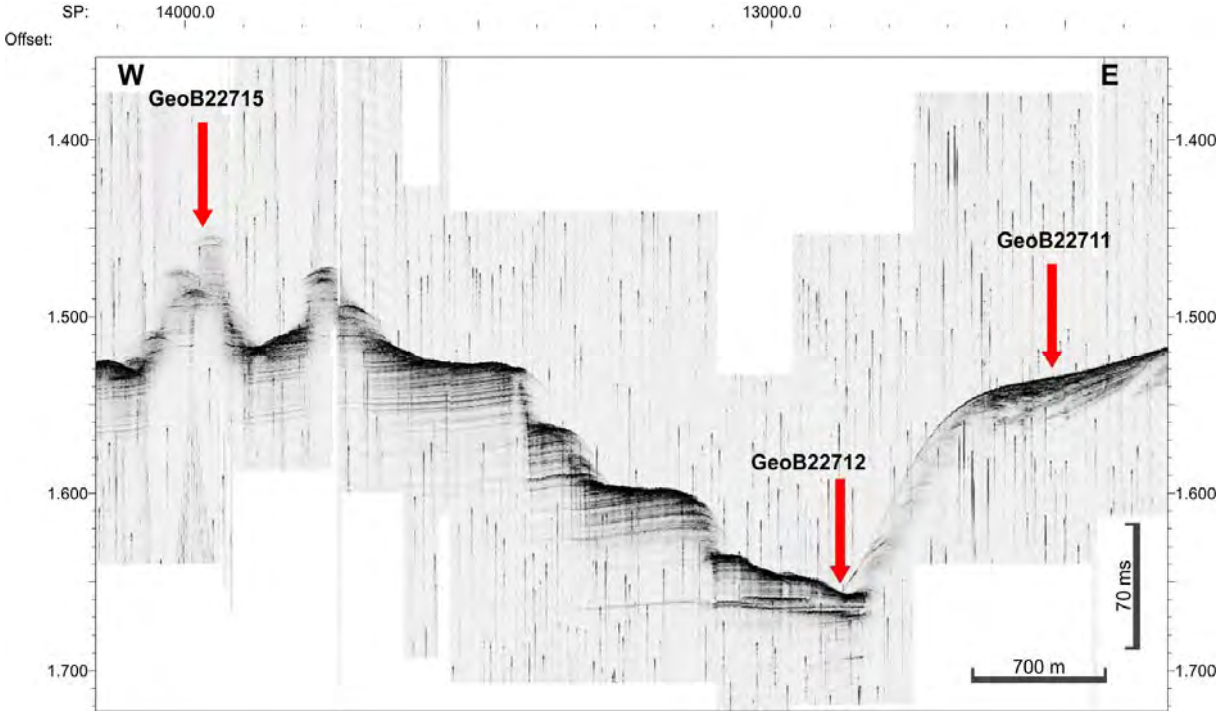
SP:
14000.0
13000.0
Offset:
W
E
GeoB22715
GeoB22711
GeoB22712
1.400
1.500
1.600
1.700
1.400
1.500
1.600
1.700
70 ms
700 m

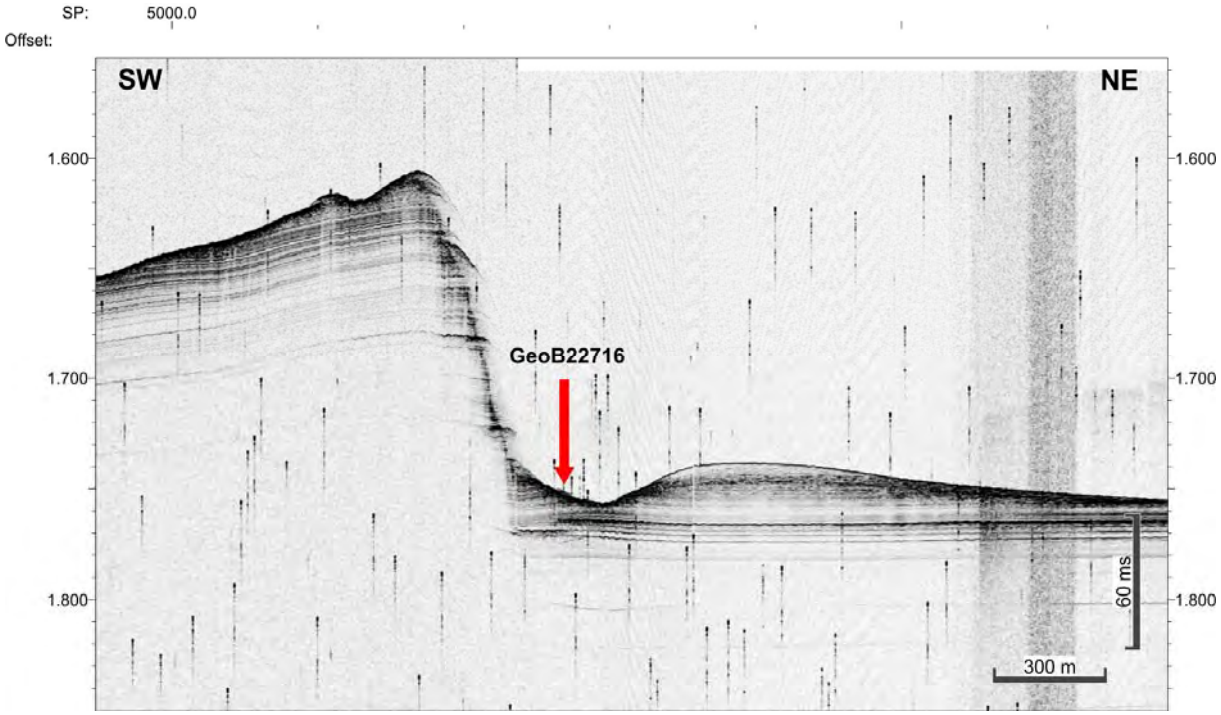
SP: 5000.0
Offset:
SW
NE
1.600
1.700
1.800
GeoB22716
60 ms
300 m

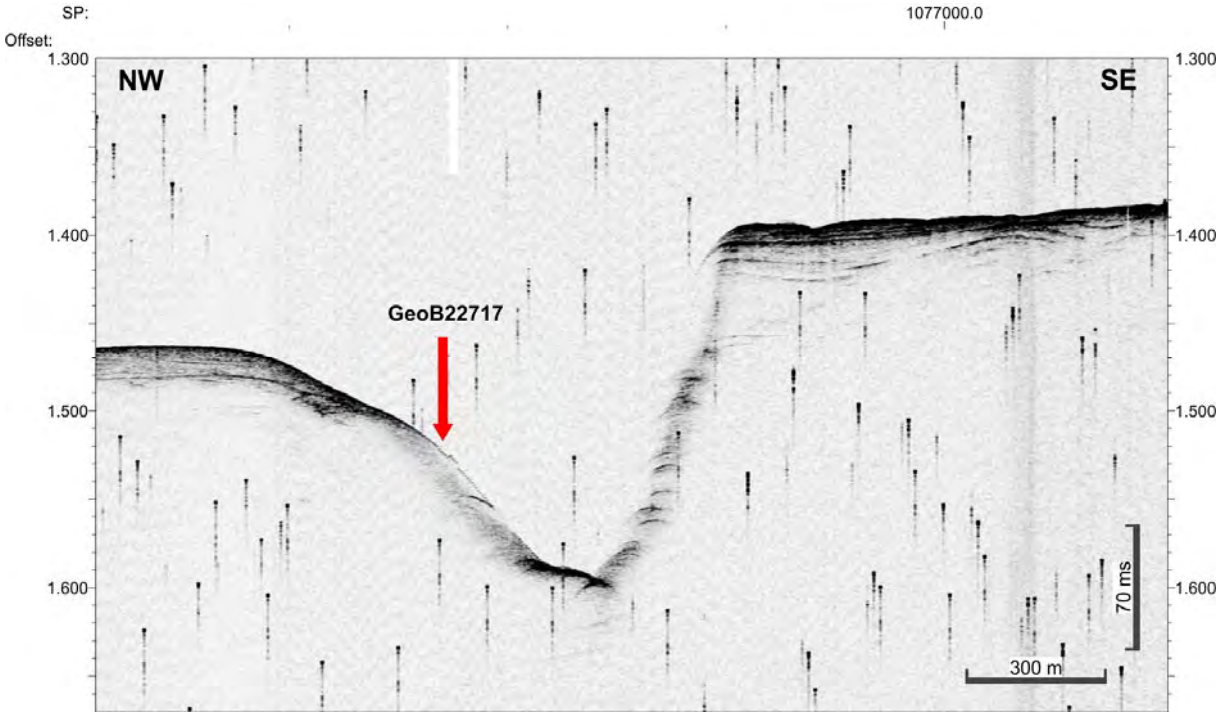
SP: 1077000.0
Offset:
NW
SE
1.300
1.400
1.500
1.600
GeoB22717
70 ms
300 m

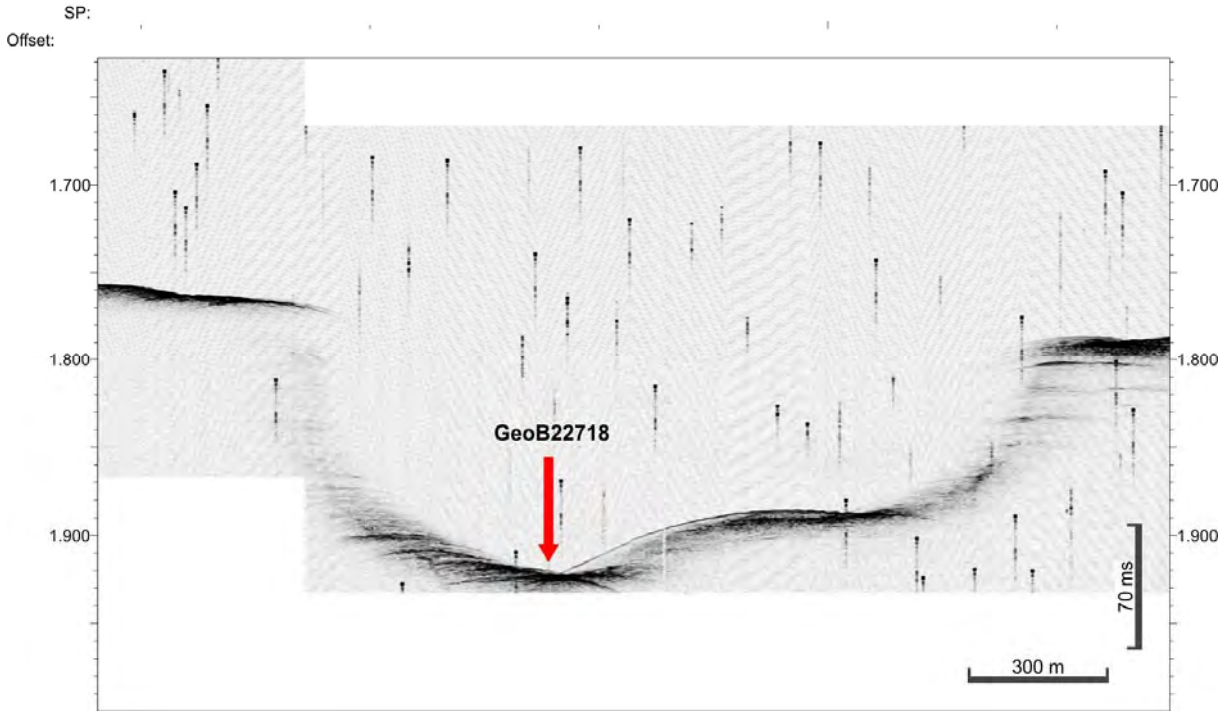
SP:
Offset:
1.700
1.800
1.900
GeoB22718
70 ms
300 m

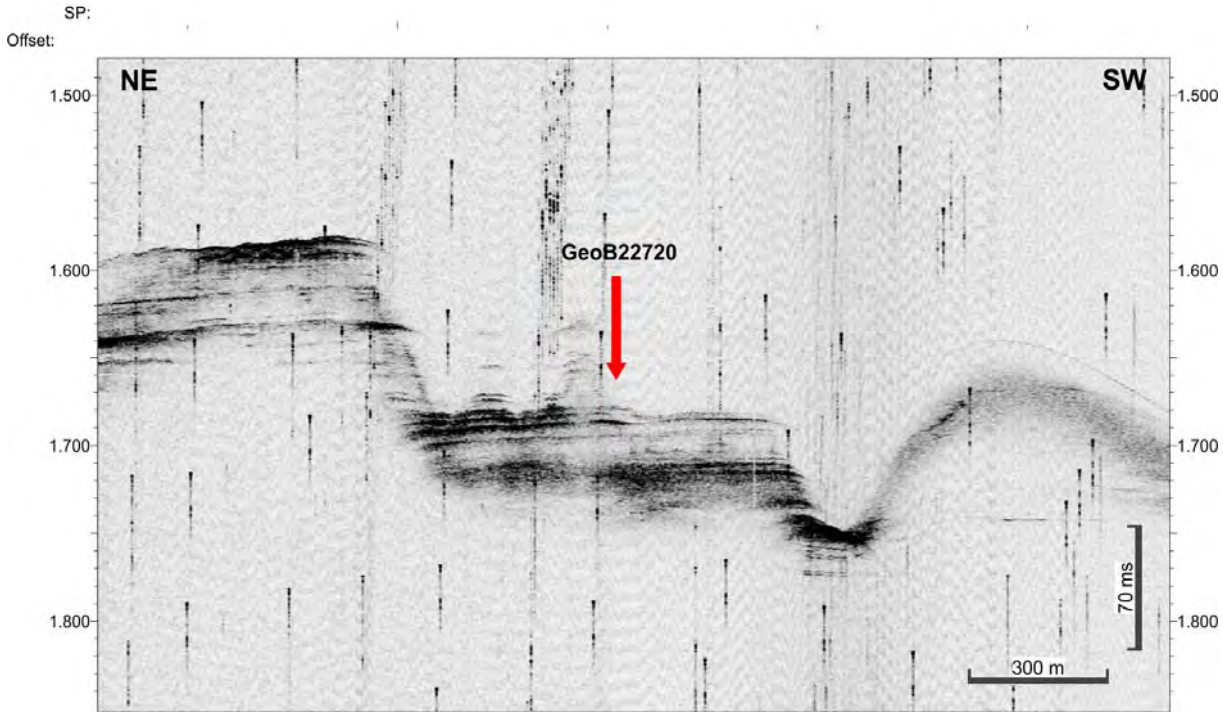
SP:
Offset:
NE
SW
1.500
1.600
1.700
1.800
GeoB22720
70 ms
300 m

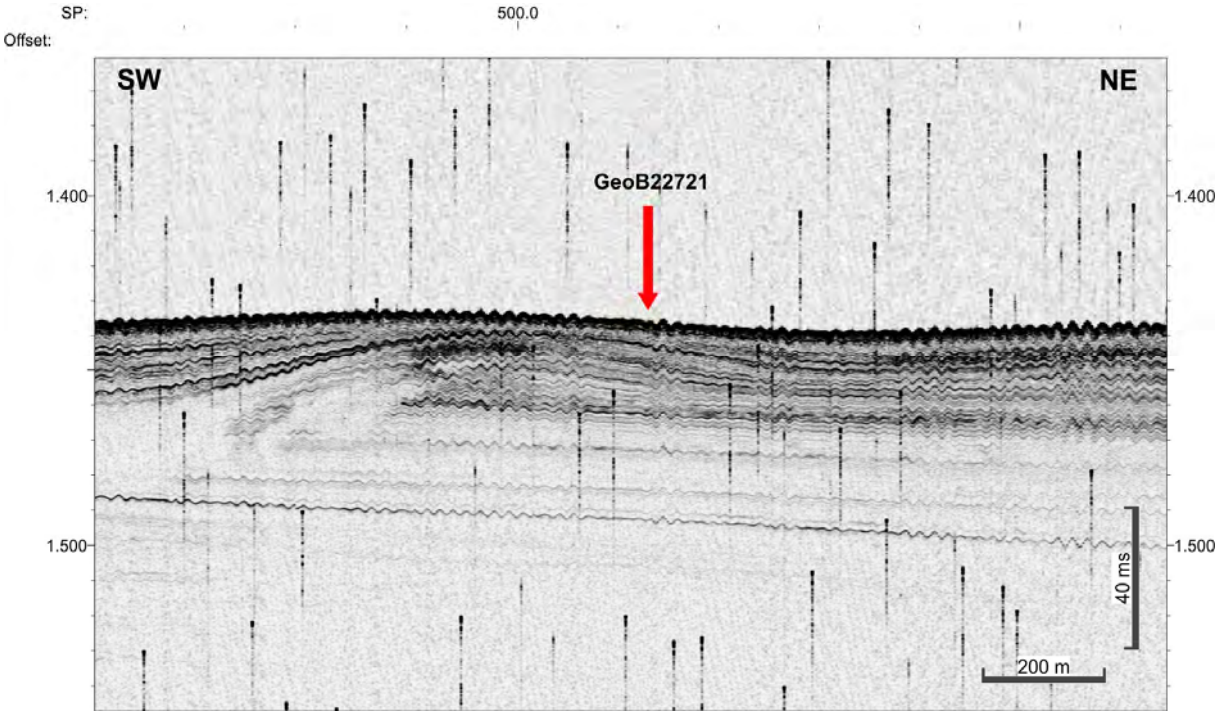
SP:
500.0
Offset:
SW
NE
GeoB22721
1.400
1.500
40 ms
200 m

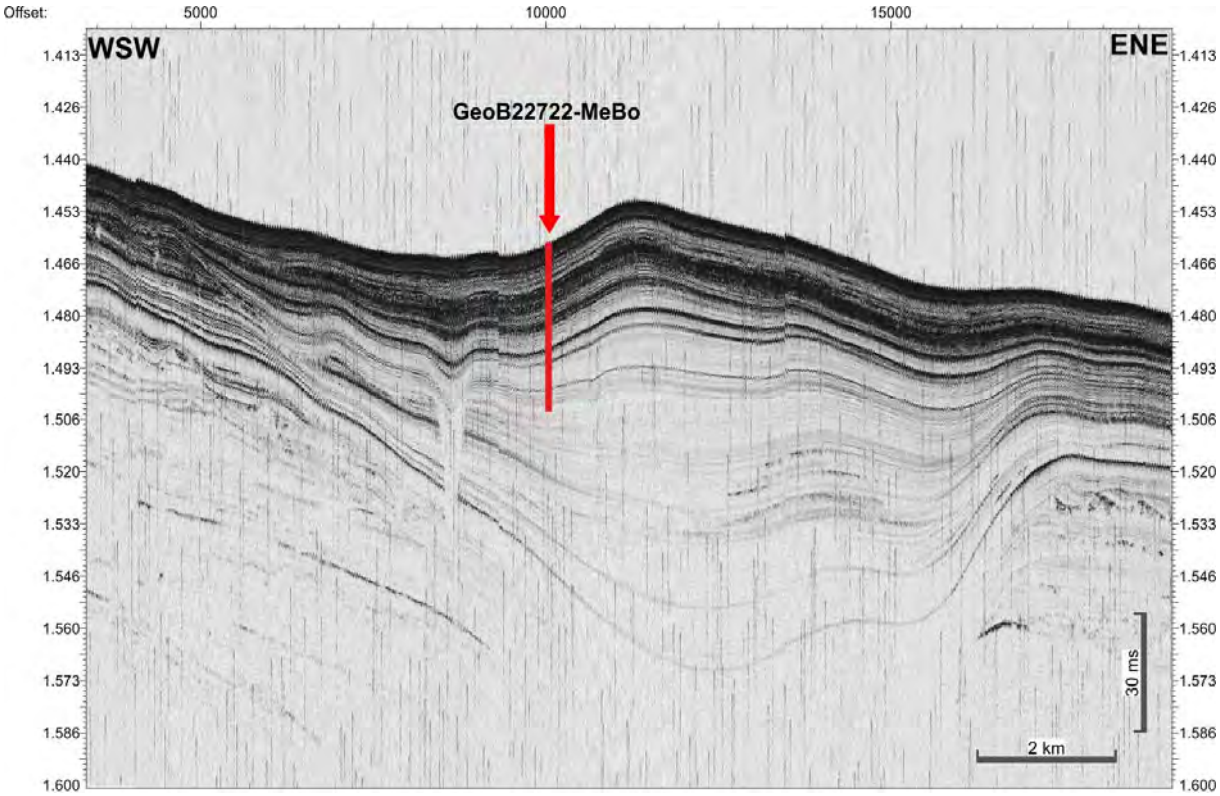
Offset:
5000
10000
15000
WSW
ENE
GeoB22722-MeBo
1.413
1.426
1.440
1.453
1.466
1.480
1.493
1.506
1.520
1.533
1.546
1.560
1.573
1.586
1.600
30 ms
2 km

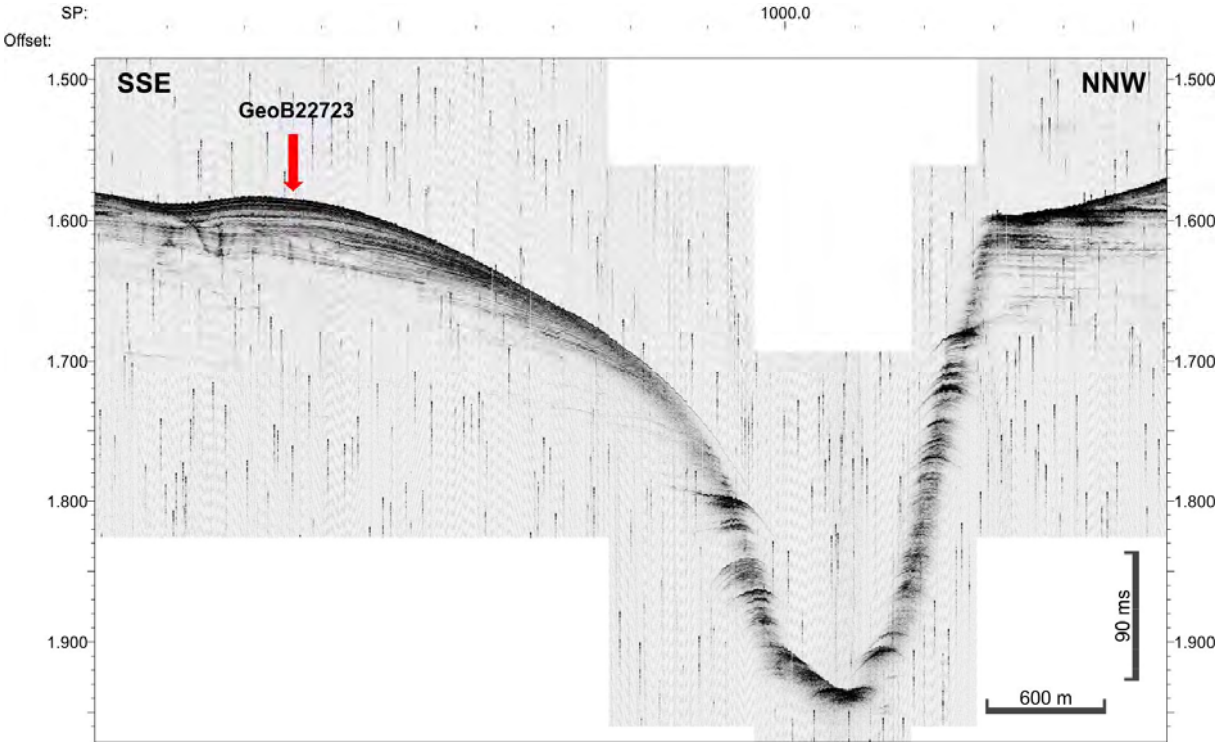
SP:
1000.0
Offset:
SSE
NNW
GeoB22723
1.500
1.600
1.700
1.800
1.900
90 ms
600 m

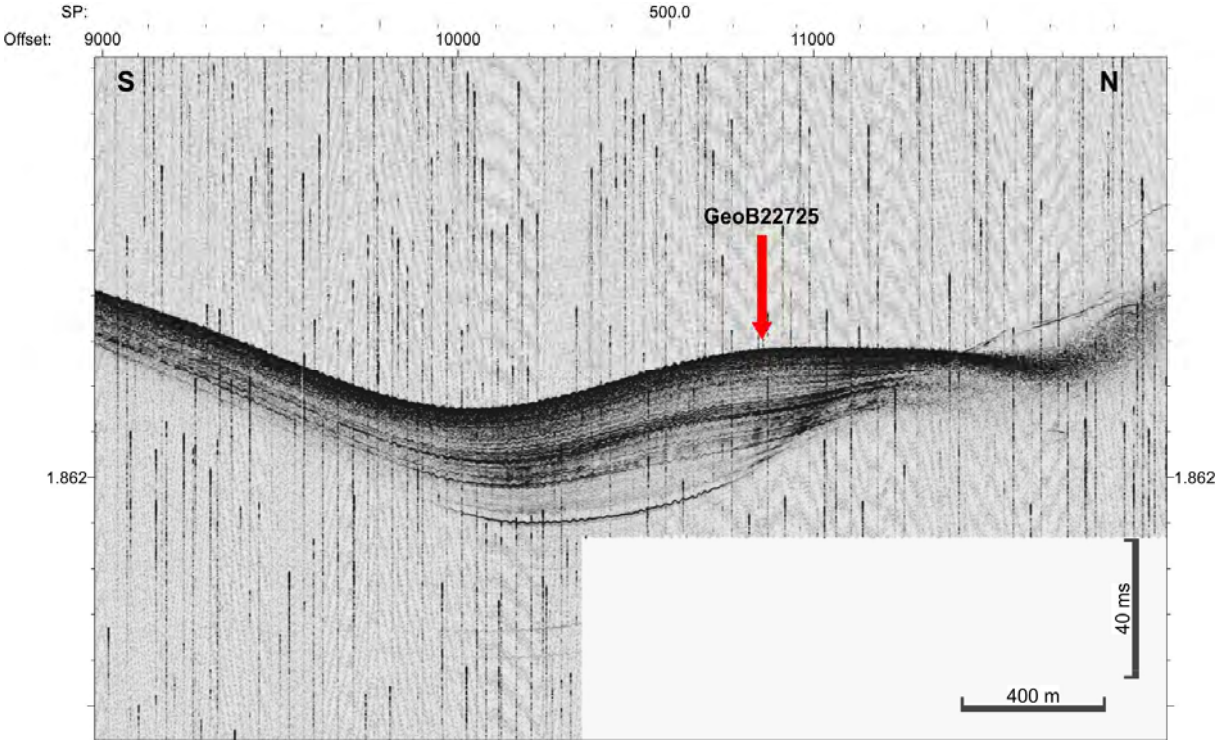
SP:
500.0
Offset:
9000
10000
11000
S
N
GeoB22725
1.862
40 ms
400 m

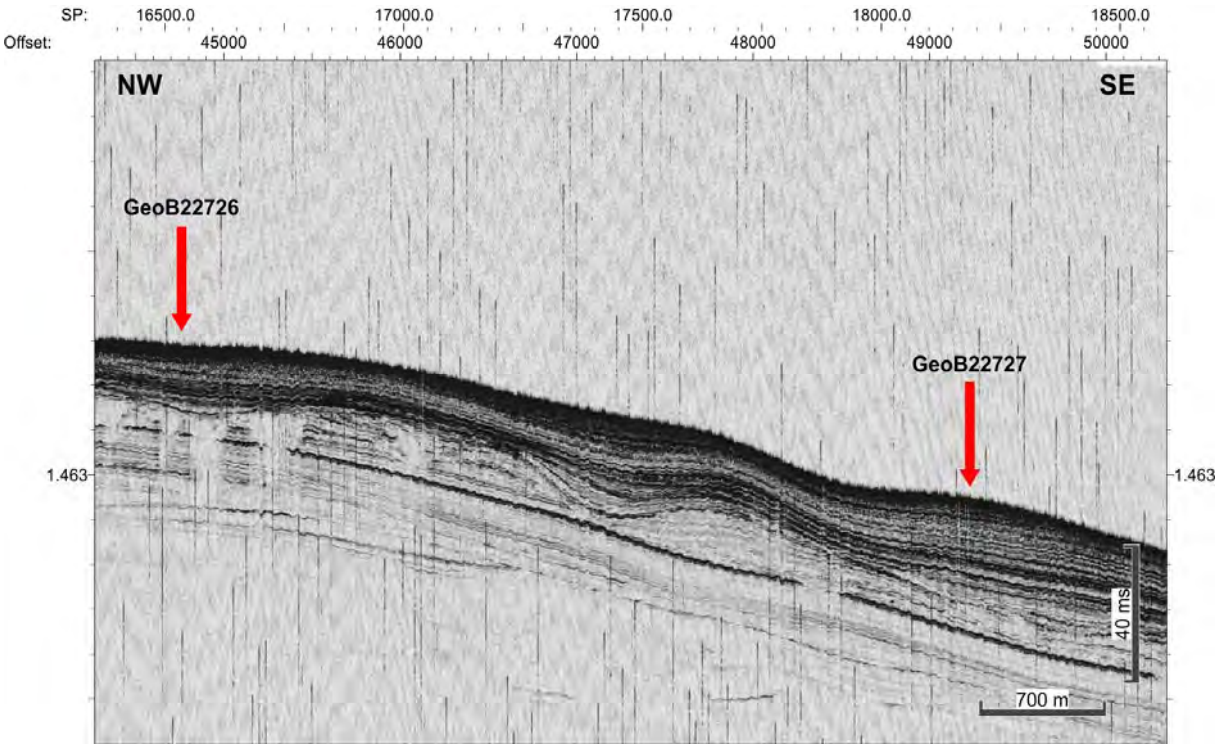
SP:
16500.0
17000.0
17500.0
18000.0
18500.0
Offset:
45000
46000
47000
48000
49000
50000
NW
SE
GeoB22726
GeoB22727
1.463
1.463
40 ms
700 m

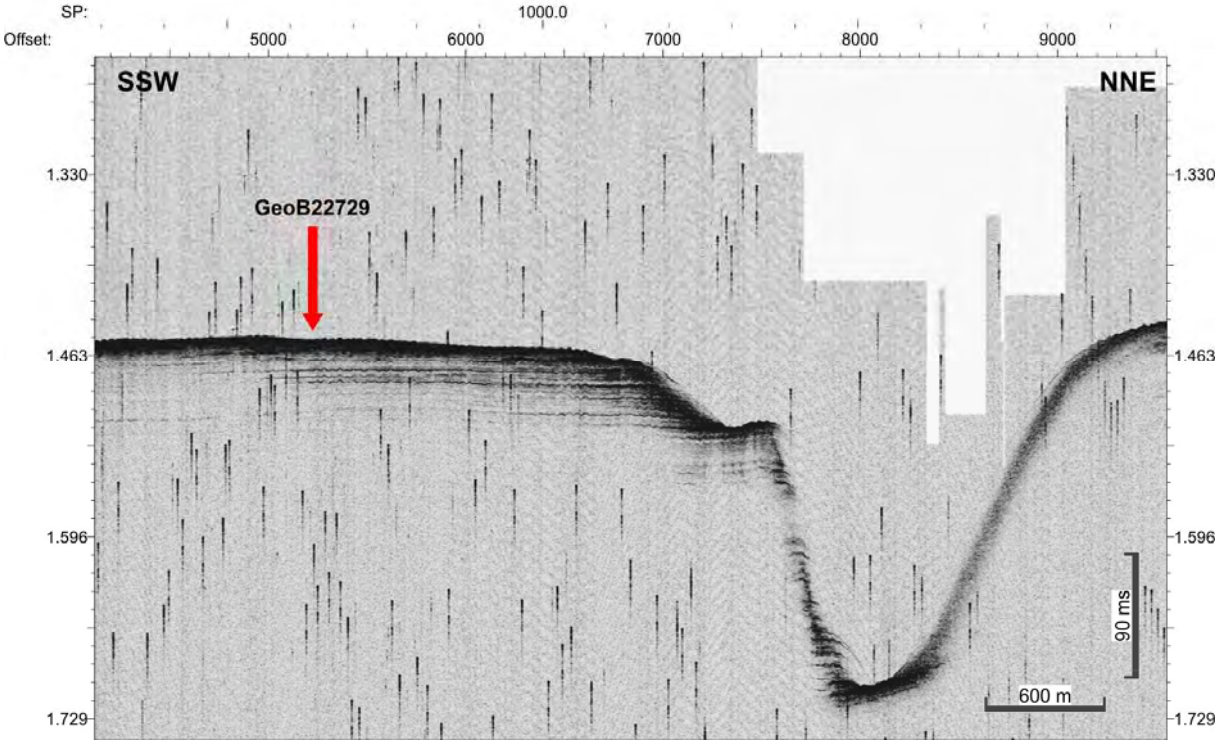
SP:
1000.0
Offset:
5000
6000
7000
8000
9000
SSW
NNE
GeoB22729
1.330
1.330
1.463
1.463
1.596
1.596
1.729
1.729
90 ms
600 m

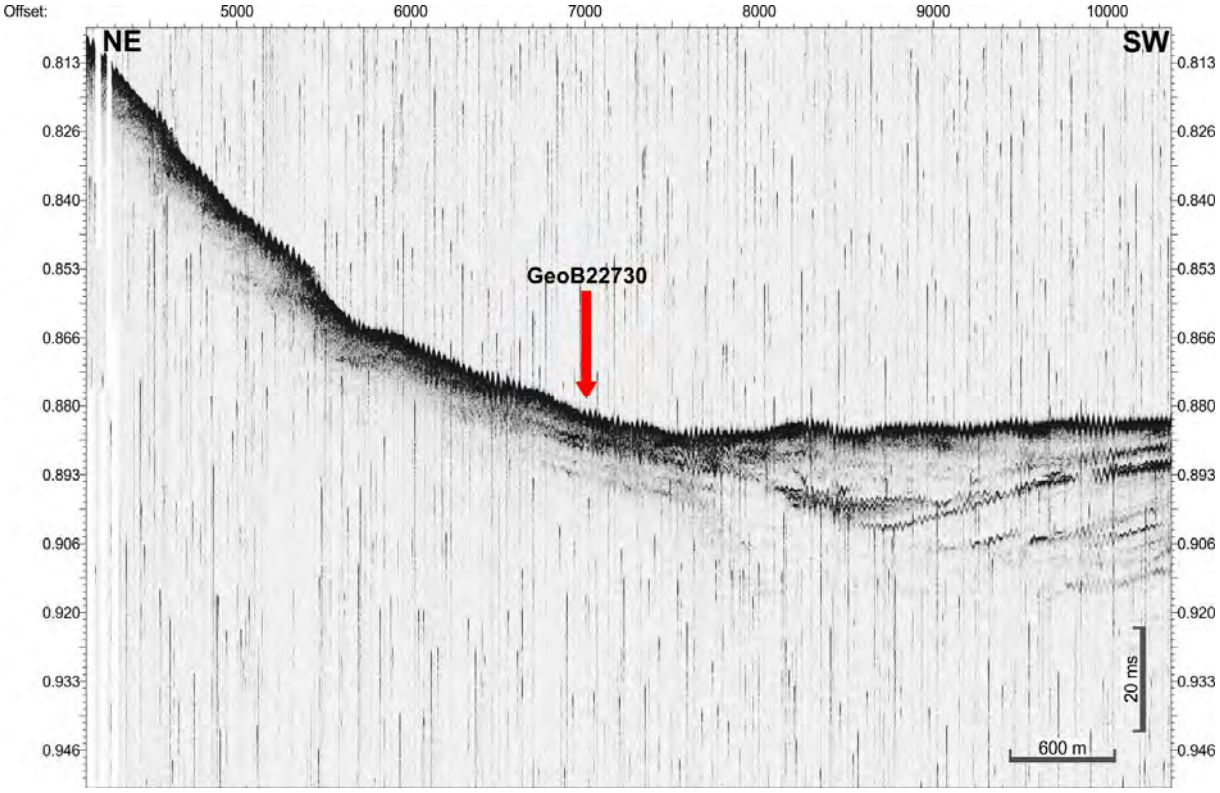
Offset:
5000
6000
7000
8000
9000
10000
NE
SW
0.813
0.826
0.840
0.853
0.866
0.880
0.893
0.906
0.920
0.933
0.946
GeoB22730
20 ms
600 m

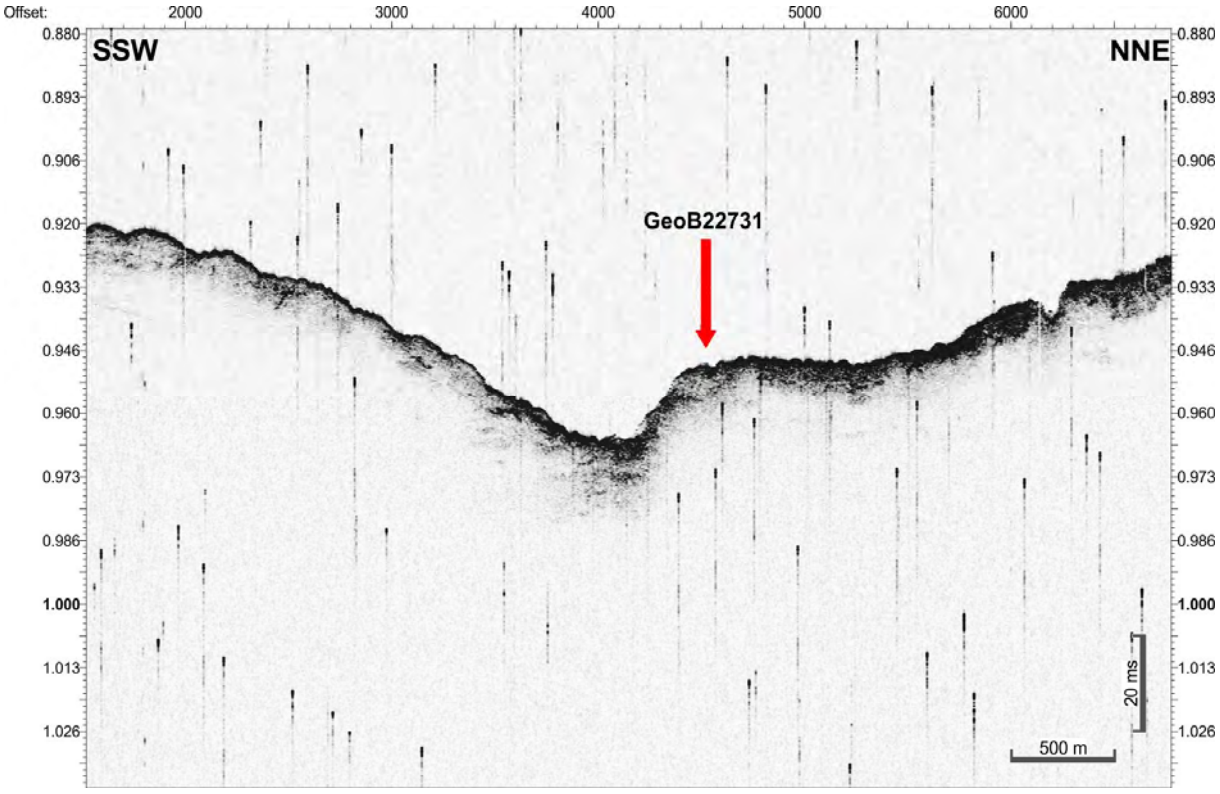
Offset:
2000
3000
4000
5000
6000
SSW
NNE
0.880
0.893
0.906
0.920
0.933
0.946
0.960
0.973
0.986
1.000
1.013
1.026
GeoB22731
20 ms
500 m

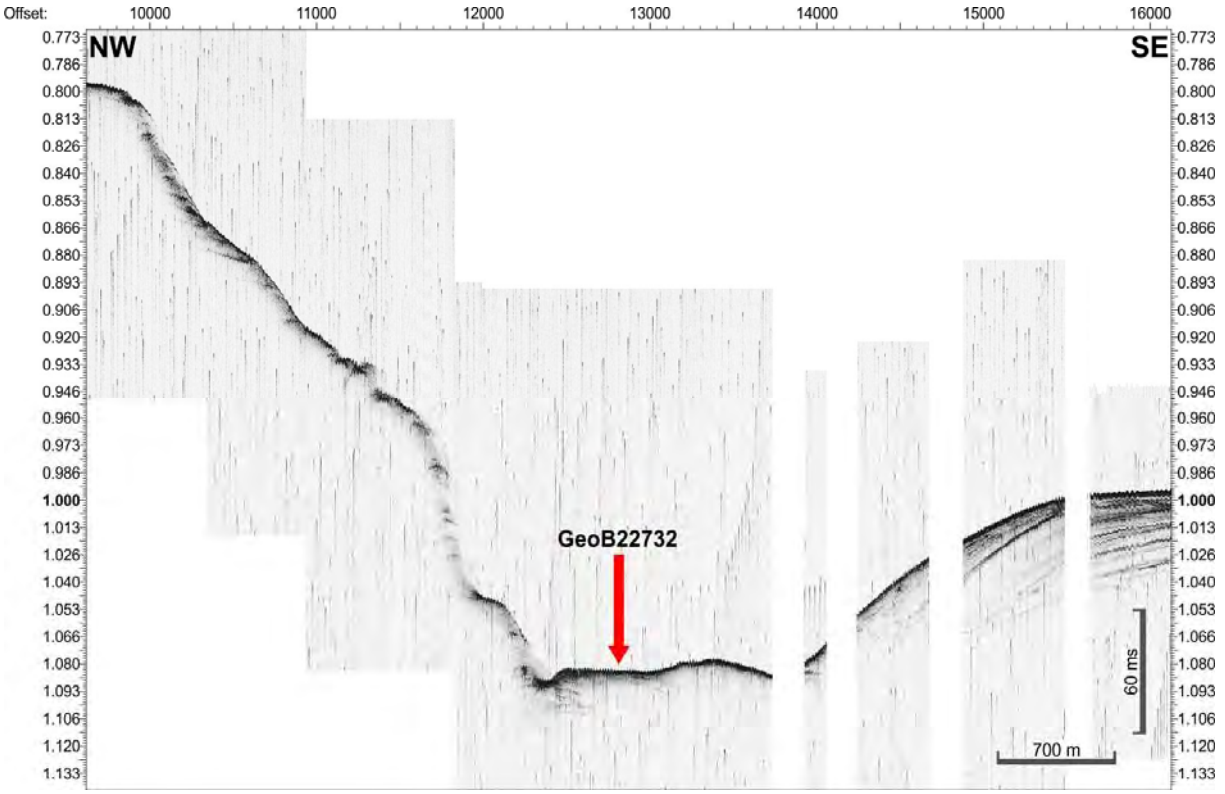
Offset:
10000
11000
12000
13000
14000
15000
16000
NW
SE
GeoB22732
60 ms
700 m

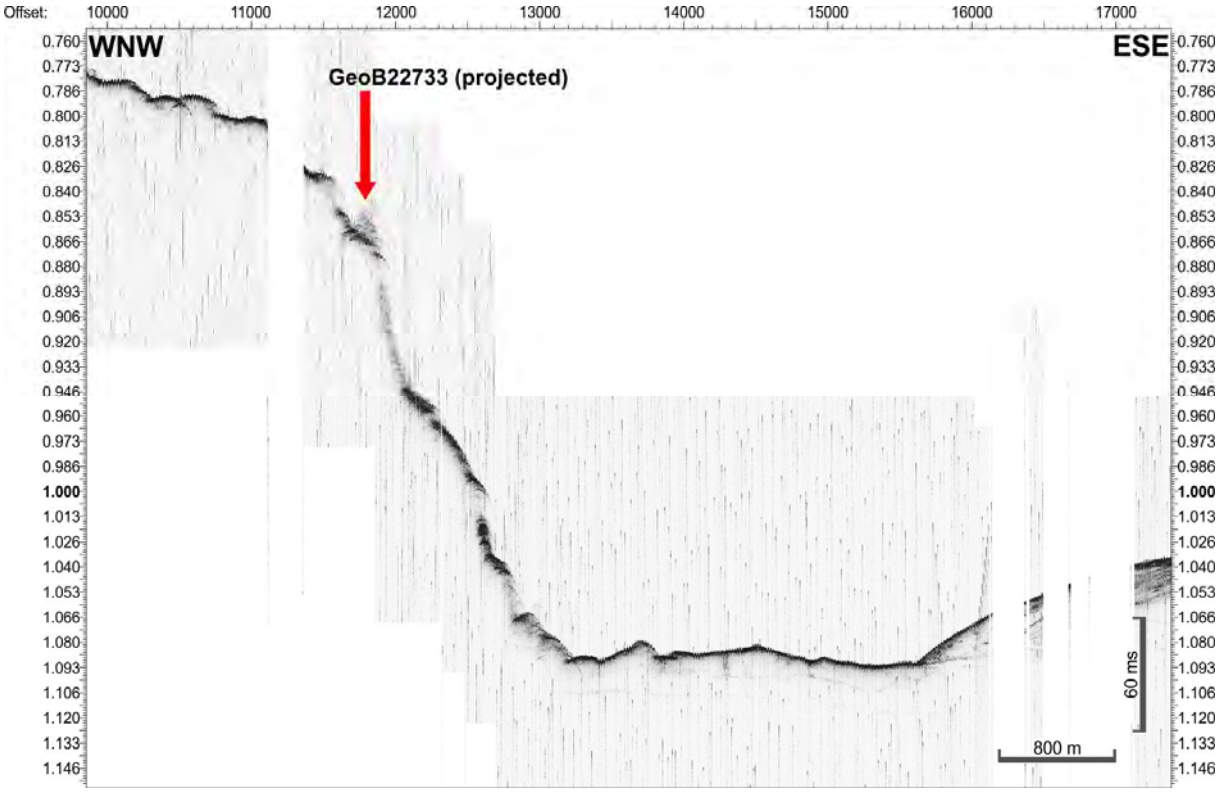
Offset:
10000
11000
12000
13000
14000
15000
16000
17000
WNW
ESE
GeoB22733 (projected)
60 ms
800 m

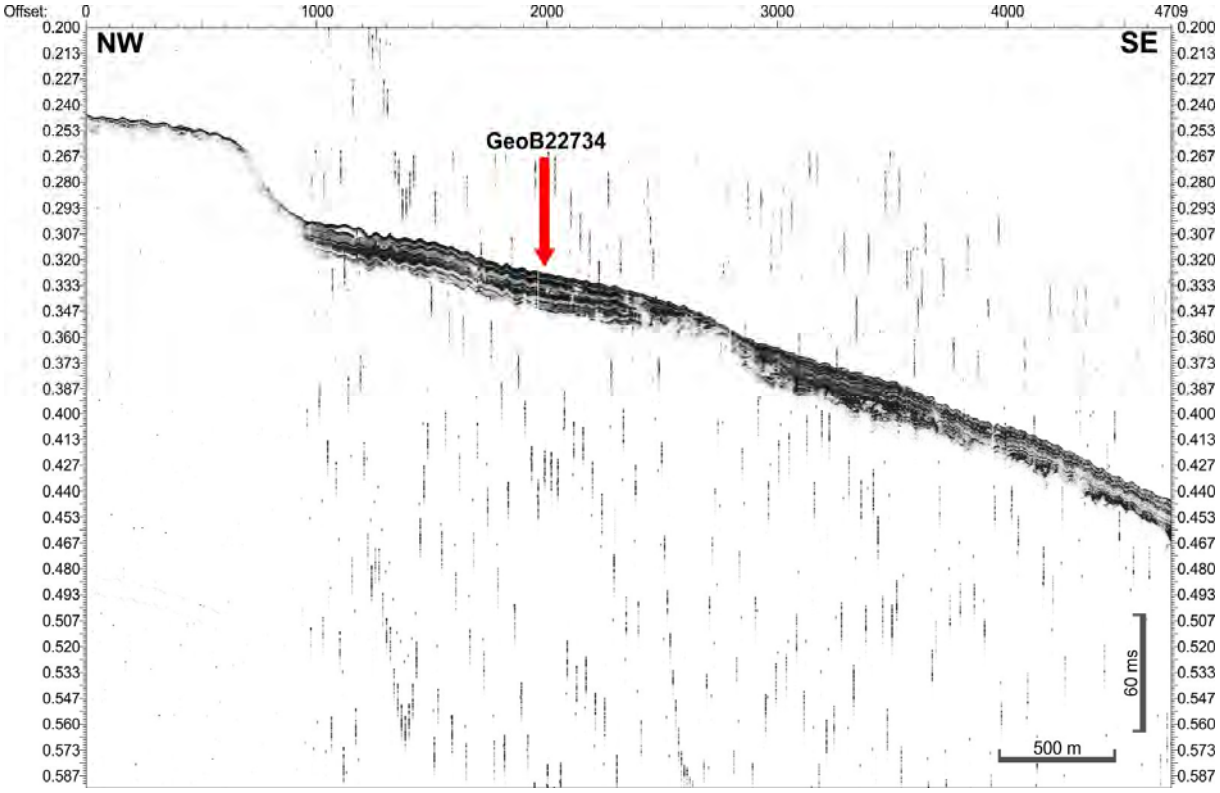
Offset: 0 1000 2000 3000 4000 4709
NW
SE
GeoB22734
60 ms
500 m

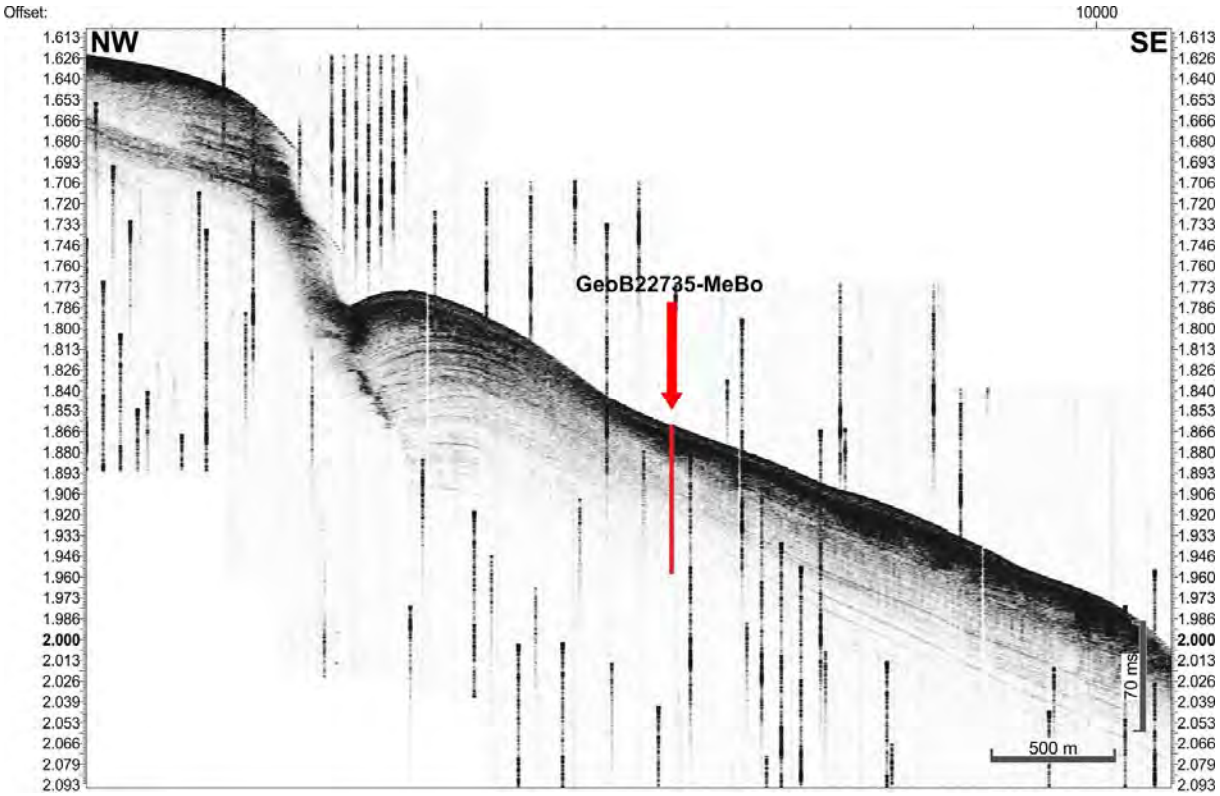
Offset: 10000
NW
SE
GeoB22735-MeBo
70 ms
500 m

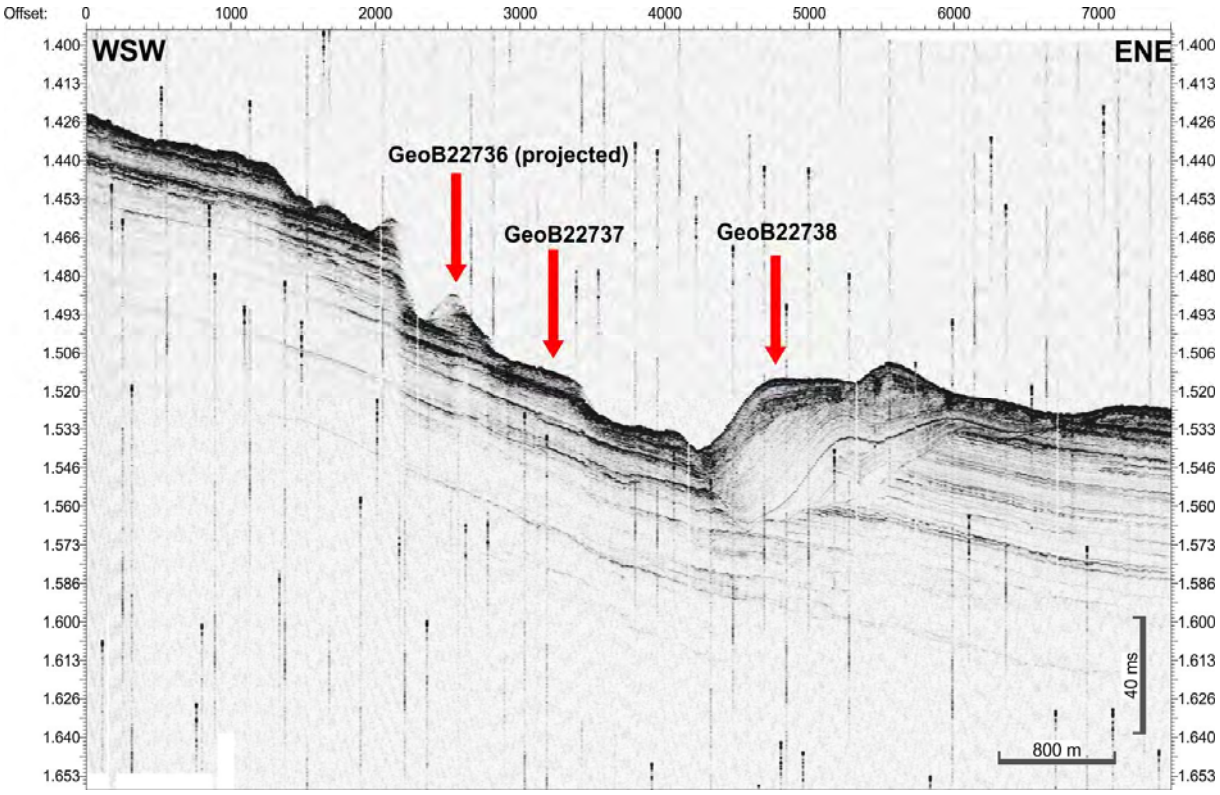
Offset: 0 1000 2000 3000 4000 5000 6000 7000
WSW
ENE
GeoB22736 (projected)
GeoB22737
GeoB22738
40 ms
800 m

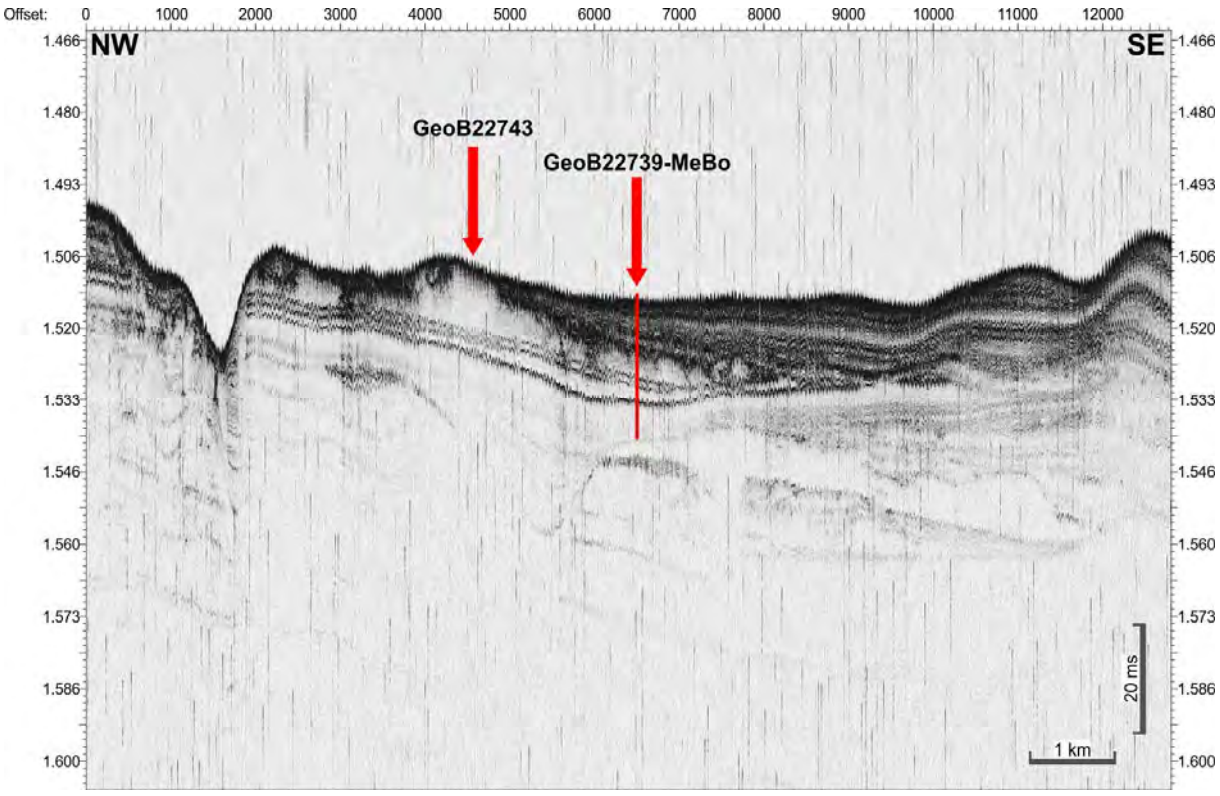
Offset: 0 1000 2000 3000 4000 5000 6000 7000 8000 9000 10000 11000 12000
NW
SE
GeoB22743
GeoB22739-MeBo
20 ms
1 km

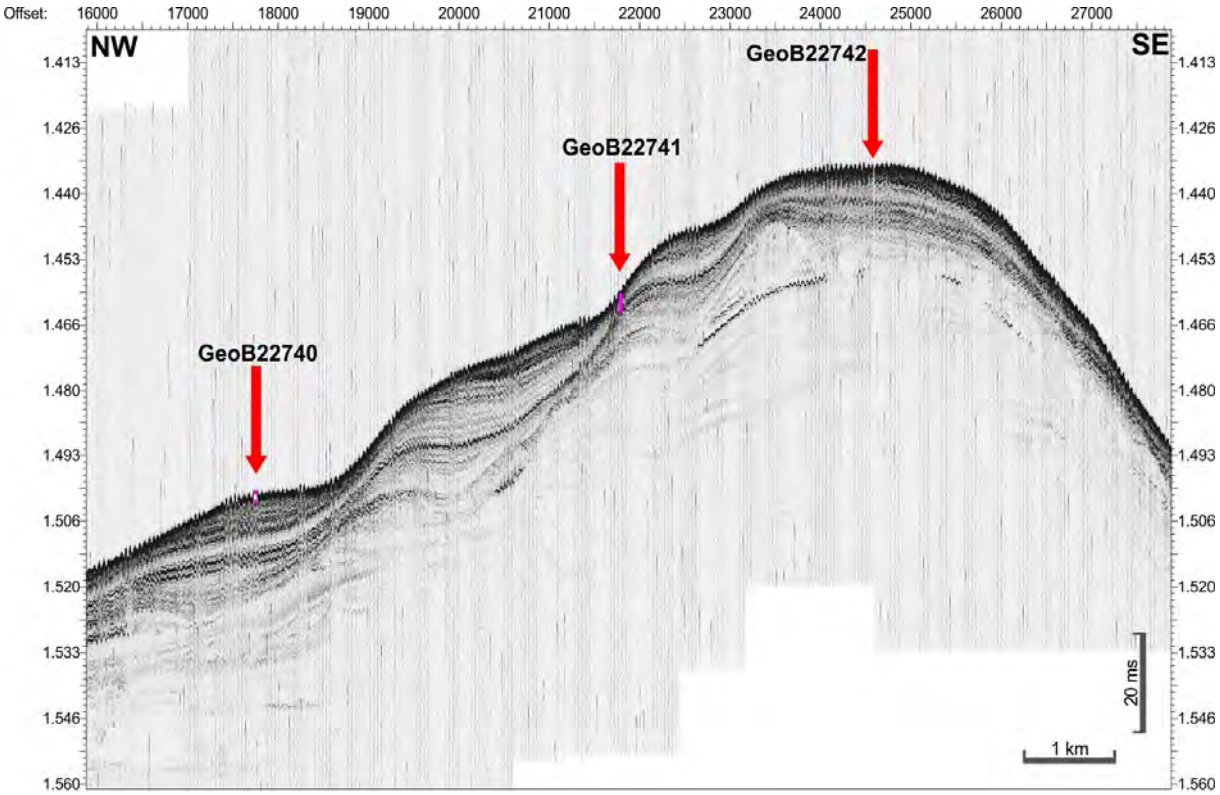
Offset: 16000 17000 18000 19000 20000 21000 22000 23000 24000 25000 26000 27000
NW
SE
GeoB22742
GeoB22741
GeoB22740
1.413 1.426 1.440 1.453 1.466 1.480 1.493 1.506 1.520 1.533 1.546 1.560
20 ms
1 km

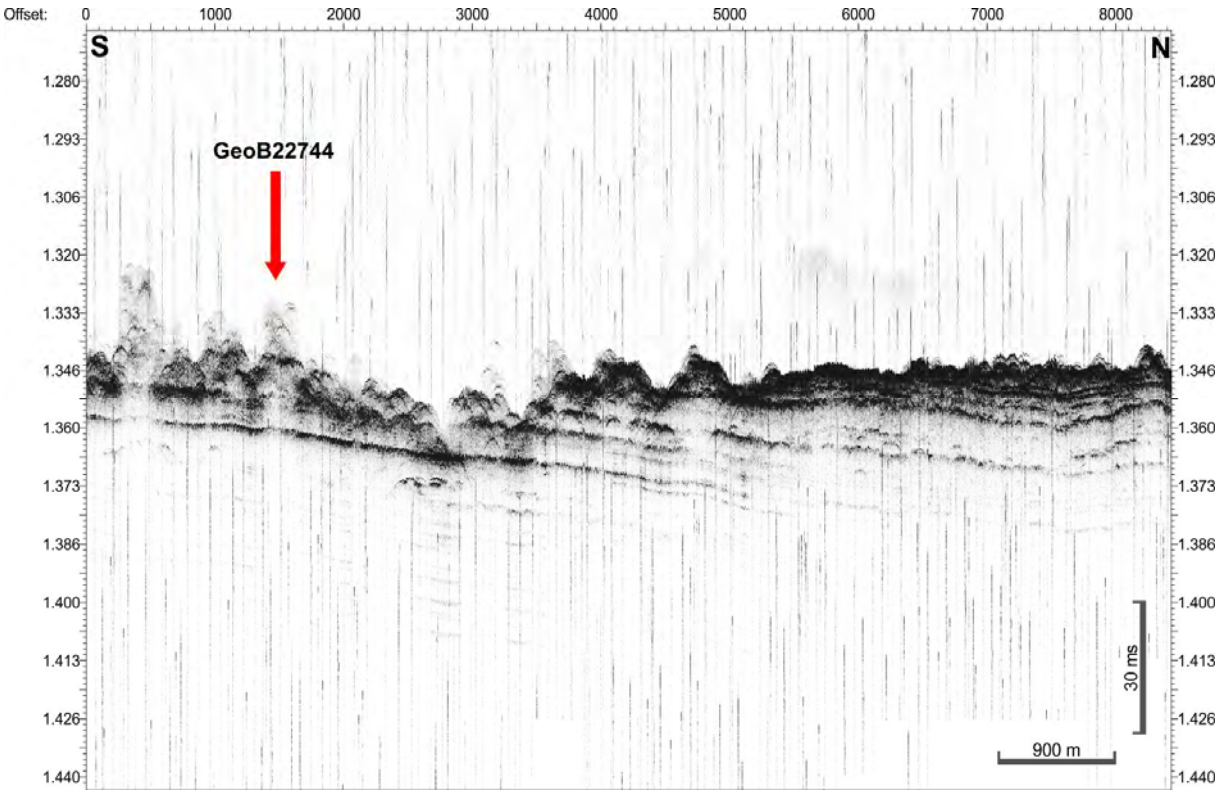
Offset: 0 1000 2000 3000 4000 5000 6000 7000 8000
S
N
GeoB22744
1.280 1.293 1.306 1.320 1.333 1.346 1.360 1.373 1.386 1.400 1.413 1.426 1.440
30 ms
900 m

Appendix 2: Core descriptions and photos

GeoB 22701-2

Date: 15.01.18
Position: 37° 48.902' S 54° 10.691 W

Water depth: 1400 m
Recovery: < 1 cm

Surface description:

Almost with no recovery. Only small amount of loose sand, terrigenous composition with small shell fragments, mud clasts and several benthic foraminifera.

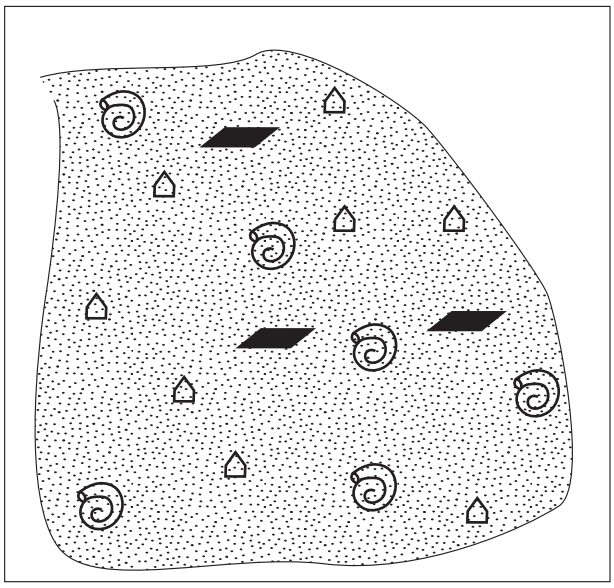

GeoB 22702-1

Date: 15.01.18
Position: 37° 48.560' S 54° 10.215 W

Water depth: 1349 m
Recovery: 43 cm

Surface description:

Olive to olive gray (5Y 4/2, 5Y 4/3) mud with silt to fine-grained sand with benthic foraminifera, small grastropods, living worms and worm tubes. Mud clasts with rock fragments are observed.

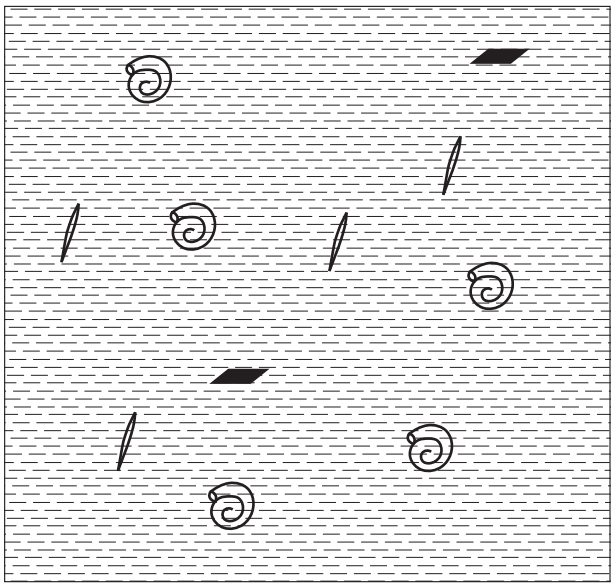

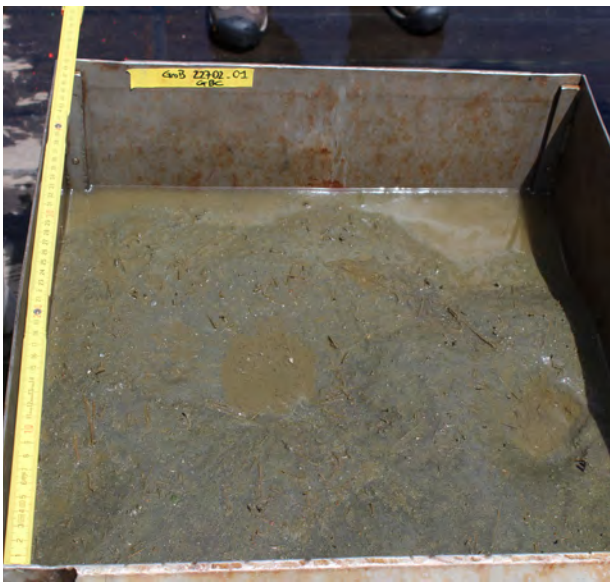

Downcore description:

From 0 - 6 cm olive and olive gray (5Y 4/3, 5Y 4/2), muddy fine-grained sands with abundant foraminifera.
From 6 - 11 cm, silty lenses.
From 11 - 43 cm, olive gray (5Y 4/2) silty to very fine-grained sands with sparse mud clasts, rock fragements and coral fragments in the last 10 cm downcore.

GeoB 22703-1

Date: 15.01.18
Position: 37° 48.252' S 54° 9.805' W

Water depth: 1320 m
Recovery: 25 cm

Surface description:

The surface may not be in place probably because the box corer was tilted during recovery. Olive gray (5Y 4/3) muddy sand with worm tubes benthic foraminifera and dark gray rock fragments.

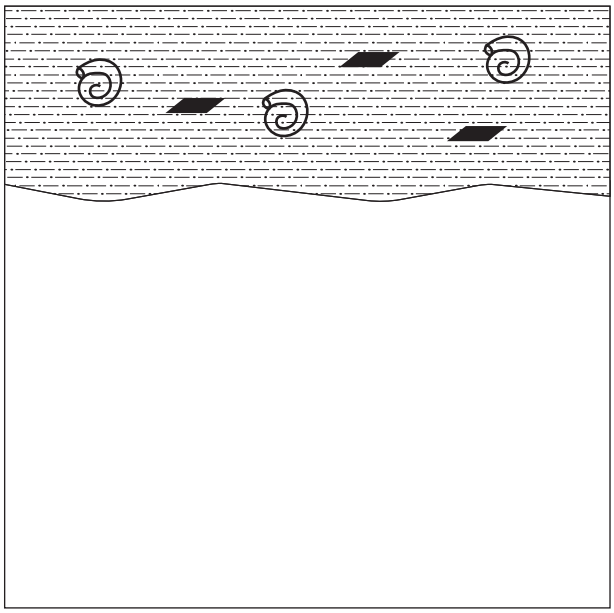

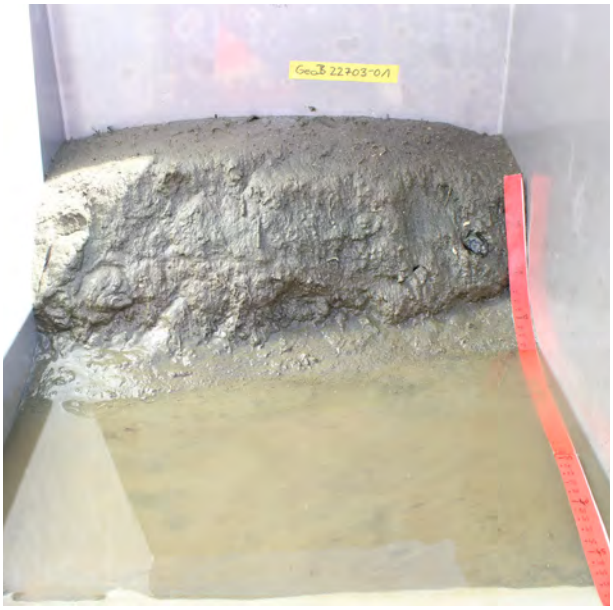

Downcore description:

From 0 - 25 cm, olive gray (5Y 4/3) sandy mud with rock fragments below 6 cm. Rock fragments with different lithologies, color and shapes.

GeoB 22704-1

Date: 15.01.18
Position: 37° 38.630' S 54° 8.492' W

Water depth: 1041 m
Recovery: 48 cm

Surface description:

Olive (5Y 4/4, 5Y 4/3) silty to fine-grained foram bearing sands with mud. Abundant epifauna including worm tubes, ophiuroids (brittle stars) and crustaceans.

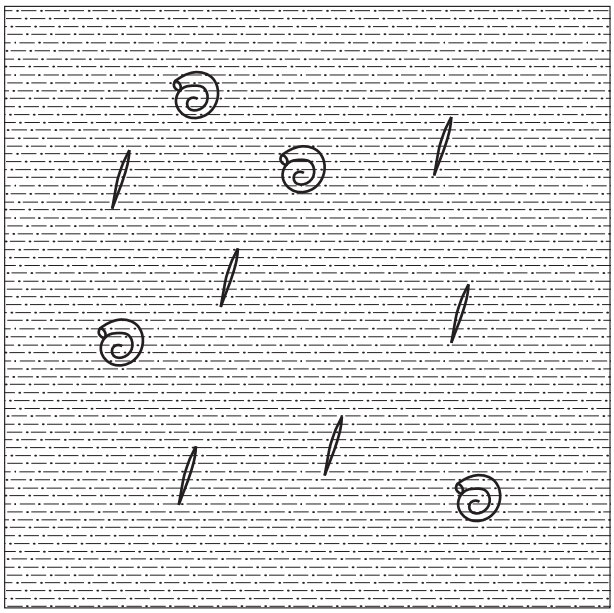

Downcore description:

From 0 - 48 cm, olive (5Y 4/4, 5Y 4/3) silty to very fine-grained sand with few sand patches. Very homogeneus structure.

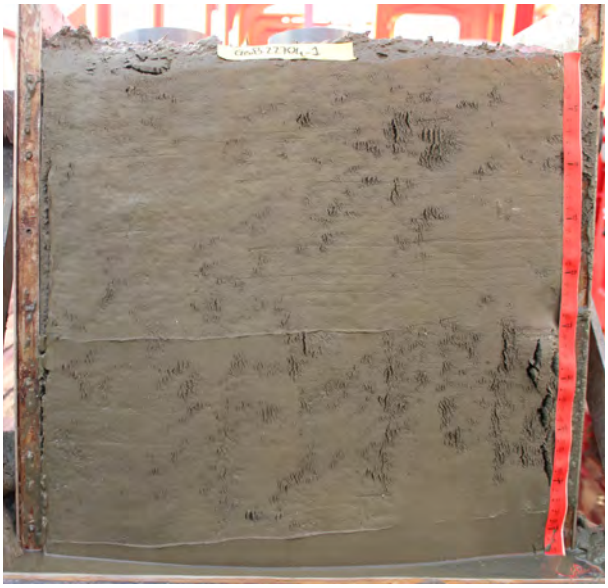

GeoB 22712-3

Date: 20.01.18
Position: 38° 19.953’ S 54° 29.665’ W

Water depth: 1214 m
Recovery: 3 kg

Surface description:

Recovered only rocks, mud clasts, coral fragments and loose medium to coarse olive gray (5Y 4/2) sand at the bottom of the box corer. Rock fragments size are up to 10 cm in diameter. Different lithologies are present with bryozoa colonies attached to the rock surfaces.

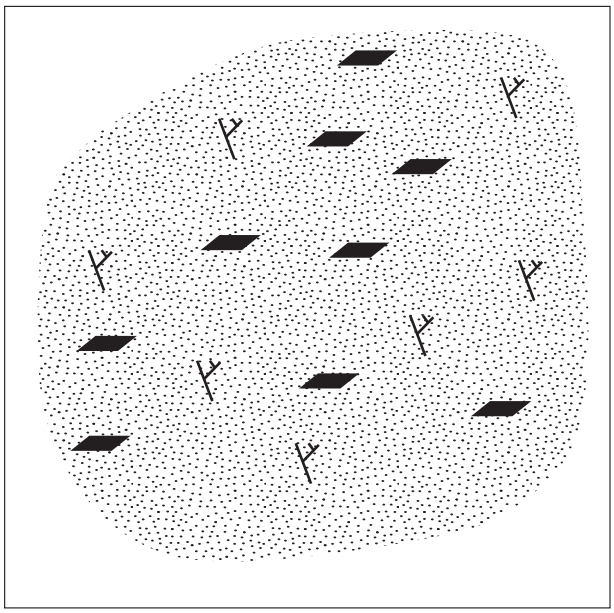

GeoB 22715-1

Date: 20.01.18
Position: 38° 19.499' S 54° 31.696' W

Water depth: 1111 m
Recovery: 39 cm

Surface description:

Olive gray (5Y 5/2) medium to coarse sand with silt. Abudant coral fragments up to 10 cm in size. Abundant epifauna including gasteropods, worm tubes, benthic foraminifera, ophiuroids, bivalves, artropods, briozoans.

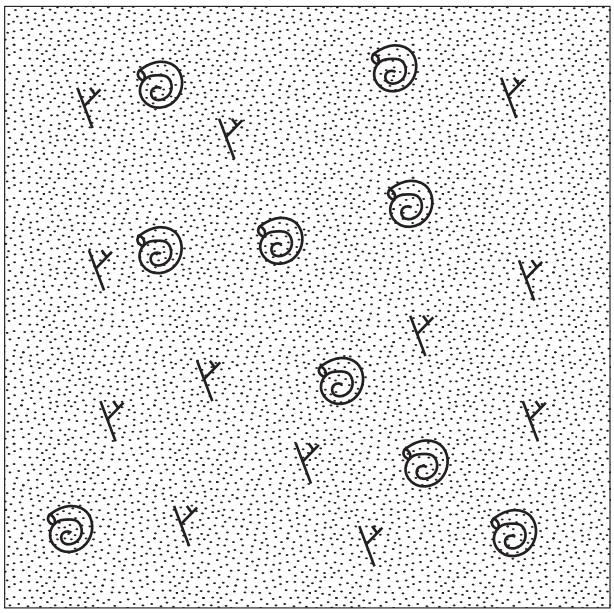

Downcore description.

From 0 - 39 cm, olive gray (5Y 5/2) silty sand with abundant coral fragments throughout the whole section. Top 5 cm are very rich in forams. Grain size decreases downwards.

GeoB 22716-1

Date: 21.01.18
Position: 38° 6.329′ S 54° 22.803′ W

Water depth: 1287 m
Recovery: Partial recovery

Surface description:

Partial recovery with only sand and rocks of different lithologies and shapes with sizes ranging from 0.5 to 10 cm in diameter. Epibenthic fauna includes benthic foraminifera, briozoans and mollusks.

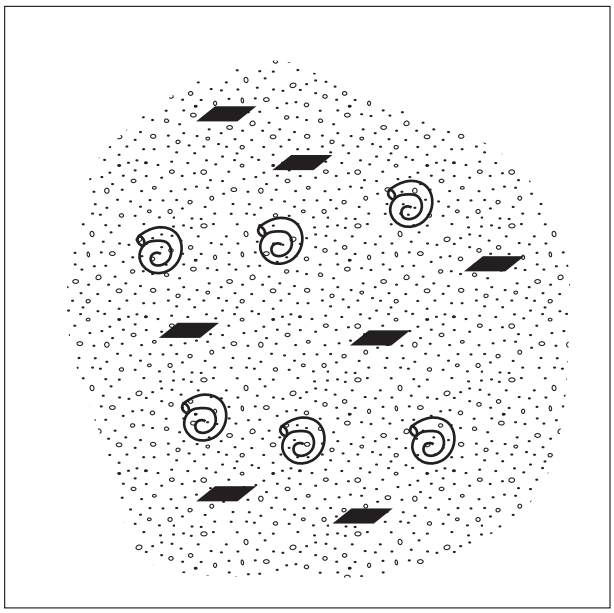

GeoB 22744-2

Date: 12.02.18
Position: 38° 18.254' S 54° 32.363 W

Water depth: 1102 m
Recovery: 27 cm

Surface description:

Brownish-gray-olive mud with coral fragments, shrimp, brachiopods, crabs, sea fern, and other living organisms.

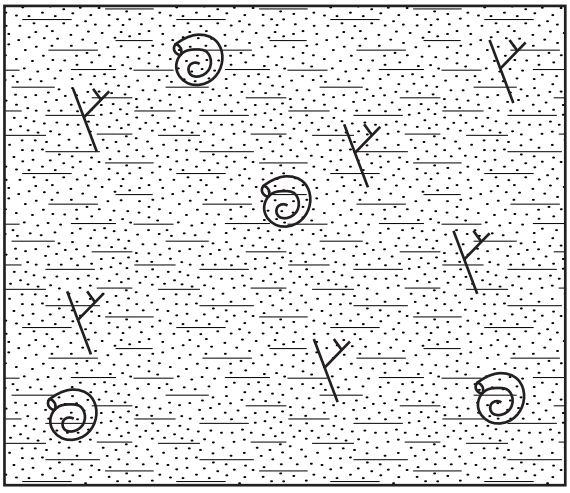

Downcore description:

From 0-27 cm Olive Gray (5Y 4/2), massive, strongly bioturbated, slightly muddy, fine to very fine-grained sand with abundant forams and dead corals.

Core Legend gravity corer and MeBo

Lithology

Sand-rich

- Sand
- Shelly Sand
- Silty Sand (some mud)

Mud-rich

- Muddy Silt (some sand)
- Mud/Silty Mud

Bioturbation

- SSS Strongly Bioturbated
- SS Bioturbated
- S Weakly Bioturbated
- Large irregular oval burrows
- Small distinct circular/ cylindrical burrows

Biogenic Material

- Shell Fragment
- White Specks (biogenic material, small shell fragments, burrow linings, etc)
- Coral
- Foram
- Spine/Spicule
- Shell hash/lag

Physical Structures

- Horizontal Lamination
- Faint Laminae or Bedding
- Normally / Inversely Graded
- Sand / Mud Lens
- M Massive/structureless
- Grain lag / Outsized Grains

Bed Contacts

- Gradational
- Sharp
- Diffuse
- Erosional

Diagenetic

- Black Grains/nodules
- Black/Dark Gray Irregular Spots
- Concretion
- Ikaite Nodule

For all structures A = abundant, C = common, and R = rare

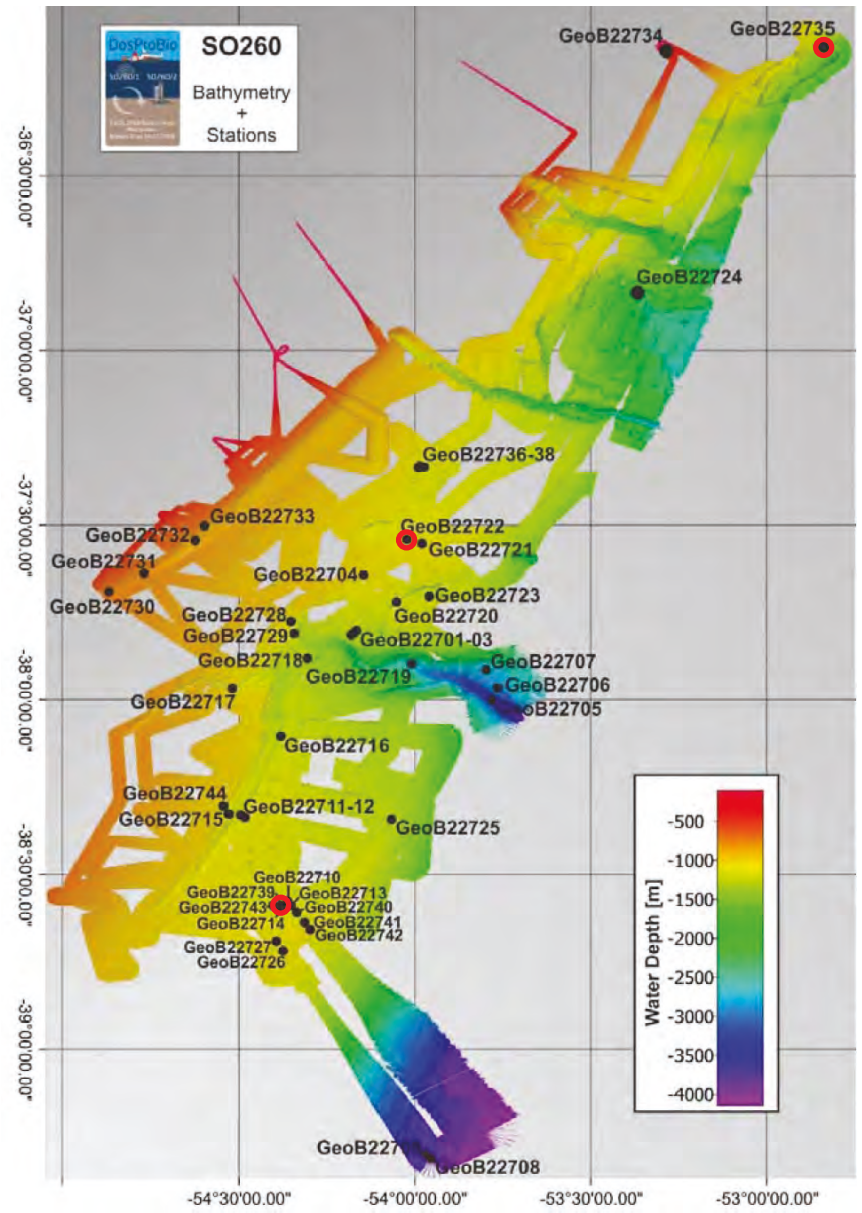

Base map provided by T. Schwenk. Open red circles indicate locations of MeBo cores.

GeoB22702-03 (GC)

Water Depth: 1,355 m

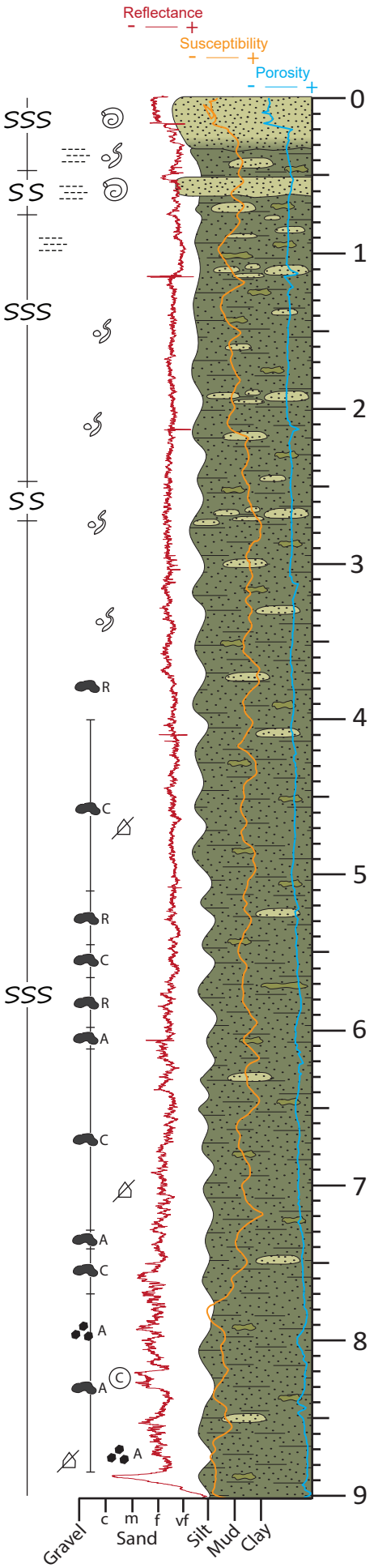

Dark Gray (5Y 3/1), well sorted, massive, fine-grained sand with mud. Abundant forams

Dark Olive Gray (5Y 3/2) and Olive (5Y 5/3) strongly to very strongly bioturbated, silty, very fine-grained sand with mud, with lenses of dark gray well-sorted very fine-grained sand.

(200 and 270 cm) Sand-rich zones, slight decrease in degree of bioturbation

Dark Olive Gray (5Y 3/2), Olive (5Y 5/3) and Black (5Y2.5/1), strongly to very strongly bioturbated, silty, very fine-grained sand with mud. Rare to abundant large, irregular, black/very dark gray burrows throughout.

(461 cm) small shell fragments (1-3 mm)

Dark Olive Gray (5Y 3/2)and Black (5Y 2.5/1), strongly to very strongly bioturbated, silty very fine-grained sand with mud. Black monosulfide (FeS) grains or small nodules are abundant throughout.

(870 cm) Shell fragments less than 1 cm in size

Described by: J. Long and J. Bösche

GeoB22704-02 (GC)

Water Depth: 1,038 m

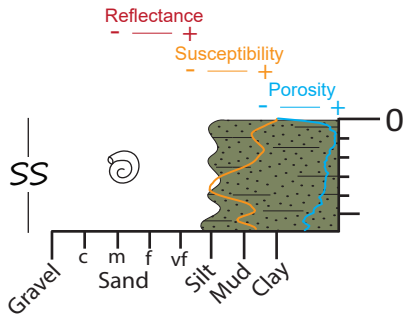

Olive (5Y4/3) and Very Dark Gray (5Y 3/1); bioturbated; silty, very fine-grained sand with mud. Forams common throughout.

Described by: J. Bösche and A. Melcher

GeoB22704-03 (GC)

Water Depth: 1,038 m

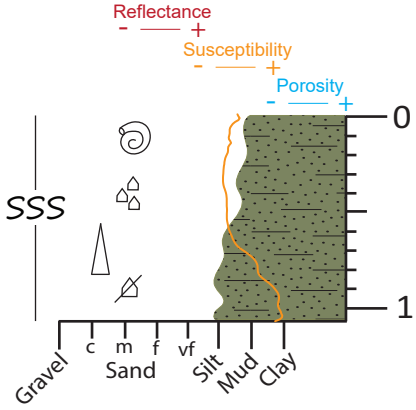

Olive (5Y 4/2) and Olive Gray (5Y 4/3); bioturbated; silty, very fine-grained sand with mud. Higher mud content than underlying unit.

Very Dark Gray (5Y 3/1) with Black (5Y 2.5/1); bioturbated; silty, very fine-grained sand with mud.

Described by: J. Bösche and A. Melcher

GeoB22706-02 (GC)

Water Depth: 2,997 m

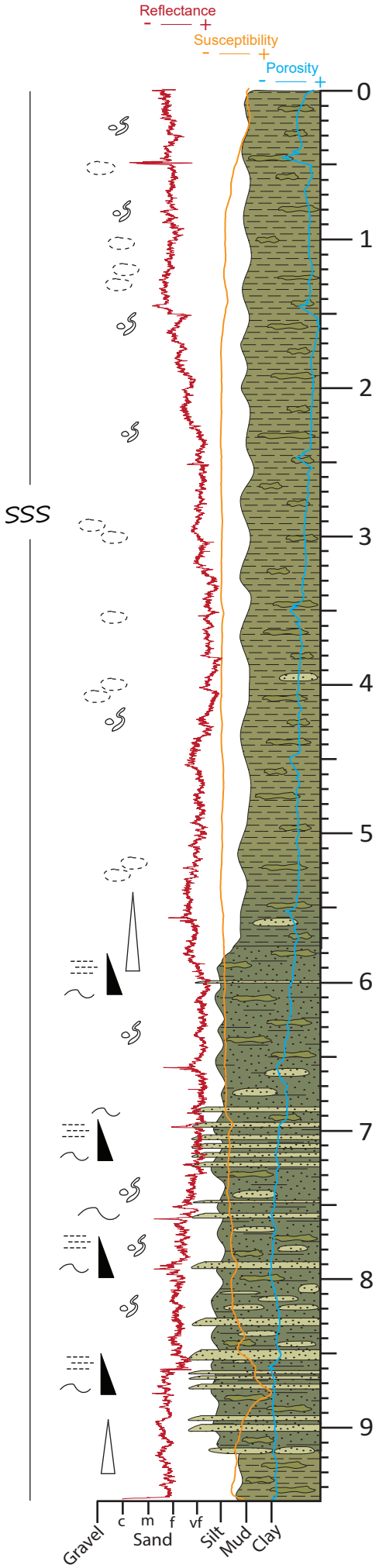

Olive Gray (5Y 4/2) and Light Olive Gray (5Y 5/2) strongly bioturbated, muddy silt with disseminated very fine-grained sand. Contains intervals within which small, circular to cylindrical, horizontal and oblique individual borrows are easily distinguished (*Chondrites*). Other intervals show faint, large (2-3 cm), irregular ovals that are a different type of borrow (*Planolites*).

Olive Gray (5Y 4/2) and Light Olive Gray (5Y 5/2), strongly bioturbated, silty, very fine-grained sand with mud interbedded with Dark Olive Gray (5Y 3/2), bioturbated, well to moderately sorted, bioturbated, very thinly bedded to thickly laminated, very fine to fine-grained sand. Sands appear to be composed of 60% of quartz, ~20% black grains, ~20% lithic grains with trace of shell fragments/forams. Sands occur as both continuous beds and discontinuous lenses and commonly define the bases of fining upwards packages.

Upper limit of fining upward successions are difficult to distinguish due to extensive bioturbation

Small muddy lenses throughout

Indivual burrows in the upper parts of these sharp-based sand beds are easily distinguishable

Described by: J. Long

GeoB22707-01 (GC)

Water Depth: 2,762 m

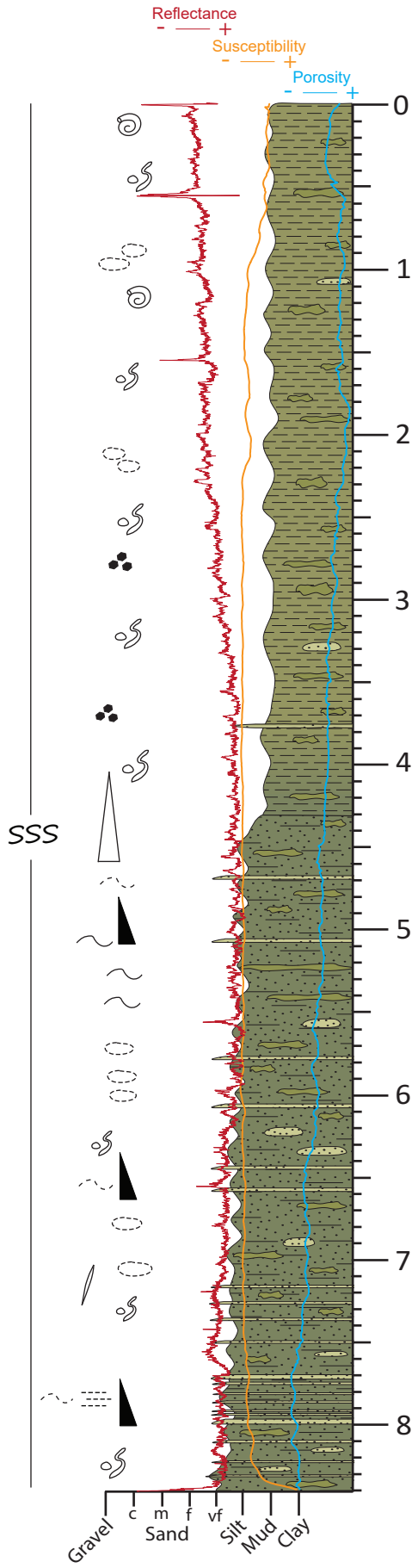

Olive Gray (5Y 4/2) and Light Olive Gray (5Y 5/2), strongly bioturbated, muddy silt with very fine-grained sand

Lenses of very fine-grained sand

Long gradational transition into overlying muddy silt with very fine-grained sand

Olive Gray (5Y 4/2) and Light Olive Gray (5Y 5/2), strongly bioturbated, silty, very fine-grained sand with mud interbedded with Dark Olive Gray (5Y 3/2), bioturbated, well to moderately sorted, bioturbated, very thinly bedded to thickly laminated, very fine to fine-grained sand. Sands occur as both continuous beds and discontinuous lenses and commonly define the bases of fining upwards packages.

GeoB22708-01 (GC)

Water Depth: 3,688 m

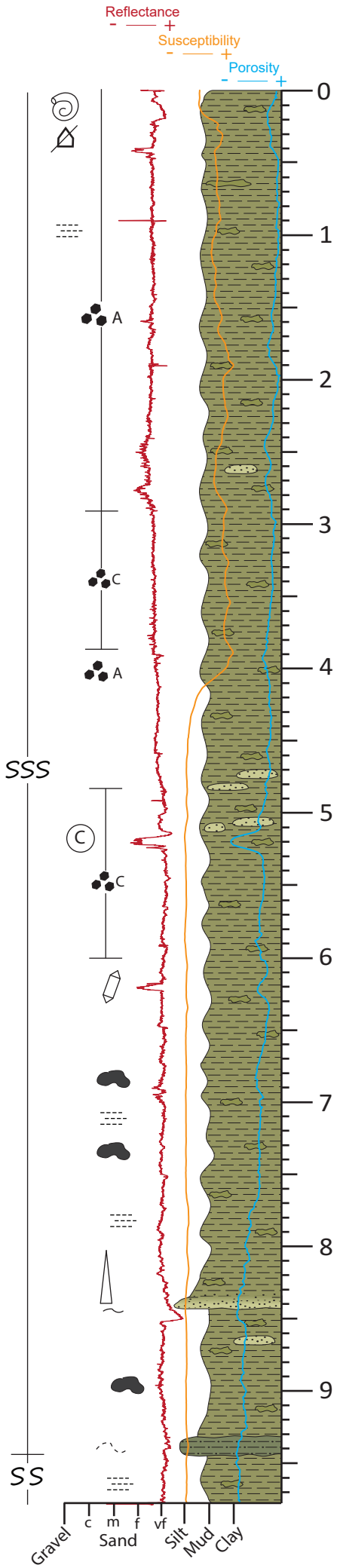

(0-50 cm) Benthic forams common

(45 cm) Large bivalve shell (2.2 cm diameter)

Olive Gray (5Y 4/2) and Very Dark Gray (5Y 3/1), strongly bioturbated, muddy silt with very fine-grained sand. Sand is typically in trace amount but infrequently occurs as small lenses. Abundant small black grains or nodules throughout and concentrated around individual burrows. Mottled appearance is related to bioturbation with burrows defined by very dark gray color (some with obvious lighter fill). Distinct burrows range from 1 to 4 mm in diameter.

(340-350 cm) indistinct change of compactation, with lower units more compacted

(405 cm) Numerous small (< 1 mm) black grains (FeS)

(475 cm) small lenses of very fine-grained sand

(766 cm) Diffuse laminae indicated by aligment and concentration of horizonatally elongated burrows

(815-844 cm) Gradational transition from lighter colored underlying sand-rich unit to overlying darker, mud silt rich unit

(936-943 cm) Slightly higher sand content. Silty, very fine-grained sand with mud

Described by: J. Long

GeoB22709-01 (GC)

Water Depth: 3,605 m

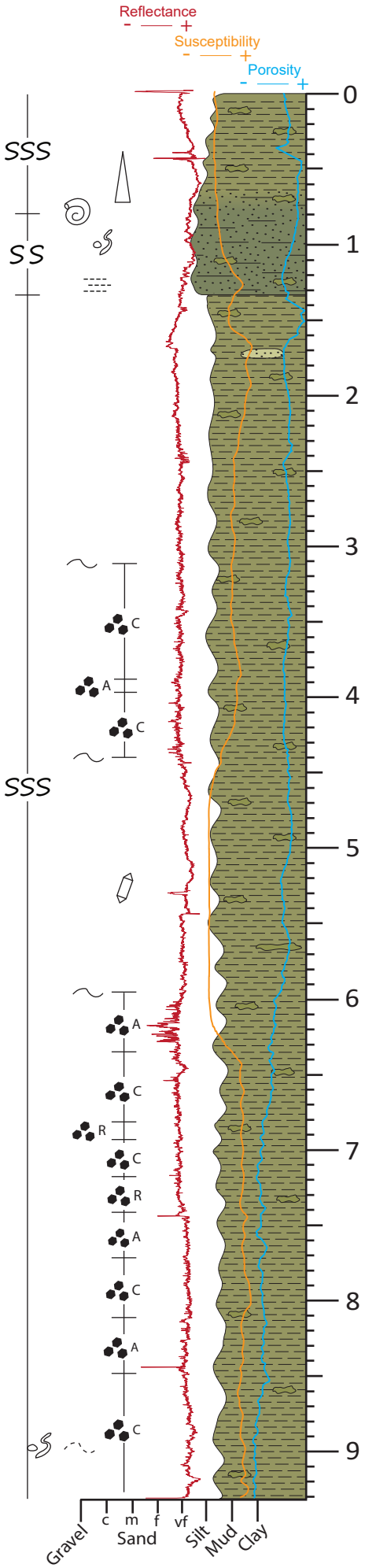

Olive Gray (5Y 4/2), with Very Dark Gray (5Y 3/1) bioturbated, very fine-grained silty sand with mud. Abundant forams throughout. Unit fines upwards to a muddy silt with very fine-grained sand.

(117cm) Single, lined horizontal borrow (paleophycus)

(167 cm) Lens of very fine-grained sand lens

Olive Gray (5Y 4/2), Very Dark Gray (5Y 3/1), Olive Gray (5Y 5/2) and Black (5Y 2.5/1) strongly bioturbated muddy silt with minor amounts of very fine-grained sand. Common to abundant, small, Very Dark Gray burrows (planolites). Discrete zones in which black monosulfide (FeS) grains are rare to abundant alternate with zones within which these grains are entirely absent.

(898 cm) Subtle color change and definable burrows mark the contact

Described by: J. Long and J. Bösche

GeoB22713-02 (GC)

Water Depth: 1,115 m

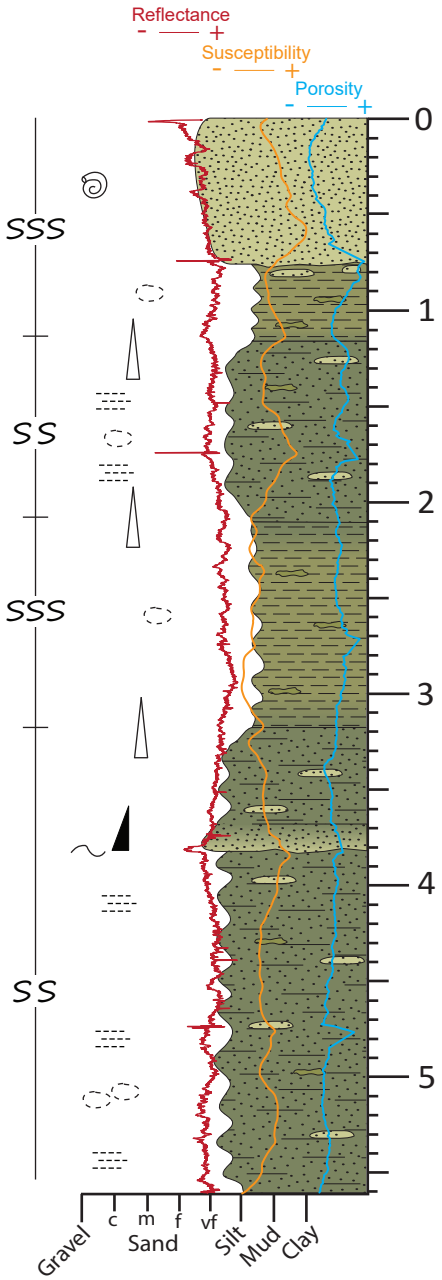

Olive Gray (5Y 4/2) with Very Dark Gray (5Y 3/1), strongly bioturbated, fine to very fine-grained sand with mud. Upper 30 cm contains abundant forams. Black color (5Y 2.5/1) associated with sand lenses

Olive gray (5Y 4/2) with Very Dark Gray (5Y 3/1), strongly bioturbated, muddy silt with very fine grained sand. Indistinct burrows

Olive gray (5Y 4/2) with Very Dark Gray (5Y 3/1), bioturbated to strongly bioturbated, very fine-grained silty sand with mud. Small sand lenses are common. Burrows are indistinct. Faint disrupted bedding in some parts, darkest colours (5Y 3/1) to black (5Y 2.5/1) associated with sand-rich intervals.

Olive gray (5Y 4/2) with Very Dark Gray (5Y 3/1), strongly bioturbated, muddy silt with very fine grained sand. Indistinct burrows

Olive gray (5Y 4/2) with Very Dark Gray (5Y 3/1), bioturbated to strongly bioturbated, very fine-grained silty sand with mud. Small sand lenses are common. Burrows are indistinct. Faint disrupted bedding in some parts, darkest colours (5Y 3/1) to black (5Y 2.5/1) associated with sand-rich intervals.

Described by: J. Long and J. Bösche

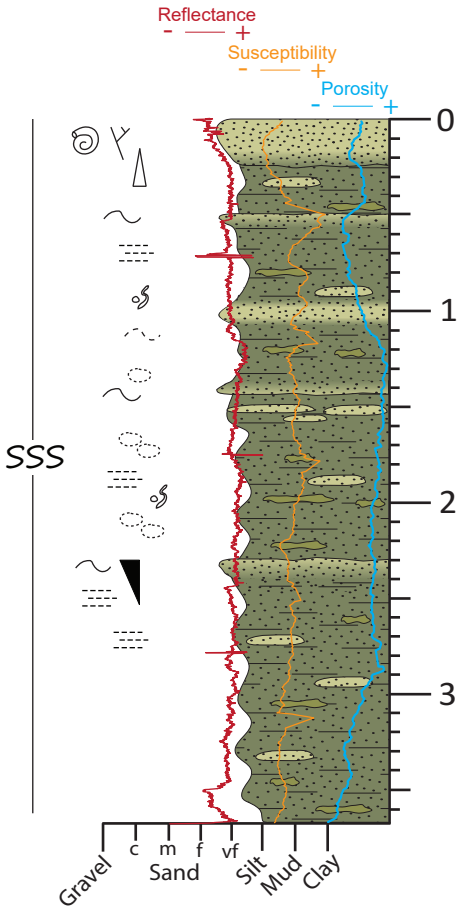

GeoB22714-01 (GC)

Water Depth: 1,110 m

Olive Gray (5Y 4/2) with Very Dark Gray (5Y 3/1) and Black bioturbated fine to very fine-grained sand. Forams abundance decreases downwards

Olive Gray (5Y 4/2) to Very Dark Gray (5Y 3/1) strongly bioturbated, very fine-grained silty sand with mud. Small sand lenses are common. Black associated with sand-rich intervals. Mud-rich intervals are more Olive Gray (5Y 4/2). Indistinct borrows.

(235 cm) Coarsening-upwards, very fine-grained sand bed. Sharp upper contact gradational lower contact.

Described by: J. Long and J. Bösche

GeoB22721-02 (GC)

Water Depth: 1,060 m

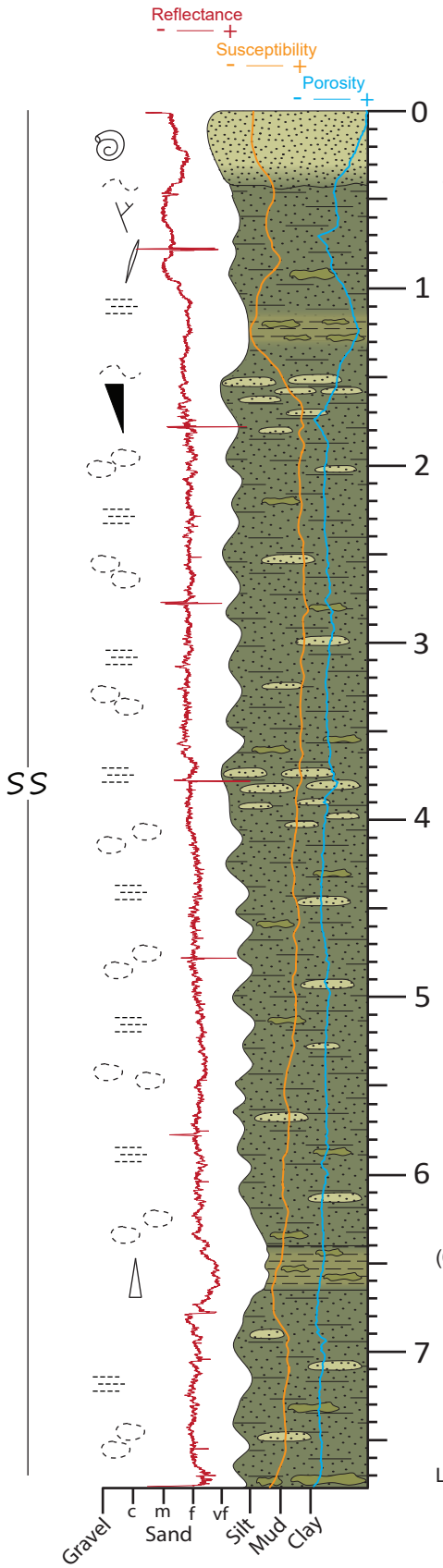

Olive (5Y 4/3) and Very Dark Gray (5Y 3/1) bioturbated, faintly laminated very fine to fine-grained sand with mud

Dark Gray (5Y 4/1), Very Dark Gray (5Y 3/1) and Black (5Y 2.5/1); bioturbated; faintly laminated, silty, very fine-grained sand with mud. Black color is associated with sands that contain 20-30% opaque minerals. Indistinct borrows throughout.

(120-138 cm) Mud-rich interval

(162-190 cm) Coarsening-upwards, sand-rich interval

(370-385 cm) Sand-rich interval

(645–665 cm) Muddy silt with very fine-grained sand

Lowest 4 cm of the core is mud-rich

Described by: J. Long and J. Bösche

GeoB22722-05 (GC)

Water Depth: 1,078 m

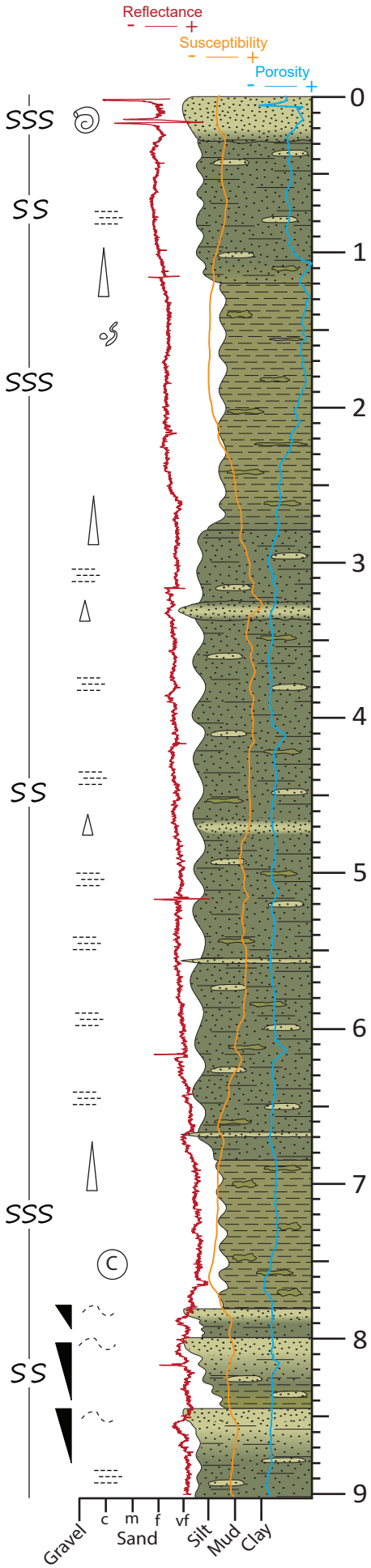

Dark Gray (5Y 3/1) well to moderately sorted, massive, fine-grained sand with mud. Abundant forams.

Dark Olive Gray (5Y 3/2) Olive Gray (5Y 4/2), Very Dark Gray (5Y 3/1) and Black (5Y 2.5/1), bioturbated, muddy, silty, very fine-grained sand. Mud lenses in lower 50 cm. Forams are abundant in the upper 60 cm. Contacts between these intervals are diffused. Faint planar laminations in many sand-rich intervals.

Olive Gray (5Y 5/2) and Very Dark Gray (5Y 3/2) bioturbated, muddy silt with some very fine-grained sand

(328-334 cm) Very fine-grained sand with gradational contact at top and base

Dark Olive Gray (5Y 3/2), Very Dark Gray (5Y 3/1) and Black (5Y 2.5/1) bioturbated, faintly laminated, muddy, silty very fined-grained sand. Mud and sand lenses throughout. Black color associated with sand grains

Olive Gray (5Y 5/2) and Very Dark Gray (5Y 3/2) bioturbated, muddy silt with some very fine-grained sand

(762 cm) Large concretion

Dark Olive Gray (5Y 3/2), Very Dark Gray (5Y 3/1) and Black (5Y 2.5/1) bioturbated, faintly laminated, muddy, silty very fined-grained sand. Mud and sand lenses throughout. Black color associated with sand grains. Three coarsening-upwards packages.

Described by: J. Long

GeoB22723-01 (GC)

Water Depth: 1,167 m

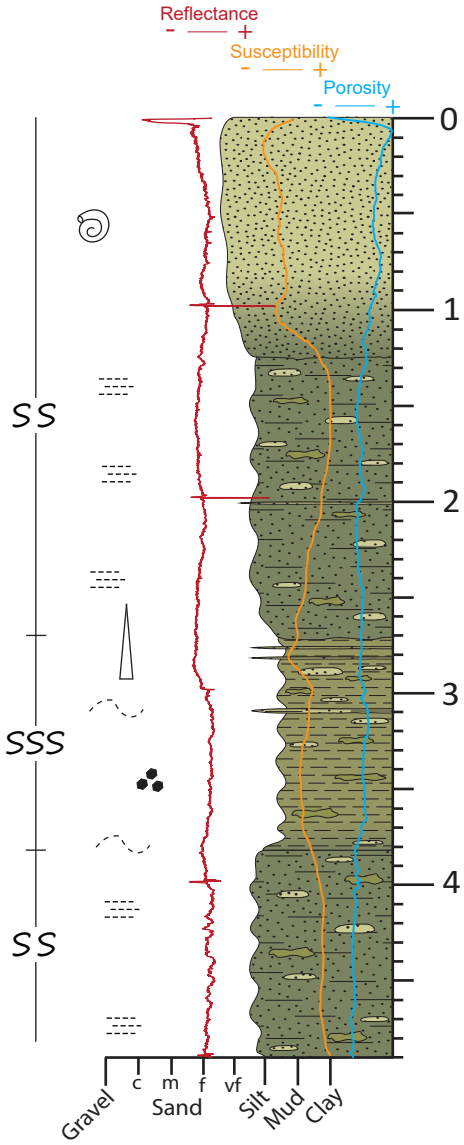

Olive (5Y 4/3), very dark gray (5Y 3/1) and black (5Y 2.5/1) bioturbated massive fine to very fine grained sand with mud and silt. Abundant forams.

Olive (5Y 4/3), very dark gray (5Y 3/1) and black (5Y 2.5/1) bioturbated, silty, very fine- grained sand with mud. Forams become more abundant towards the top. Slightly better sorting towards the top.

(240 cm) Isolated very thin (<5 mm) mud lenses. These define faint bedding.

(278 and 285 cm) Thin silty very fine-grained sand beds

Olive gray (5Y 4/3) and very dark gray (5Y 3/1). Strongly bioturbated muddy silt with very fine grained sand

---

Olive gray (5Y 4/2) and very dark gray (5Y 3/1) with black (5Y 2.5/1) bioturbated silty very fine grained sand with mud. Dark colors (5Y 3/1, 5Y 2.5/1) are associated with black sand grains

Described by: J. Long and J. Bösche

GeoB22725-02 (GC)

Water Depth: 1,061 m

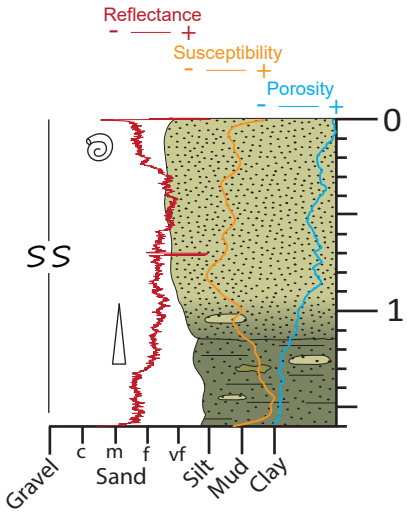

Olive Gray (5Y4/2) with Very Dark Gray (5Y 3/1) bioturbated, silty, fine-grained sand with mud. Abundant benthic forams.

Lenses of Very Dark Gray (5Y 3/1) very fine-grained sand

Very Dark (5Y 3/1), bioturbated, silty very fine-grained sand with mud

Described by: G. Warratz and J. Bösche

GeoB22734-02 (GC)

Water Depth: 240 m

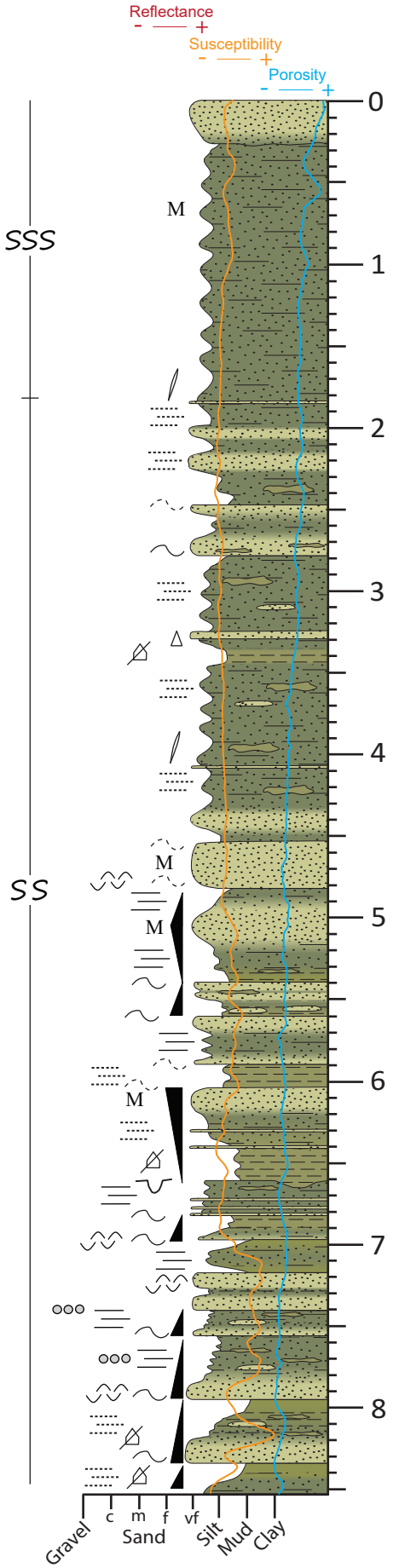

Very Dark Gray (5Y 3/1); bioturbated; massive; muddy, silty very fine-grained sand.

Dark Gray (5Y3/2) and Olive Gray (5Y4/2); bioturbated; massive; muddy, silty, fine to very fine-grained sand.

Dark Gray (5Y3/2) and Olive Gray (5Y4/2); bioturbated; faintly laminated; muddy, silty, fine to very fine-grained sand. Mud and sand lenses common throughout. Lower 1.5 meters contain sands that are better sorted.

Dark Gray (5Y4/1) and Very Dark gray (5Y3/1) weakly to moderately bioturbated; laminated to thinly bedded; intercalated fine to very fine-grained sands, silty sands, and muddy silts. Most of this unit is well bedded with numerous fining-upwards successions ranging in thickness from 3-20 cm and defined by sharp-based sands or silty sands. Shell fragments throughout and shell lags are common at the base of finin-upwards successions.

Sharp, irregular contact is likely a scour but may be a coring-induced feature

Interlaminated silty sand and muddy silts

Described by: J. Long

GeoB22735-01 (GC)

Water Depth: 1,376 m

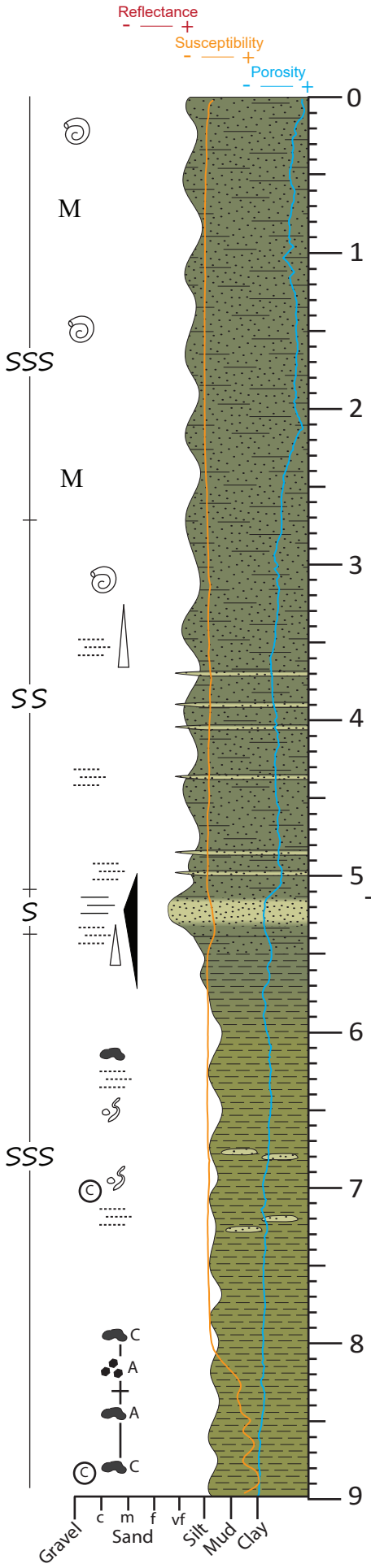

Olive (5Y 4/3); bioturbated; massive to faintly laminated (lower part) silty, very fine-grained sand. Forams common to abundant. High water content.

Dark Olive Gray (5Y 3/2), Very Dark Gray (5Y3/1), and Black (5Y 2.5/1); bioturbated; faintly laminated; muddy, silty, very fine-grained sand. Mud and sand lenses common throughout. Sand is ~60% Quartz, 20% gray and green lithic fragments, and 20% black minerals.

Olive (5Y 5/3), Olive Gray (5Y4/2), Very Dark Gray (5Y 3/1), and Black (5Y 2.5/1); bioturbated; muddy silt with with minor amount of very fine-grained sand.Black mottling in lower 1 m and black monosulfide grains at the top of this mottle zone. Slightly sandier at the base of core. Upper ~50 cm coarsens upwards into a silty, very fine-grained sand.

Large concretion

Described by: J. Long

GeoB22740-01 (GC)

Water Depth: 1,103 m

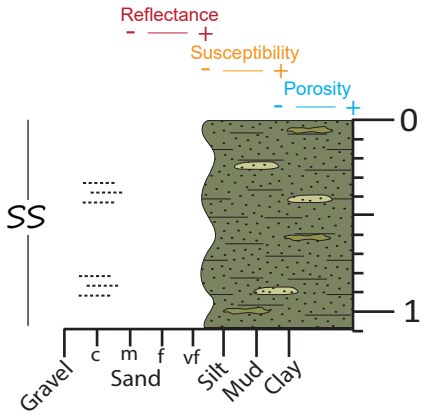

Dark Gray (5Y 4/1) and Very Dark Gray (5Y 3/1); bioturbated; faintly laminated; muddy, silty, very fine-grained sand. Thin sand and mud lenses throughout.

Lower ~50 cm is disturbed

GeoB22741-01 (GC)

Water Depth: 1,072 m

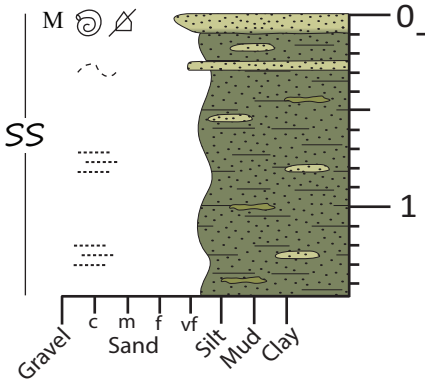

Olive Gray (5Y 4/3); massive; slightly muddy, fine to very fine-grained sand.

Dark Gray (5Y 4/1) and Very Dark Gray (5Y 3/1); bioturbated; faintly laminated; silty, very fine-grained sand with mud. Mud and sand lenses throughout.

Described by: J. Long

GeoB22722-06 (MeBo)

Total Core Depth: 2.5 m
Recovery: 0.80 m
Water Depth: 1,077 m

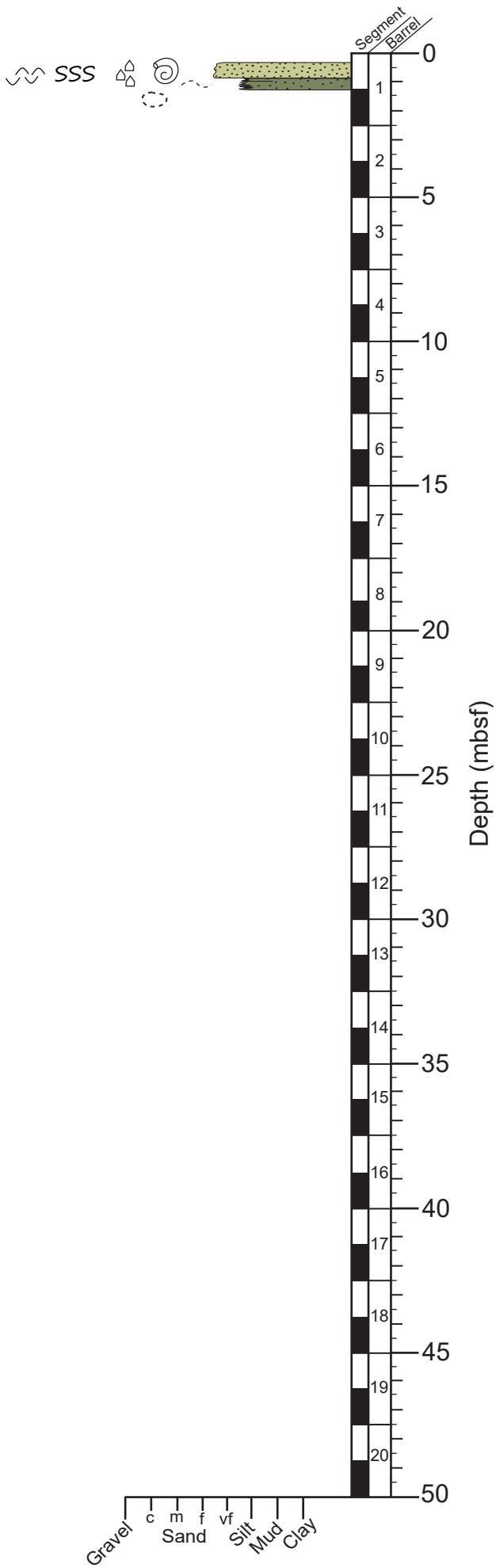

-Olive (5Y4/3), massive, strongly bioturbated, very fine to fine-grained sand with mud
-Very Dark Gray (5Y3/1) and Black (5Y2.5/1), silty, very fine-grained sand with mud

GeoB22722-07(MeBo)

Total Core Depth: 30 m
Recovery: 14.4 m (47%)
Water Depth: 1,076 m

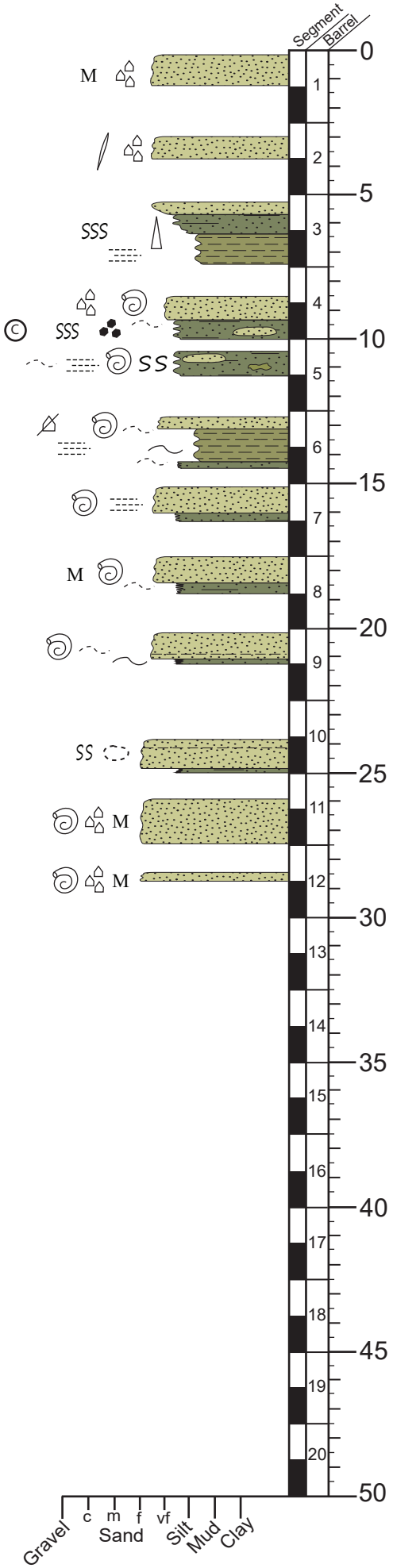

-Very Dark Gray (5Y3/1), well-sorted, massive, very fine to fine-grained sand

-Very Dark Gray (5Y3/1), well-sorted, massive, very fine to fine-grained sand

-Very Dark Gray (5Y3/1), well-sorted, very fine-grained sand
-Dark Gray (5Y4/1) to Very Dark Gray (5Y3/1), silty, very fine-grained sand with mud
-Dark Gray (5Y4/1) to Very Dark Gray (5Y3/1), strongly bioturbated, muddy silt with very fine-grained sand

-Very Dark Gray (5Y3/1), well-sorted, massive, very fine to fine-grained sand
-Olive Gray (5Y4/2), Very Dark Gray (5Y3/1), and Black (5Y2.5/1), strongly bioturbated, muddy silt with fine-grained sand. Large worm tube
-Dark Gray (5Y4/1) to Very Dark Gray (5Y3/1), silty, very fine-grained sand with mud

-Very Dark Gray (5Y3/1), well-sorted, massive, very fine to fine-grained sand
-Dark Gray (5Y4/1) to Very Dark Gray (5Y3/1), strongly bioturbated, muddy silt with very fine-grained sand
-Dark Gray (5Y4/1) to Very Dark Gray (5Y3/1), silty, very fine-grained sand with mud

-Olive Gray (5Y4/2), very fine-grained sand with mud
-Dark Gray (5Y4/1), silty, very fine-grained sand with mud

-Dark Gray (5Y4/1), massive, very fine to fine-grained sand with mud
-Dark Gray (5Y4/1), silty, very fine-grained sand

-Dark Gray (5Y4/1), massive, very fine to fine-grained sand with mud
-Very Dark Gray (5Y3/1), silty, very fine-grained sand

-Dark Gray (5Y4/1), massive, very fine to fine-grained sand with mud
-Olive Gray (5Y4/2), silty, very fine-grained sand with mud

-Very Dark Gray (5Y3/1), well-sorted, massive, fine-grained sand

-Very Dark Gray (5Y3/1), well-sorted, massive, fine-grained sand

GeoB22735-05 (MeBo)

Total Core Depth: 70 m
Recovery: 51.7 m (74%)
Water Depth: 1,392 m

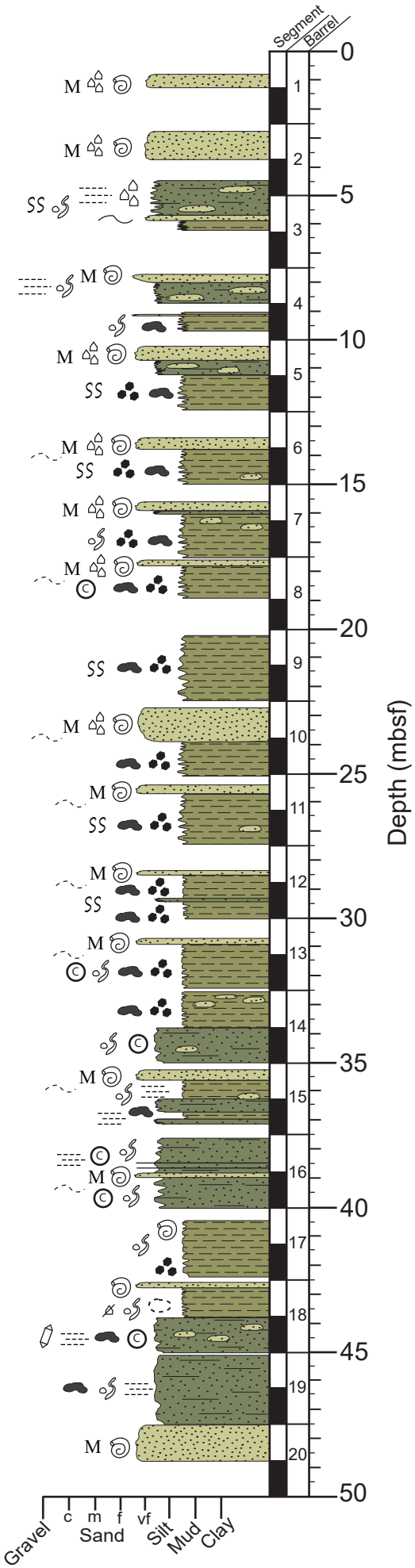

-Very Dark Gray (5Y3/1), well to moderately-sorted, massive, very fine to fine-grained sand. Forams common to abundant

-Olive Gray (5Y4/3), Dark Gray (5Y4/1) and Very Dark Gray (5Y3/1), bioturbated, muddy, silty very fine-grained sand. Thin, well-sorted very fine to fine-grained sand bed at the base (no forams)

-Dark Gray (5Y4/1), faintly laminated, bioturbated, silty very fine-grained sand with mud

-Very Dark Gray (5Y3/1), Dark Olive Gray (5Y3/2) and Black (5Y2.5/1), strongly bioturbated, muddy silt with minor amounts of very fine-grained sand

-Dark Gray (5Y4/1) and Very Dark Gray (5Y3/1), bioturbated, silty very fine-grained sand with mud

-(11.5-33.5 m) Very Dark Gray (5Y3/1), Dark Olive Gray (5Y3/2) and Black (5Y2.5/1), strongly bioturbated, muddy silt with minor amounts of very fine-grained sand interbedded with Very Dark Gray (5Y3/1), well to moderately sorted sands containing abundant forams. Sands occur only at the tops of individual core barrels

-Dark Gray (5Y4/1) and Very Dark Gray (5Y3/1), bioturbated, silty very fine-grained sand with mud

-Very Dark Gray (5Y3/1), well-sorted, massive, very fine to fine-grained sand

-Dark Gray (5Y4/1), Very Dark Gray (5Y3/1), and Black (5Y2.5/1), interbedded bioturbated, muddy, silty, very fine-grained sand and sandy, muddy silt

-Dark Gray (5Y4/1) and Very Dark Gray (5Y3/1), bioturbated, faintly laminated, silty very fine-grained sand with mud. Well preserved bedding in lower half of segment 1

-Very Dark Gray (5Y3/1), Dark Olive Gray (5Y3/2) and Black (5Y2.5/1), strongly bioturbated, muddy silt with minor amounts of very fine-grained sand

-Dark Gray (5Y4/1), Very Dark Gray (5Y3/1), and Black (5Y2.5/1), bioturbated, muddy, silty, very fine-grained sand

-Very Dark Gray (5Y3/1), well-sorted, massive, very fine to fine-grained sand

GeoB22735-05 (MeBo) continued

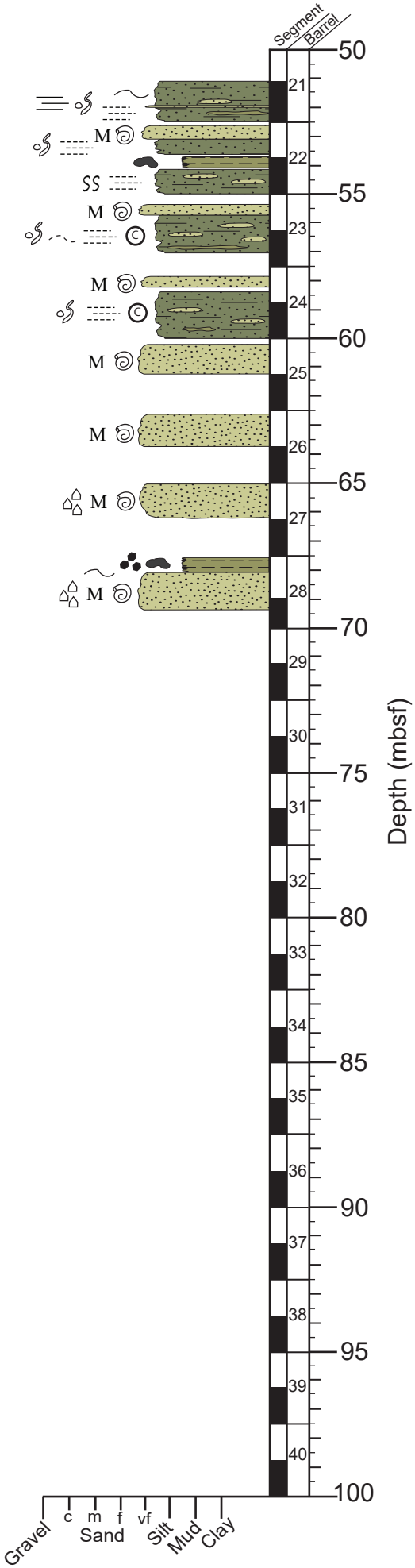

-Dark Gray (5Y4/1), bioturbated, faintly laminated, very fine-grained, silty sand with mud. Isolated sand and mud laminae

-Very Dark Gray (5Y3/1), well-sorted, massive, very fine to fine-grained sand

-Very Dark Gray (5Y3/1) and Dark Gray (5Y4/1) strongly bioturbated, muddy silt with sand

-Dark Gray (5Y4/1), bioturbated, faintly laminated, very fine-grained, silty sand with mud

-Very Dark Gray (5Y3/1), well-sorted, massive, very fine to fine-grained sand

-Dark Gray (5Y4/1), bioturbated, faintly laminated, very fine-grained, silty sand with mud

-Very Dark Gray (5Y3/1), well-sorted, massive, very fine to fine-grained sand

-Dark Gray (5Y4/1), bioturbated, faintly laminated, very fine-grained, silty sand with mud

-Very Dark Gray (5Y3/1), well-sorted, massive, very fine to fine-grained sand

-Very Dark Gray (5Y3/1), well-sorted, massive, very fine to fine-grained sand

-Very Dark Gray (5Y3/1), well-sorted, massive, very fine to fine-grained sand

-Dark Gray (5Y4/1), Very Dark Gray (5Y3/1), and Black (5Y2.5/1), strongly bioturbated, muddy silt with minor very fine-grained sand

-Very Dark Gray (5Y3/1), well-sorted, massive, very fine to fine-grained sand. Rotary core

GeoB22739-02 (MeBo)

Total Core Depth: 20 m
Recovery: 4.79 m (24%)
Water Depth: 1,112 m

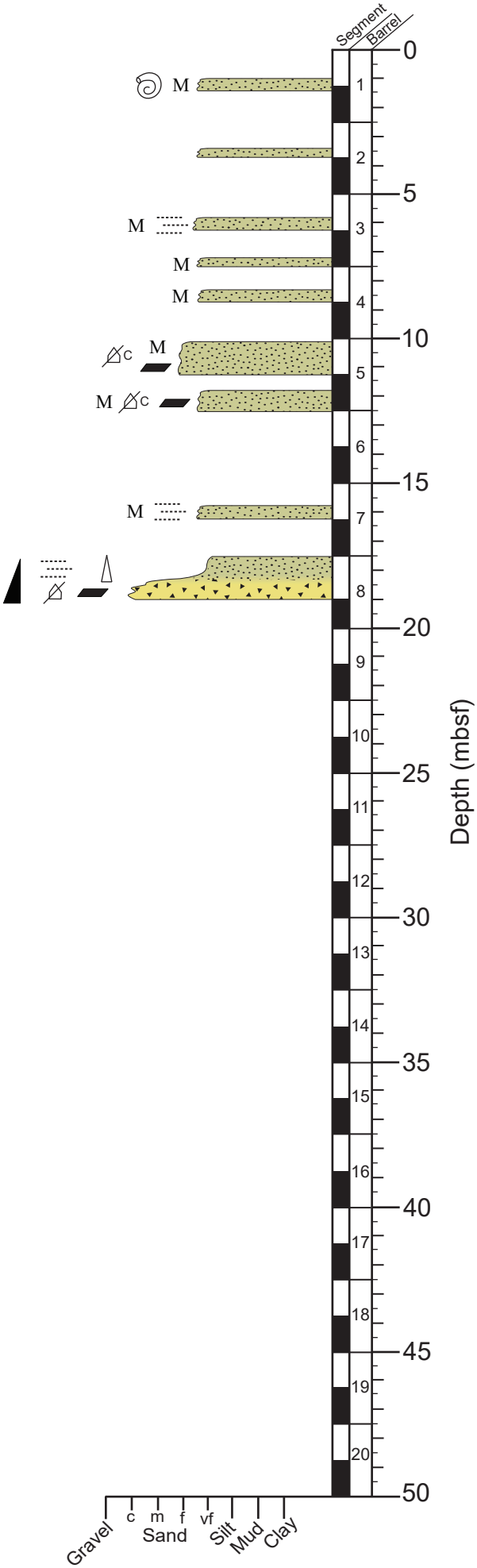

-Olive Gray (5Y4/2) massive, fine to very fine-grained sand
-Dark Gray (5/Y4/1) and Very Dark Gray (5Y 3/1) massive, well-sorted, fine to very fine-grained sand

-Very Dark Gray (5Y 3/1) fine to very fine-grained sand

-Dark Gray (5Y4/1) and Very Dark Gray (5Y3/1), massive, well-sorted, very fine-grained sand

-Very Dark Gray (5Y3/1), massive, well-sorted, fine to medium-grained sand. Mudclasts and small shell fragments common throughout

-Very Dark Gray (5Y 3/1) massive to faintly laminated, well-sorted, fine to very fine-grained sand

-Very Dark Gray (5Y 3/1), Dark Gray (5Y4/1), and Gray (5Y5/1), intercalated fine to coarse-grained, shelly sand and well-sorted sand. Shelly sands are ~30% small shell fragments (1-7 mm), 40% quartz, and 30% lithic fragments and opaque minerals. Poorly sorted overall

Appendix 2c: Grab Photos

GeoB22717-1:

GeoB22718-1:

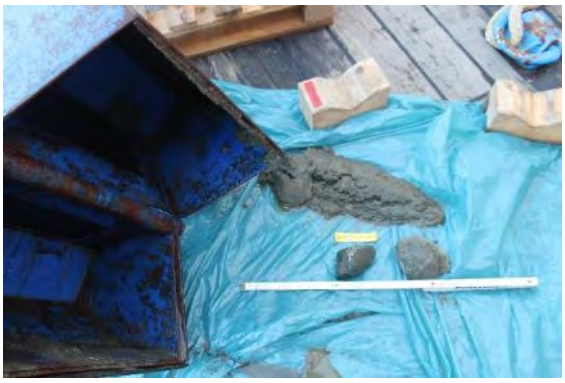

GroB22720-1:

GeoB22726-2:

GeoB22727-1:

GeoB22730-1:

GeoB22731-1:

GeoB22732-1:

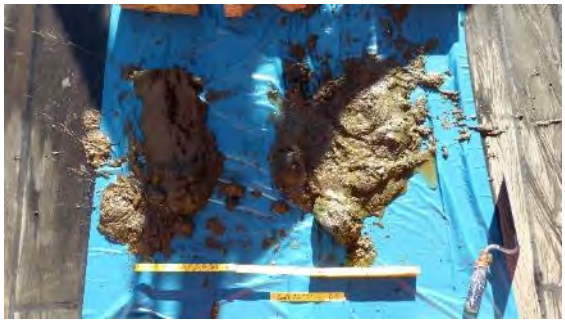

Geob22733-1:

GeoB22736-1:

GeoB22738-1:

Appendix 3: Physical properties

22702-3

Date: 15/01/2018 Position: 37°48.57'S 054°10.21'W
Water depth: 1355 m Core length: 9.02 m

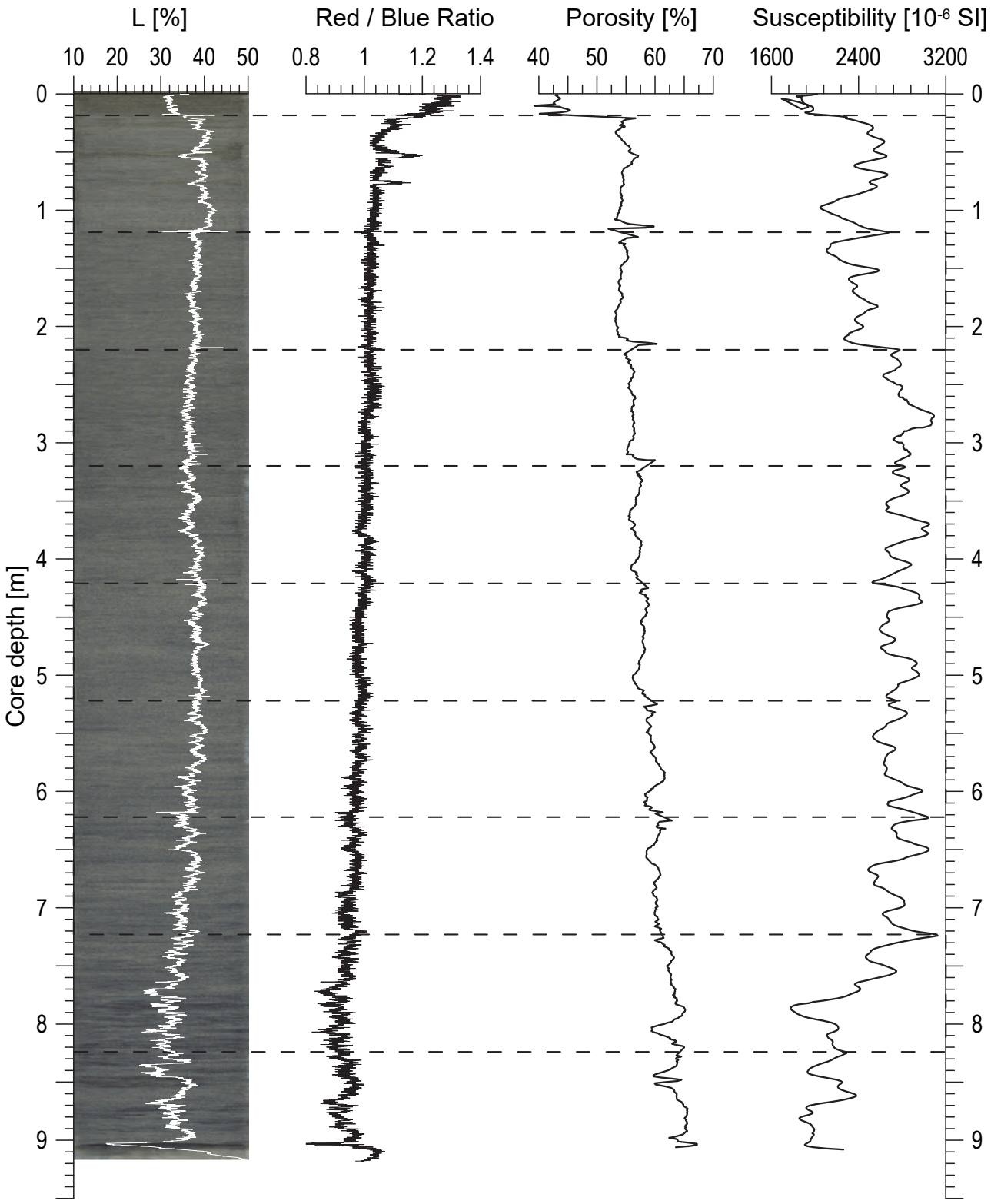

22704-2

Date: 22/01/2018 Position: 37°38.63'S 054°08.49'W
Water depth: 1040 m Core length: 0.59 m

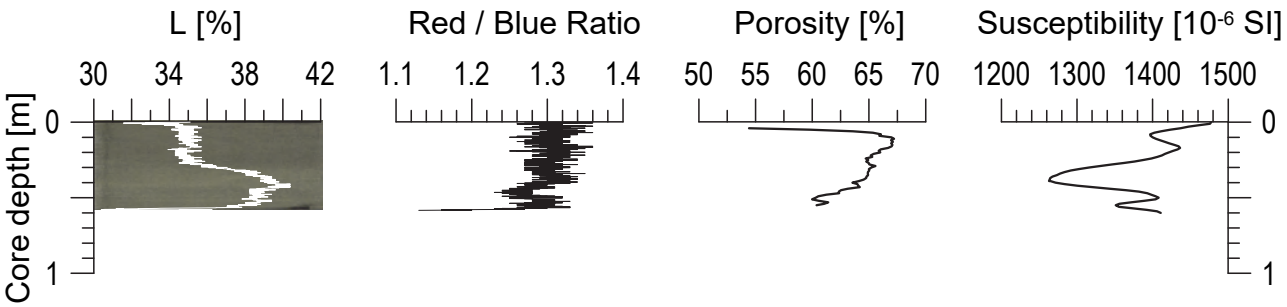

22704-3

Date: 22/01/2018 Position: 37°38.64'S 054°08.48'W
Water depth: 1038 m Core length: 1.05 m

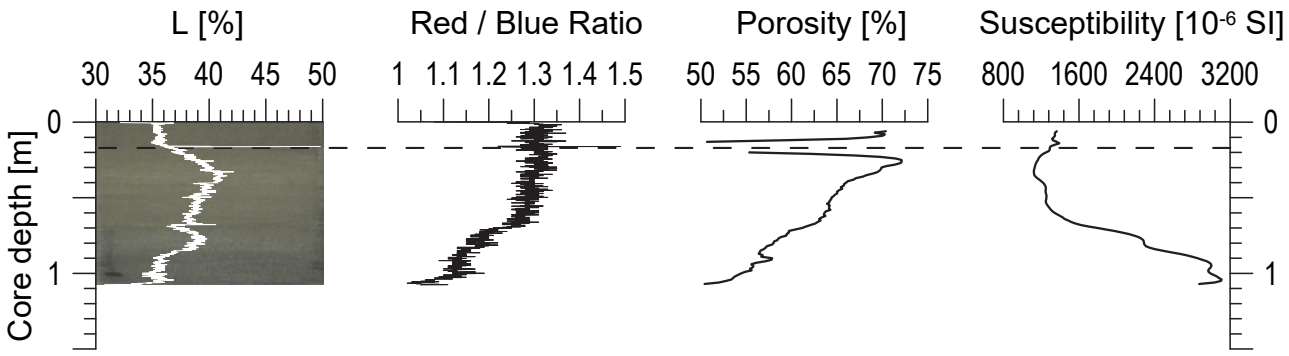

22706-2

Date: 16/01/2018 Position: 37°58.04'S 053°45.79'W
Water depth: 3011 m Core length: 9.35 m

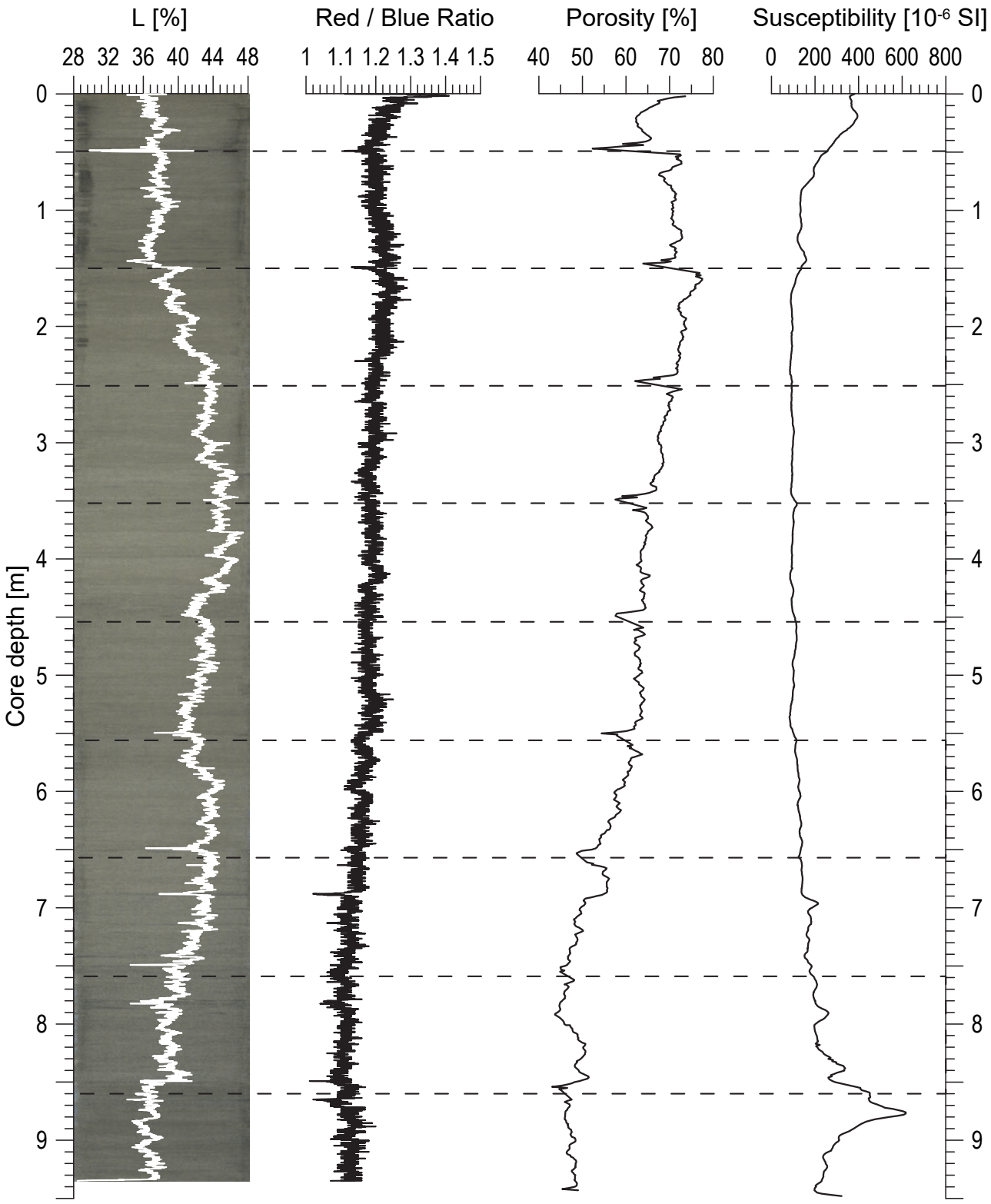

22707-1

Date: 16/01/2018 Position: 37°54.83'S 053°47.72'W
Water depth: 2762 m Core length: 8.40 m

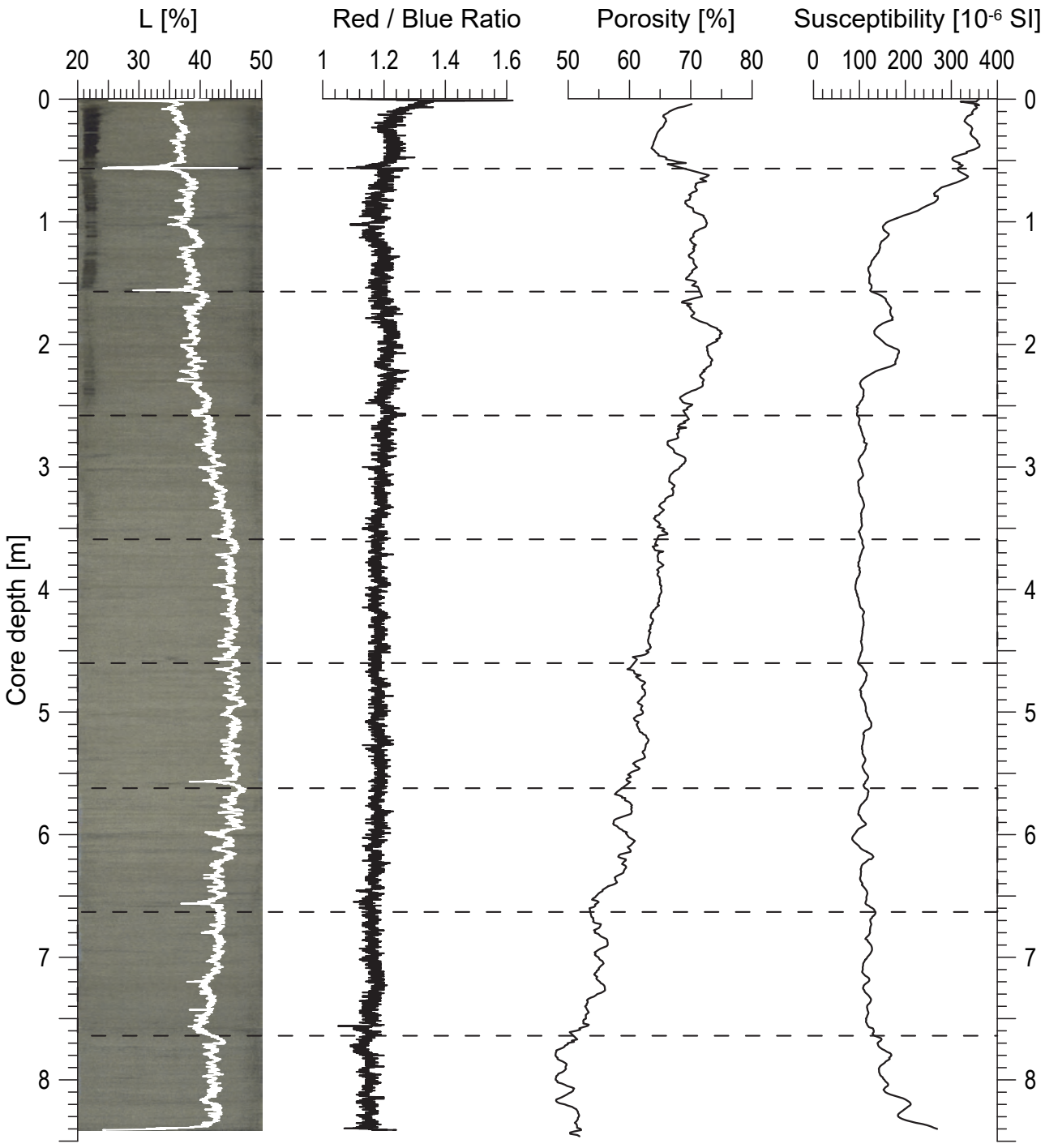

22708-1

Date: 17/01/2018 Position: 39°18.70'S 053°57.15'W
Water depth: 3690 m Core length: 9.76 m

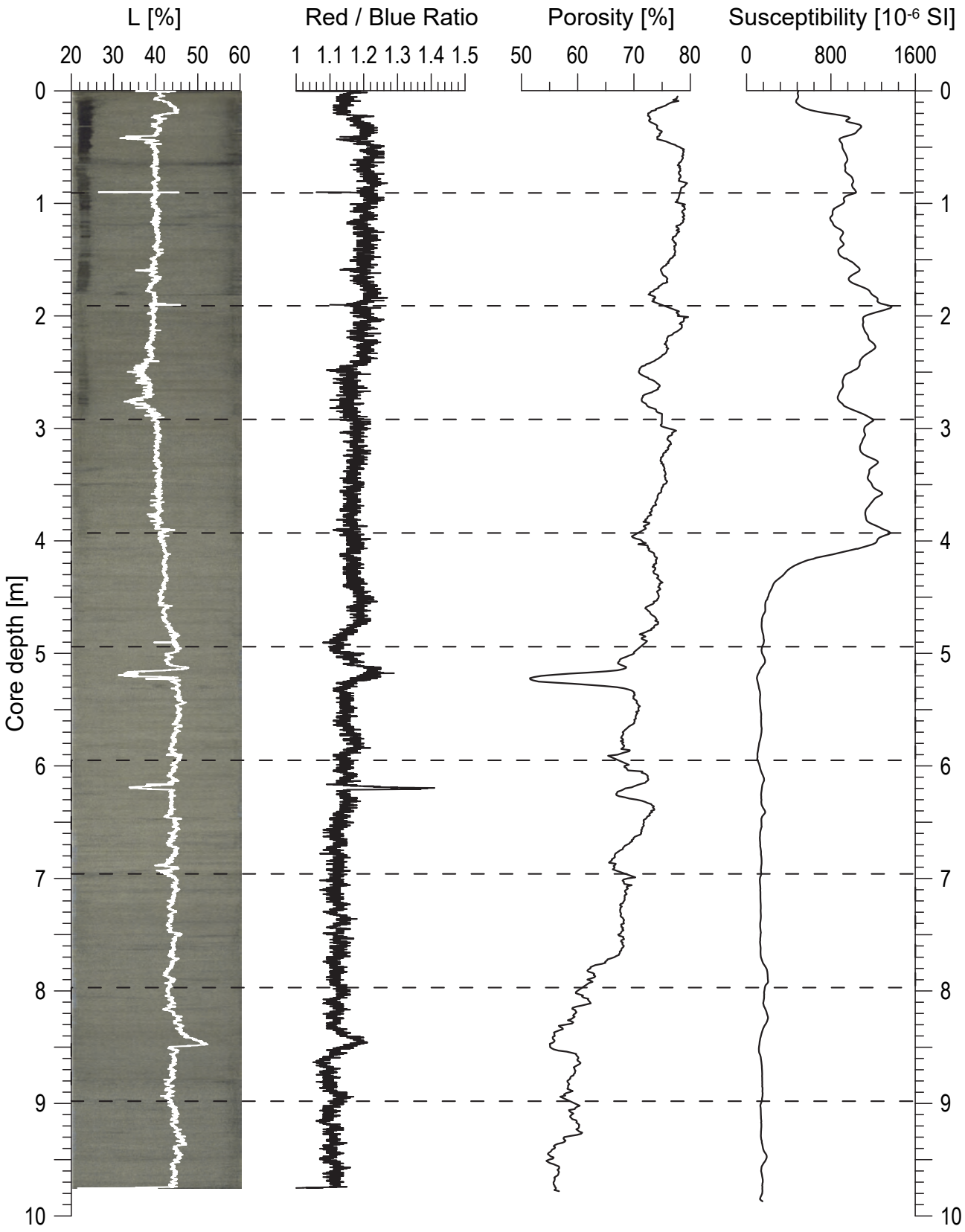

22708-2

Date: 17/01/2018 Position: 39°18.70'S 053°57.17'W
Water depth: 3679 m Core length: 9.60 m

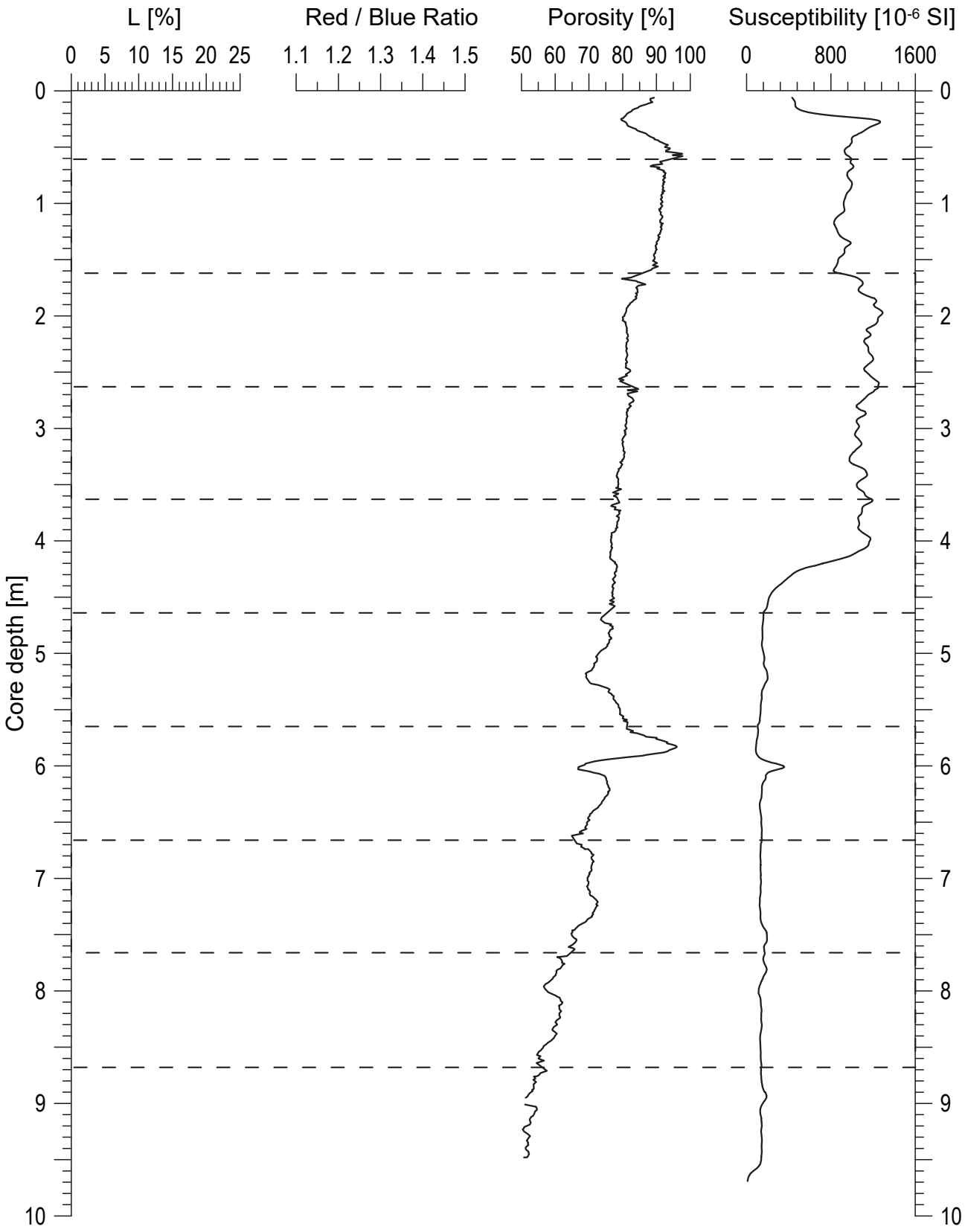

22709-1

Date: 17/01/2018 Position: 39°18.06'S 053°58.03'W
Water depth: 3611 m Core length: 9.32 m

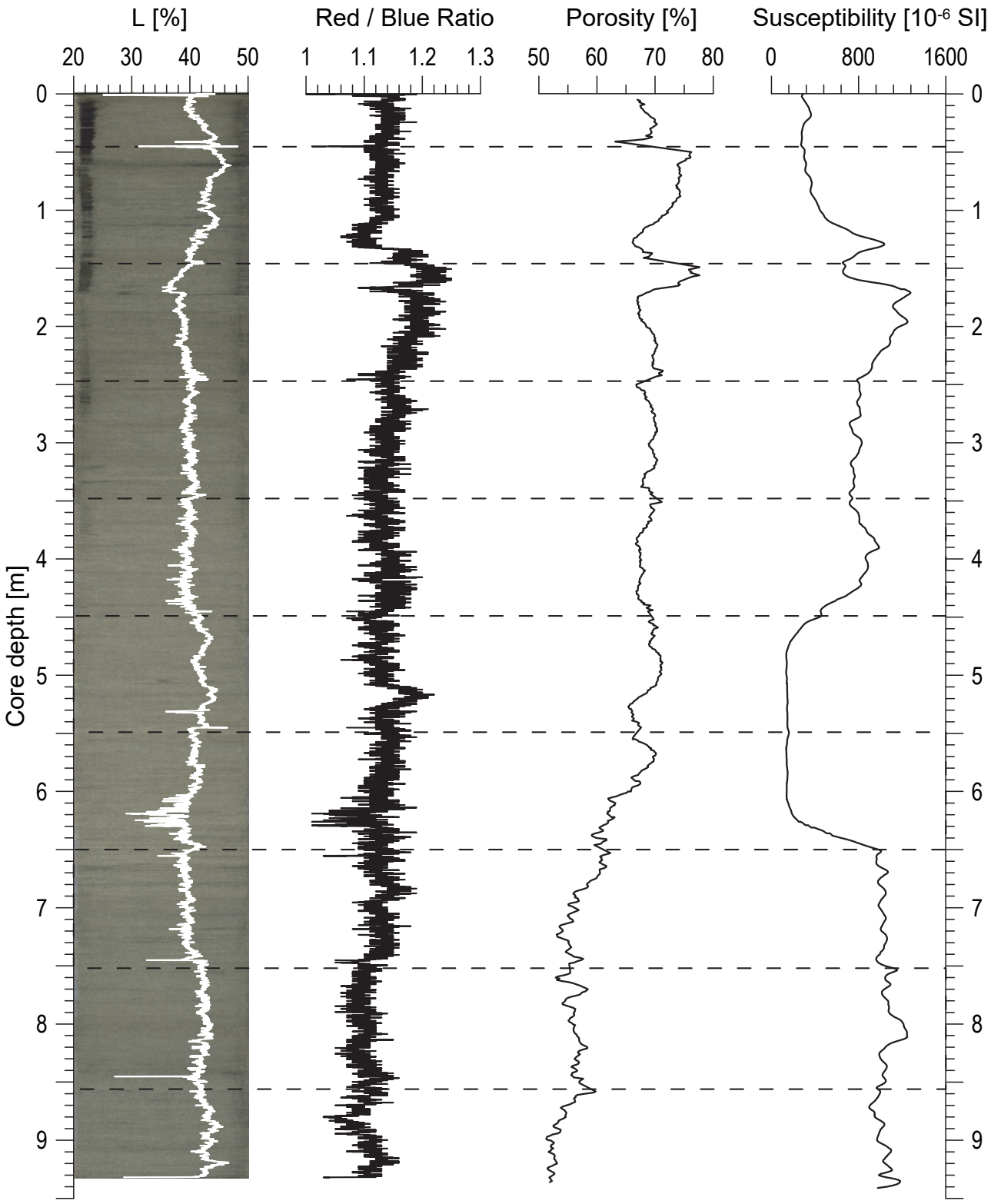

22709-2

Date: 17/01/2018 Position: 39°18.06'S 053°58.02'W
Water depth: 3612 m Core length: 9.64 m

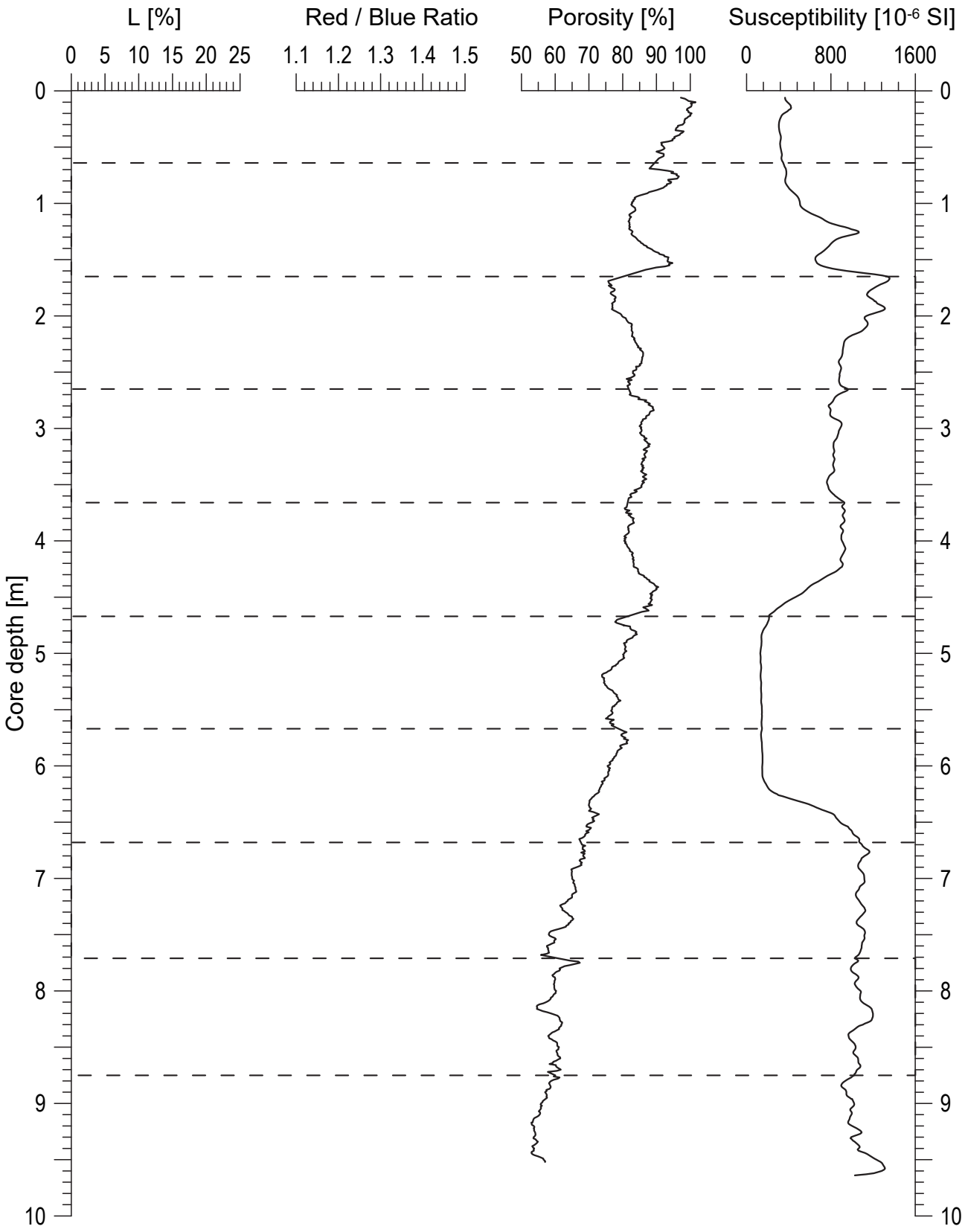

22713-2

Date: 20/01/2018 Position: 38°35.32'S 054°21.08'W
Water depth: 1115 m Core length: 5.61 m

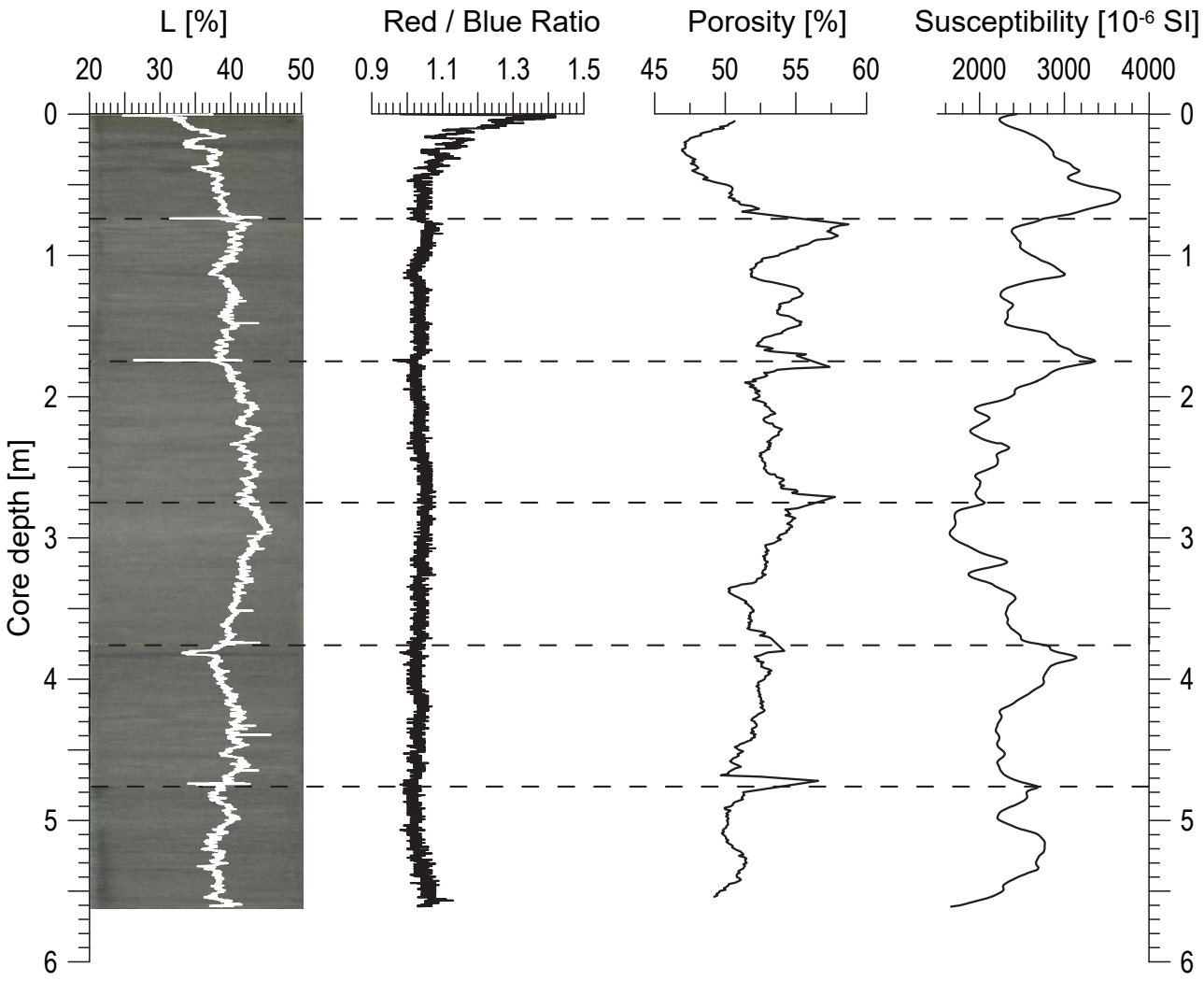

22714-1

Date: 20/01/2018 Position: 38°35.77'S 054°22.73'W
Water depth: 1111 m Core length: 3.57 m

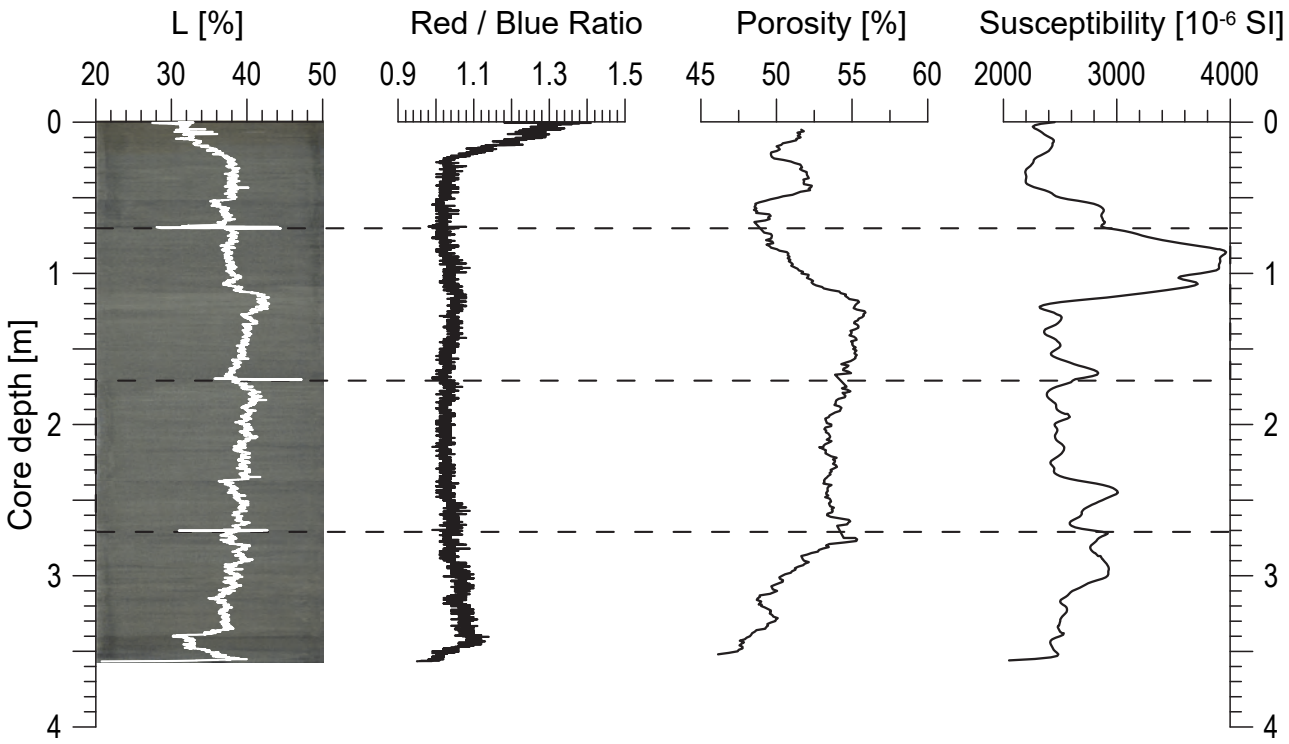

22715-2

Date: 20/01/2018 Position: 38°19.48'S 054°31.65'W
Water depth: 1105 m Core length: 5.54 m

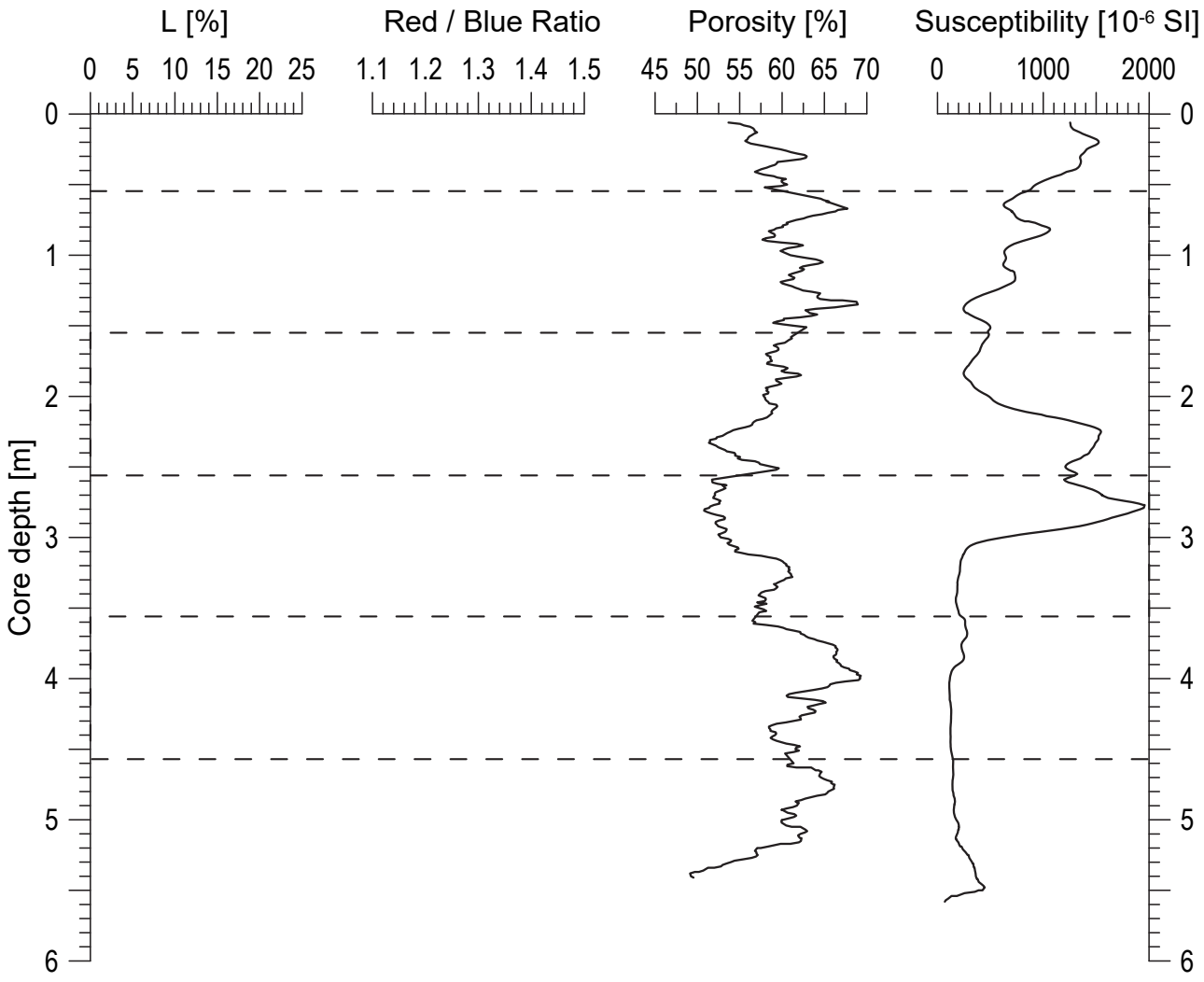

22721-2

Date: 22/01/2018 Position: 37°33.32'S 053°58.71'W
Water depth: 1060 m Core length: 7.77 m

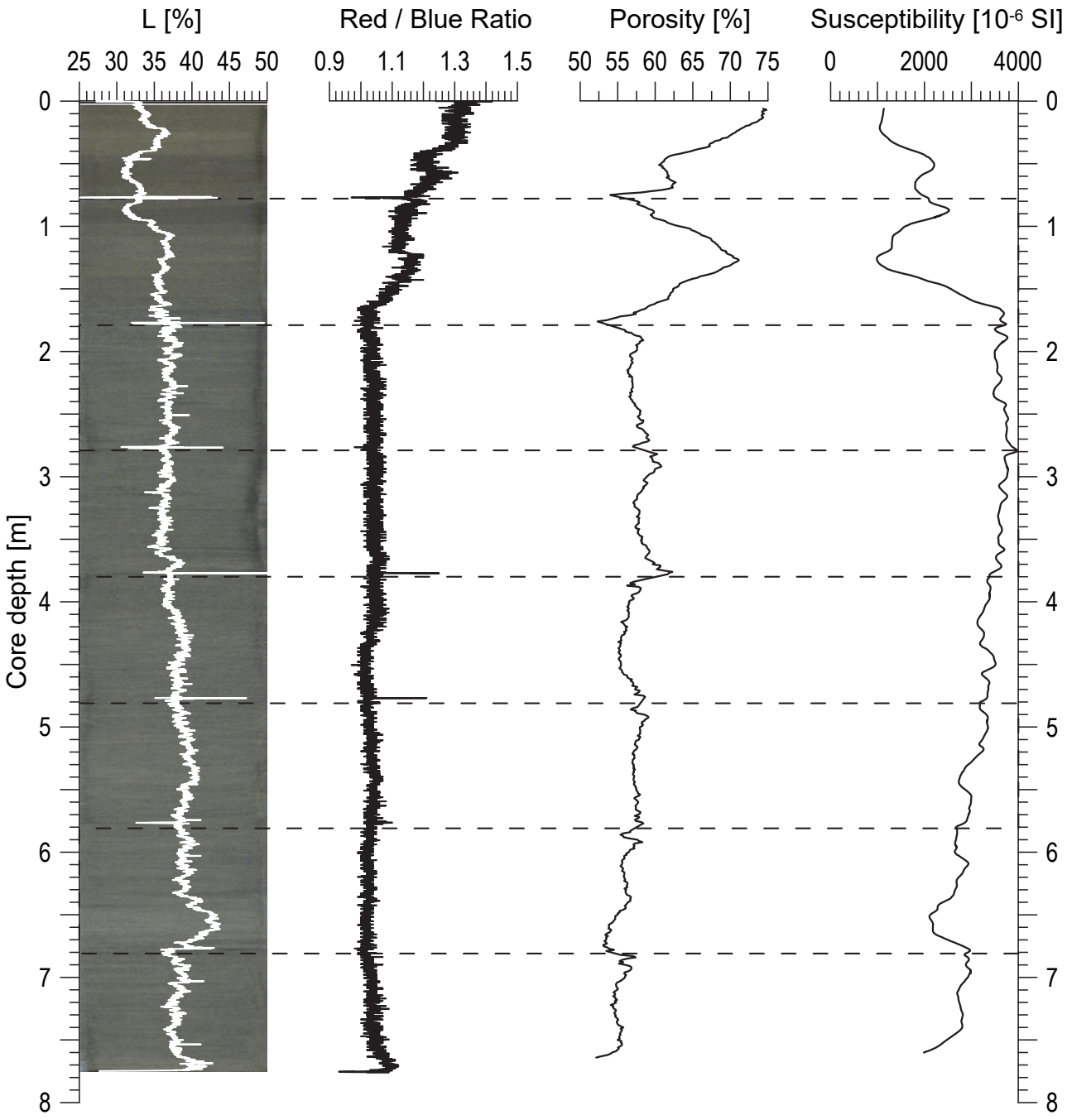

22722-4

Date: 24/01/2018 Position: 37°32.40'S 054°01.33'W
Water depth: 1077 m Core length: 5.71 m

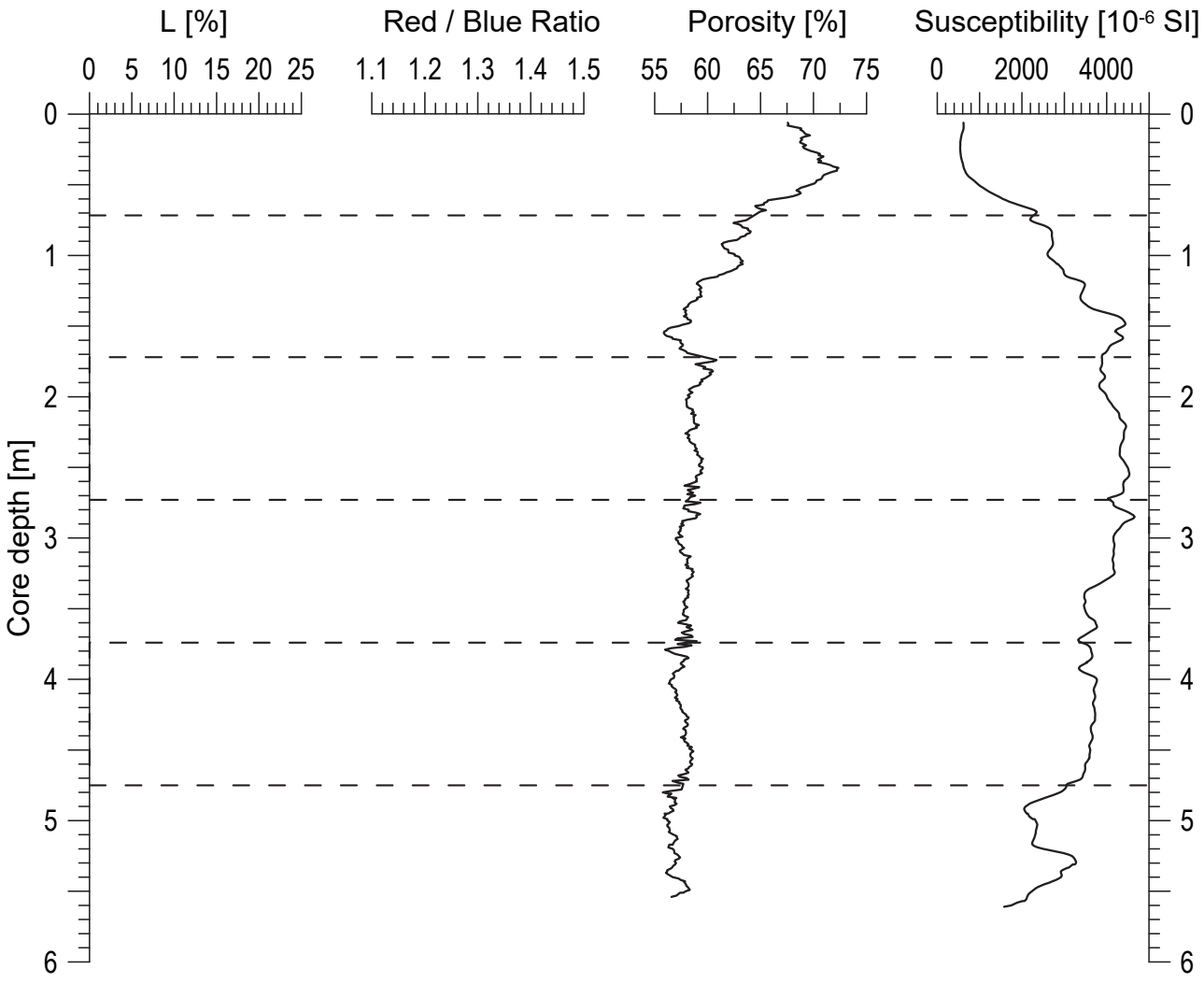

22722-5

Date: 24/01/2018 Position: 37°32.40'S 054°01.38'W
Water depth: 1073 m Core length: 9.01 m

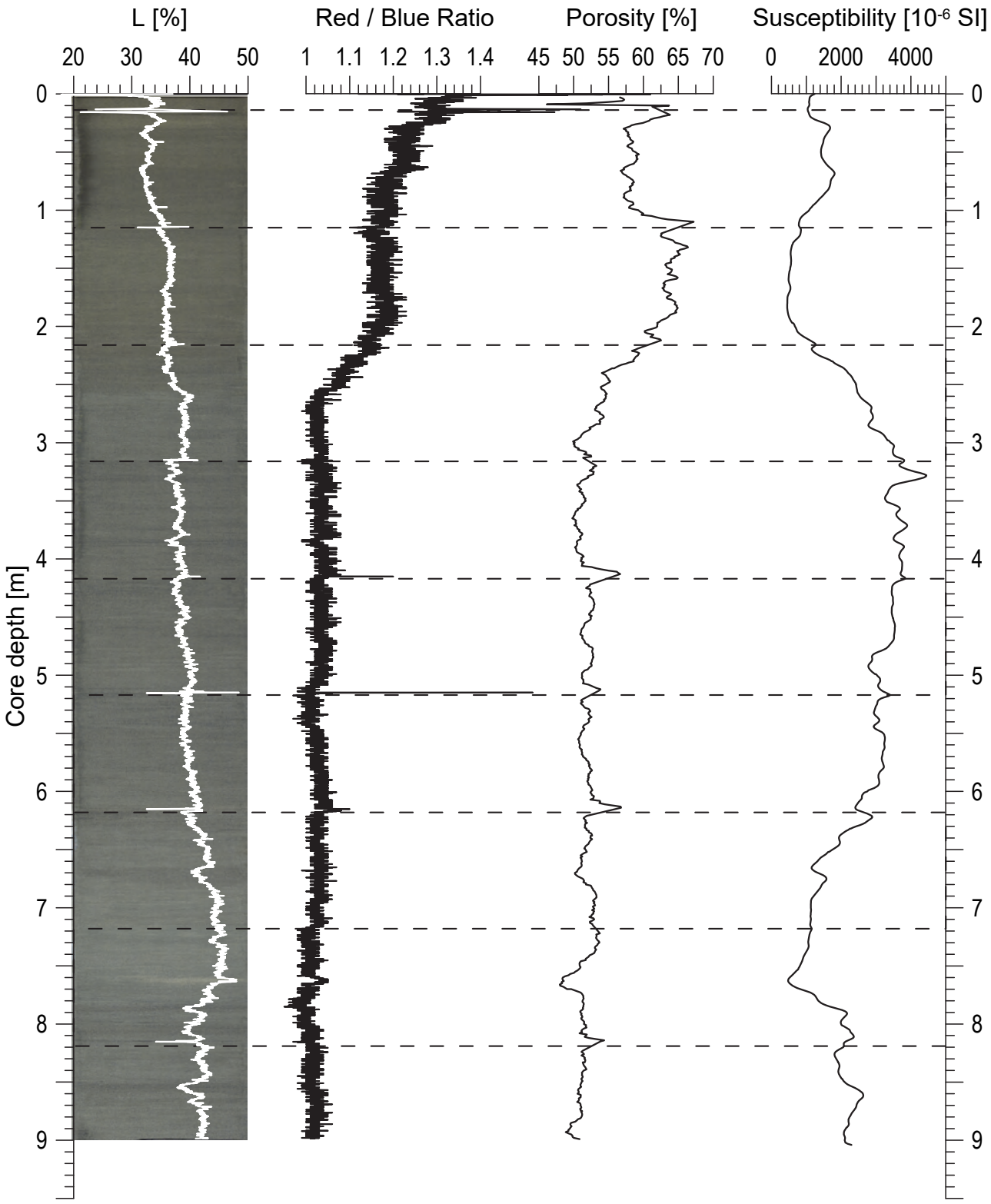

22722-6

Date: 05/02/2018 Position: 37°32.37'S 054°01.33'W
Water depth: 1076 m Recovery: 0.80 m

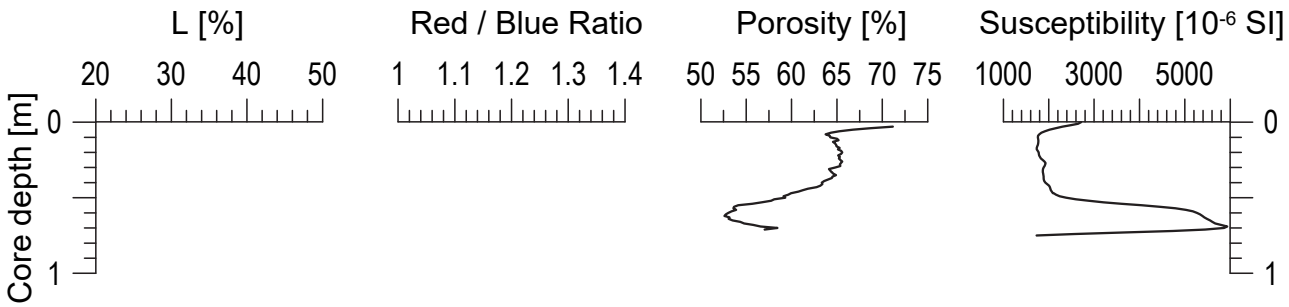

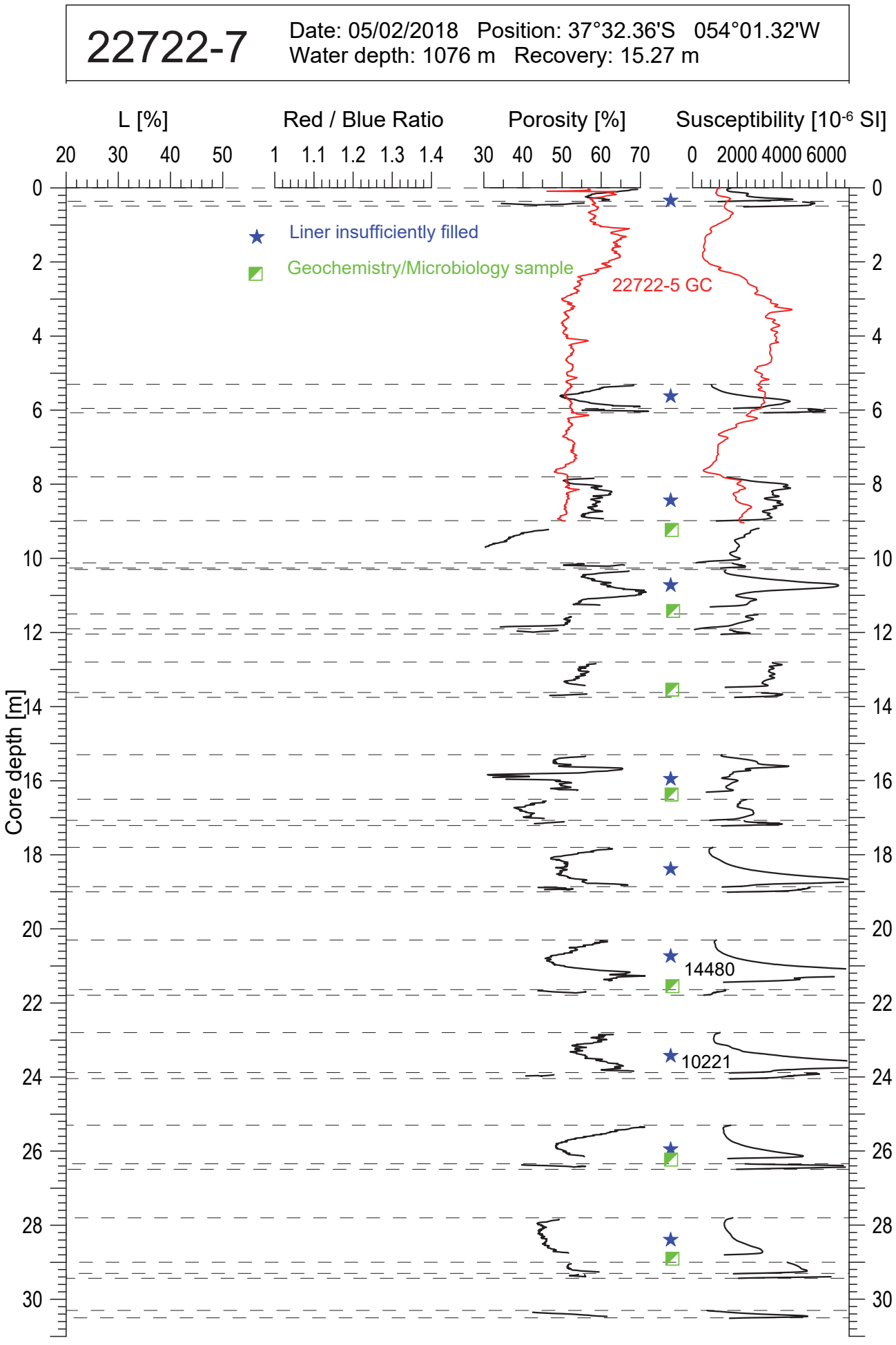
22722-7
Date: 05/02/2018 Position: 37°32.36'S 054°01.32'W
Water depth: 1076 m Recovery: 15.27 m
L [%]
Red / Blue Ratio
Porosity [%]
Susceptibility [10-6 SI]
20 30 40 50
1 1.1 1.2 1.3 1.4
30 40 50 60 70
0 2000 4000 6000
Liner insufficiently filled
Geochemistry/Microbiology sample
22722-5 GC
14480
10221
Core depth [m]
0 2 4 6 8 10 12 14 16 18 20 22 24 26 28 30

22723-1

Date: 24/01/2018 Position: 37°42.22'S 053°57.51'W
Water depth: 1167 m Core length: 4.90 m

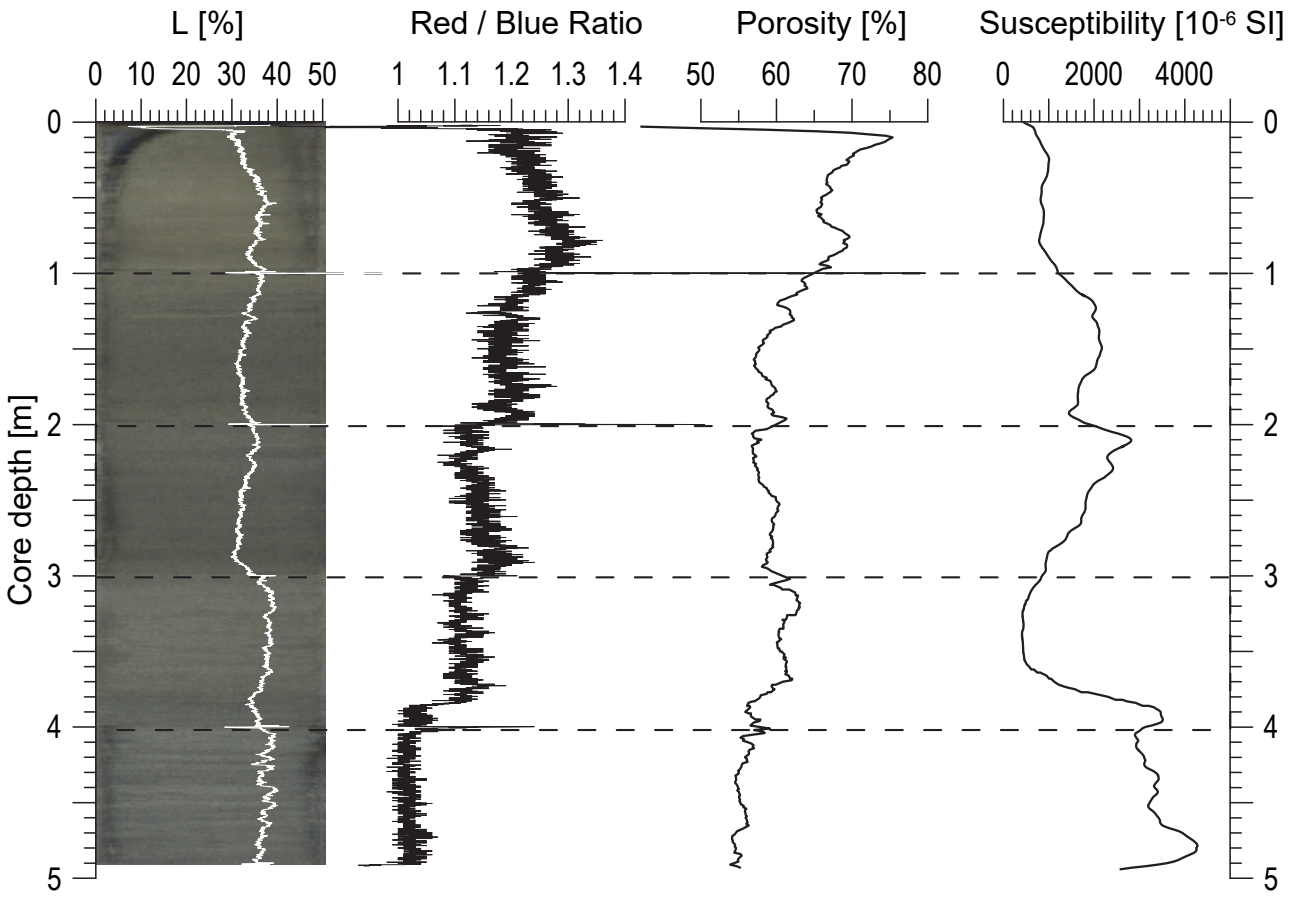

22723-3

Date: 26/01/2018 Position: 37°42.22'S 053°57.50'W
Water depth: 1168 m Core length: 4.31 m

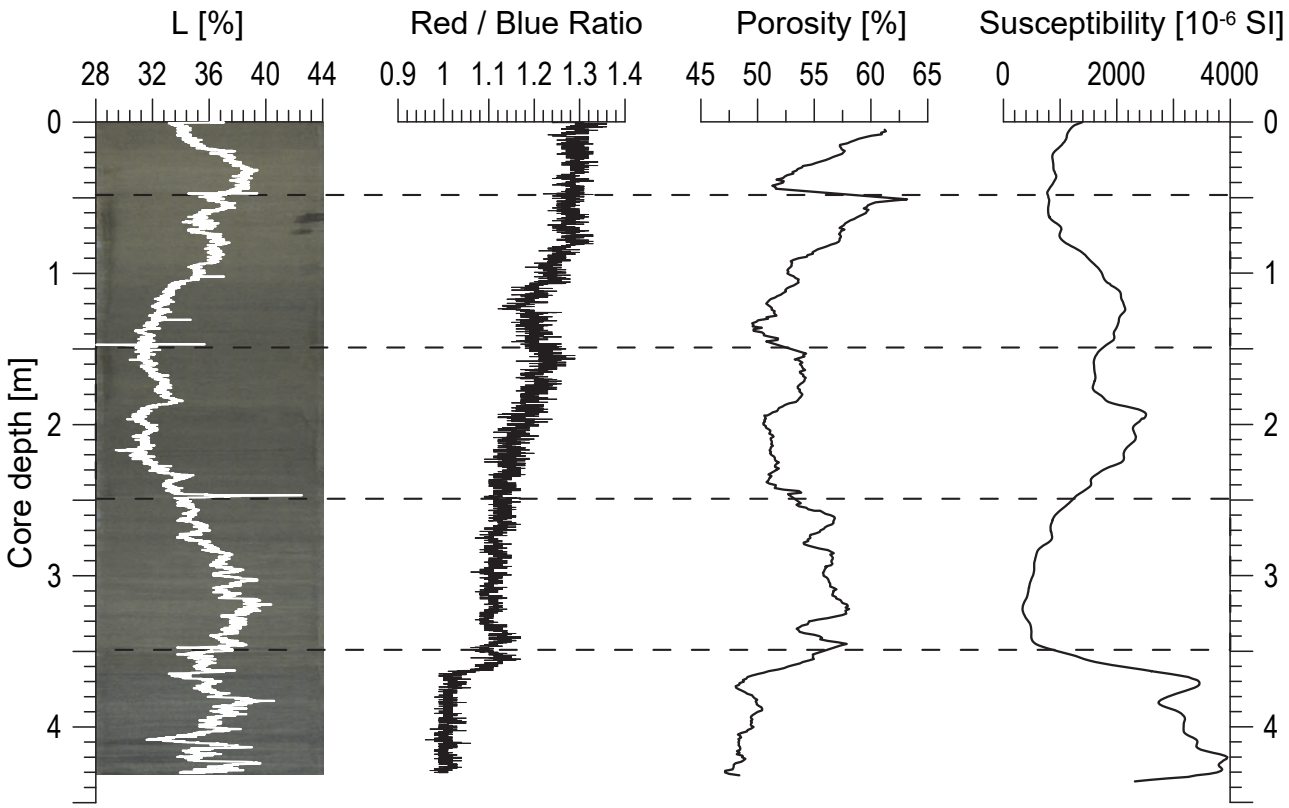

22725-2

Date: 27/01/2018 Position: 38°20.51'S 054°03.86'W
Water depth: 1345 m Core length: 1.60 m

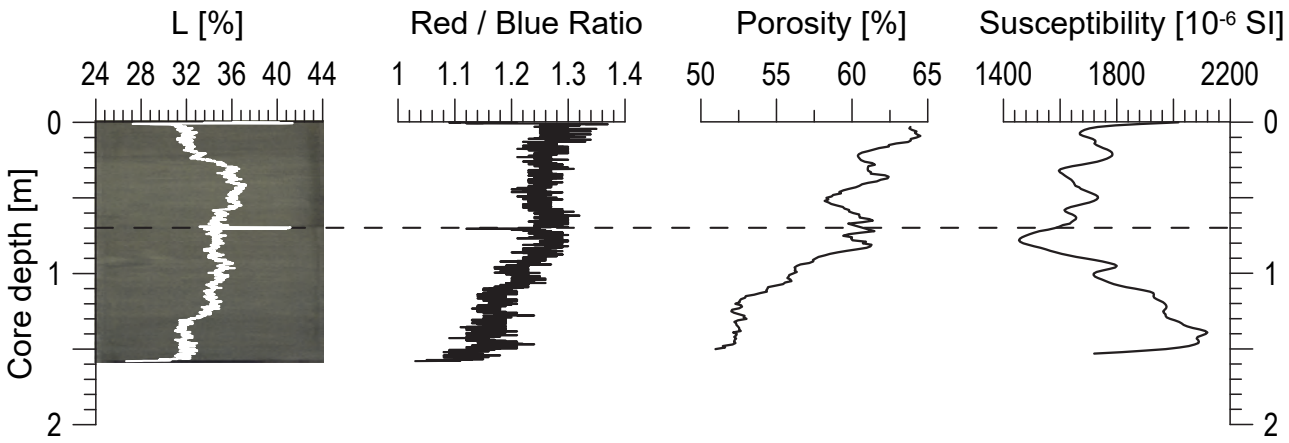

22729-1

Date: 28/01/2018 Position: 37°48.44'S 054°20.11'W
Water depth: 1202 m Core length: 1.83 m

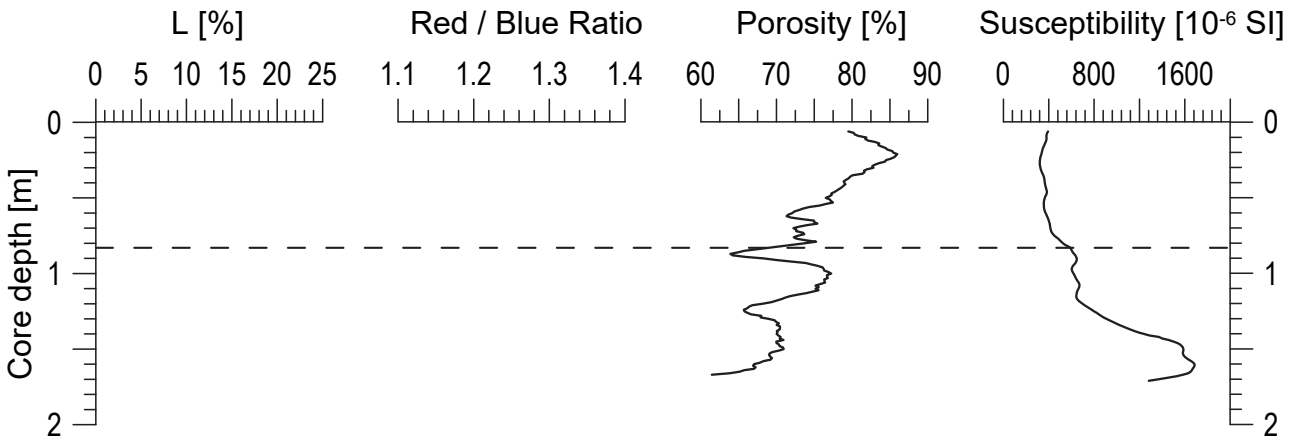

22733-2

Date: 29/01/2018 Position: 37°30.12'S 054°35.79'W
Water depth: 635 m Core length: 0.47 m

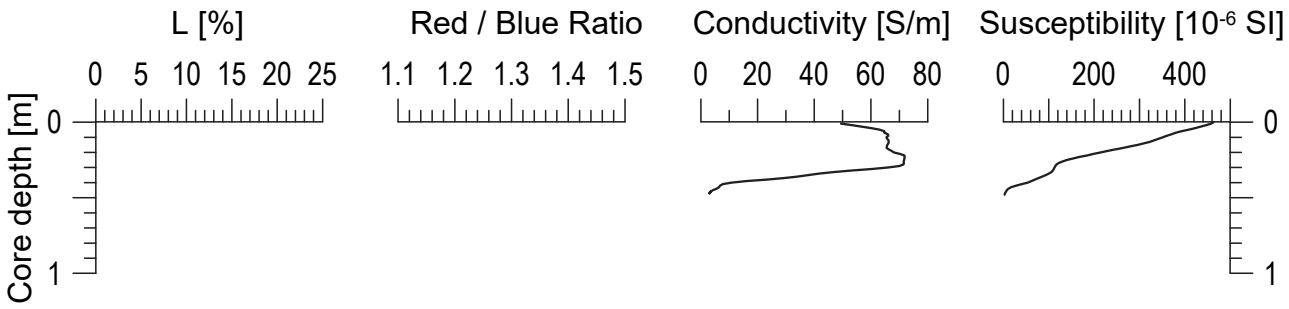

22733-3

Date: 29/01/2018 Position: 37°30.12'S 054°35.80'W
Water depth: 634 m Core length: 0.18 m

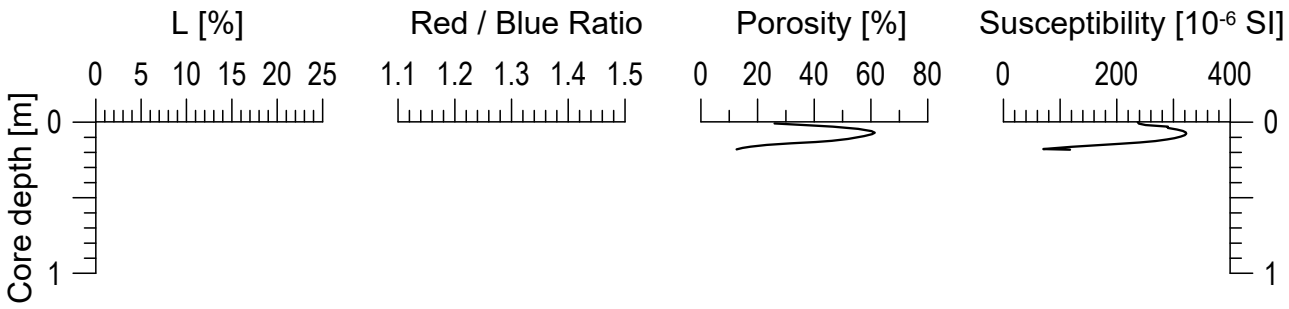

22734-2

Date: 03/02/2018 Position: 36°08.49'S 053°17.15'W
Water depth: 242 m Core length: 8.54 m

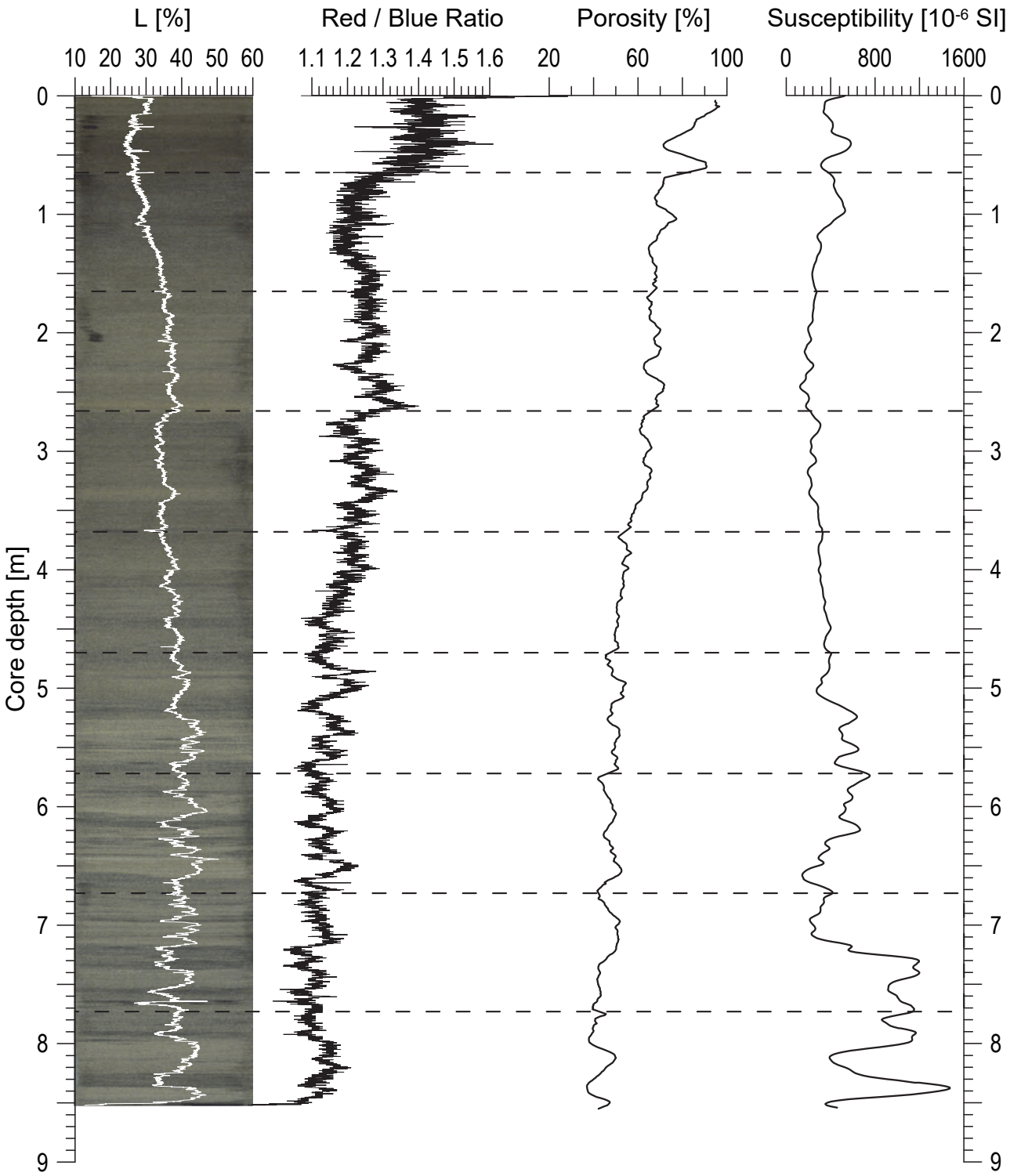

22734-3

Date: 03/02/2018 Position: 36°08.49'S 053°17.15'W
Water depth: 240 m Core length: 7.18 m

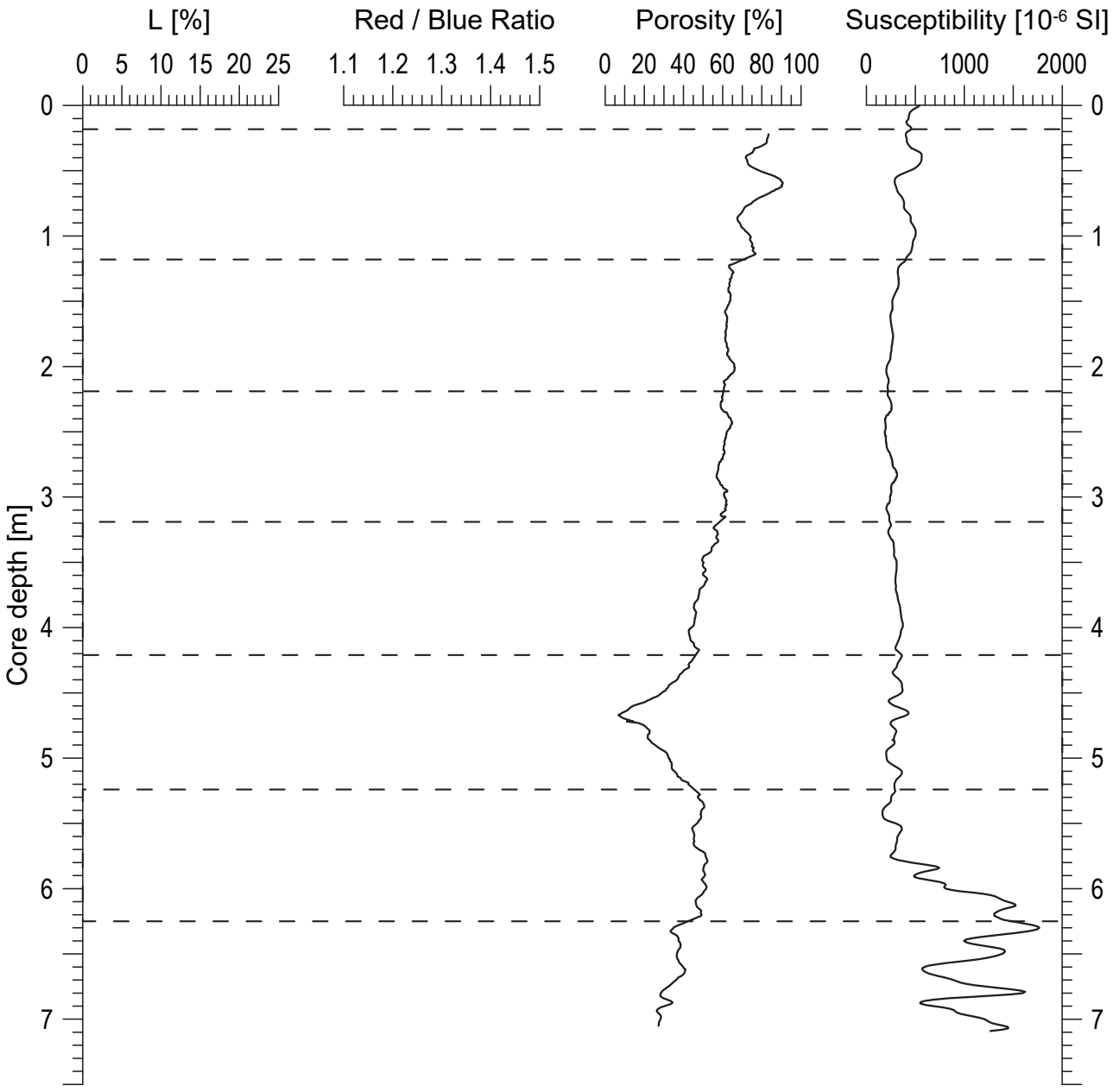

22735-1

Date: 03/02/2018 Position: 36°07.66'S 052°49.90'W
Water depth: 1384 m Core length: 8.99 m

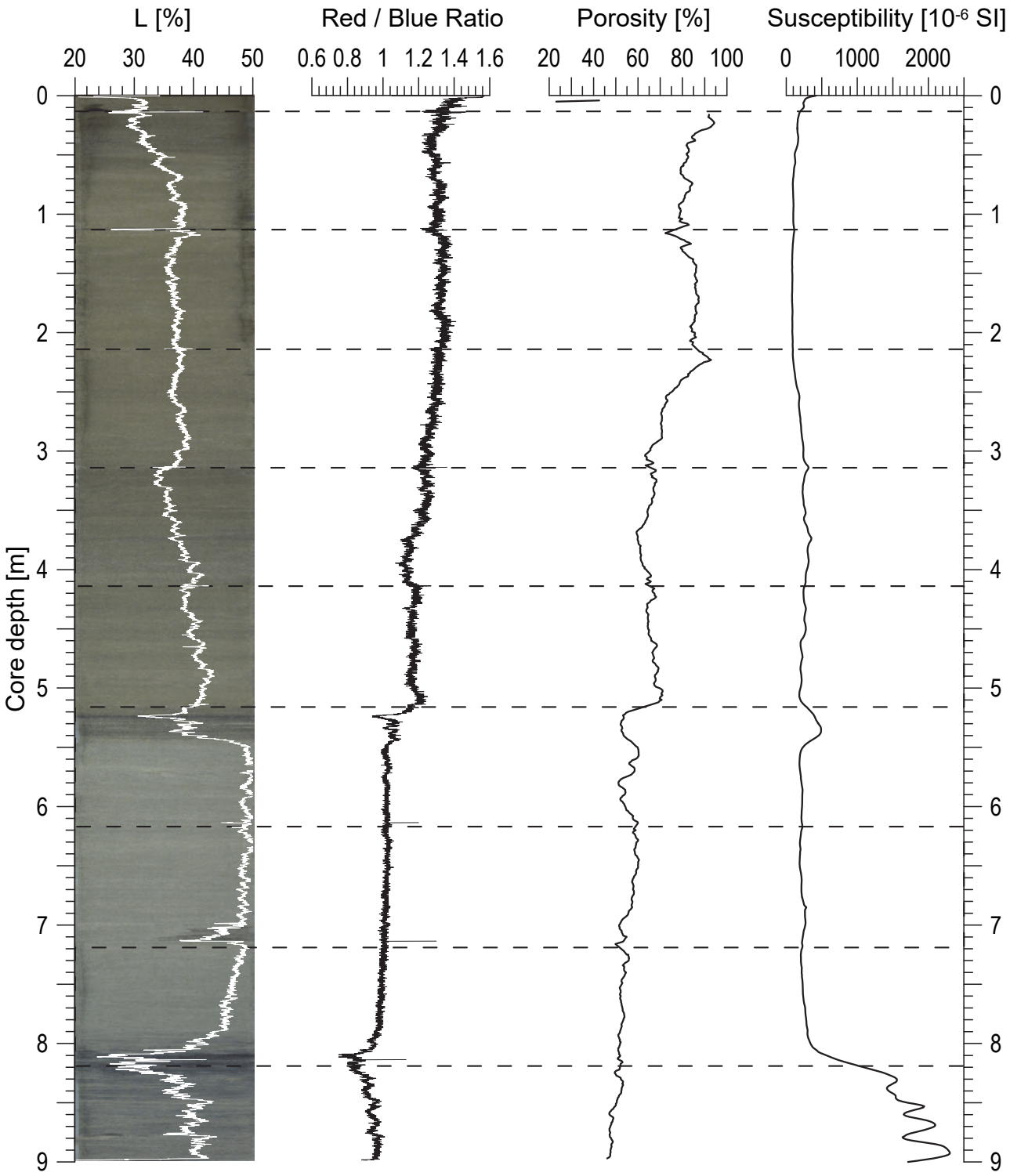

22735-5

Date: 07/02/2018 Position: 36°07.61'S 052°49.89'W
Water depth: 1388 m Recovery: 59.79 m

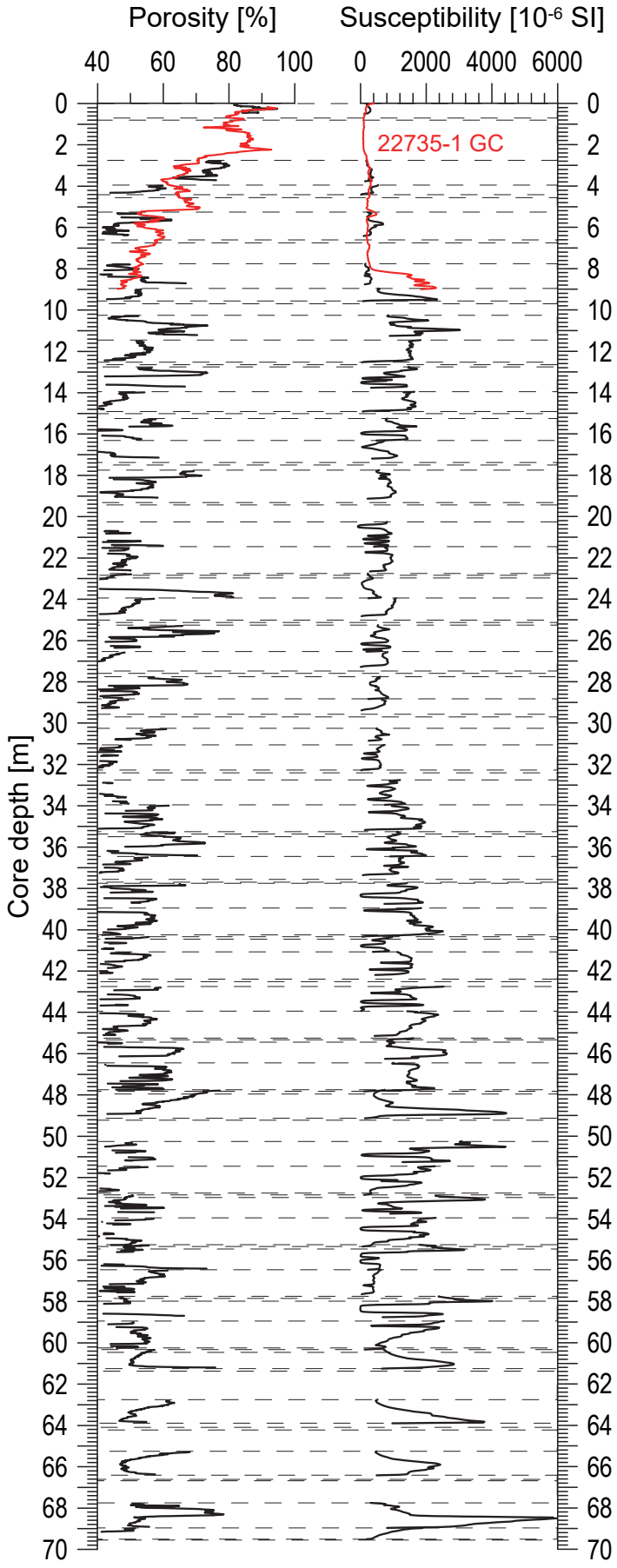

22739-2

Date: 11/02/2018 Position: 38°35.56'S 054°22.80'W
Water depth: 1112 (1406) m Recovery: 5.365 m

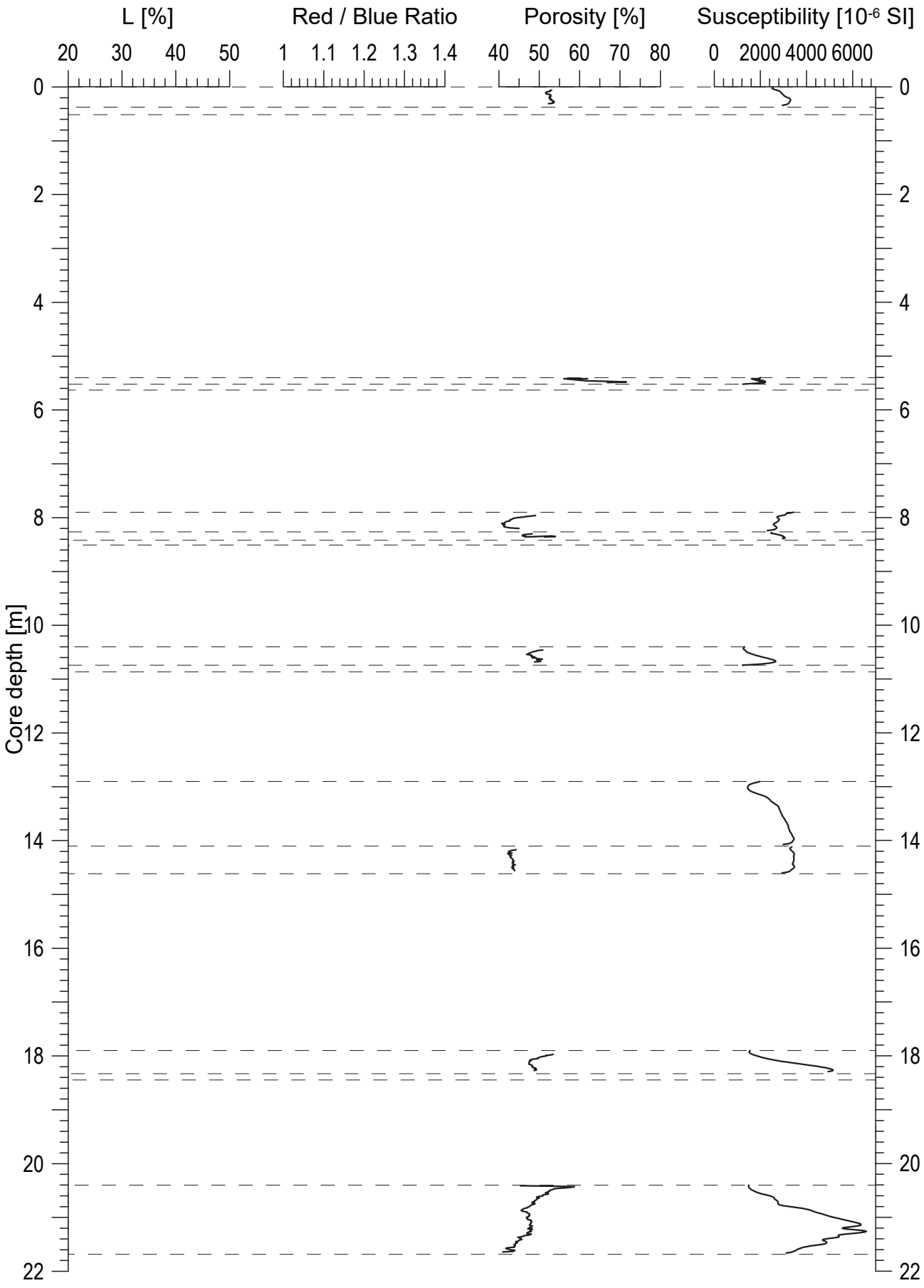

22740-1

Date: 10/02/2018 Position: 38°36.58'S 054°20.11'W
Water depth: 1102 m Core length: 1.62 m

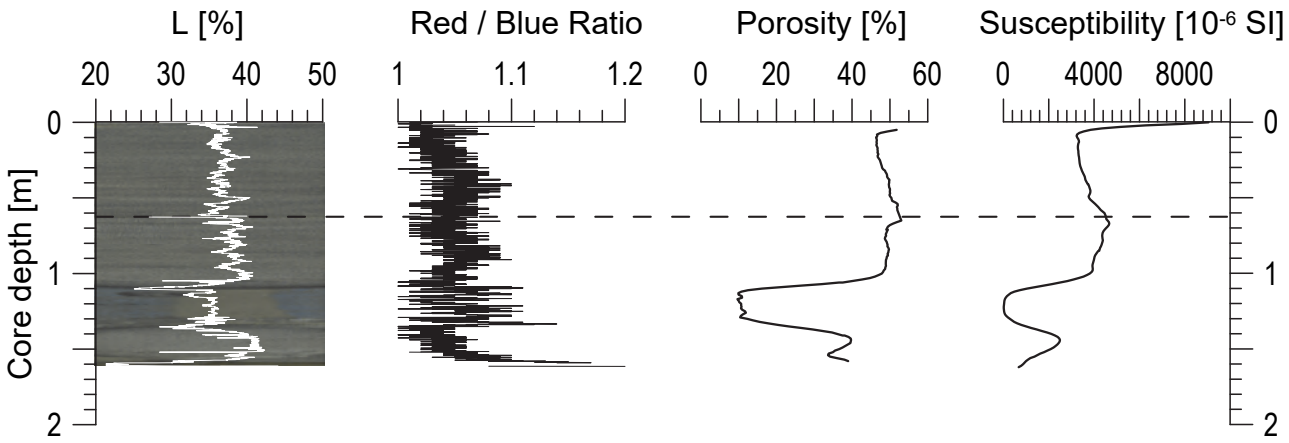

22741-1

Date: 10/02/2018 Position: 38°38.22'S 054°18.67'W
Water depth: 1072 m Core length: 2.41 m

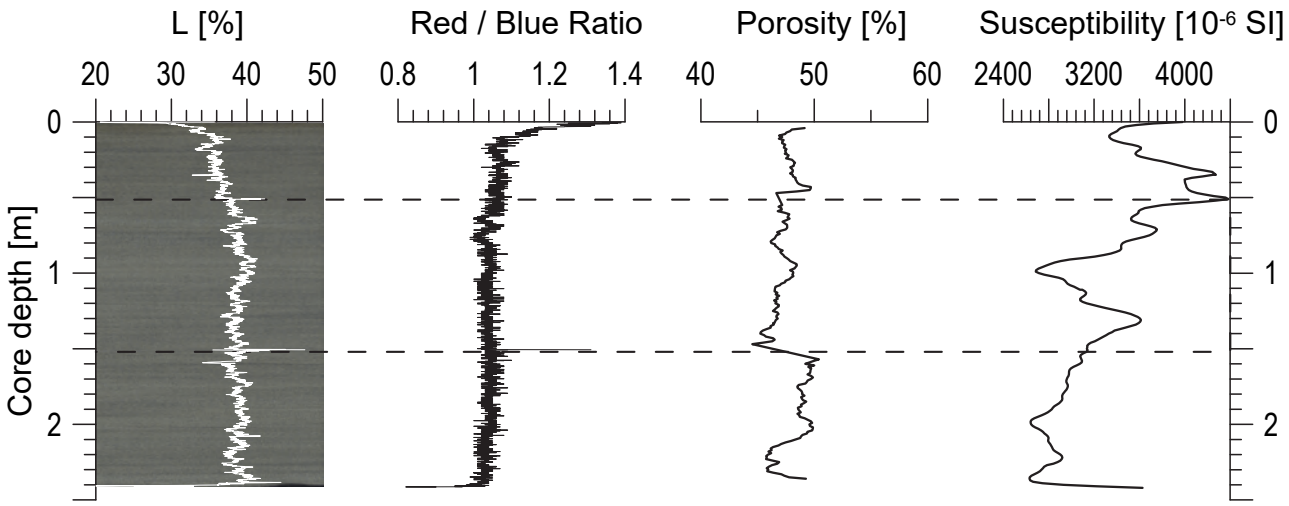

22744-1

Date: 12/02/2018 Position: 38°18.25'S 054°32.36'W
Water depth: 992 m Core length: 5.07 m

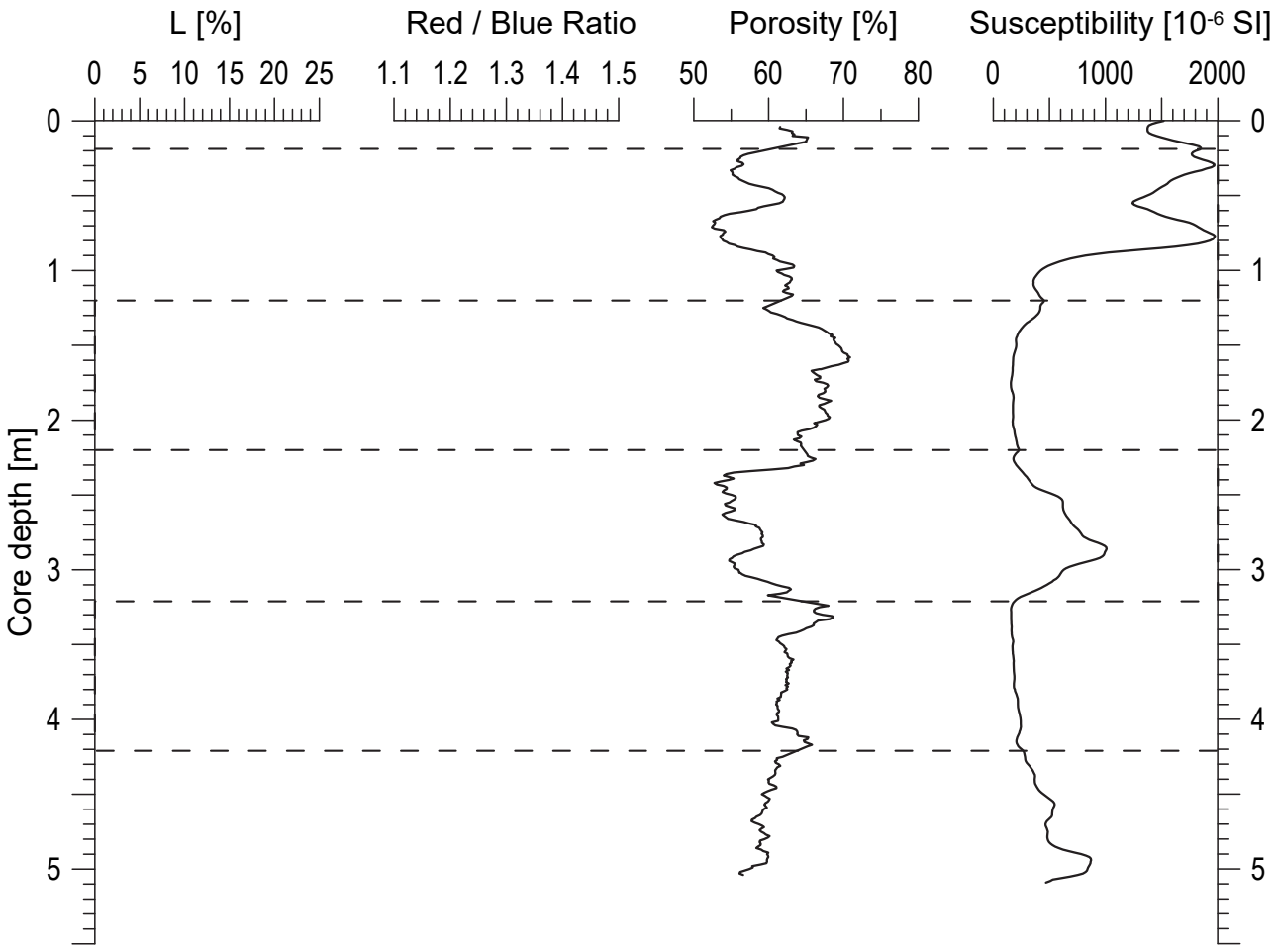

Appendix 4: Core labels and depths of samples taken for rock magnetic studies

Appendix 4 Core labels and depths of samples taken for rock magnetic studies

Depth(cm) 22702-3	Depth(cm)	Depth(cm) 22706-2	Depth(cm) 22708-1	Depth(cm)	Depth(cm) 22709-1	Depth(cm)
9.5	847	10	9.5	841	9.5	849.5
31	872	40	29	860	30	869.5
52	887.5	70	50	880.5	50.5	889.5
77		99.5	70	899.5	70	910
92		129.5	85.5	919.5	90.5	924.5
112		158	98.5	939.5	110.5	
130.5		188	119.5	960	130	
150		228.5	139.5		149.5	
175		275.5	159.5		169.5	
190.5		288.5	180		189.5	
210		318.5	199.5		210	
229		358	220		230	
249.5		387.5	239		250	
274		417.5	260		270	
289		455	280		290	
310		485.5	299.5		310	
328		515.5	320		330	
348.5		560	340		350	
373.5		589	360		370	
388		620	380		390	
409		657.5	399		409.5	
427.5		687	420		429.5	
447.5		717	439		449.5	
472.5		756	459		470	
487.5		786	479.5		489.5	
507.5		816	500		509.5	
526		859	524.5		530	
546		889	540		549.5	
571		920	559		570	
585.5			579		590	
606			599.5		610	
627.5			620		630	
648			639.5		649.5	
673			660.5		669.5	
688			679.5		589.5	
708			699		709	
727			720		729.5	
747.5			739.5		750	
772.5			759		770	
787.5			779.5		790	
807			799		810	
827			820.5		830	

Appendix 4 (continued)

Depth(cm) 22713-2	Depth(cm) 22721-3	Depth(cm) 22722-5	Depth(cm) 22723-1	Depth(cm) 22723-3	Depth(cm) 22725-2
3.5	9.5	9	19	9	10
24.5	39.5	30	49.5	20	20
43.5	69.5	60	80	40	34.5
64.5	99.5	89.5	119.5	60	50
94.5	129.5	129	149.5	80	65.5
124	159.5	159.5	179.5	100	80
154	189.5	189	220	120	95
184.5	219.5	229	250	140.5	110.5
214.5	250	259	280	159	125.5
244.5	289.5	290	320	180	140
284.5	320	329.5	350	200	149.5
314.5	350.5	360	379.5	220	
345	389.5	389.5	419.5	240	
385	419.5	429	449	260.5	
414.5	450	460	479	280	
445	489.5	489		300	
485	519.5	529.5		320	
514.5	549.5	559.5		340	
544.5	589.5	590		360	
	619.5	630		380	
	649.5	660.5		399.5	
	689.5	690.5		420	
	720	729			
	740	753.5			
		790			
		830.5			
		860.5			
		890			

Appendix 4 (continued)

Depth(cm) 22734-2	Depth(cm) 22735-1	Depth(cm) 22741-1
8.5	20	10
19	40	25
24.5	60	40
54.5	80	60
75	100	80
95	130	100
115	160	120
135	190	140
155	230	160
175	260	180
195	290	200
215	330	220
235	360	230
255	390	
275	430	
295	460	
315	490	
335	530	
355	560	
375	590	
395	630	
415	660	
435	690	
455	730	
475	760	
495	790	
515	805	
535	820	
555	835	
575	850	
595	870	
615	890	
635		
655		
675		
695		
715		
735		
755		
775		
795		
815		
835		
845		

Appendix 5: List of samples collected for microbiological analyses

Appendix 5 Detailed information on samples collected for future microbiological analysis

Date	Event	Coordinates	Water depth (m)	Gear	Nature of sample	Microbiology (DNA extraction)	Whole core sampling
15.01.18	GeoB22701-1	37° 48, 093'S, 054°10, 694'W	1390	CTD/ Rosette	Water column filter	×	
15.01.18	GeoB22702-2	37° 48, 563'S, 054°10, 214'W	1355	MUC	Solid phase sediment	×	
15.01.18	GeoB22702-3	37° 48, 567'S, 054°10, 211'W	1355	GC	Solid phase sediment	×	
16.01.18	GeoB22706-1	37° 58, 028'S, 053°45, 807'W	3006	MUC (	Solid phase sediment	×	
16.01.18	GeoB22706-2	37° 58, 035'S, 053°45, 789'W	3011	GC	Solid phase sediment	×	
17.01.18	GeoB22708-1	39° 18, 701'S, 053°57, 153'W	3690	GC	Solid phase sediment	×	
17.01.18	GeoB22708-2	39° 18, 702'S, 053°57, 165'W	3670	GC	Solid phase sediment		×
17.01.18	GeoB22708-3	39° 18, 700'S, 053°57, 167'W	3677	MUC	Solid phase sediment	×	
18.01.18	GeoB22709-1	39° 18, 064'S, 053°58, 030'W	3611	GC	Solid phase sediment	×	
18.01.18	GeoB22709-2	39° 18, 060'S, 053°58, 023'W	3615	GC	Solid phase sediment	×	×
18.01.18	GeoB22710-1	38° 34, 561'S, 054°21, 726'W	1110	CTD/ Rosette	Water column	×	
20.01.18	GeoB22711-1	38° 20, 037'S, 054°28, 950'W	1127	MUC	Solid phase sediment	×	
20.01.18	GeoB22713-1	38° 35, 328'S, 054°21, 079'W	1115	MUC	Solid phase sediment	×	
20.01.18	GeoB22713-2	38° 35, 320'S, 054°21, 081'W	1115	GC	Solid phase sediment	×	
21.01.18	GeoB22718-2	38° 52, 814'S, 054°18, 333'W	1445	CTD/R osette	Water column	×	
22.01.18	GeoB22719-1	37° 52, 078'S, 054°00, 049'W	2785	CTD/R osette	Water column	×	
24.01.18	GeoB22722-1	37° 32, 398'S, 054°01, 336'W	1076	CTD/R osette	Water column	×	
25.01.18	GeoB22724-1	36° 49, 998'S, 053°22, 001'W	1820	CTD/R osette	Water column	×	
22.01.18	GeoB22721-1	37° 33, 318'S, 053°58, 710'W	1060	MUC	Solid phase sediment	×	
22.01.18	GeoB22721-2	37° 33.315'S 53° 58.718'W	1060	GC	Solid phase sediment	×	
24.01.18	GeoB22722-3	37° 32, 392'S, 054°01, 342'W	1076	MUC	Solid phase sediment	×	
24.01.18	GeoB22722-5	37° 32.399'S 54° 01.377'W	1073	GC	Solid phase sediment	×	
24.01.18	GeoB22723-1	37° 42, 224'S, 053°57, 508'W	1167	GC	Solid phase sediment	×	
25.01.18	GeoB22723-2	37° 42.230'S, 53° 57.505'W	1168	MUC	Solid phase sediment	×	
25.01.18	GeoB22723-3	37° 42.221'S 53° 57.497'W	1168	GC	Solid phase sediment	×	
27.01.18	GeoB22725-1	38° 20, 536'S, 054°03, 862'W	1343	MUC	Solid phase sediment	×	
27.01.18	GeoB22725-2	38° 20, 541'S, 054°03, 864'W	1345	GC	Solid phase sediment	×	
29.01.18	GeoB22731-1	37° 38, 437'S, 054°45, 998'W	708	GS	Coral + slime, surface sediment	×	

Date	Event	Coordinates	Water depth (m)	Gear	Nature of sample	Microbiology (DNA extraction)	Whole core sampling
29.01.19	GeoB22732-1	37° 32, 578'S, 054°37, 244'W	799	GS	2 Undefined, potentially living samples, 1 worm (Annelida)	×	
03.02.18	GeoB22734-1	36° 08. 488'S, 53° 17. 163'W	242	MUC	Solid phase sediment	×	
03.02.18	GeoB22734-2	36° 08.483’S 53° 17.160’W	240	GC	Solid phase sediment	×	
03.02.18	GeoB22734-3	36° 08.489'S, 53° 17.149'W	240	GC	Solid phase sediment		×
03.02.18	GeoB22735-1	36° 07. 662'S, 52° 49. 899'W	1384	GC	Solid phase sediment	×	
03.02.18	GeoB22735-2	36° 07.668'S 52° 49.808'W	1381	MUC	Solid phase sediment	×	
05.02.18	GeoB22722-7	37° 32. 358'S, 54° 01. 318'W	1076	MeBo	Solid phase sediment	×	
07.02.18	GeoB22735-5	36° 07.613'S, 52° 49. 887'W	1388	MeBo	Solid phase sediment	×	
10.02.18	GeoB22741-1	38° 38. 216 'S, 54° 18. 674'W	1072	GC	Solid phase sediment	×	

Appendix 6: List of samples collected for organic geochemical analysis

Appendix 6 Detailed information for samples collected for organic geochemistry analysis

Date	Event	Coordinates	Water depth (m)	Gear	Nature of sample	IPLs/TOC	DOM	Cell counts	Double L-Channel
15.01.18	GeoB22702-2	37° 48, 563'S, 054°10, 214'W	1355	MUC	Solid phase, PW	×	×		
15.01.18	GeoB22702-3	37° 48, 567'S, 054°10, 211'W	1355	GC	Solid phase, PW	×	×		
16.01.18	GeoB22706-1	37° 58, 028'S, 053°45, 807'W	3006	MUC	Solid phase, PW	×	×		
16.01.18	GeoB22706-2	37° 58, 035'S, 053°45, 789'W	3011	GC	Solid phase, PW	×	×		
17.01.18	GeoB22708-1	39° 18, 701'S, 053°57, 153'W	3690	GC	Solid phase	×			×
17.01.18	GeoB22708-2	39° 18, 702'S, 053°57, 165'W	3670	GC	Solid phase		×		
17.01.18	GeoB22708-3	39° 18, 700'S, 053°57, 167'W	3677	MUC	Solid phase	×	×		
18.01.18	GeoB22709-2	39° 18, 060'S, 053°58, 023'W	3615	GC	Solid phase, PW	×	×	×	×
20.01.18	GeoB22711-1	38° 20, 037'S, 054°28, 950'W	1127	MUC	Solid phase	×			
20.01.18	GeoB22713-1	38° 35, 328'S, 054°21, 079'W	1115	MUC	Solid phase, PW	×			
20.01.18	GeoB22713-2	38° 35, 320'S, 054°21, 081'W	1115	GC	Solid phase, PW	×	×		
22.01.18	GeoB22721-1	37° 33, 318'S, 053°58, 710'W	1060	MUC	Solid phase, PW	×	×		
22.01.18	GeoB22721-2	37° 33.315'S 53° 58.718'W	1060	GC	Solid phase, PW	×	×		
24.01.18	GeoB22722-3	37° 32, 392'S, 054°01, 342'W	1076	MUC	Solid phase, PW	×	×		
24.01.18	GeoB22722-5	37° 32.399'S 54° 01.377'W	1073	GC	Solid phase, PW	×	×		
24.01.18	GeoB22723-1	37° 42, 224'S, 053°57, 508'W	1167	GC	Solid phase, PW	×	×		
25.01.18	GeoB22723-2	37° 42.230'S, 53° 57.505'W	1168	MUC	Solid phase	×			
25.01.18	GeoB22723-3	37° 42.221'S 53° 57.497'W	1168	GC	Solid phase, PW	×	×		
27.01.18	GeoB22725-1	38° 20, 536'S, 054°03, 862'W	1343	MUC	Solid phase, PW	×	×		
27.01.18	GeoB22725-2	38° 20, 541'S, 054°03, 864'W	1345	GC	Solid phase, PW	×	×		
28.01.18	GeoB22729-1	37°48,445'S,54 °20,113'W	1202	GC	PW		×		
03.02.18	GeoB22734-1	36° 08. 488'S, 53° 17. 163'W	242	MUC	Solid phase, PW	×	×		
03.02.18	GeoB22734-2	36° 08.483’S 53° 17.160’W	240	GC	Solid phase	×		×	×
03.02.18	GeoB22734-3	36° 08.489'S, 53° 17.149'W	240	GC	Solid phase, PW		×		
03.02.18	GeoB22735-1	36° 07. 662'S, 52° 49. 899'W	1384	GC	Solid phase, PW	×	×	×	
03.02.18	GeoB22735-2	36° 07.668'S 52° 49.808'W	1381	MUC	Solid phase, PW	×	×		
05.02.18	GeoB22722-7	37° 32. 358'S, 54° 01. 318'W	1076	MeBo	Solid phase sediment	×			
07.02.18	GeoB22735-5	36° 07.613'S, 52° 49. 887'W	1388	MeBo	Solid phase sediment	×			
10.02.18	GeoB22741-1	38° 38. 216 'S, 54° 18. 674'W	1072	GC	Solid phase sediment	×			
12.02.18	GeoB22744-1	38° 18. 25 'S 054° 32. 36 'W	992	GC	Pore water		×		

Appendix 7: List of samples from Rosette-casts for investigation of coccolithophore assemblages

Appendix 7 List of samples from Rosette-casts for investigation of coccolithophore assemblages.

GeoB No.	Sample No.	Date	Location Latitude (S)	Longitude (W")	Water Depth [m]	Sampling Depths [m]	Filtered Volume [l]	Remarks
22701-1	I-1		37° 48,9'	54° 10,7'	1391	10	2,0	
	I-2					20	4,0	
	I-3					40	5,0	
	I-4					60	5,0	
	I-5					80	5,0	
	I-6					100	5,0	
	I-7					125	5,0	
	I-8					150	5,0	
	I-9					200	5,0	
22705-1	II-1	16.1.18	37° 59,8'	53° 46,3'	3562	60	3,0	bottles at
	II-2					80	2,5	10m, 20m,
	II-3					100	5,0	and 40m
	II-4					125	5,0	have not
	II-5					150	5,0	closed
	II-6					200	5,0	
	II-7					3500	6,6	
22710-1	III-1	18.1.18	38° 34,5'	54° 22,7'	1125	10	1,5	
	III-2					20	2,0	
	III-3					40	5,0	
	III-4					60	5,0	
	III-5					80	4,5	
	III-6					100	5,0	
	III-7					125	5,0	
	III-8					150	5,0	
	III-9					200	5,0	
	III-10					1075	6,5	
22712-1	IV-1	20.1.18	38° 19,9'	54° 29,6'	1220	10	1,5	

	IV-2					20	1,5	
	IV-3					40	5,0	
	IV-4					60	5,0	
	IV-5					80	5,0	
	IV-6					100	5,0	
	IV-7					125	5,0	
	IV-8					150	5,0	
	IV-9					200	5,0	
	IV-10					1167	8,0	
22718-2	V-1	21.1.18	37° 52,8'	54° 18,3'	1411	10		not closed
	V-2					20	3,0	
	V-3					40	5,0	
	V-4					60	5,0	
	V-5					80	5,5	
	V-6					100	5,0	
	V-7					125	5,5	
	V-8					150	5,0	
	V-9					200	5,5	
	V-10					1352	8,5	
22719	VI-1	22.1.18	37° 53,8'	54°00,5'	2785	10	2,0	
	VI-2					20	2,0	
	VI-3					40	4,5	
	VI-4					60	5,0	
	VI-5					80	4,0	
	VI-6					100	5,0	
	VI-7					125	5,0	
	VI-8					150	5,0	
	VI-9					200	5,0	
	VI-10					2730	4,5	
	VI-11					2758	5,0	
22722-1	VII-1	24.1.18	37° 32,6'	54° 01,3'	1074	10	1,5	
	VII-2					20	1,5	

	VII-3					40	3,5
	VII-4					60	4,0
	VII-5					80	5,0
	VII-6					100	5,0
	VII-7					125	5,0
	VII-8					150	5,0
	VII-9					200	5,0
	VII-10					1074	6,0
22724-1	VIII-1	25.1.18	36° 50,0'	53° 22,0'	1818	10	4,5
	VIII-2					20	4,5
	VIII-3					40	4,5
	VIII-4					60	5,0
	VIII-5					80	5,0
	VIII-6					100	5,0
	VIII-7					125	5,0
	VIII-8					150	5,0
	VIII-9					200	5,0
22728-1	IX-1	28.1.18	37° 46,6'	54° 21,0'	1254	10	2,0
	IX-2					20	3,5
	IX-3					40	4,0
	IX-4					60	5,0
	IX-5					80	5,0
	IX-6					100	5,0
	IX-7					125	5,0
	IX-8					150	5,0
	IX-9					200	5,0
	IX-10					1238	8,0